Identification of RabGGTase inhibitors and mechanistic studies of Rab GTPase prenylation and recycling using fluorescent sensors

Dissertation

zur Erlangung des akademischen Grades
eines Doktors der Naturwissenschaften (Dr. rer. nat.)
des Fachbereichs Chemie der Technischen Universität Dortmund

Angefertigt am Max-Planck-Institut für molekulare Physiologie
in Dortmund

vorgelegt von

Yaowen Wu
aus China

Dortmund, Dezember 2007

1. Gutachter : Prof. Dr. R.S. Goody
2. Gutachter : Prof. Dr. H. Waldmann

Erklärung/Declaration

Die vorliegende Arbeit wurde in der Zeit von August 2004 bis December 2007 am Max-Planck-Institut für molekulare Physiologie in Dortmund unter der Anleitung von Prof. Dr. Roger S. Goody, Dr. Kirill Alexandrov und Prof. Dr. Herbert Waldmann durchgeführt.
Hiermit versichere ich an Eides statt, dass ich die vorliegende Arbeit selbständig und nur mit den angegebenen Hilfsmitteln angefertigt habe

The present work was accomplished from August 2004 to Dezember 2007 at Max-Planck-Institute for molecular physiology in Dortmund under the guidance of Prof. Dr. Roger S. Goody, Dr. Kirill Alexandrov and Prof. Dr. Herbert Waldmann.
I hereby declare that I performed the work presented independently and did not use any other but the indicated aids.

Dortmund, December 2007

Yaowen Wu

Contents

Abbreviations

Å	Angstrom (1 Å = 0.1 nm = 10^{-10} m)
AA	Amino acid
CBD	Chitin-binding domain
CBR	C-terminus binding region
CHAPS	3-[(3-Cholamidopropyl)-dimethylammonio]-propansulfonat
CHM	Choroideremia
CMC	Critical micelle concentration
CTAB	Cetyltrimethylammoniumbromide
Da	Dalton
Dans / Dansyl	5-Dimethylaminonaphtalin-1-sulfonyl
DDMAB	*N*-Dodecyl-*N*,*N*-(dimethylammonio)butyrate
DTE	1,4-Dithioerythritol
EPL	Expressed protein ligation
FA	Formic acid
FTase	Farnesyltransferase
FRET	Fluorescence resonance energy transfer
GAP	GTPase activating protein
GDF	GDI displacement factor
GDI	GDP dissociation inhibitor
GdmHCl	Guanidinium hydrochloride
GEF	Guaninenucleotide exchange factor
GF	Gel filtration
GG	Geranylgeranyl
GGPP	Geranylgeranylpyrophosphate
GGTase	Geranylgeranyltransferase
GST	Glutathione S-transferase
GTPase	Guaninetriphosphate phosphatase
HPLC	High performance liquid chromatography
HOPS	Homotypic fusion and vacuole protein sorting
Hsp	Heat shock protein
IPTG	Isopropyl-β-D-thiogalactoside
LC-MS	Liquid chromatography-mass spectrometry
MALDI-TOF-MS	Matrix assisted laser desorption/ionization-time of flight mass spectrometry
MEL	Mobile effector loop
MetAP	Methionylaminopeptidase
MWCO	Molecular weight cut off
NBD	7-Nitrobenz-2-oxa-1,3-diazol-4-yl
NCL	Native chemical ligation
NSF	*N*-ethyl-maleimide sensitive fusion protein
OD_{600}	Optical density at 600 nm
Rab	Ras-like (protein) from Rat brain
Ras	Rat adeno sarcoma
REP	Rab escort protein
RP-HPLC	Reversed-phase high performance liquid chromatography
RRF	Rab recyling factor
RT	Room temperature
SDS	Sodium dodecyl sulfate

Sec	Secretory protein
SNAP	Soluble NSF attachment protein
SNARE	Soluble NSF attachment protein receptor
SPPS	Solid phase peptide synthesis
S*t*Bu	*S-tert*-butyl
TEV	Tobacco Etch Virus
TFA	Trifluoroacetic acid
TX-100	Triton X-100
Yip	Ypt-interacting protein
Ypt	Yeast protein transport

Zusammenfassung

Prenylierte Rab-GTPasen regulieren den intrazellulären Transport in eukaryotischen Zellen durch Assoziation mit spezifischen Membranen sowie durch Rekrutierung einer Reihe von Rab-spezifischen Effektorproteinen. Die Katalyse der Prenylierung der mehr als 60 Mitglieder der Rab-GTPase-Familie erfolgt durch die Rab-Geranylgeranyltransferase (RabGGTase), wobei die Rab-Proteine mit dem *Rab Escort Protein* (REP) komplexiert sind. Das Recycling der Rab-GTPasen wird durch ein dem REP verwandten Protein, dem *GDP dissociation inhibitor* (GDI), reguliert. Diese zwei Regulatoren besitzen beide die Fähigkeit, einen Komplex mit prenylierten Rab-Proteinen zu bilden und dadurch als molekulare Chaperone zu fungieren, um unspezifische Aggregation zu verhindern, sowie prenylierte Rabs zu ihren Zielmembranen zu transportieren. Erst kürzlich wurde die gezielte Beeinflussung der Prenylierung von Rab-GTPasen als hoffnungsvolle Krebs- und Osteoporosetherapie beschrieben.

Mechanistische Studien der Rab-Prenylierung und die Identifizierung von RabGGTase-Inhibitoren setzen einen sensitiven und zweckmäßigen Rab-Prenylierungsassay voraus. Zudem kann die Untersuchung der Interaktion prenylierter Rabs mit REP/GDI dem Verständnis des molekularen Mechanismus des Rab-Recyclings durch REP/GDI und der funktionalen Segregation beider Regulatoren dienen. Die biophysikalische Analyse der Interaktion wird jedoch aufgrund der geringen Löslichkeit prenylierter Proteine in wässriger Lösung kompliziert.

In der vorliegenden Doktorarbeit wurden Methoden des Proteinengineerings, der organischen Synthese sowie der *Expressed Protein Ligation* (EPL) angewandt, um ein Ensemble semisynthetischer, fluoreszenter Rab7-Konjugate herzustellen. Hierzu wurde eine Vielzahl an Fluorophoren unterschiedlicher Anregungswellenlängen an Cystein- oder Lysin-Aminosäurereste in der Nähe des Prenylierungsmotives gekoppelt. Zwei Konstrukte, Rab7CCK(NBD) und Rab7SCCC-dans, zeigten einen 200%igen bzw. 50%igen Anstieg der Fluoreszenz in Folge von Prenylierung. Des Weiteren wiesen Rab7-Konstrukte mit einem dans-, NBD-, I-BA- oder I-SO-Label eine 2-10-fache Fluoreszenzänderung nach Bindung an REP oder RabGGTase auf. Diese fluoreszenzsensitiven Sensoren wurden zur Untersuchung der Bildung des

binären Rab:REP-Komplexes sowie des ternären Rab:REP:RabGGTase-Komplexes herangezogen.

Außerdem zeigte ein synthetisches fluoreszentes Analog des Phosphoisoprenoids, NBD-Farnesylpyrophosphat (NBD-FPP), einen 23-fachen Fluoreszenzanstieg nach Einbau in das Rab-Protein. Kinetische und thermodynamische Analysen wiesen auf, dass dieser Prozess verschieden von der Prenylierung mit dem physiologischen Substrat Geranylgeranyl-pyrophosphat (GGPP) erfolgt. NBD-FPP wurde dazu genutzt, die Rab-Prenylierung *in vitro* zu verfolgen und einen fluorometrischen Assay im Hochdurchsatzformat für die Prenylierung durch RabGGTase zu entwickeln, welches die Identifizierung von RabGGTase-Inhibitoren ermöglichte.

Mittels dieses Assay wurde eine Peptidbibliothek von etwa 400 chemischen Verbindungen gescreent. Dies führte zur Identifizierung mehrerer potenter (niedrige mikromolare IC_{50}-Werte), spezifischer sowie zellulär aktiver RabGGTase-Inhibitoren mit aromatischen Aminosäureresten (Phe, His, Tyr) im zentralen Kern des Peptides (R^2-R^4), einer langen Lipidkette oder einem Arylring am N-Terminus (R^5) und einer potentiell Zink-bindenden Gruppe wie dem N-Methyl-2-Ethylpyridin am C-Terminus (R^1). Die Untersuchung der Spezifität gegenüber den zwei anderen Prenyltransferasen FTase und GGTase-I sowie die kinetische Analyse des Inhibitionsmechanismus ergaben, dass Verbindung **5** und **10**, die sich nur in einem Aminosäurenrest unterscheiden (R^3), nicht-kompetitive bzw. kompetitive Inhibitoren zu NBD-FPP sind. Diese Beobachtungen legen nahe, dass der zentrale Kern des Peptids (R^2-R^4) die Bindungskonfiguration der Peptidverbindungen bestimmt. *Structure activity relationship*- (SAR) und Spezifitätsstudien zeigten, dass der C-terminale (R^1) Rest die Aktivität des Peptids in hohem Maße beeinflusst, wohingegen die chemische Gruppe am N-Terminus (R^5) kritisch für die Selektivität zwischen den drei Prenyltransferasen zu sein scheint. Die strukturelle Analyse weist ebenfalls darauf hin, dass die mutmaßliche Bindungsstelle des Isoprenoids des mono-prenylierten Rabs in der RabGGTase ein vielversprechendes Target für die zukünftige Identifizierung spezifischer RabGGTase-Inhibitoren darstellt.

Des Weiteren ermöglichte der sensitive fluorometrische Assay für die Rab-Prenylierung die Untersuchung der Prenylierung von C-terminalen Rab- Mutanten. Sequenzanalysen zeigten, dass das mutmaßliche C-terminale Rab- Interaktionsmotiv (CIM), in dem zwei nicht-polare Aminosäurereste einen polaren Aminosäurerest

umschließen, in der gesamten Rab-Familie vorhanden (**IKL** in Rab7) und für die Rab-Prenylierung essentiell ist. Mutationen in diesem Motiv führen zur partiellen oder sogar totalen Inhibition der Prenylierung. Im Gegensatz dazu gab es keine bestimmenden Faktoren für die Rab-Prenylierung innerhalb des Peptidlinkers, der das CIM- und das Prenylierungsmotiv verbindet. Das CIM fungiert somit als Anker zur Konzentrierung des C-terminalen Rab-Peptids in der aktiven Stelle der RabGGTase. Thermodynamische Analysen zur Bildung des binären Rab:REP-Komplexes sowie des ternären Rab:REP:RabGGTase-Komplexes wurden unter Anwendung der fluoreszenten Sensoren durchgeführt. Mutationen oder Verkürzungen des CIM führten zu einer Reduktion der Affinität des Rab:REP-Komplexes um zwei Größenordnungen, welches nahe legt, dass das CIM-Motiv signifikant zur hochaffinen Rab:REP-Bindung beiträgt, jedoch in geringerem Ausmaß als die GTPase-Domäne des Rab-Proteins selbst. Die Bildung des ternären Komplexes scheint durch sequentielle Formation der Rab-GTPase-Domäne-REP RBP (*Rab binding platform*) Interaktion, der Rab CIM-REP CBR (*Rab C-terminal binding region*) Interaktion sowie der REP-RabbGGTase-Bindungsoberfläche zu erfolgen. Somit assoziiert das C-terminale Rab-Peptid mit der RabGGTase in einer nicht-spezifischen Weise und positioniert die C-terminalen Cysteine an das reaktive Zn^{2+}-Zentrum zur Prenylierung. Dies liefert ein Erklärung dafür, warum die Rab-Prenylierungsmaschinerie sämtliche Rab-Proteine trotz ihrer hypervariablen C-terminalen Region als Substrat erkennen kann.

In weiterführenden Arbeiten wurde ein fluoreszentes Analog eines prenylierten Rab-Proteins, Rab7-NBD-farnesyl (Rab-NF), durch *Expressed Protein Ligation* hergestellt. Trotz einer hohen Löslichkeit in Abwesenheit von Detergenzien zeigte es ein ähnliches Verhalten wie die durch RabGGTase-Katalyse prenylierte Rab7-GTPase. Um Informationen über die Interaktion von nativ mono- und di-geranylgeranylierten Rab7-GTPasen mit REP und GDI zu erhalten, wurden die prenylierten GTPasen in Lösung durch Verwendung der β-Untereinheit der RabGGTase stabilisiert, welche als unspezifisches Chaperon von prenylierten Proteinen identifiziert wurde. Unter Anwendung kompetitiver Titrationen nativ-prenylierter und fluoreszenter Rab-Proteine konnte gezeigt werden, dass mono-geranylgeranyliertes Rab7 mit einem K_d-Wert von etwa 70 pM an REP bindet. Die Affinität des doppelt-prenylierten Rab7 ist etwa 20-fach schwächer. Im Gegensatz dazu bindet GDI beide prenylierten Formen mit vergleichbaren Affinitäten (K_d = 1-5

nM), jedoch nur sehr schwach an unprenylierte Rab-Proteine. Die erhaltenen Daten erlauben nun die Aufstellung eines thermodynamischen Modells für die Interaktion von RabGTPasen mit ihren Regulatoren und Membranen, welches die Notwendigkeit der Existenz von sowohl REP als auch GDI für die korrekte physiologische Funktion von Rab-Proteinen erklärt.

1. Abstract

Prenylated Rab GTPases regulate intracellular vesicular transport in eukaryotic cells by association with specific membranes and recruiting a multitude of Rab-specific effector proteins. Prenylation of more than 60 members of the Rab GTPase family in the human genome is catalyzed by Rab geranylgeranyl transferase (RabGGTase) while Rabs are complexed to Rab escort protein (REP). Recycling of Rab GTPases is regulated by a REP-related protein, GDP dissociation inhibitor (GDI). These two regulators share the ability to form a complex with prenylated Rab proteins, thereby functioning as molecular chaperones to prevent their aggregation, and the capability of delivery of prenylated Rabs to the target membrane. Recently, interference with prenylation of Rab GTPases has emerged as a very promising approach in cancer and osteoporosis therapy.

Mechanistic studies of Rab prenylation and identification of RabGGTase inhibitors require a sensitive and convenient assay for Rab prenylation. Moreover, investigation of the interaction of prenylated Rab with REP/GDI can facilitate understanding the molecular mechanism of Rab recycling by REP/GDI and the functional segregation of these two regulators. However, biophysical analysis of the interaction of prenylated proteins is complicated by their low solubility in aqueous solutions.

In this work, a combination of protein engineering, organic synthesis and expressed protein ligation was used to construct a family of semi-synthetic Rab7 fluorescent conjugates. A variety of fluorophores (excitation from UV to far red light) were coupled to a Cys or Lys amino acid residue at different places in the vicinity of the prenylation site. Two constructs, Rab7CCK(NBD) and Rab7SCCC-dans, displayed 200% and 50% fluorescence increase upon prenylation. Moreover, dans, NBD, I-BA and I-SO labeled Rab7 conjugates exhibited 2-10 fold fluorescence change upon binding to REP or RabGGTase. These fluorescently sensitive sensors were used to investigate the assembly of Rab:REP binary complex and Rab:REP:RabGGTase ternary complex.

In addition, a synthetic fluorescent analogue of phosphoisoprenoid, NBD-farnesyl pyrophosphate (NBD-FPP), displayed 23-fold fluorescence enhancement upon incorporation into Rab. The kinetic and thermodynamic analysis of the

prenylation using NBD-FPP showed that it is quite different from the native prenylation using geranylgeranyl pyrophosphate (GGPP). NBD-FPP was used to report Rab prenylation *in vitro* and develop a high-throughput fluorometric assay for RabGGTase, which facilitated the rapid identification of RabGGTase inhibitors.

A peptide library containing ca. 400 compounds was screened using this assay. Several potent (low micromolar IC_{50} values), specific and cellularly active RabGGTase inhibitors were identified, with the features of aromatic amino acid residues (Phe, His, Tyr) at the peptide central core (R^2-R^4), a long lipid chain or an aryl ring at the N-terminus (R^5) and a potential zinc binding group, such as *N*-methyl 2-ethyl pyridine, at the C-terminus (R^1). The specificity over the other two protein prenyltransferases, FTase and GGTase-I, and the inhibition mechanism of these inhibitors were characterized. Compound **5** and **10**, which differ in only one amino acid residue (R^3), are non-competitive and competitive to NBD-FPP, respectively. This finding suggests that the peptide central core (R^2-R^4) determines the binding configuration of the peptide compounds. Structure activity relationship (SAR) and specificity studies revealed that the C-terminal (R^1) residue strongly influences the activity of the peptide, while the chemical moiety at the N-terminus (R^5) appears to be critical for the selectivity among the three prenyltransferases. Structural analysis also suggests that targeting the putative binding site for the isoprenoid of mono-prenylated Rab in RabGGTase would be a very promising approach for future identification of specific RabGGTase inhibitors.

The sensitive fluorometric assay for Rab prenylation also allowed the investigation of prenylation of Rab C-terminal mutants. Sequence analysis revealed that the putative Rab C-terminal interacting motif (CIM), which has the property of two non-polar amino acid residue flanking a polar amino acid residue, is present throughout the Rab family (**I**K**L** in Rab7). The CIM motif is essential for Rab prenylation. Mutations of the CIM motif resulted in reducing the prenylation efficiency of Rab prenylation. In contrast, there are no determinants for Rab prenylation within the linker peptide connecting the CIM and the prenylation motif. However, the length of the linker peptide is critical for proper Rab prenylation. Therefore, the CIM functions as an anchor to concentrate the Rab C-terminal peptide in the active site of RabGGTase for prenylation. Thermodynamic analysis of the assembly of the Rab:REP binary complex and the Rab:REP:RabGGTase ternary complex was performed using the fluorescent sensors described above. Mutations or truncations

of CIM led to reduction of the affinity of the Rab:REP complex by 2 order of magnitude, suggesting that the CIM motif significantly contributes to Rab:REP binding. However, the CIM is not such a critical determinant for the ternary complex association as the GTPase domain. The ternary complex appears to assemble by the sequential formation of the Rab GTPase domain-REP RBP (Rab binding platform) interaction, the Rab CIM-REP CBR (Rab C-terminal binding region) interaction and the REP-RabGGTase interface. These three anchors ensure the assembly of the ternary catalytic complex. Thus, the Rab C-terminal peptide non-specifically associates with RabGGTase and positions the C-terminal cysteines to the reactive center Zn^{2+} for prenylation. This provides an explanation for how Rab prenylation machinery can process the whole Rab family despite the hypervariable C-terminal region.

In further work, a fluorescent analogue of prenylated Rab, Rab7-NBD-farnesyl (Rab-NF) was constructed by expressed protein ligation. This molecule was demonstrated to be soluble in the absence of detergent but otherwise similar in its behavior to naturally prenylated Rab7 GTPase. In order to obtain information on the interaction of natively mono- and di-geranylgeranylated Rab7 GTPases with REP and GDI molecules, the former molecules were stabilized in solution by using the β-subunit of RabGGTase, which was demonstrated to function as an unspecific chaperone of prenylated proteins. Using competitive titrations of mixtures of natively prenylated and fluorescent Rab, mono-geranylgeranylated Rab7 was shown to bind to the REP protein with a K_d value of ca. 70pM. The affinity of doubly prenylated Rab7 is ca. 20 fold weaker. In contrast, GDI binds both prenylated forms of Rab7 with comparable affinities (K_d = 1 to 5 nM), but has extremely low affinity to unprenylated Rab molecules. The obtained data allows the formulation of a thermodynamic model for the interaction of RabGTPases with their regulators and membranes and leads to an explanation for the requirement for both REP and GDI in Rab function.

2. Introduction

2.1 Protein prenylation and prenyltransferases

Posttranslational modifications of proteins are vital to the regulation of their physiological function. Whereas some important posttranslational modifications like phosphorylation and glycosylation have been well studied, lipid modification is an emerging field that has attracted more and more attention (Resh, 2006; Gelb, 1997). In particular, prenylation, a type of lipid modification with 15-carbon farnesyl and 20-carbon geranylgeranyl isoprenoids, is of increasing interest since many prenylated proteins are involved in signal transduction pathways controlling cell growth and differentiation, cytoskeletal rearrangement, and vesicular transport (Zhang and Casey, 1996). Covalent attachment of either of the isoprenyl moieties via thioether linkages to the C-terminal cysteine residues is critical for proper function of the modified proteins. The conjugated prenyl group is not only a mediator of membrane association but also functions as a molecular handle for specific protein-protein interactions, such as GDI interaction that allows cycling the prenylated proteins between different membranes (Zhang and Casey, 1996). Although a search of the human proteome revealed about 300 proteins which are potentially prenylated, only a fraction of these have been reported (Sebti, 2005). The majority of identified prenylated proteins belong to signal transducing Ras superfamily of small GTPases.

2.1.1 Discovery of protein prenylation

The first reports of prenylated peptides described secreted yeast sex hormones, which contain a farnesylated cysteine residue at the C-terminus (Tsuchiya et al., 1978; Sakagami et al., 1978). In the 1980s, the elucidation of the cholesterol biosynthesis pathway with respect to the cell cycle in human cells formed the basis for the discovery of prenylated proteins. A crucial early step in cholesterol formation is the synthesis of mevalonic acid by HMG CoA reductase (Goldstein and Brown, 1990). A specific inhibitor of HMG CoA reductase, compactin, made it possible to manipulate the metabolism of mevalonic acid in cells (Endo, 1992; Brown et al., 1978). In a set of studies, an intermediate of mevalonate metabolism other than cholesterol was found to be essential for DNA synthesis in the cell (Endo, 1992;

Fairbanks et al., 1984; Brown et al., 1978). The search for the required metabolite of mevalonate, which involved following the destiny of exogenously supplemented (Van Voorhis et al., 1991) mevalonate to compactin-treated cells, revealed that metabolites of mevalonic acid are incorporated into proteins (Maltese and Sheridan, 1987; Schmidt et al., 1984). Extensive structure elucidation studies revealed that these proteins contain cysteine-linked farnesyl and geranylgeranyl groups (Farnsworth et al., 1990; Farnsworth et al., 1989) (for a review see (Glomset et al., 1990)). These two isoprenoids are donated from soluble farnesyl pyrophosphate (FPP) and geranylgeranyl pyrophosphate (GGPP), metabolites in the mevalonate pathway (Swanson and Hohl, 2006; Goldstein and Brown, 1990) (Scheme 2-1 and 2-2). FPP and GGPP consist of 3 and 4 basic five-carbon building blocks, termed isoprene units, respectively (Scheme 2-2). Formation of FPP and GGPP is the result of chain elongation catalyzed by isoprenyl pyrophosphate synthases (IPPSs). In this biosynthesis pathway, condensation between 5-carbon isopentenyl pyrophosphates (IPP) and an isomer of IPP, dimethylallyl pyrophosphate, results in 10-carbon geranyl pyrophosphate, which is subsequently coupled consecutively with IPP to form FPP and GGPP (Scheme 2-1, a review see (Liang et al., 2002)).

Scheme 2-1. The biosynthesis of isoprenoids in animals

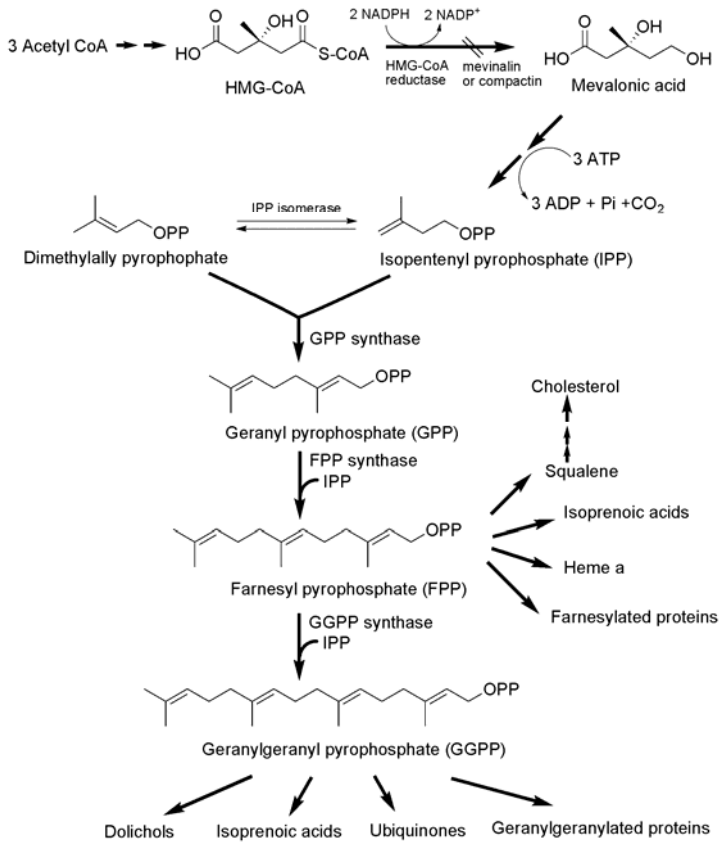

Scheme 2-2. Protein prenylation and post-prenylation modifications

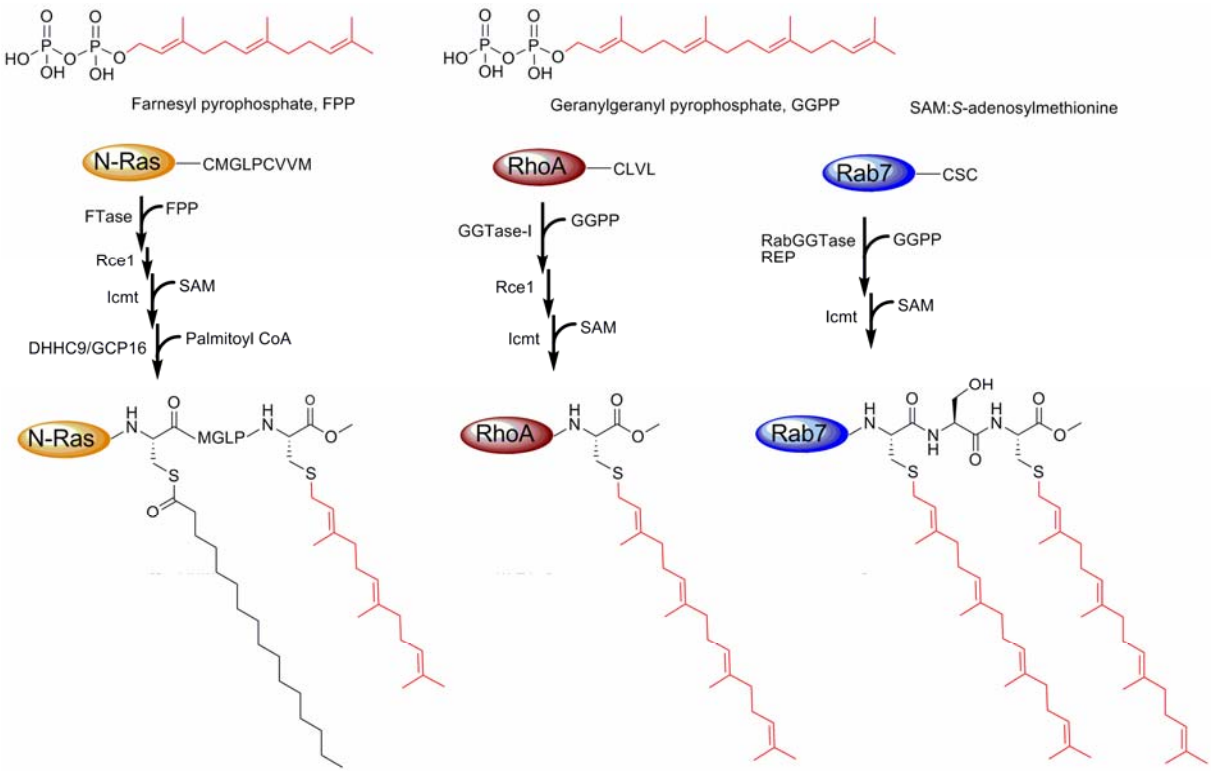

2.1.2 Protein prenyltransferases and their substrates

So far three protein prenyltransferases responsible for isoprenoid addition to proteins have been identified (for reviews see (Maurer-Stroh et al., 2003; Casey and Seabra, 1996)). They can be classified into two categories according to their functions. One is the CAAX prenyltransferases: protein farnesyltransferase (FTase) (Reiss et al., 1990) and protein geranylgeranyltransferase type I (GGTase-I) (Seabra et al., 1991) share the same motif CAAX box (C is cysteine, A is usually but not necessarily an aliphatic amino acid, and X can be one of a variety of amino acids) in their substrates. The other is the non-CAAX prenytransferase: Rab geranylgeranyltransferase (RabGGTase), also called protein geranylgeranyltransferase type II (GGTase-II) (Seabra et al., 1992b), processes different substrates, Rab GTPases.

FTase and GGTase-I are heterodimers that share an α subunit and have 30% amino acid identity in their β subunits. They are designated CAAX prenyltransferases because both of them recognize a C-terminal CAAX motif and transfer either farnesyl (FTase) or geranylgeranyl (GGTase-I) to the invariant cysteine residue located at the fourth from the C-terminus of the protein (Scheme 2-2). Substrates for FTase include Ras GTPases, which regulate signal transduction involved in cellular growth; nuclear lamins A and B, which form structural lamina on the inner nuclear membrane; the

γ subunit of heterotrimeric G-protein transducin, which functions in visual signal transduction in the retina; the large-antigen component of the hepatitis δ virus; and yeast mating factors (Clarke, 1992). Known targets of GGTase-I include most γ subunits of heterotrimeric G-proteins (Marrari et al., 2007) and many small GTPases such as the Rho/Rac family (Glomset and Farnsworth, 1994).

The rules for specificity in recognition of CAAX motifs by FTase and GGTase-I are not fully understood. These two enzymes possess distinct but overlapping protein substrate specificity that is determined primarily by the sequence identity of the CAAX motif. The X residue of CAAX is the most decisive element for differential recognition by FTase versus GGTase-I (Hartman et al., 2005; Roskoski, Jr. and Ritchie, 1998; Yokoyama et al., 1991; Casey et al., 1991)] (see Table 2-1). The AA part of the CA_1A_2X motif is also important for specificity of FTase and GGTase-I, with a relaxed requirement at the A_1 residue and more restricted in the A_2 residue (Reid et al., 2004; Reiss et al., 1991). It has also been shown that the presence of an upstream polybasic region enhances the dual specificity of these substrates (Hicks et al., 2005). In contrast to the variety in the peptide substrate specificity, FTase only efficiently transfers the lipid substrate FPP, while GGTase-I prefers transferring GGPP with FPP as a moderately effective substrate. Therefore, FTase and GGTase-I show mixed specificity under certain conditions (Yokoyama et al., 1995; Armstrong et al., 1995b; Trueblood et al., 1993; Adamson et al., 1992; Yokoyama et al., 1991). However, FTase binds FPP 15-fold tighter than GGPP and GGTase-I binds GGPP 330-fold tighter than FPP (Yokoyama et al., 1997), indicating that *in vivo* GGTase-I and FTase will likely predominantly bind to GGPP and FPP, respectively. A “molecular ruler” mechanism (Liang et al., 2002) was proposed for lipid substrate specificity base on the crystal structures of FPP bound FTase (Strickland et al., 1998; Long et al., 1998) and GGPP bound GGTase-I (Taylor et al., 2003), where the appropriate prenyl pyrophosphate is recognized by the depth of the active site. Although the properties of the C-terminal residue of the protein substrate affect reactivity with FTase and GGTase-I, it is not yet clear whether the nature of the prenyl group causes differential behavior *in vivo*, such as targeting to a specific membrane. However, the overlapping protein substrate specificity between the FTase and GGTase-I allows the modified substrates having a range of features, suggesting that in some cases the farnesyl versus geranylgeranyl distinction might not be very important (see section 2.3).

Table 2-1. Properties of protein prenyltransferases

Type	CAAX prenyltransferases		RabGGTase (GGTase-II)
	FTase	GGTase-I	
Subunit composition (mammalian)	44 kDa (α) 48 kDa (β)	44 kDa (α) 43 kDa (β)	65 kDa (α) 37 kDa (β)
Metal requirements	Zn^{2+}, Mg^{2+}	Zn^{2+}	Zn^{2+}, Mg^{2+}
Isoprenoid substrate	FPP	GGPP	GGPP
Protein substrates	Ras, nuclear lamins, trimeric G-protein transductin γ subunit	Rho, Rac, most trimeric G-protein γ subunits	Rab (requires REP)
C-terminal motif of protein substrate	$-CA_1A_2X$ X=S, M, A, Q, F a_1: no restriction, a_2: preference for I, V	$-CA_1A_2X$ X=L, F a_1: no restriction, a_2: preference for I, L	Usually double Cys motifs -CC, -CXC, CCX, -CCXX, -CCXXX, in a few cases single Cys motif -CXXX

RabGGTase is also a heterodimer, with its α subunit having 27% identity with the α subunit of FTase and GGTase-I, and the β subunit showing 29% identity to the β subunit of FTase (Sebti, 2005). However, RabGGTase stands quite apart from the other two protein prenyltransferases both functionally and structurally. RabGGTase has a very strict substrate preference and acts only on members of Rab GTPase family, which play a central role in membrane trafficking in eukaryotic cells (Stenmark and Olkkonen, 2001). Unlike FTase and GGTase-I, RabGGTase does not recognize a short C-terminal sequence but requires an additional factor termed Rab escort protein (REP) to recruit Rab protein (Andres et al., 1993). REP interacts with the unprenylated Rab protein preferentially in its GDP-bound form (Alexandrov et al., 1998; Seabra, 1996b; Sanford et al., 1993) and mediates its recognition by RabGGTase (Pylypenko et al., 2003; Alexandrov et al., 1999; Anant et al., 1998). Upon catalytic quaternary complex (Rab:REP:RabGGTase:GGPP) formation, consecutive double prenylation without dissociation of the mono-prenylated intermediate from enzyme (Thoma et al., 2001c). To ensure complete di-prenylation of Rab, the mono-prenylated Rab still tightly associate with REP so that they cannot be disrupted by liposome or detergent (Shen and Seabra, 1996). Following double prenylation, binding of another GGPP molecule triggers the release of the prernylated Rab:REP complex (Thoma et al., 2001b), which is then ready for membrane delivery of prenylated Rabs (Alexandrov et al., 1994). After that, REP is released and supports another round of Rab prenylation.

Intriguingly, some Rab proteins have only one prenylatable C-terminal cysteine, ending in CXXX. Most, but not all, of them contain sequences that do not conform to the classic CAAX motif. Conversely, Rab8 contains a CVLL motif, which may be geranylgeranylated by both RabGGTase and GGTase-I *in vitro*. Nevertheless, the majority of Rab8 appears to be geranylgeranylated *in vivo* by RabGGTase (Wilson et

al., 1998). Recently, FPP was found to be incorporated into Rab by RabGGTase resulting in formation of a di-farnesylated product. On the other hand, RabGGTase binds to GGPP with 100-fold preference over FPP, which may represent a thermodynamic proofreading of lipid substrate for RabGGTase *in vivo*. Evidence for farnesylated Rab in cells has not been forthcoming (Wu, et al. unpublished data).

2.1.3 Mechanism of protein prenylation

All three protein prenyltransferases are Zn^{2+}-dependent metalloenzymes, and each contains a single zinc atom necessary for reactivity (Chen et al., 1993; Moomaw and Casey, 1992; Reiss et al., 1992; Seabra et al., 1992b). The Zn^{2+} functions as a reactive center that coordinates the cysteine sulfur so as to reduce the pK_a of the thiol resulting in formation of a bound thiolate at physiological pH (Hightower et al., 1998; Strickland et al., 1998; Huang et al., 1997). Zinc-catalyzed sulfur alkylation has been proposed as the general mechanism for the greater family of zinc metalloproteins that facilitate the transfer of an alkyl group to sulfur and selenium residues (Hightower and Fierke, 1999). In FTase mediated farnesylation, the activated thiolate of Cys acts as a nucleophile to attack the polarized C1 of the farnesyl chain by Mg^{2+} coordination of the pyrophosphate leaving group (Saderholm et al., 2000). Stereochemical (Clausen et al., 2001; Edelstein et al., 1998; Mu et al., 1996), kinetic (Huang et al., 2000; Dolence and Poulter, 1995) and kinetic isotope effect (KIE) analyses (Lenevich et al., 2007; Pais and Fierke, 2007; Pais et al., 2006; Weller and Distefano, 1998) reveal that the condensation between cysteine thiol and prenyl pyrophosphate is mainly through an associative (S_N2) mechanism with an “exploded” transition state (Figure 2-1).

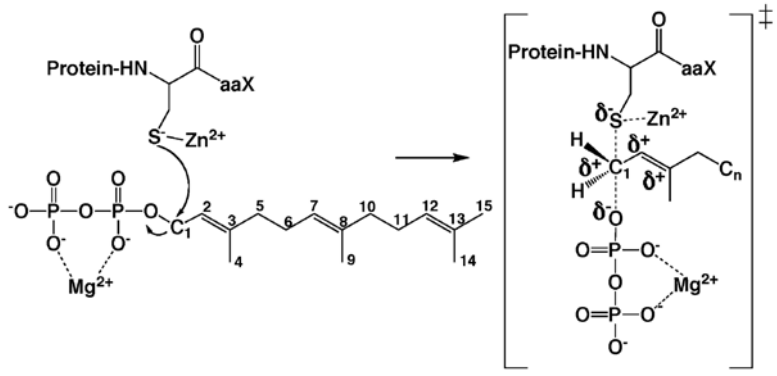

Figure 2-1. Transition state model for FTase catalysted farnesylation (Pais et al., 2006).

Over the past decade, high-resolution crystal structures of FTase and GGTase-I complexed with various substrates, products, and inhibitors have provided insights into the mechanism of these enzymes. Structures representing each of the major steps along the reaction pathway of CAAX prenyltransferases have been solved (Figure 2-2) (Taylor et al., 2003; Long et al., 2002). Steady-state kinetic studies reveal an random order sequential mechanism in FTase and GGTase-I (Zhang et al., 1994; Pompliano et al., 1992b). Nevertheless, a preferred catalytic pathway is through initial binding of isoprenoid to the enzyme followed by association of the CAAX substrate (Yokoyama et al., 1995; Pompliano et al., 1993). Reaction of the CAAX substrate with the FPP bound enzyme is functionally irreversible, accompanied by a rapid chemical step to form the enzyme-bound farnesylated peptide product (Huang et al., 2000; Yokoyama et al., 1997; Furfine et al., 1995). Product release is the rate-limiting step of the reaction and occurs only in the presence of excess of either substrate, particularly isoprenoid diphosphate (Tschantz et al., 1997; Furfine et al., 1995). This reaction cycle effectively maintains FTase in a substrate- or product-bound complex at all times. On account of this, one interesting possibility is that CAAX prenyltransferase itself could serve as a chaperone for the nascent prenylated Ras and Rho proteins and may deliver them to the endoplasmic reticulum (ER).

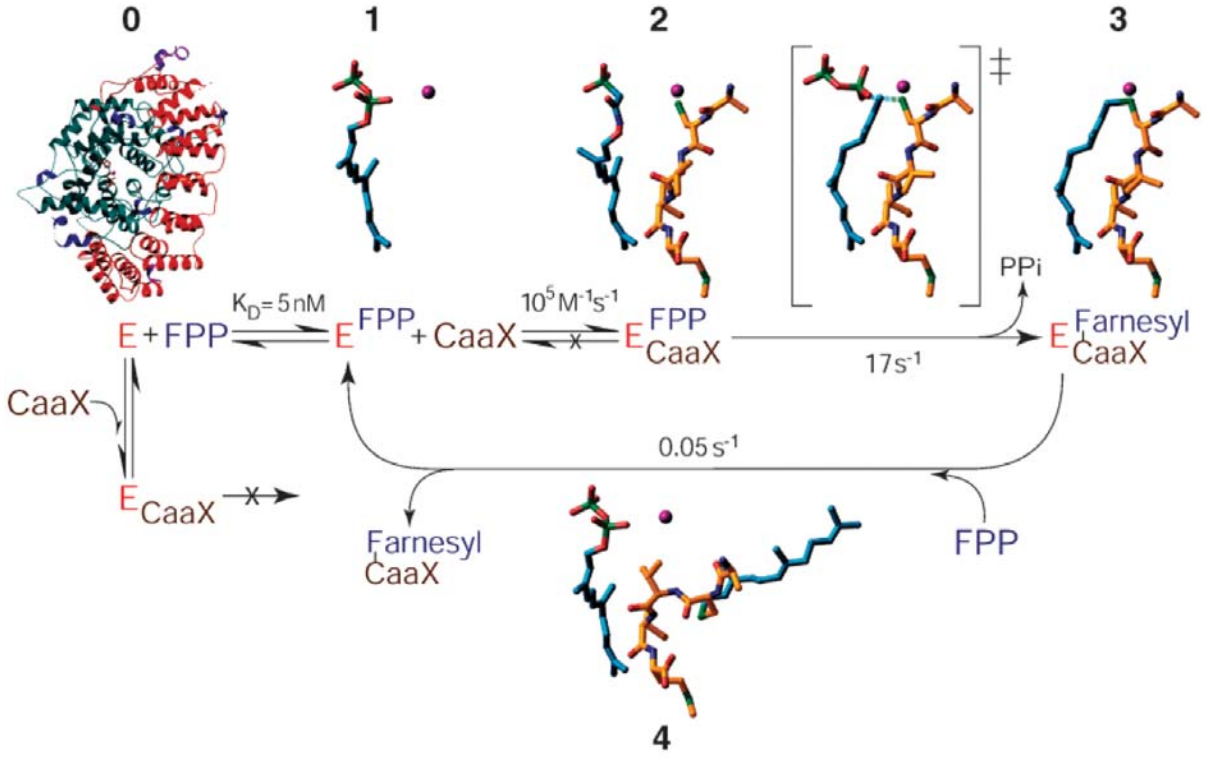

Figure 2-2. Structures along the FTase reaction pathway (Lane and Beese, 2006). In each of these complexes, the enzyme acts as a rigid scaffold, therefore, for clarity, only the substrates and products

are shown as they bind in the active site. The path begins with the unliganded (apo) enzyme (0) (PDB ID 1FT1), with the α subunit shown in red and the β subunit in blue. The FPP molecule binds to form a binary substrate complex (1) (PDB ID 1FT2), followed by binding of the CAAX substrate to form a ternary substrate complex (2) (PDB ID 1D8D). The resulting farnesylated product remains bound in the active site (3) (1KZP). Excess substrate, particularly FPP, facilitates product displacement, demonstrated by a complex in which binding of a new FPP molecule expelled the farnenylated product to the "exit groove", ready for dissociation from enzyme (4) (1KZO). The double dagger symbol indicates a modeled transition state along the reaction coordinate between 2 and 3 (see Figure 2-1 for a more detailed view of the transition state). Throughout this figure, the isoprenoid is shown in blue, the CAAX in yellow, and the catalytic zinc ion in magenta. Also shown are the kinetic parameters determined for this reaction.

2.1.4 Post-prenylation modification

Prenylation of proteins enables them to associate with the endoplasmic reticulum, where they are further modified in subsequent post-prenylation reactions. The three C-terminal amino acid residues (AAX) of CAAX protein are removed by the endoprotease Rce1 (Ras converting enzyme 1) (Trueblood et al., 2000; Boyartchuk et al., 1997) and the α-carboxyl group of the newly exposed isoprenylcysteine is methylated by Icmt (isoprenylcysteine carboxymethyltransferase) (Clarke, 1992; Clarke et al., 1988). Embryonic lethality of either $Rce1^{-/-}$ or $Icmt^{-/-}$ knockout mouse argues for the physiological significance of post-prenylation CAAX processing (Bergo et al., 2004; Bergo et al., 2001). It was proposed that 15-carbon farnesyl modification is below the threshold for promoting membrane association and requires AAX proteolysis and carboxyl methylation (Wright and Philips, 2006). This hypothesis is correlated with the finding that carboxy-methylation of farnesylated peptide increases the affinity for vesicles by more than 40-fold (Silvius and l'Heureux, 1994). Although carboxy-methylation of prenylated proteins has been suggested to be reversible (Chelsky et al., 1985), and therefore could represent a regulatory event, no *in vivo* evidence has been observed until now.

At the Golgi apparatus, some GTPases, such as N-Ras, H-Ras and K-Ras4A, then undergo another lipid modification – palmitoylation, a conjugation of a 16-carbon fatty-acid chain to the thiol group of an upstream cysteine via a thioester bond (Hancock et al., 1989) (for a recent review see (Mitchell et al., 2006)). A Golgi-associated protein, GCP16 complexed with one of the DHHC family proteins (protein containing an Asp-His-His-Cys domain), DHHC9, has shown palmitoyl acyltransferase (PAT) activity towards H-Ras and N-Ras (Swarthout et al., 2005). Scheme 2-2 shows the structures of the C-termini of example prenylated proteins after prenylation and post-prenylation modifications. Palmitoylation for H-Ras, N-Ras

and K-Ras4A, and a polybasic, lysine-rich sequence for K-Ras4B (Hancock et al., 1991) provide a second signal for targeting of these proteins to the plasma membrane via vesicular transport. Depalmitoylation of H-/N-Ras at the plasma membrane triggers the back transport of the farnesylated proteins to the Golgi via a nonvesicular pathway (Goodwin et al., 2005; Rocks et al., 2005). The eukaryotic acyl protein thioesterase 1 (APT1) has been found to function in removal of palmitate from proteins on the cytosolic face of plasma membranes (Duncan and Gilman, 1998). The reversible palmitoylation is essential for regulation of partitioning of Ras isoforms between plasma membrane and Golgi. In contrast, the association of K-Ras4B with plasma membrane is controlled by an electrostatic switch regulated by protein kinase C, which phosphorylates K-Ras4B on serine 181 within the polybasic region and thereby partially neutralizes the charge of the polylysine sequence (Bivona et al., 2006). This modification may reduce the affinity of K-Ras4B with negatively charged phosphatidylinositol 4,5-bisphosphate (Heo et al., 2006) and phosphatidylinositol 3,4,5-trisphosphate (Heo et al., 2006) clusters on the plasma membrane, resulting in dissociation from PM (Heo et al., 2006).

Similar post-prenylation modifications (proteolysis and methylation) seem to apply to Rho GTPases except that they bind to the cytosolic protein RhoGDI (Rho-guanine nucleotide dissociation inhibitor) (Wright and Philips, 2006), which keeps them soluble in the cytosol and regulate the membrane binding of Rho GTPases (Michaelson et al., 2001; Hoffman et al., 2000).

After (usually) doubly geranylgeranylation, Rab GTPases ending in CXC undergo carboxymethylation by Icmt at ER membrane, whereas those having CC and CCXX sequences in their C-termini are not carboxyl-methylated (Gelb et al., 1995; Smeland et al., 1994; Li and Stahl, 1993a). Recently, some Rab GTPases containing an analogous CAAX motif, like Rab8a(CVLL), Rab13(CSLG), Rab18(CSVL) and Rab23(CSVP), were also found to undergo the same AAX proteolysis and carboxy-methylation at the endoplasmic reticulum as other CAAX proteins (Leung et al., 2007). However, the regulatory function of carboxymethylation of Rab proteins is still unclear. One example showed that carboxy-methylation of Rab3D is developmentally regulated and coincides with the acquisition of stimulus–secretion coupling in rat pancreas and the rat pancreatic acinar tumor cell line AR42J (Qiu et al., 2001; Valentijn and Jamieson, 1998). Carboxy-methylation of Rab proteins may increase their affinity to membranes. It has been shown that carboxy-

methylation of a di-geranylgeranylated peptide decreases the rate of interbilayer transfer by more than 10-fold (Silvius and l'Heureux, 1994). This correlates with the observation that more carboxylmethylated Rabs partition into membranes when they are subjected to RabGDI extraction (Leung et al., 2007; Li and Stahl, 1993b). Carboxy-methylation may also result in an indirect pathway for Rab membrane targeting. In the indirect pathway, prenylated Rabs that require methylation may first contact with the ER and the fully processed Rabs are then redirected to their target membrane, in a step probably mediated through a soluble complex with their chaperone, RabGDI (Leung et al., 2007).

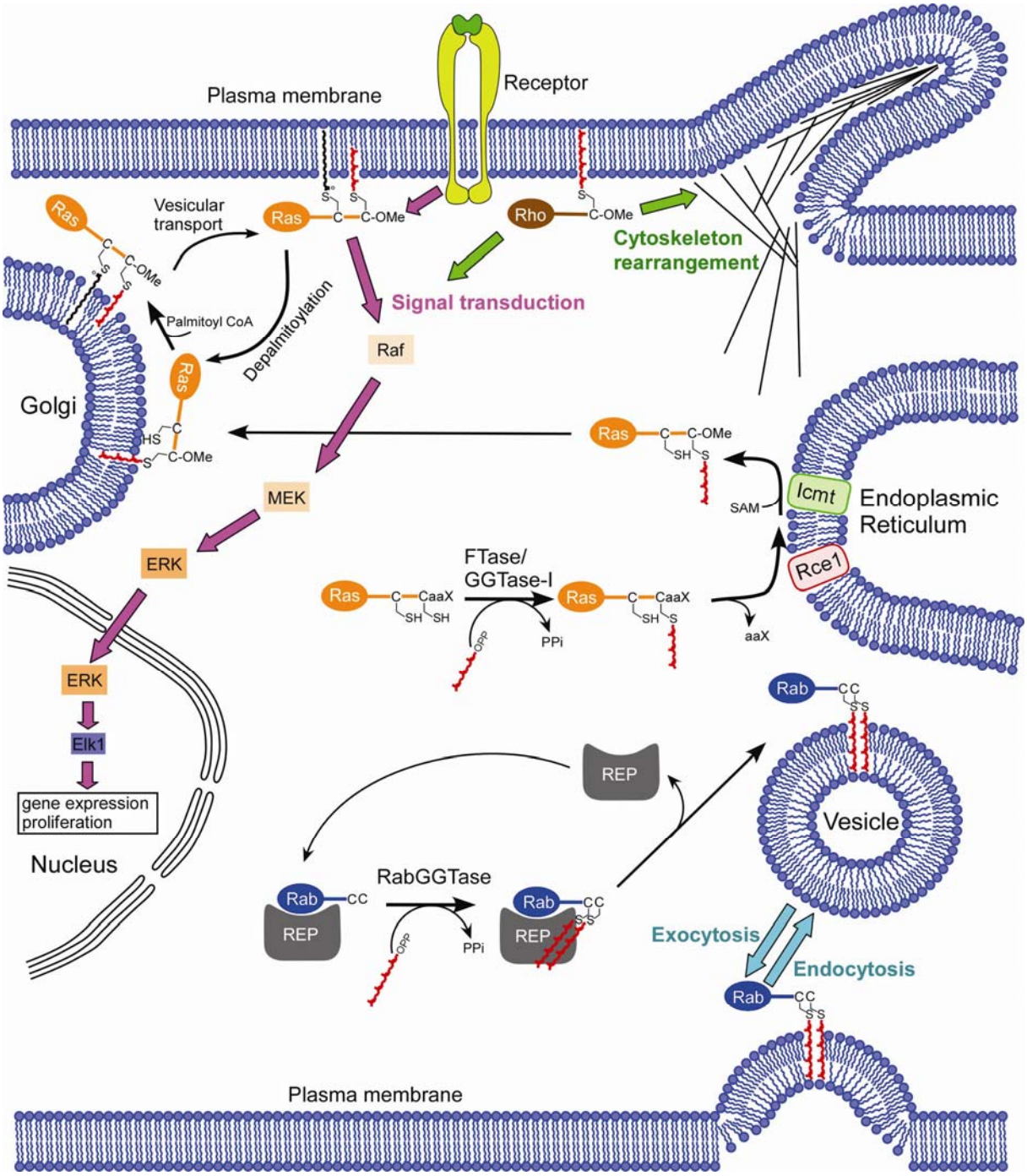

Figure 2-3. Overview of protein prenylation, post-prenylation modification and function of prenylated proteins. CAAX protein prenyltransferases (FTase and GGTase-I) attach a farnesyl or geranylgeranyl group to the C-terminal CAAX motif of certain cytosolic proteins (shown examples are Ras in orange, and Rho in dark red). The prenylated proteins undergo C-terminal AAX proteolysis by Rce1 (light red), and afterward carboxylmethylated by Icmt (light green) at the ER. Some Ras proteins, such as N-Ras, H-Ras and K-Ras4A are subsequently palmitoylated at the one or two upstream C-terminal cysteines after transfer to the Golgi membranes. This reaction is catalyzed by DHHC9-GCP16 in mammals using palmitoyl coenzyme A (CoA) as the fatty-acid donor (palmitoyl group is shown in black and farnesyl group is in red). The palmitoylation controls plasma membrane localization of Ras proteins. After its insertion into the membrane via its lipid tail, Ras proteins transduce signals from plasma membrane to nucleus, upon activation into GTP-bound form. A simplified depiction of the Ras signaling pathway is also illustrated (shown in pink arrows) (Vojtek and Der, 1998). Rho family proteins exert their function on the membrane, and are involved in regulation of cytoskeletal rearrangement and gene expression. Rab proteins are geranylgeranylated by RabGGTase with the aid of REP. REP presents prenylated Rab proteins to the target membrane. Once associate with membranes, Rab proteins regulate vesicular transport including endo- and exocytosis. Abbreviation: Icmt, isoprenylcysteine carboxylmethyltransferase; Rce1, Ras converting enzyme 1; PPO, pyrophosphate; SAM, S-adenosylmethionine; MEK, mitogen-activated protein (MAP) or extracellular signal-regulated kinase (ERK) kinase.

Modification of Rab GTPases by two long (20-carbon) hydrophobic moieties allows them to stably associate with membranes (Shahinian and Silvius, 1995), and serves as a molecular handle for specific interaction with RabGDI that extracts prenylated Rab from membranes (Pylypenko et al., 2006; Rak et al., 2003; Alory and Balch, 2001). The reversibility of this association is of particular importance, since it allows recycling of Rab proteins between different membranes upon completion of their functional cycle. Points concerning Rab recycling will be discussed in section 2.2.4.

2.2 Function of small GTPases

2.2.1 GTPase cycle

GTP-binding proteins (also called GTPases or G proteins) are responsible for regulation of a host of functions ranging from transduction of signals from plasma membrane receptors to regulation of the cytoskeleton, membrane traffic, nuclear transport, and protein synthesis in eukaryotic cells (Figure 2-3). The main families of G proteins include the monomeric small G proteins, the heterotrimeric G proteins, elongation factors and dynamin-related G proteins. Most identified prenylated proteins belong to small G proteins (also referred to as small GTPases). Of the small G proteins, the Ras superfamily of GTPases is the most studied and consists of over 150 human members with a typical size of 20–25 kDa (Wennerberg et al., 2005). This superfamily is classified into five major subfamilies: Ras, Rho/Rac, Rab, Sar1/Arf and Ran (Takai et al., 2001). These proteins function as regulators of a variety of important biological processes: the Ras family regulates gene expression, the Rho family regulates cytoskeletal reorganization and gene expression, the Rab and Sar1/Arf families regulate vesicle trafficking, and the Ran family regulates nucleocytoplasmic transport and microtubule organization (for recent reviews see (Konstantinopoulos et al., 2007; Rocks et al., 2006; Souza-Schorey and Chavrier, 2006; Pfeffer and Aivazian, 2004; Quimby and Dasso, 2003; Etienne-Manneville and Hall, 2002)). Among these proteins, Arfs are myristoylated, but Ran GTPases are not modified and are soluble in the cytosol and the nucleosol, while Ras, some Rho and all Rab GTPases are prenylated as described in section 2.1.

All G proteins share a conserved GTPase domain that binds a guanine nucleotide and use a common enzymatic cycle between GTP-bound and GDP-bound state to switch the protein “on” and “off”, (the GTPase cycle; Figure 2-4) (Sprang, 1997). The GTP-bound conformation is active, since it interacts with effector proteins, which stimulate downstream signaling events. The GDP-bound conformation is inactive for it does not bind effectors. Hydrolysis of GTP to GDP switches G proteins from the active state to the inactive state. Thus, within G proteins are found clocks (hetertotrimeric G protein α subunits), molecular switches (Ras superfamily), and sensors (translation elongation factors, EF-Tu and EF-G).

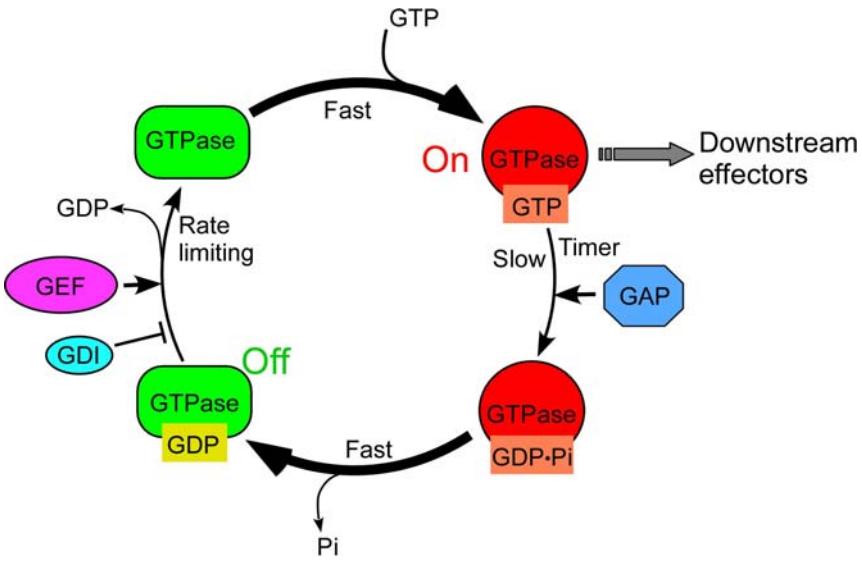

Figuer 2-4. GTPase cycle. The size of the arrows indicates the relative rate of the reactions. GAP: GTPase-activating protein; GDI: guanine nucleotide dissociation inhibitor; GEF: guanine nucleotide exchange factor.

The GTPase cycle is highly regulated by guanine nucleotide exchange factors (GEFs) that induce the release of the bound GDP to be replaced by the more abundant GTP and by GTPase-activating proteins (GAPs) that accelerate the intrinsic GTP hydrolysis of GTPases (for reviews see (Bos et al., 2007; Cherfils and Chardin, 1999; Scheffzek et al., 1998)). For a subset of small G proteins (Rho and Rab proteins) guanine nucleotide dissociation inhibitors (GDIs) provide an additional level of control. These proteins remove membrane-anchored small G proteins from membranes by sequestration of their lipid tails, and inhibit the release of GDP, The prenylated proteins are unloaded from GDI by GDI displacement factors (GDFs) on membranes.

GDP release is the rate limiting step in the GTPase cycle with a half-life on the order of one or more hours. GEFs accelerate the exchange reaction by several orders of magnitude (Vetter and Wittinghofer, 2001), and thus activation of G proteins in biological processes occurs within minutes or less. Since the binding of a GEF reduces the affinity for the nucleotide, and visa versa, the nucleotide weakens the affinity for the GEF, the nucleotide-free G protein binds with either the GEF or the nucleotide in high-affinity binary complexes. In the exchange reaction the GEF displaces the bound nucleotide, and in the reverse reaction rebinding of GDP or GTP results in the dissociation of the GEF. Binding of GTP is fast and is favored over GDP since the cytoplasmic concentration of GTP (about 1 mM) is ten times higher than that of GDP, resulting in preferential binding of GTP.

The intrinsic GTP hydrolysis of GTPase is very slow, occurring with half-lives in tens of seconds to hours, depending on the GTPase. Efficient hydrolysis requires the association with a GAP, which accelerates the cleavage of the γ-phosphate group by several orders of magnitude. The first major insight into GAP-assisted GTP hydrolysis was obtained from the structure of the Ras-RasGAP complex (Scheffzek et al., 1997). The RasGAP stabilizes the interaction of the conserved $_{ras}$Gln61 with the attacking water, and in addition, inserts an “arginine finger” into the phosphate-binding site, thus stabilizing the transition state by neutralizing negative charge at the γ-phosphate. The interactions are conserved between the Ras, Rho, and trimetric G-protein families. In contrast, RabGAP supplies two catalytic fingers, an analogous arginine finger and a glutamine finger that substitutes for the glutamine in the conserved DxxGQ motif of the GTPase (Pan et al., 2006). Subsequent dissociation of inorganic phosphate is fast and reverses the conformational change of switch I and II. This inactivates GTPases by dismantling the binding site for effector proteins. The net rate of GTP hydrolysis serves as a timing mechanism to limit the duration of interaction with effectors.

2.2.2 The structural basis of Rab GTPases function

All GTPases share a core GTP-binding domain with a minimum size of about 160-170 residues. The basic architecture of this domain has been maintained during the evolutionary divergence of the various GTPases. The common GTP-binding domain (also referred to as the G protein fold) consists of a 6-stranded β sheet sandwiched between 5 α helices (Sprang, 1997) (Figure 2-6). In this domain the elements responsible for the guanine nucleotide and Mg^{2+} binding and GTP hydrolysis are located in five loops (designated G1 to G5), which are the most highly conserved and define the G protein superfamily (Valencia et al., 1991; Bourne et al., 1991).

The G1 motif (also called the P-loop) with the consensus sequence GxxxxGK(S/T) connects the β1 strand to the α1 helix and contacts the α- and β-phosphates of the guanine nucleotide. The G2 motif (T) located between the α1 helix and the β2 strand, and the G3 motif [DxxG(Q/H/T)] at the N-terminus of the α2 helix associate with Mg^{2+} and the γ-phosphate of GTP. The guanine is recognized, in part, by the conserved NKxD sequence (G4) that links the β5 strand and α4 helix and the

G5 box that connects β6 and α5 with the consensus sequence, (C/S)A(K/L/T) (Wennerberg et al., 2005) (Figure 2-5).

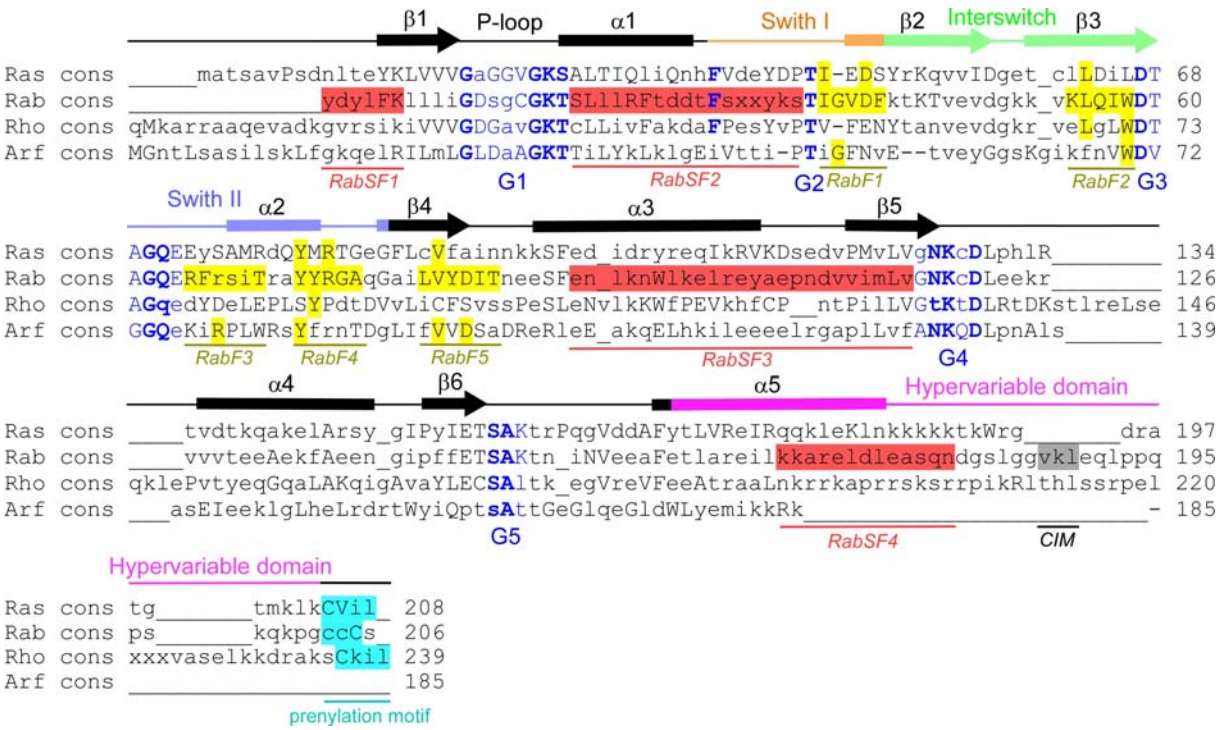

Figure 2-5. Consensus sequence alignment of profile hidden Markov models (HMM) of Ras, Rab, Rho and Arf family (Pereira-Leal and Seabra, 2000). The uppercase/lowercase coding represents the probabilities (*p*) of the profile HMM, in which uppercase characters were found at *p*>0.5. *Blue* characters denote the conserved nucleotide binding motifs (G motif) with conserved residues indicated in *boldface type*. RabF residues are highlighted in *yellow*, and the corresponding residues conserved in other families are also highlighted in yellow. RabSF regions are highlighted in *red*. Putative CBR interacting motif (CIM) is highlighted in *gray*. Prenylation motif is highlighted in *turquoise*.

The availability of high resolution structures of both the GDP- and GTP-bound form of GTPases enables definition of the requirements of the molecular switch (Figure 2-6). The extent of the conformational change between GDP- and GTP-bound forms are usually subtle but may turn out to be quite large in some cases, and involves extra elements for some proteins. The regions of major conformational changes are confined primarily to two segments, called switch I and switch II, first observed in Ras (Schlichting et al., 1990; Milburn et al., 1990). The trigger for the conformational change is most probably universal. In the GTP-bound form, switch I and II are bound to the γ-phosphate via the main chain NH groups of the invariant Thr (G2 motif) and Gly (part of the G3 motif, Dxx**G**) residues, respectively. Release of the γ-phosphate after GTP hydrolysis allows the two switch regions to relax into the GDP-bound conformation, which is characterized as a loaded-spring mechanism (Vetter and Wittinghofer, 2001).

It is mainly through the conformational changes in these two switches that regulatory proteins and effectors sense the nucleotide bound state of the GTPases (Figure 2-6). This implies that regulator and effector binding involves the switch regions of GTPases, and this is indeed supported by the structural and functional studies (Vetter and Wittinghofer, 2001).

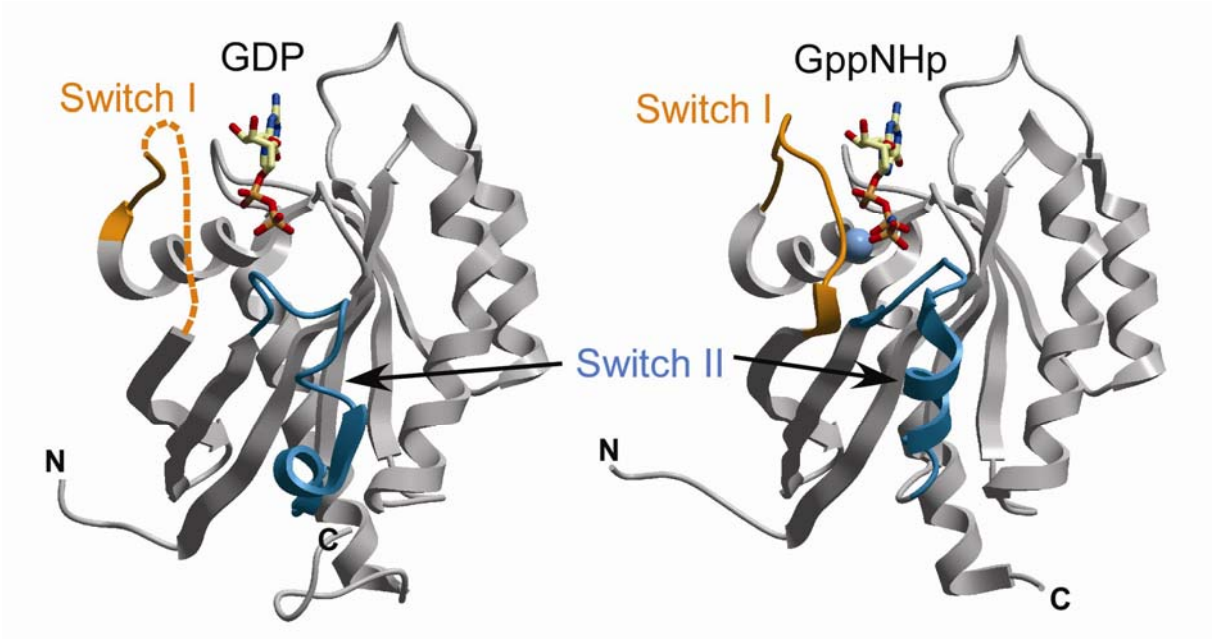

Figure 2-6. Structures of Rab4a in GDP (PDB code: 2BMD) and GppNHp (non-hydrolysable analogue of GTP) (PDB code: 2BME) bound form. Rab4a is displayed in ribbon representation, nucleotides in stick representation and Mg^{2+} in cyan sphere. Switch I is *orange* and switch II is *light blue*. The dashed ribbon in Rab4a-GDP represents the invisible part in the crystal structure.

Despite conservation of critical residues involved in nucleotide binding and hydrolysis, Rab GTPases are only distantly related to other small GTPases in sequence (< 30% identity) (Dumas et al., 1999). Conformational changes in switch I and II during GDP/GTP cycling were also observed in Rab GTPases (Huber and Scheidig, 2005; Pasqualato et al., 2004; Constantinescu et al., 2002; Stroupe and Brunger, 2000) (Figure 2-6). As for other small GTPases, these two segments are crucial for the interaction of Rab GTPases with regulators and effectors. For example, the crystal structure of Rab3a complexed with the effector domain of Rabphilin-3A shows that the binding specificity for active/inactive conformations is determined by the switch regions of Rab3a (Ostermeier and Brunger, 1999).

Analysis of sequence conservation in the mammalian Rab family revealed the existence of five Rab-specific regions that cluster in and around switch regions, termed Rab family (RabF) motifs (Pereira-Leal and Seabra, 2000). These RabF motifs were proposed to provide criteria for the Rab family classification. Furthermore, four Rab subfamily (RabSF) motifs have been identified to define the ten Rab

subfamilies (Pereira-Leal and Seabra, 2000; Moore et al., 1995) (Figure 2-5). RabSF regions are located on two subfamily-specific surfaces of Rab proteins. They were suggested to determine specific binding of effectors and regulators, since the conserved switch regions among all Rabs might not be sufficient to define the binding to specific effectors and regulators, given that these proteins must discriminate between GDP/GTP-bound states of Rab GTPases (Pereira-Leal and Seabra, 2000).

This model is not universal in the Rab family. But it is indeed supported by some crystal structures of Rab-effector complexes (Figure 2-7). The Rab3a-Rabphilin complex revealed that the interaction involves both switch regions and RabSF1, 3 and 4 (Ostermeier and Brunger, 1999). The structure of Rab7-RILP complex showed that RabSF1 and RabSF4 regions of Rab7 are important for interaction with RILP (Wu et al., 2005).

However, in some cases different subsets of residues within the switch regions determine specificity (Figure 2-7). Rabex-5 VPS9 domain, a RabGEF, selects for the Rab5 subfamily primarily through a strict requirement for a small nonacidic residue preceding the invariant phenylanaline in the switch I **T**(I/V)GA(A/S)**F** motif, while the selectivity for Rab21 also involves Gln53 in the TLQASF motif (Delprato and Lambright, 2007; Delprato et al., 2004). Sec2p, the specific GEF for Sec4p GTPase, discriminates its substrates via the switch regions (Dong et al., 2007). In contrast, MSS4, which is a less specific RabGEF and activates a range of Rabs, interacts with switch I, interswitch regions, and the N-terminus, but not with switch II (Itzen et al., 2006). Different elements contribute to the interacting specificity between Rab and its effectors. In the Rab11–FIP3-RBD complex the unique Rab11 switch II structure is essential for its specific interaction with FIP3-RBD independent of the RabSF regions (Shiba et al., 2006). Rabaptin5 specifically binds to Rab5 probably through some distinct residues in switch and interswitch regions (Zhu et al., 2004). Furthermore, other nonconserved residues in Rab that alter the conformation of those conserved residues in direct effector contacts may also contribute to the binding specificity (Merithew et al., 2001). A family-wide analysis of RabGTPases interaction with effector rabenosyn-5 revealed that the specificity is determined by a combination of structural diversity in the active conformation, which governs the plasticity of critical conserved recognition, and sequence determinants in the switch and interswitch regions (Eathiraj et al., 2006).

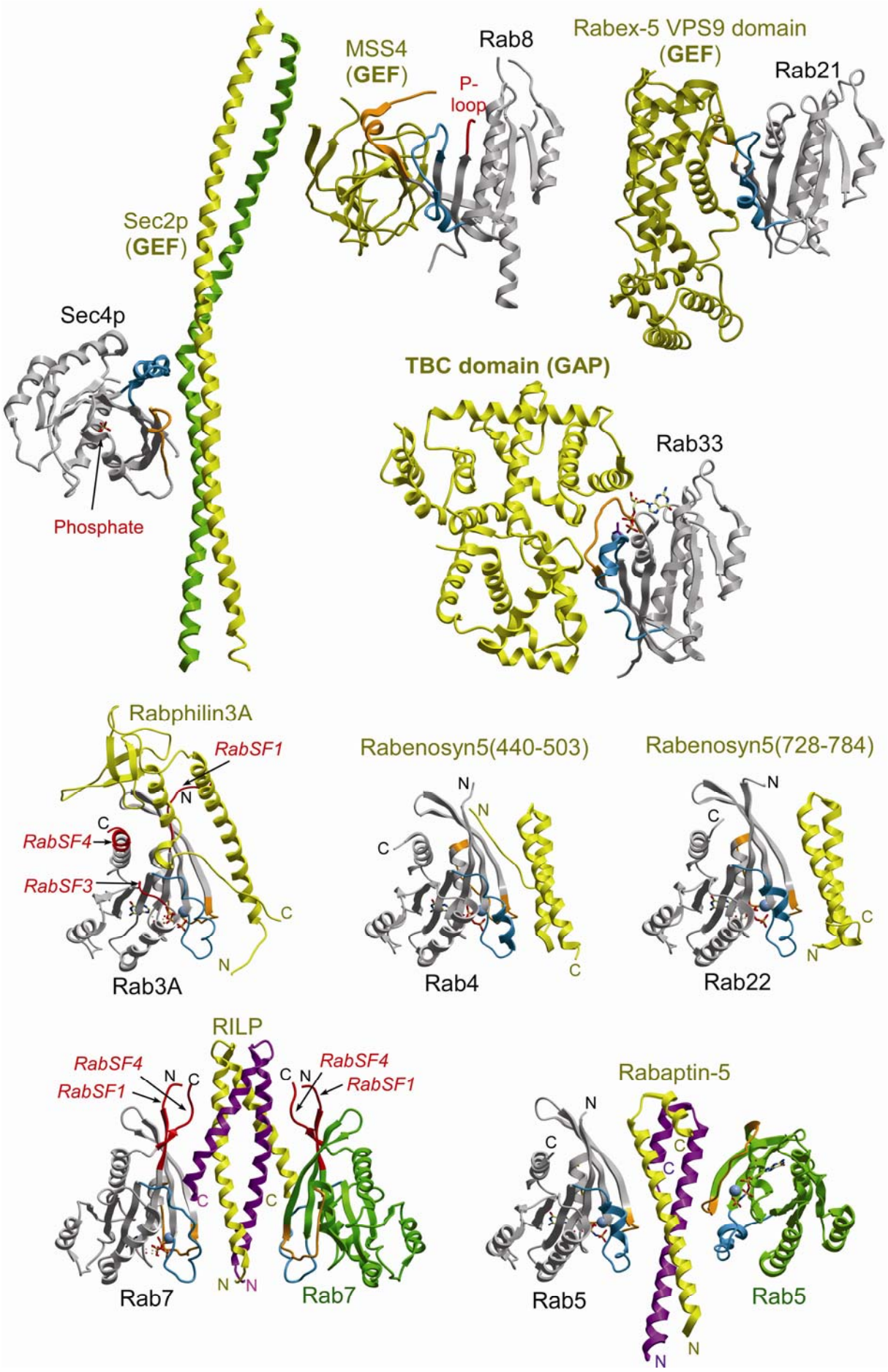
MSS4
(GEF)
Rab8
P-
loop
Rabex-5 VPS9 domain
(GEF)
Rab21
Sec2p
(GEF)
Sec4p
Phosphate
TBC domain (GAP)
Rab33
Rabphilin3A
RabSF1
RabSF4
RabSF3
Rab3A
Rabenosyn5(440-503)
Rab4
Rabenosyn5(728-784)
Rab22
RILP
RabSF4
RabSF1
Rab7
Rab7
Rabaptin-5
Rab5
Rab5

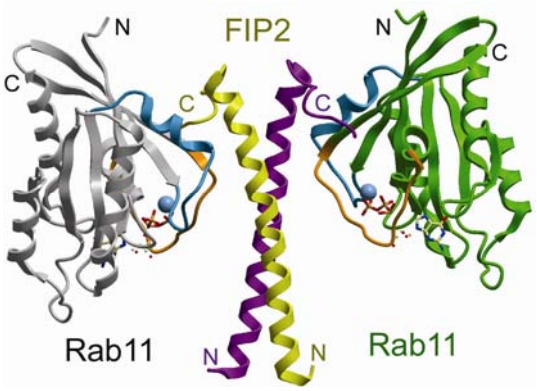

Figure 2-7. Structures of the complexes of Rabs with GEFs, GAP, and effectors. Rabs are shown in *gray*, while effectors and regulators are shown in *yellow*. The Switch I region of Rab is highlighted in *orange*, and Switch II in *light blue*. GEFs are in complex with nucleotide free Rabs, and GAP is in complex with GDP·AlF3-bound Rab, while effectors are in complex with GTP-bound Rabs. In Rab3A-Rabphilin3A and Rab7-RILP complexes, the RabSF regions involved in interaction are highlighted in *red*.

According to this model, it was proposed that the binding of general Rab-specific regulators such as REP and GDI involves RabF regions. This hypothesis is confirmed by the crystal structures of the Rab-GDI complex (Rak et al., 2003) and the Rab-REP complex (Rak et al., 2004). Moreover, an additional important binding motif (CBR interacting motif, CIM) was identified in these interactions. In this motif, two key hydrophobic residues make critical contacts with REP and GDI and mount the Rab C-terminal hypervariable domain (see below) onto REP/GDI. This interaction may facilitate the insertion of geranylgeranyl moieties into the lipid binding site of REP/GDI (Pylypenko et al., 2006).

Apart from the GTP-binding domain, the so called C-terminal hypervariable domain, which is consist of ca. 30-40 amino acid residues, is another important structural element of Rab GTPases. Rab hypervariable domains represent the most divergent parts of Rab sequences and are primarily unstructured (Pfeffer, 2005) (Figure 2-5). This domain is presumed to contain a targeting signal for Rab proteins (Stenmark et al., 1994b; Brennwald and Novick, 1993; Chavrier et al., 1991). The targeting signal can be some special residues, for instance, the polybasic cluster in Rab35 C-termini that is responsible for targeting to the plasma membrane via interaction with negatively charged phosphatidylinositol 4,5-bisphosphate (PI(4,5)P2) and phosphatidylinositol 3,4,5-trisphosphate (PI(3,4,5)P3) lipids (Heo et al., 2006). The hypervariable domain of Rab9 is involved in membrane localization by interacting with the effector protein TIP47 (tail-interacting protein of 47 kDa) (Aivazian et al., 2006). Subsequent studies show that Rab localization is likely to be more

complex and involve additional determinants (Aivazian et al., 2006; Ali et al., 2004; Beranger et al., 1994; Stenmark et al., 1994b).

At or near the C-terminus, the conserved cysteine(s) in the Rab prenylation motif (CC, CXC, CCX, CCXX, CCXXX, CXXX) are post-translationally modified by geranylgeranyl group(s) (as described in section 2.1). This hydrophobic modification of Rab GTPases enables reversible association with membranes, which is essential for proper Rab functioning (see section 2.2.3, 4).

2.2.3 Rabs function in vesicular transport

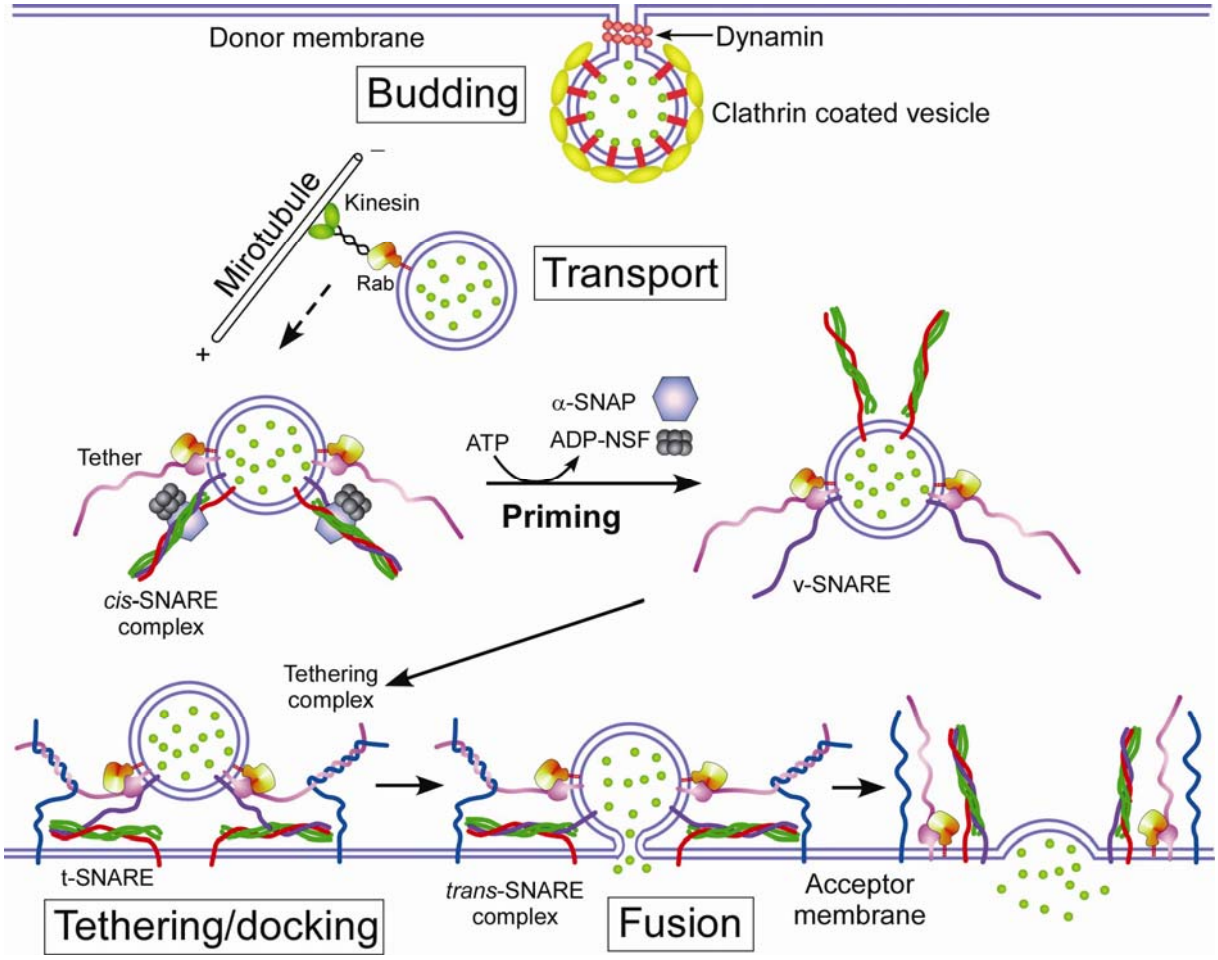

Figure 2-8. The essential steps of vesicular transport (endocytosis from the plasma membrane as an example). (1) Budding. A specific transport intermediate (vesicle or tubule) carrying the selected cargo is formed during assembly of the coat. Dynamin mediates scission and release of the vesicle from the donor organelle. (2) Transport. The vesicle is subsequently transported to its destination using motor proteins (kenesins/dyneins and myosins) to drive the movement of vesicles along microtubules and actin filaments, respectively. (3) Tethering and docking. ATP hydrolysis drives the disassembly of *cis*-SNARE complexes by NSF and α-SNAP. GTP-Rabs mediate the recruitment of tethering factors and SNAREs into a microdomain. Vesicle and target membrane are then brought into close proximity by formation of tethering complexes (coiled-coiled tethers or multimeric tethering complexes). This process facilitates the *trans*-SNARE pairing between the cognate v-SNAREs on vesicles and t-SNAREs on the target compartment, which is referred to as “docking”. (4) Fusion. The assembly of *tans*-SNARE complexes drives membrane fusion. Transported cargo is incorporated into the

membrane of the target compartment of released into its lumen. The tethers dissociated from the membrane or remain stably associated with the target membrane.

Eukaryotic cells, due to the spatial differentiation of intracellular organelles, require a sophisticated system of vesiculo-tubular transport that ensures the communication between different compartments. In the exocytic pathway, newly synthesized proteins and lipids are sorted from the endoplasmic reticulum, via the Golgi apparatus to their destination at the lysosome, the plasma membrane and the extra cellular space. On the other hand, the endocytic pathway is required for the uptake of nutrients and signaling molecules, and the internalization of receptors. The newly internalized cargos are transported to the early endosome, and subsequently proteins destined for recycling are sorted to recycling endosomes and then to the plasma membrane, while proteins destined for degradation are transported to late endosomes and then to the lysosome (Zerial and McBride, 2001) (Figure 2-13).

Vesicular transport takes place in four essential steps (Figure 2-8) that comprise vesicle budding, transport, tethering/docking, and fusion. Rab GTPases have been implicated in regulation of each of these steps (Grosshans et al., 2006) (Figure 2-8, 2-14).

Vesicle budding is a process of cargo selection combined with formation of a vesicle or tubular intermediate. Packaging of cargo into transport container involves the coat protein complexes (CPCs) machinery (Figure 2-9), including the clathrin (Fotin et al., 2004a; Fotin et al., 2004b), coat protein complex-I(COPI) (Presley et al., 2002) and coat protein complex-II (COPII) (Fath et al., 2007; Stagg et al., 2006). The clathrin CPC functions at the Golgi and the plasma membrane (Edeling et al., 2006), the COPII coat machinery mediates the exocytic pathway at the ER (Gurkan et al., 2006), whereas the COPI coat machinery is involved in recycling of proteins between the compartments of the Golgi and from the Golgi apparatus to the ER (Lippincott-Schwartz and Liu, 2006). The small GTPases Arf and Sar1 regulate the assembly of the COPI and COPII vesicular coats, respectively (Memon, 2004). The coat assembly and disassembly are dictated by the GTP- and GDP-bound Arf/Sar1, which are controlled by GEFs and GAPs (see section 2.2.1). CPCs include adaptor proteins (APs) that recognize sorting motifs present in cargo proteins, which provide the “first line” of cargo-sequestration specificity on budding machinery (Sato and Nakano, 2007; McNiven and Thompson, 2006). Clathrin coated vesicle (CCV) fission and release are proposed to be driven by a mechanochemical molecule, dynamin. CCV assembly results in the formation of a deeply invaginated coated pit. The GTPase

dynamin is targeted to coated pits and, upon binding GTP, self-assembles into a helical collar at the necks of deeply invaginated coated pits (Figure 2-8). Dynamin oligomerization stimulates GTPase activity, and GTP hydrolysis may drive membrane tubulation, fission and vesicle release (Praefcke and McMahon, 2004; Hinshaw, 2000). Whereas in the case of COPII coated vesicles, membrane curvature and vesicle fission are promoted by the Sar1 N-terminal amphipathic α helix that is regulated by GTP-binding and hydrolysis (Lee et al., 2005; Bielli et al., 2005). Upon GTP binding by Sar1, membrane insertion of the N-terminal amphipathic α helix initiates membrane tubulation. Therefore, the initiation of COPII vesicle budding by Sar1 GTPase couples the formation of membrane curvature with coat protein assembly and cargo selection.

Figure 2-9. Molecular model of COPII-cage (left) (Fath et al., 2007) and a 7.9 Å (cryo-EM) reconstruction of clathrin-cage (right) (Fotin et al., 2004b). In the left, the COPII-cage is built by fitting Sec13/31 crystal structures into a Cryo-EM map. The molecular model of the cage comprises 24 copies of the assembly unit with octahedral or 432 symmetry. The full-length Sec13 proteins are shown in red and orange and the central α-solenoid domains of Sec31 are shown in light and dark green. In the right, there are 36 clathrin triskelions in the structure, which has D6 symmetry. Thus, there are three symmetry-independent triskelions (or nine symmetry-independent legs). The coloured triskelions show one choice of the three independent clathrin triskelions.

Rabs have been implicated in cargo selection and vesicle formation (Pagano et al., 2004; McLauchlan et al., 1998; Jedd et al., 1997; de Hoop et al., 1994). For example, GTP bound Rab9 increases the affinity of its effector TIP47 for mannose 6-phosphate receptors (MPRs), resulting in the enrichment of MPRs within vesicles that recycle MPRs from late endosomes back to the Golgi for additional rounds of transport (Carroll et al., 2001; Diaz and Pfeffer, 1998).

The vesicles are delivered to their target compartment, often using motor proteins (kinesins/dyneins and myosins) to drive the movement of vesicles along microtubules and actin filaments, respectively. In animal cells, microtubules provide

high-speed, long-range transport, whereas the actin network usually facilitates slower and short-range local transport events (Jordens et al., 2005). The first indications that Rab proteins might be involved in cytoskeleton-mediated vesicle delivery come from the observations that actin-mediated movement of vesicles was largely dependent on Rab8 activity (Peranen et al., 1996). Subsequently, the identification of specific interaction of GTP-Rab6 with Rabkinesin-6(RB6K) provided the first view of a Rab protein linked to a motor protein (Echard et al., 1998). From then on, an emerging number of findings have revealed that Rabs control recruitment of motor proteins through direct interactions and/or via effectors (Figure 2-10).

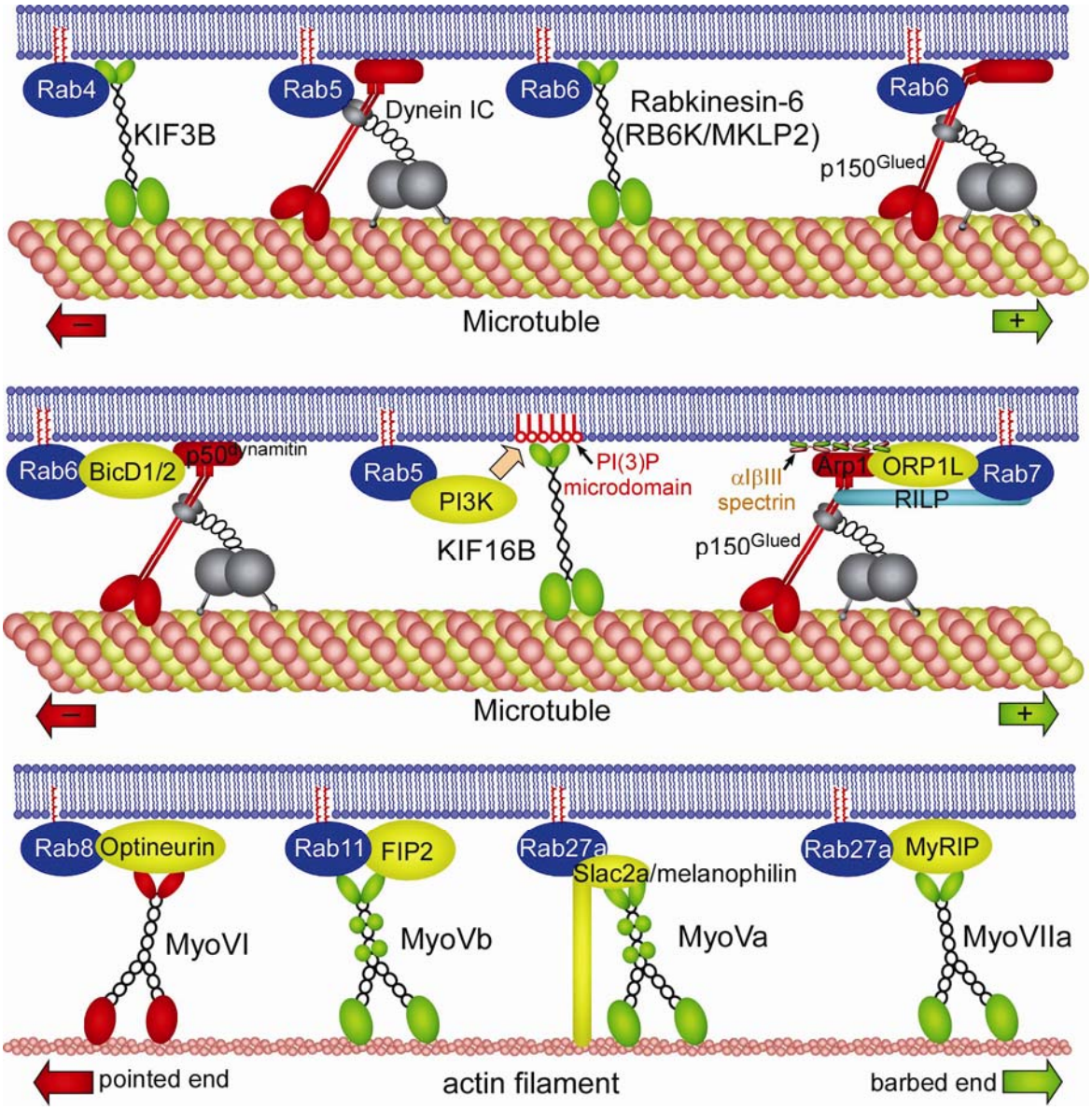

Figure 2-10. Rab-mediated connection of microtubule- and actin filament-based motor proteins for delivery of vesicles. Red and green indicate, respectively, minus-end- and plus-end-directed motors. In dynein/dynactin motors, dyneins are shown in gray, dynactins in red. Rab effectors are shown in yellow. Rab7 effector RILP is shown in light blue (see text for details).

There are many examples of Rab proteins associating with the actin-based myosin motors (for recent reviews see ref (Desnos et al., 2007; Seabra and Coudrier, 2004)). An interaction between the class V myosin Myo2p and a yeast Rab GTPase, Sec4p, is required for secretory vesicle transport to the sites of vesicle delivery during budding and mating (Pruyne et al., 2004; Wagner et al., 2002). Rab11 binds to the mammalian class V myosin homologue, myosin Vb, directly or via family of Rab11-interacting proteins (FIPs) (Hales et al., 2002) (Figure 2-7, structure of Rab11-FIP2 complex). They function in the delivery of recycling endosomes to the cleavage furrow of plasma membrane, which is essential for plasma membrane expansion of the associated furrow ingression and/or during the abscission and separation of daughter cells (Wilson et al., 2005; Fielding et al., 2005).

A fast-growing field about myosin-dependent vesicle transport is the trafficking of melanosome, the pigment-containing organelle of melanocytes, due to its connection to Griscelli syndrome (for review see (Desnos et al., 2007)). Melanosomes are delivered rapidly to the melanocyte cell periphery via kinesin motor traveling along microtubles (Wu et al., 1998b). At the melanocyte periphery, melanosomes are captured to actin filaments through melanosome-residing Rab27a, which attaches the melanosome to the actin motor myosin-Va (MyoVa) via its effector melanophilin/Slac2a (synaptotagmin-like protein homologue lacking C2 domain A) (Fukuda and Kuroda, 2002; Fukuda et al., 2002; Strom et al., 2002; Nagashima et al., 2002; Wu et al., 2002a; Wu et al., 2002b). The slow and local transport along actin filaments lead to the retention of melanosomes at the cell periphery for their final transfer to the neighboring keratinocytes (Wu et al., 1998b). Therefore, mutations in *MY05A*, *RAB27A* and *MLPH*, the genes encoding MyoVa, Rab27a and melanophilin, correspondingly, lead to albinism (a pigmentary dilution of skin and hair) and Griscelli syndrome. Griscelli syndrome type I (GS1) is a recessive disease characterized by partial albinism and primary neurological disorders. The primary defect in GS1 was localized to MyoVa that functions in synaptic vesicle transport in neurons. Moreover, since Rab27a and its effector are also necessary for various secretory events, patients with mutations in Rab27a (Griscelli syndrome type II) display a combination of albinism and immunodeficiency, which is due to the loss of cytotoxic killing activity in T-lymphocytes (Menasche et al., 2003; Menasche et al., 2000).

An interesting example of the recruitment of microtubule-based dynein/dynactin motors to the target compartment is the Rab7 GTPase-mediated stepwise assembly

of the complex transport machinery (Johansson et al., 2007). Rab7 controls late endocytic transport by recruiting the dynein/dynactin motor through a series of mutual interactions mediated by its effectors, Rab7-interacting lysosomal protein (RILP) and oxysterol-binding protein-related protein 1L (ORP1L). GTP-Rab7 binds to RILP and ORP1L to form a heterotrimeric complex (Figure 2-7 shows the structure of a dimer of Rab7-RILP complex). The N-terminal domain of RILP binds to the C-terminal region of the dynactin projecting arm $p150^{Glued}$, resulting in the recruitment of the 2.4-MD dynein/dynactin motor to late endosomes (LEs). In addition, ORP1L is required to direct the entire complex to αIβIII spectrin. The interaction is mediated by Arp1 binding to βIII spectrin, which is the general dynein receptor on LEs, Golgi and other organelles (Johansson et al., 2007; Cantalupo et al., 2001; Jordens et al., 2001).

After the delivery of a vesicle to the target membrane, the tethering factors serve in the initial recognition between a vesicle and its target and bring them in close proximity. Two types of tethering factors have been described: long coiled-coiled tethers and large multisubunit complexes (for review see (Sztul and Lupashin, 2006)).

Coiled-coiled tethers are characterized by long, extended rod-like structures appearing to function as long fibrous connections that have been observed between vesicles and Golgi membranes. Rab proteins have been shown to be involved in assembly of tethering complexes. For example, GTP-Rab1 is required to recruit the tethering factor p115 to COPII vesicles derived from the ER (Allan et al., 2000). The *cis*-Golgi coiled-coiled tethering protein GM130 complexed with GRASP65 functions as a Rab1 effector complex that directly interacts with GTP-Rab1 (Moyer et al., 2001). The interaction of p115 with the GM130-GRASP65 complex is thought to tether ER-derived COPII vesicles to the Golgi membrane, which is required for vesicle targeting/fusion with the Golgi (Sztul and Lupashin, 2006) (Figure 2-11 **A**). In addition to the tethering of COPII vesicles, p115-GM130 together with giantin have been proposed to mediate the tethering of recycling COPI vesicles. The COPI vesicle-residing coiled-coiled tether giantin also binds to GTP-Rab1. Giantin and GM130 associate with the C-terminal, acidic domain of p115, thus releasing the autoinhibitory intramolecular interaction of p115 so as to facilitate p115 binding to Rab1 (Beard et al., 2005). This study suggests that the tethering factors GM130 and giantin regulate recruitment of p115 for further downstream events rather than merely forming a bridge.

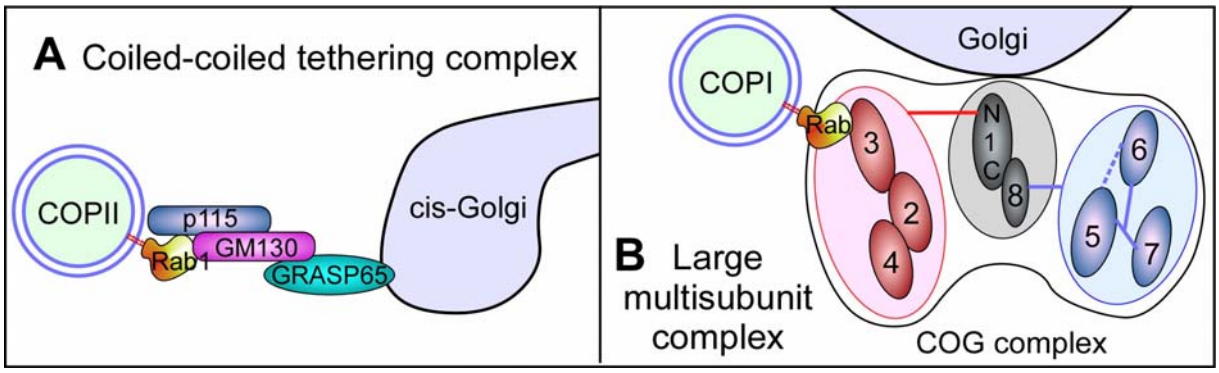

Figure 2-11. Two types of tethering complexes and the roles of Rab GTPases in membrane tethering. (**A**) GTP-Rab1 is required for the recruitment of its effector, coiled-coiled protein p115 into ER-derived COPII vesicles. At the *cis*-Golgi membrane, GTP-Rab1 binds a coiled-coiled protein GM130 complexed with GRASP65, directly via GM130. This interaction might then facilitate the formation of the tripartite p115-GM130-GRASP65 protein complex, which seems to be essential for the tethering of COPII vesicles to the *cis*-Golgi. (**B**) Potential COG complex-mediated bridge formation between COPI vesicles and the Golgi in a Rab-dependent manner. The mammalian COG architecture is show in detail (Ungar et al., 2005). Numbers represent COG subunits, with the N- and C-terminal regions of Gog1 indicated. Two herterotrimeric subcomplexes (Gog2-4 and Gog5-7) are linked by a heterodimeric unit containing Cog1 and Cog8.

The second type of tethering factor, multisubunit complexes, represent examples of *in vivo* function of proteins as parts of large macromolecular machines. Large multisubunit complexes, including COG (8 subunits), GARP (4 subunits), Dsl1 (3 subunits), TRAPP I (7 subunits), TRAPP II (10 subunits) and Exocyst (8 subunits), have been shown to regulate distinct steps of membrane traffic (Sztul and Lupashin, 2006). One example is the conserved oligomeric Golgi (COG) complex, an eight-subunit complex essential for normal Golgi structure and function (for review see (Ungar et al., 2006)). COG complex was initially suggested to be involved in membrane trafficking in yeast. The COG complex has been shown to interact with SNARE proteins that mediate membrane fusion, Ypt/Rab GTPases, and the COPI coat (Figure 2-11 **B**). These findings led to the hypothesis that the COG complex functions as a tether connecting COPI vesicles with *cis*-Golgi membranes during retrograde trafficking (Suvorova et al., 2002). Very recently, the TRAPP I complex was found to link to a component of COPII cargo adaptor complex, Sec23, via Bet3 subunit. These findings reveal an additional role for vesicle coats and indicate that ER-derived COPII vesicles tether to their target membrane before uncoating (Cai et al., 2007).

Once a vesicle is brought to the proximity of its target membrane by tethering, the vesicle undergoes membrane fusion with the target membrane. Soluble *N*-ethylmaleimide-sensitive factor attachment protein receptors (SNAREs) mediate membrane fusion in all of the trafficking steps of the secretory pathway (for review

see (Jahn and Scheller, 2006; Hong, 2005)). SNAREs contain a transmembrane domain at their C-terminal ends, a conserved SNARE motif that are arranged in heptad repeats, and N-terminal domains.

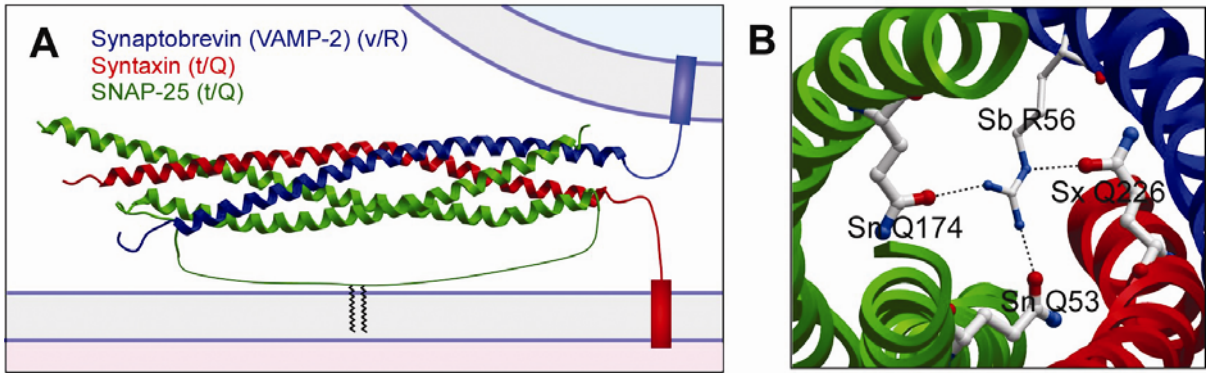

Figure 2-12. Structure of SNARE complex (PDB file: 1SFC). (**A**) The 4-helix bundle of *trans*-SNARE pair in a structural view. Synaptobrevin (VAMP-2) is a v/R-SNARE shown in blue, syntaxin is a t/Q-SNARE shown in red, and SANP-25 is a t/Q-SNARE shown in green. (**B**) The central ionic layer of the SNARE complex (looking down the coiled-coil from the C-terminus) illustrates the critical arginine of synaptobrevin (R-SNARE) forming hydrogen-bonding with glutamines of syntaxin (Q-SNARE) and SNAP-25 (Q-SNARE).

Vesicle-associated SNAREs (v-SNAREs) and SNAREs at the target membrane (t-SNAREs) recognize each other and form four-helix bundles, with the associated release of free energy being used to drive membrane fusion (see Figure 2-8, 2-12). This has been referred to as a "zippering" hypothesis (Nichols et al., 1997; Hanson et al., 1997; Lin and Scheller, 1997). Structural analysis shows that the four-helix bundle of SNAREs depends on interactions of an arginine from one helix with glutamines from three other helices, which results in a structure-based classification of SNAREs into R- and Q-SNAREs, based on the presence of these critical arginine (R) and glutamine (Q) residues (Ossig et al., 2000; Sutton et al., 1998; Fasshauer et al., 1998) (Figure 2-12 **B**). The *cis*-SNARE complexes, i.e. complexes formed between SNAREs located on the same membrane, are disassembled by the ATPase NSF (*N*-ethylmaleimide-sensitive factor) together with its cochaperone α-SNAP (soluble NSF attachment protein), driven by ATP hydrolysis (Mayer et al., 1996; Sollner et al., 1993). This process is called initial priming. Upon tethering and priming, the activated SNAREs associated with the vesicle and the target compartment, respectively, participate in the docking through a process termed *trans*-SNARE paring. *Trans*-SNARE complexes proceed from a loose state to a tight state (zippering), which may exert a mechanical force on the membranes through the stiff linkers between the transmembrane domains and the helical bundle of SNARE motifs, resulting in opening the fusion pore (McNew et al., 2000; McNew et al., 1999).

Although SNAREs reconstituted into liposomes are enough to mediate a fusion reaction on the order of minutes (Weber et al., 1998), intracellular fusion reactions, which often happen in the microsecond range, also requires Rab GTPases and Rab effectors, SM (Sec1/Munc18-related) proteins, and some other regulatory factors (like calmodulin, synaptotagmin).

A large amount of evidence indicates that Rab GTPases indirectly regulate SNARE function. They bind the SNARE machinery (SNAREs and NSF) via effectors (such as tethering factors) (reviewed in (Lupashin and Sztul, 2005; Zerial and McBride, 2001)). For example, Rab5 effectors Rabaptin-5/Rabex-5 (Figure 2-7, structure of Rab5-Rabaptin complex and Rab21-Rabex-5 VPS9 domain complex) and coiled-coiled tethering factor EEA1 recruit the t-SNARE, syntaxin-13, via EEA1 in an NSF-dependent manner. This interaction is required to drive homotypic early endosome fusion (McBride et al., 1999). A proposal for Rab GTPase regulation of a membrane fusion is that Rab and its effectors create a so called “Rab domain” on specific membrane, and selective incorporation of *cis*-SNARE complexes into a Rab domain leads to *trans*-SNARE paring between cognate SNAREs upon tethering (Zerial and McBride, 2001). One good example to support this model comes from a recent report by William Wickner and coworkers (Starai et al., 2007). They showed that Rab-independent liposome fusion needs high levels of SNAREs, but Ypt7 enhanced the rate constant of 4SNARE/HOPS complex formation by many thousand-fold. Therefore, Rabs function in membrane fusion by concentrating SNAREs, SM proteins and key lipids in a microdomain. Rab GTP hydrolysis seems to define the timeframe for Rab effector assembly and therefore influences the tethering, docking and fusion steps (Rybin V et al., 1996; Stenmark et al., 1994a). Some evidence also showed that disassembly of SNAREs is required for tethering of COPII vesicle, suggesting that on the contrary SNAREs determine the recruitment of the tether as well (Bentley et al., 2006). This may represent a “dead end” tethering elimination mechanism, since tethering would only happen at focal sites containing appropriated poised SNAREs.

Although the list of Rab GTPases, Rab effectors, tethers, other regulatory proteins is still growing, the exact functions of these trafficking machineries are still somewhat elusive (Pfeffer, 2007).

2.2.4 Regulation of Rab membrane localization and recycling

Rab GTPases compromise the largest subgroup of the Ras superfamily, with more than 60 members in humans and 11 members in yeast (Pereira-Leal and Seabra, 2001). It seems that the increased complexity throughout evolution results from a higher level of cell organization and intracellular transport in the differentiated cells of multicellular organisms. Rab GTPases localize to distinct intracellular compartments and direct vesicular transport through specific interaction with effectors (as discussed in section 2.2.3). Evolutionarily conserved Rab proteins tend to be expressed in all cell and tissue types and regulate fundamental transports, whereas certain family members function in specialized transport events observed in different cell types (Figure2-13).

As discussed in section 2.2.1, the regulatory principle of Rab GTPases lies in their ability to cycle between active GTP- and inactive GDP-bound conformations, therefore functioning as molecular switches to exert temporal and spatial control of vesicular transport (Figure 2-14). Malfunction of these regulations may lead to defects in eukaryotic cells. For example, hijacking Rab1GAP, TBC1D20 of host cells by hepatitis C viruses (HCV) is involved in HCV infection. Rab1 GTPase has been implicated in the regulation of anterograde traffic between the ER and the Golgi (Figure 2-13). Interaction of HCV protein NS5A with TBC1D20 was proposed to locally inactivate Rab1 at the sites of nascent viral protein synthesis, thus, promote redirection from a Golgi-bound pathway to viral-induced membrane structures supporting HCV RNA replication (Sklan et al., 2007).

Interestingly, Rab activation and deactivation seem often to be concentrated to the site (membrane) of its function, namely the Rab machinery. Two factors may contribute to this restriction. First, in the cytosol Rab proteins normally bind to REP/GDI, which serves as a chaperone for prenylated Rab soluble in cytosol (Sanford JC et al., 1995). REP and GDI also act as GDP dissociation inhibitors, which helps prevent Rab proteins from inadvertent activation (Alexandrov et al., 1994; Sasaki et al., 1990) (Figure 2-14). Second, a number of GEFs are actually members of large protein complexes (like the TRAPP tethering complex) that function as Rab effectors as well (Liang et al., 2007; Jones et al., 2000; Wurmser et al., 2000). Yeast homologues of Rab, Ypt31/32 have been shown to recruit Sec2p, a GEF for Sec4p

GTPase (Figure 2-7 shows the structure of Sec4-Sec2), leading to the activation of Sec4p on secretory vesicles (Ortiz et al., 2002). Recent studies showed that the Rab machinery is peripherally associated with the membrane in a dynamic equilibrium that depends on the balance between GEFs and GAPs. Interaction of GTP-Rab5 with the class C VPS/HOPS complex, which contains Vps39p (the GEF for Rab7), is required to recruit Rab7 so as to exchange Rab5 for Rab7 at the interface between early and late endosomes (Rink et al., 2005).

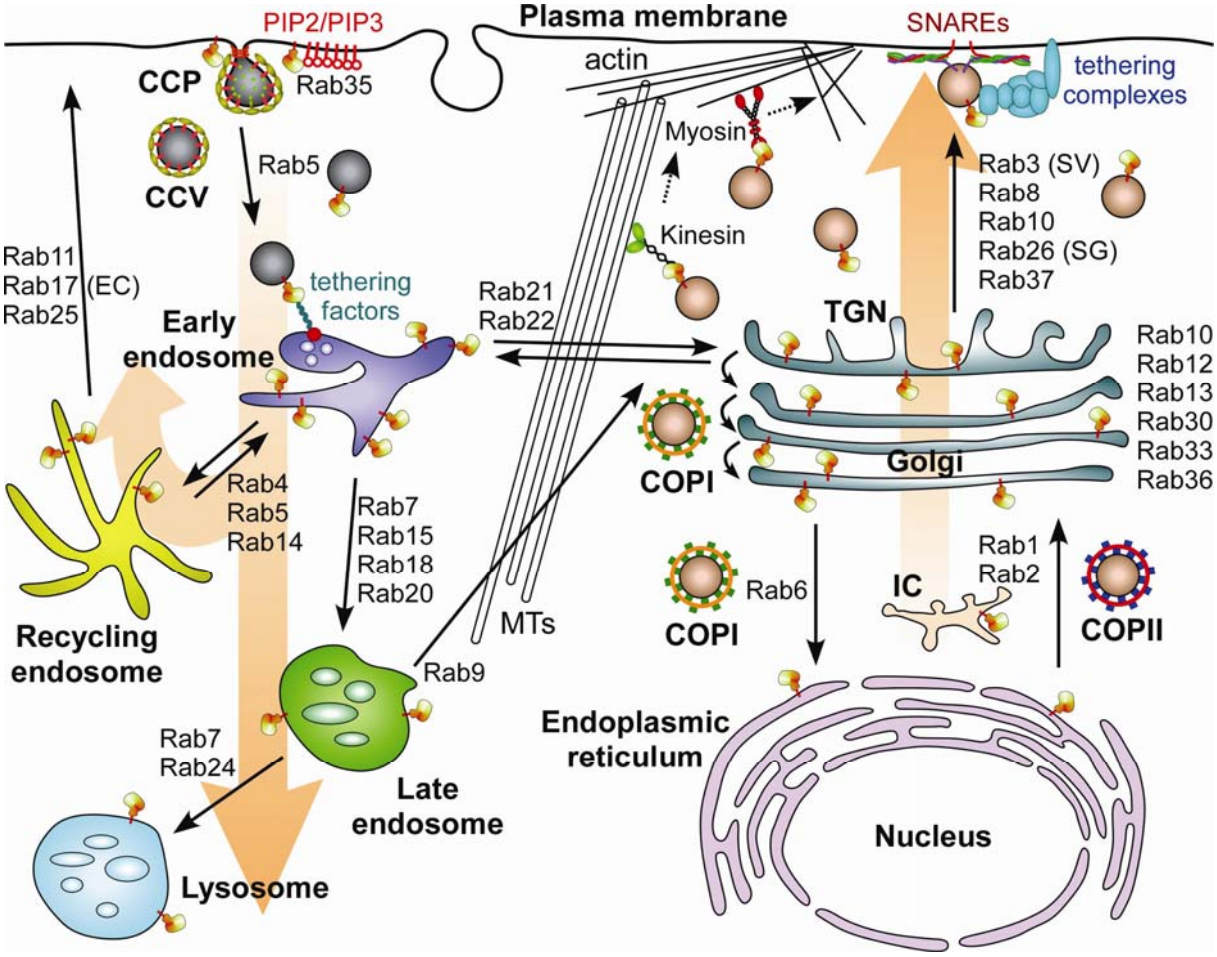

Figure 2-13. Intracellular localization of Rab proteins and Rab-regulated vesicular transport. The large, orange arrows indicate endocytosis, recycling and exocytosis. Appropriated cargos are selected and internalized by clathrin-coated vesicles. Rab5 mediates transport of vesicles to early endosomes. Recruitment of cargos into Rab4-containing microdomains within early endosomes leads to transport back to the plasma membrane directly or via recycling endosomes. While sorting into Rab5 microdomains results in transport either to recycling endosomes or toward late endosomes. Cargos sorted to recycling endosomes are subsequently recycled to the plasma membrane, involving Rab11. Transport from early endosomes to late endosomes is facilitated by Rab7, whereas recycling of mannose 6-phosphate receptors (M6PRs) from late endosome to TGN is mediated by Rab9. Rab7 also regulates the transport of molecules to lysosomes for degradation, through its effectors RILP and ORP1L interaction with motor dynein/dynactin. Exocytosis begins with movement of COPII vesicles from ER to the Golgi apparatus, which involves Rab1. Rab6 controls the retrograde Golgi-ER and intra-Golgi transport of COPI vesicles, which recycles components involved in anterograde transport. Rab33b is localized to the medial Golgi cisternae and may play a role in intra-Golgi transport. Successful passage through the Golgi complex brings the products to the TGN, the major distribution center along the biosynthetic pathway, where they are packaged and sent to different destinations.

Rab3a facilitates the secretion of synaptic vesicles in neurons. Rab8 is involved in TGN-plasma membrane transport. In yeast, a Rab homologue, Sec4p is required for delivery of TGN-derived, secretory vesicles into the bud. Some Rabs are cell- (for example, Rab3a in neurons) or tissue-specific (for example, Rab17 in epithelia), or exhibit cell-type-specific localization (for example, Rab13 in tight junction of epithelial cells). Abbreviations: CCP, clathrin-coated pit; CCV, clathrin-coated vesicle; COP, coat protein complex; IC, ER-Golgi intermediated; TGN, *trans*-Golgi network; EC, epithelial cell; SG, secretory granules; SV, synaptic vesicles; PIP2, PIP3, phosphatidylinositol bi/trisphosphate (see section 2.2.2).

Post-translational addition of geranylgeranyl moieties at (usually) two cysteine residues in the C-termini of Rab proteins enable them to associate with membranes, which is essential for Rab function on membranes. This reaction is catalyzed by RabGGTase with the aid of REP (Rab prenylation is discussed in section 2.1). In addition to support Rab prenylation, REP acts as a molecular chaperone of prenylated Rab to make it soluble in cytosol and is responsible for delivery of prenylated Rab to the target membrane (Figure 2-14). REP-mediated delivery may involve some unknown release factor that facilitates insertion of Rab into membranes and disrupts the Rab-REP interaction. The GDI displacement factors (GDF) that are capable of displacing GDI (discussed below) from Rab are candidates as release factor, if there is an analogous function towards REP. Once prenylated Rab is presented to the membrane, REP is released and recycled to the cytosol for additional rounds of function (Figure 2-14). Two isoforms of REP (REP-1 and REP-2) have been identified in mammalian cells (Cremers et al., 1994; Seabra et al., 1992a).

Prenylation is known to be crucial for the proper function of Rab proteins. The roles of lipid modification can be divided into three parts. First, double hydrophobic moieties enable Rabs to stably associate with membranes through hydrophobic interaction with the lipid bilayer (Shahinian and Silvius, 1995). Unprenylated Rabs are cytosolic proteins and are not able to attach to membranes and exert their function on membrane events.

Second, prenylation serves as one of the determinants of Rab targeting. The majority of Rab proteins contain two cysteine residues at the C-termini. Some evidence reveals that double prenylation is required for correct localization of dicysteine Rab proteins, while mutant Rab proteins that contain only one prenylatable cysteine are retained on the ER membrane and are not delivered to their target locations (Gomes et al., 2003). However, this seems not to apply to several Rabs that natively process only one prenylatable cysteine (see section 2.1). Another similar study has revealed that single-cysteine mutants of Ypt1 and Sec4 were mislocalized and lost function (Calero et al., 2003). In contrast, Rab1b mutated to GGTaseI

substrate CAAX box containing a single prenylation site (Rab1bCLLL) correctly targets to Golgi/ER and is functional in ER -> Golgi transport (Overmeyer et al., 2001). Furthermore, the lipid tail of Rab proteins could be circumvented by replacing the prenylation motif with a transmembrane domain, given that the transmembrane domain brought them to the correct location (Ossig et al., 1995).

Third, the prenyl moities are required for interactions of Rabs with effectors and regulators. For example, RabGDI does not bind to unprenylated Rab but only with prenylated Rab (Musha et al., 1992). Ypt interacting protein1 (Yip1) interacts preferentially with digeranylgeranylated Rab proteins but not with mono-geranylgeranylated Rabs (Calero et al., 2003). Rab3 subfamily-specific GAP and GEF show activity on lipid-modified Rab3 but not on the lipid-unmodified Rab3 (Fukui et al., 1997; Wada et al., 1997).

After completion of their designated functions in a round of transport, GTP hydrolysis accelerated by GAPs leads to inactivation of Rab proteins. Inactive GDP-Rab is sequestered by Rab GDP dissociation inhibitor (RabGDI) that inhibits Rab reactivation upon binding (Sasaki et al., 1990) and extracts Rab molecules from membranes (Sanford JC et al., 1995) (Figure 2-14). Rab recycling factors (RRFs) have been postulated to be involved in initiating Rab extraction from membranes (Luan et al., 1999). A possible RRF is the heat shock protein 90 (Hsp90)-containing chaperone complex, including Hsp90, Hsc70 and cysteine string protein. Interaction of αGDI with the complex via GDI mobile effector loop (MEL) is required for efficient Rab3A membrane extraction and neurotransmitter release (Sakisaka et al., 2002). Later, the Hsp90 chaperone complex was found to function in Rab1-dependent ER to Golgi transport as well (Chen and Balch, 2006). RabGDI subsequently delivers prenylated Rabs back to donor membrane for another rounds of transport, representing Rab recycling. The membrane bound GDI displacement factors (GDFs) serve as RabGDI-Rab receptor and dislodge prenylated Rab from GDI (Dirac-Svejstrup AB et al., 1997). Human Yip3 was shown to catalyze dissociation of endosomal Rab-RabGDI complex (Sivars et al., 2003). Very recently, a bifunctional protein, SidM from *Legionella pneumophila*, was found to act as both GEF and GDF for Rab1 (Machner and Isberg, 2007). In this bifunctional factor, GDI displacement, Rab binding, and nucleotide exchange activity located in the same protein. This discovery suggests the possibility of the existence of similar factors in eukaryotic cells, despite a lot of evidence showing that nucleotide exchange appears to happen

after the release of REP/GDI from the membrane (Soldati et al., 1994; Ullrich et al., 1994). However, the molecular mechanism of GDI displacement mediated by GDF is still unclear.

REP and GDI are similar in both sequence (30% identity) and structure (Rak et al., 2004; Rak et al., 2003) and functionally related. Both proteins can bind prenylated Rab, inhibit GDP dissociation, make them soluble in cytosol, and deliver them to target membrane. Nevertheless, in contrast to REP, GDI cannot support Rab prenylation due to its low affinity to unprenylated Rabs, whereas REP is less efficient in retrieving Rab molecules from membranes than GDI (Pylypenko et al., 2006). The functional segregation of these two Rab regulators determines their precise role in Rab processing and recycling. Therefore, an effort to generate a variant of REP or GDI that could perform both functions was only partially successful (Alory and Balch, 2003).

Considering the number and importance of intracellular events controlled by Rab GTPases, it is not surprising that dysfunction of Rab and regulatory proteins links is correlated to human diseases (Seabra et al., 2002). Mutations in Rab27a result in Griscelli syndrome due to malfunction of melanosome transport in melanocytes and cytotoxic granule secretion by T cells, as described in section 2.2.3. Mutations in RabGDIα lead to X-linked non-specific mental retardation. Defects in Rab prenylation give rise to abnormalities in mammals. Mutation in RabGGTase gene causes a mouse model of Hermansky-Pudlak syndrome (Detter et al., 2000), characterized by partial albinism, tendency for bleeding, and lysosomal accumulation of ceroid liposuscin. Mutations in REP-1 gene leads to choroideremia (CHM) (Seabra, 1996a; Seabra et al., 1993), an X-linked inherited disease characterized by progressive retinal degeneration leading to blindness by middle age.

In the case of CHM, due to the presence of REP-2, loss of REP-1 function does not completely abolish the ability of processing Rabs in CHM cells. However, REP-2 cannot compensate the loss of REP-1 function absolutely, since CHM lymphoblast cell lines accumulate unprenylated Rab27A (Seabra et al., 1995). This was proposed to be a consequence of a result of low affinity of RabGGTase for the Rab27A:REP-2 complex (Larijani et al., 2003). Later studies showed that Rab27 binds in lower affinity to REP-2 than other Rab proteins, leading to a proposal that the competition among Rab proteins for limiting REP-2 molecules results in hierarchical prenylation

of Rab proteins (Rak et al., 2004). However, much more work needs to be done to prove this model *in vivo*.

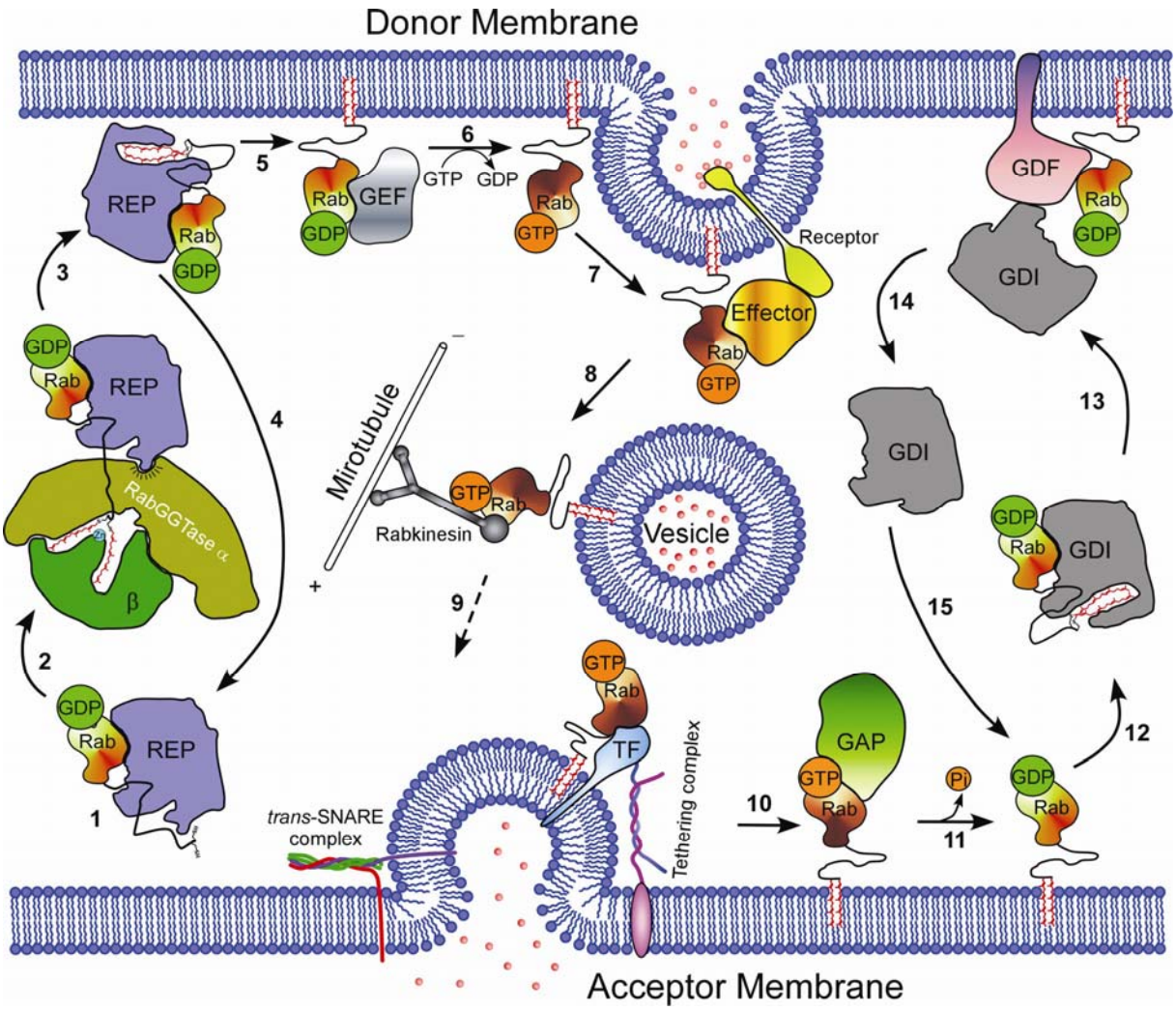

Figure 2-14. Rab biogenesis, regulation of vesicular transport and recycling. (1) Newly synthesized Rab proteins bind to REP. (2) REP presents Rab proteins to heterodimeric RabGGTase for modification of (usually) two geranylgeranyl moieties. (3) REP delivers the prenylated Rab proteins to their target membranes. (4) Once REP is released, it recycles into cytosol to support additional rounds of Rab prenylation. (5) Prenylated Rab proteins associate with the membrane. (6) Subsequently GEFs facilitate exchange of GTP for GDP. (7) GTP bound Rab proteins can bind to effectors that are involved in vesicle budding and cargo selection. (8) GTP-Rab proteins directly or via effectors recruit motor proteins to drive the movement of vesicles along microtubules and actin filaments. (9) The vesicles are transported to the target compartment. GTP-Rab proteins mediate recruitment of effectors, tethering factors, SNAREs, facilitating tethering, docking and fusion of vesicles at the target membrane. (10, 11) Hydrolysis of GTP is accelerated by GAPs, resulting dissociation of related effectors. (12) Extraction of GDP bound Rab proteins from membranes is medicated by GDI. This extraction process may involve Rab recycling factors (13) GDI makes prenylated Rab proteins soluble in cytosol and delivers them to the donor membrane. GDF facilitates dislodgement of prenylated Rab proteins from GDI, enabling them to re-associate with the donor membrane. (14, 15) GDI is released and is reused in additional rounds of Rab extraction.

2.3 Protein prenyltransferase inhibitors

2.3.1 Farnesyl transferase inhibitors (FTIs)

As described in section 2.1, Ras proteins play a pivotal role in cellular signal transduction controlling cell proliferation, division, and differentiation (Barbacid, 1987). Mutation in Ras can lead to loss of its GTPase activity and permanent activation of Ras signaling independent of upstream activation (namely oncogenic Ras). A similar effect arises from mutation induced increase in the rate of GDP dissociaction. Oncogenic Ras genes are among the most common oncogenes found in human tumors. They have been found in approximately 20-30% of a wide variety of human cancers (Bos, 1988). Particularly, mutations in K-Ras are prevent in >50% of colon cancers, >90% of pancreatic cancers, and ~30% of lung cancer. Mutations in N-Ras are present in 10-20% melanoma and some hematologic malignancies. Mutations in H-Ras are rare in human cancer but have been documented in 15-20% of bladder cancers (Basso et al., 2006). The extensive involvement of mutated Ras in the development of a number of cancers provides strong indicatives that interfering with Ras activity might offer new opportunities for the development of anti-cancer agents. One straightforward approach was proposed to be intervention of Ras membrane localization (Gibbs, 1991), since Ras proteins require post-translational modification with lipids to associate with plasma membrane in order to exert their biological function. The discovery that FTase inhibitors (FTIs) can reverse transformed phenotype of cancer cells dramatically stimulated interest in the development of FTIs (Kohl et al., 1993). Subsequently, one of the FTIs developed by Merck has been demonstrated to induce tumor regression in *ras* transgenic mice without systemic toxicity. This finding suggests that FTIs may be safe and effective anti-tumor agents (Kohl et al., 1995).

Over the past ~15 years, a number of FTIs have been developed (Gibbs et al., 2001; James et al., 1993), showing inhibitory activities *in vitro* and *in vivo* up to the low nanomolar range with high selectivities. These include natural products, tetrapeptide CAAX analogues, nonpeptidic and CAAX-competitive inhibitors, farnesyl pyrophosphate analogues and bisubstrate inhibitors. Four of them, R115777 (tipifarnib) from Janssen, SCH66336 (lonafarnib) from Schering group, BMS214662 from Bristol-Myers Squibb, and L778,123 from Merck, have advanced into clinical

trials. These compounds are highly potent and selective against FTase (>1000-fold preference over GGTase-I), except L778,123 which shows moderate selectivity between FTase and GGTase-I (Figure 2-15).

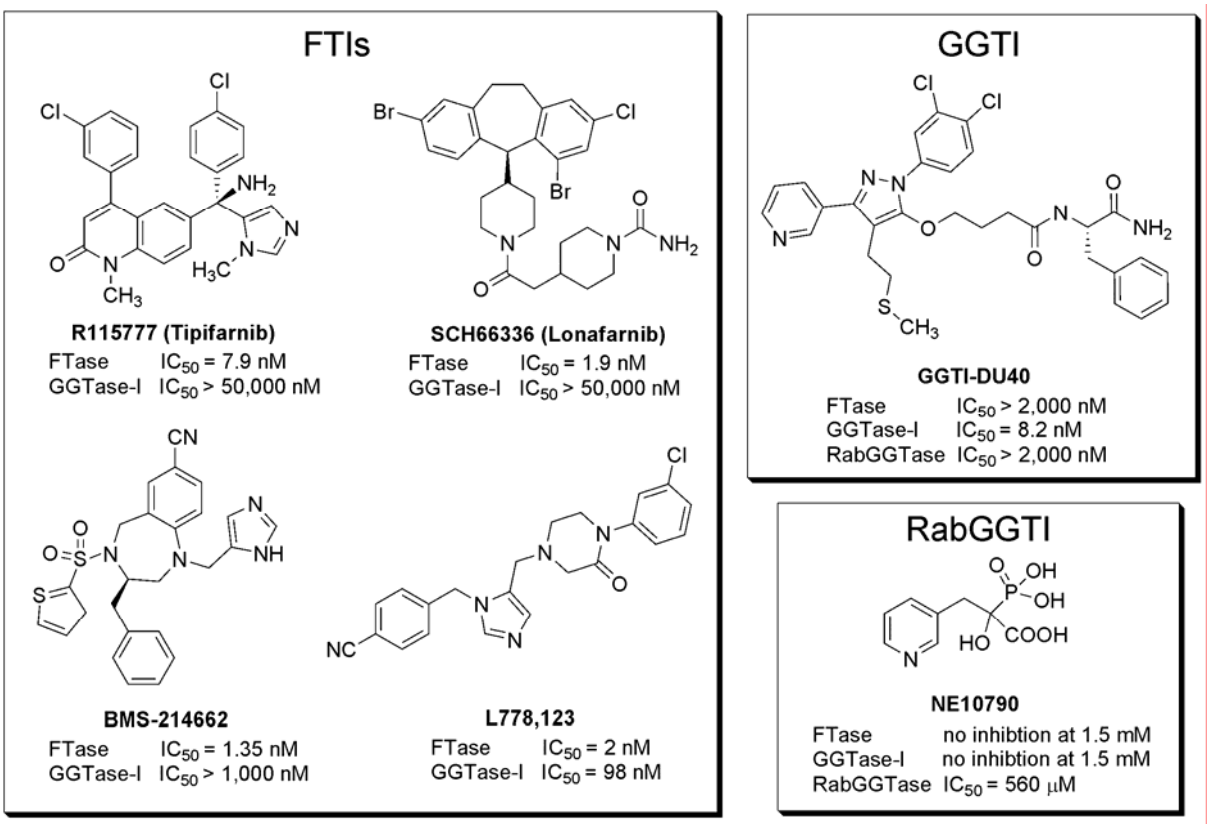

Figure 2-15. Farnesyl transferase inhibitors (FTIs) in clinical trials; GGTI, a selective, potent and cellularly active GGTase-I inhibitor; RabGGTI, a selective and cellularly active RabGGTase inhibitor.

2.3.2 Mechanism of FTIs action

The mechanisms of FTIs action are not fully understood. The lack of toxicity to untransformed cells (at pharmacologically relevant drug concentrations) could be related to several points (Waldmann and Thutewohl, 2001). First, some geranylgeranylated Ras-related proteins (like TC21) that shares indistinguishable transforming and differentiating activities with Ras might compensate for the loss of Ras function (Graham et al., 1999; Graham et al., 1996). Second, cancer cells may be more vulnerable to FTIs than normal cells, probably due to the differential reaction to the inhibition of Ras activity. The dose-limiting toxicities of FTIs in clinical trials may be evidence for this assumption. Third, prenylation of two Ras isoforms, K-Ras4B and N-Ras, are not so efficiently blocked by FTIs as H-Ras (James et al., 1996). Thus, normal cells may be less sensitive to FTIs because they express K-Ras4B and

N-Ras. Two reasons may account for this consequence. One is that K-Ras4B is a better substrate for FTase than H-Ras (James et al., 1995). The other is that N-Ras and K-Ras4B are also substrates for GGTase-I, while H-Ras is not (Zhang et al., 1997). On account of this, in FTI treated cells K-Ras4B and N-Ras are alternatively geranylgeranylated by GGTase-I, resulting in persistent membrane association for K-Ras4B and N-Ras (Whyte et al., 1997; Rowell et al., 1997). Fourth, other signaling pathways may be activated when Ras is not active.

Furthermore, this property of FTIs also makes them useful in the treatment of malaria and African sleeping sickness caused by the parasites *Plasmodium falciparum* and *Trypanosoma brucei*, respectively. FTIs are cytotoxic to these parasites while lacking toxicity to humans, perhaps because these protozoa contain FTase but lack GGTase-I (Gelb, 2007; Eastman et al., 2006).

Although geranylgeranylated Ras oncoproteins are also able to transform cells (Cox et al., 1994), FTIs inhibit the growth of numerous tumors in preclinical models, including K-Ras4B and N-Ras transgenic mouse models (Omer et al., 2000; Mangues et al., 1998). In addition, Rat1 fibroblast cells transformed by a myristylated Ras construct, which thereby would be expected to associate with membrane independent of prenylation, remained susceptible to growth inhibition by FTIs (Lebowitz et al., 1995). Moreover, clinical activities of FTIs seem to be largely lack of correlation with the inhibition of Ras, since FTIs are also active on the cancer cell lines without oncogenic Ras mutations (Gelb et al., 2006; Head and Johnston, 2003).

It is possible that the anticancer action of FTIs may involve synergetic effects on other farnesylated target proteins. These include RhoB, Rheb, CENP-E/F, PRL, HDJ, and nuclear lamins (Basso et al., 2006). However, there is no direct evidence linking inhibition of the farnesylation of these targets to the mechanism of anticancer activity of FTIs (Sebti, 2005). The antiproliferative and proapoptotic activity of FTIs seems to be related to their ability to inhibit the PI3K/Akt (Jiang et al., 2000), RheB (Castro et al., 2003), and/or mTOR/p70s6k pathways (Law et al., 2000).

Among these target proteins, RhoB has attracted attention owing to its role in mediating the cellular response to FTIs (Prendergast, 2001). Rho family proteins are not mutated in cancer cells. They regulate actin stress fiber formation. The evidence that prompted the concerning on RhoB as a target of FTIs action comes from the work of Prendergast and coworkers (Prendergast et al., 1994). They found that the morphological reversion observed in FTI-treated and Ras-transformed Rat1 fibroblast

cells is rapid (detectable within 18h) so as to outpace the kinetics of elimination of processed Ras from cells (a half-life of ~24h), but correlates with the short-lived RhoB (a half-life of ~2h). Moreover, FTIs induced actin stress fiber formation in both normal and transformed cells. Additionally, expression of a myristylated RhoB but not a myristylated Ras in Ras-transformed Rat1 cells leads to FTI resistance (Lebowitz et al., 1995).

RhoB is a substrate for both FTase and GGTase-I, and therefore exists in both farnesylated and geranylgeranylated forms in intact cells, with the geranylgeranylated form being more abundant (up to 70%) (Adamson et al., 1992). Some of the responses to FTI treatment may result from a loss of farnesylated RhoB (RhoB-F) and a gain of function of geranylgeranylated RhoB (Rho-GG). FTIs block formation of RhoB-F, leading to accumulation of RhoB-GG. The shifted pattern of RhoB prenylation is associated with mislocalization of RhoB-GG away from its target endosomal compartment (Lebowitz et al., 1997; Lebowitz et al., 1995). A gain of growth-inhibitory function of RhoB-GG has been proposed by the findings that overexpression of an engineered RhoB isoform to be only geranylgeranylated reverses the phenotype of Ras-transformed Rat1 fibroblast cells (Du et al., 1999), and mediates growth inhibition and apoptosis in human tumor cells (Du and Prendergast, 1999). Furthermore, knocking out the *RhoB* gene has no consequence in wild type mice (Liu et al., 2001), but in Ras-transformed mice leads to resistance to FTI-treatment. In agreement with this, transformed murine fibroblasts that were genetically null for *RhoB* showed defects in their FTI response, although farnesylation of mutant Ras was inhibited to the same extent in both $Rho^{-/-}$ and $Rho^{+/-}$ cells (Liu et al., 2000). In contrast, FTI-induced alteration of RhoB has strong effects in Ras-transformed cells. Therefore, Prendergast *et al.* postulated that targeting RhoB with a transformation-selective property might be one of the reasons for the selective effects of FTIs toward transformed cells.

These studies suggested that RhoB-GG may be crucial to the FTI response. A most interesting feature might be RhoB's ability to mediate the FTI-induced apoptosis of transformed cells. FTI or RhoB-GG suppressed the activity of the survival kinase Akt-1 in COS cells and MCF-7 breast carcinoma cells (Liu and Prendergast, 2000). A study from another group also demonstrated that RhoB-F enhanced and RhoB-GG suppressed cell growth and induced apoptosis of Ras-transformed NIH-3T3 cells. RhoB-GG, but not RhoB-F, inhibited Ras-induced activation of the tumor survival

pathways of Akt and NF-κB (Mazieres et al., 2005). Moreover, suppression of Cyclin B1 by FTI is linked to gain of function of RhoB-GG and the fate of cell apoptosis (Kamasani et al., 2004). Recently, the downstream adaptor protein mDia was shown to be critical for the RhoB-dependent cell death mechanism induced by FTI (Kamasani et al., 2007).

Regardless of these findings on RhoB involvement in the FTI response, some other observations suggested that RhoB is not a critical target of FTIs. Sebti and coworkers showed that RhoB was as potent as the tumor suppressor p53 at inhibiting cell focus formation and growth in soft agar of the human pancreatic tumor cell line Panc-1. They demonstrated that RhoB, RhoB-F and RhoB-GG inhibit anchorage-dependent and -independent Panc-1 cell growth, induce apoptosis, inhibit insulin-like growth factor-1 stimulation of Akt and constitutive activation of Erk, and suppress tumor growth in nude mice (Chen et al., 2000). Furthermore, RhoB tumor-suppressive and proapoptotic activities require palmitoylation at Cys192 and prenylation at Cys193 (Wang and Sebti, 2005). Thus, they argued that RhoB-F is not a target of FTIs. The role of RhoB in mediating the cellular response to FTIs is still controversial. To resolve the contradiction may require further investigation of the cellular functions of the two prenylated forms of RhoB.

2.3.3 GGTase-I and RabGGTase as therapeutic targets

In spite of the extensive studies summarized above, there are still a lot of questions remaining unanswered concerning the mechanism of FTI action. Recently, the proapoptotic activity of FTIs has been found to be a consequence of RabGGTase inhibition (Lackner et al., 2005). Direct inhibition of RabGGTase activity by certain FTIs from Bristol-Myers Squibb triggers p53-dependent apoptosis in the nematode *C.elegans* model. Genetic screens implicated Rab proteins (like Rab7 and Rab5 that are involved in endosomal trafficking) and RabGGTase in apoptosis. Moreover, knockdown of RabGGTase induced apoptosis in several mammalian cancer cell lines. Finally, both subunits of RabGGTase were found to be overexpressed in a variety of human tumors. These findings suggested that RabGGTase could be a novel target for cancer therapy. Moreover, if the character of these FTIs can be extended to other FTIs, particularly those in clinical trials, this would contribute to a better understanding and interpretation of biological response of FTIs. However, the approach of targeting RabGGTase should be further proved by investigation of the

toxicity of RabGGTase inhibitors (RabGGTIs), since inhibition of RabGGTase is related to blood clotting malignance and retinal degeneration (Seabra et al., 2002).

Compared to various effective and specific inhibitors discovered for FTase (Gibbs et al., 2001) and GGTase-I (El et al., 2006), the development of potent inhibitors for RabGGTase has lagged behind. This is despite the relative importance of RabGGTase, which is linked with some skeletal diseases, such as excessive osteoclast-mediated bone resorption which can cause tumor-induced osteolysis and post-menopausal osteoporosis (Coxon et al., 2001). Only one weak (IC_{50} = 560 μM) but specific inhibitor for RabGGTase (Figure 2-15), a phosphonocarboxylate analogue of biphosphonate risedronate (RIS), was identified so far and proposed as possible lead compound in the development of antitumor (Roelofs et al., 2006) and anti-osteoporosis drugs (Coxon et al., 2001).

GGTase-I has recently emerged as another important target for cancer therapy. The interest in GGTase-I inhibitors (GGTIs) was stimulated from the finding that N-Ras and the most abundant human oncogenic Ras precursor protein K-RasB can be geranylgeranylated by GGTase-I when FTase is inhibited (as described before). Thus, GGTIs may be used in combination with FTIs to inhibit both FTase and GGTase-I. Moreover, the geranylgeranylated proteins RalA (Lim et al., 2005) and RhoC (Clark et al., 2000) have been suggested to play a critical role in Ras-induced tumorgenesis of several human cancer cells and cancer metastasis, respectively. Some recent *in vitro* studies provided evidence that targeting these two proteins by GGTIs is linked to anticancer and anti-metastasis activities of GGTIs. In COS-7 cells and human pancreatic MiaPaCa2 cancer cells, suppressing prenylation of RalB and RalA by GGTI-2417 correlated with inhibition of anchorage-dependent cell growth and induction of apoptosis, and with inhibition of anchorage-independent cell growth, respectively (Falsetti et al., 2007). The transendothelial migration of MDA-MB-231 human breast cancer cells was inhibited potently by GGTI-298, associated with inhibition of the membrane localization of RhoA and RhoC (Kusama et al., 2006).

In addition, GGTI-2154 has been shown to induce breast tumor regression in H-Ras transgenic mice and suppress constitutively activated phospho-Erk1/2 and phospho-Akt and induce apoptosis of breast carcinoma cells (Sun et al., 2003). GGTI-298 and GGTI-2166 were found to induce apoptosis of human ovarian epithelial cancer cells by inhibition of PI3K/AKT and survivin pathways (Dan et al., 2004). Interesting results have been obtained in pre-clinical models of tumor

progression with dual inhibition of these enzymes (Morgan et al., 2005; Morgan et al., 2003; Lobell et al., 2001). Notably, the toxicity associated with GGTI treatment *in vivo* may somewhat limit their therapeutic application (Lobell et al., 2001). Recently, the first nonpeptidic GGTI, named GGTI-DU40 (Figure 2-15), has been identified with an IC_{50} of 8 nM against GGTase-I and no inhibition to the other two prenyltransferases at 2 μM (Peterson et al., 2006).

Furthermore, GGTIs may be potentially valuable agents for the treatment of smooth muscle hyperplasia in relation to restenosis/atherosclerosis (Finder et al., 1997), multiple sclerosis (Walters et al., 2002), osteoporosis (Woo et al., 2005; Coxon et al., 2000), and hepatitis C virus infection (Ye et al., 2003).

Finally, despite the enigmatic mechanisms of action of prenyltransferases inhibitors, a number of efficient compounds provide powerful tools to modulate physiological events, which can help to understand molecular mechanisms of cancer and other diseases and open up new opportunities for anti-tumor therapy.

2.4 Chemical protein ligation

2.4.1 Native chemical ligation

Chemical synthesis is an attractive alternative to biological methods of protein production. Synthetic chemistry provides almost unlimited modulation of the structure of a polypeptide chain in order to understand the protein function. However, since proteins are large molecules, applying chemical synthesis to them is a considerable challenge (Dawson and Kent, 2000).

In the early 1990s a breakthrough approach using chemoselective reaction to couple unprotected peptide segments in chemical protein synthesis was devised in the Kent laboratory (Schnolzer and Kent, 1992). In 1994, Kent and coworkers introduced the approach of native chemical ligation (NCL), which is now a general method in chemical protein synthesis (Dawson et al., 1994). In this method, two unprotected synthetic peptide fragments are joined together in neutral aqueous conditions with the formation of a native peptide bond at the ligation site.

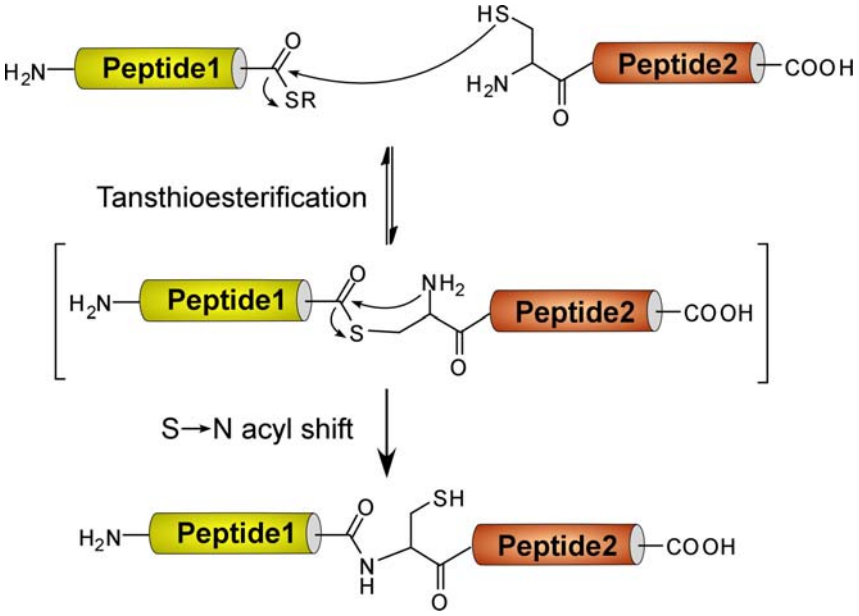

Figure 2-16. Principle of native chemical ligation. Both peptide fragments are fully unprotected and the reaction proceeds in aqueous and neutral conditions, given that one contains a C-terminal α-thioester and the other contains N-terminal cysteine.

The principle of NCL is depicted in Figure 2-16. The approach is based on the chemoselective reaction between a peptide containing a C-terminal thioester and another peptide containing an N-terminal cysteine. The initial chemoselective transthioesterification in NCL is essentially reversible, whereas the subsequent S→N

acyl shift is spontaneous and irreversible. Thus, the reaction is driven to form an amide bond specifically at the ligation site, even in the presence of unprotected internal cysteine residues.

NCL has been widely used in the total chemical synthesis of small proteins and protein domains, with a number of refinements in ligation methodology and strategy, such as auxiliary group-facilitated ligation (Offer et al., 2002; Meutermans et al., 1999), catalytic thiol cofactors (Johnson and Kent, 2006; Dawson et al., 1997b), kinetically controlled ligation (KCL) (Bang et al., 2006), and convergent chemical protein synthesis (Durek et al., 2007). However, the scope of NCL was significantly widened upon introduction of the approach termed expressed protein ligation (EPL) from the Muir laboratory (Severinov and Muir, 1998; Muir et al., 1998). In this method, both fragments containing the required C-terminal thioester and N-terminal cysteine can be produced recombinantly.

2.4.2 Expressed protein ligation

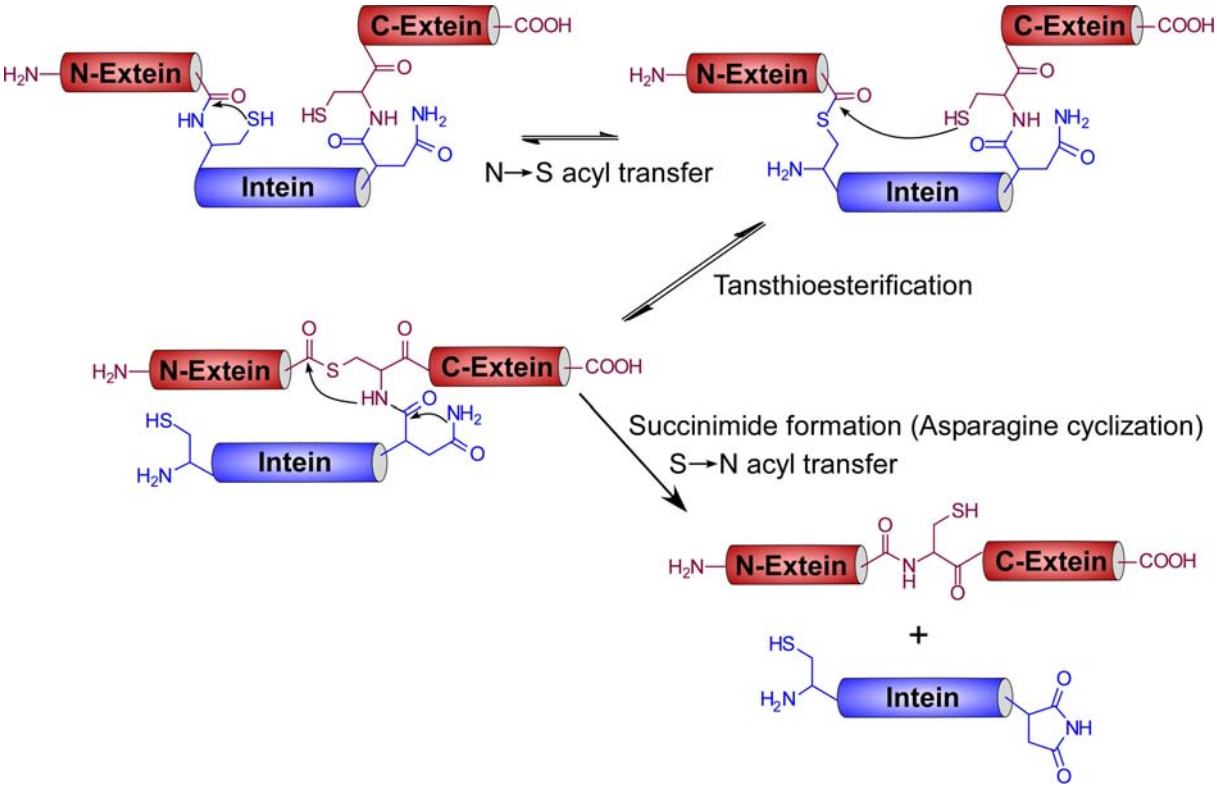

Figure 2-17. Protein splicing mechanism.

EPL emerged as a result of the advances in the use of self-cleavable affinity tags for recombinant protein purification using intein chemistry (Chong et al., 1997).

Inteins are protein insertion sequences flanked by host protein sequences (N- and C-exteins) and are eventually removed by a posttranslational process termed protein splicing (Kane et al., 1990). Protein splicing does not require specific sequences in either of the exteins, whereas inteins are characterized by several conserved motifs with over a hundred members of this protein domain in eubacteria, archaea, low eukaryotes including fungi and yeast (www.neb.com/neb/inteins.html).

As shown in Figure 2-17, the first step in typical protein splicing involves an N→S(O) acyl rearrangement in which the N-extein is moved to the side chain of a conserved cysteine or serine residue at the immediate N-terminus of the intein (Shao et al., 1996). This thermodynamicly unfavorable process may be in part catalyzed by the intein domain, which twists the scissile amide bond into a conformation with higher energy (Romanelli et al., 2004; Klabunde et al., 1998). Next, trans(thio)esterification occurs when the (thio)ester is attacked by the side chain of a conserved Cys/Ser/Thr residue located at the immediate N-terminus of the C-extein (+1 position of intein-C-extein junction) (Xu et al., 1993). The resulting branched intermediate is resolved through a cyclization reaction involving a conserved asparagine residue at the C-terminus of the intein. The intein is thereby excised as a C-terminal succinimide derivative (Xu et al., 1994). The final step of protein splicing resembles the second step of NCL, where a spontaneous S(O)→N acyl shift results in formation of amide bond linking the N- and C-exteins (Shao and Paulus, 1997).

Although the biological role of protein splicing is still unclear, it was used to make intein-mediated protein purification and engineering tools, including engineered inteins and split inteins (see next section). The former make use of knowledge of the protein splicing mechanism. Mutated inteins containing a C-terminal Asp→Ala substitution have been designed to keep their ability for the initial N→S acyl shift without proceeding to later steps of protein splicing (Xu and Perler, 1996). Therefore, proteins fused to the N-terminal of these engineered inteins can be cleaved by thiol reagents (such as 2-mercapoethanesulfonic acid) via an intermolecular transthioesterification reaction, releasing the α-thioester-tagged proteins (Figure 2-18) (Chong et al., 1997). Commercially available vectors harbor introduced affinity tags (chitin binding domain, CBD), which facilitate purification of target-intein-CBD fusion protein by chitin agarose beads and allow inducible self-cleavage of target protein from the beads.

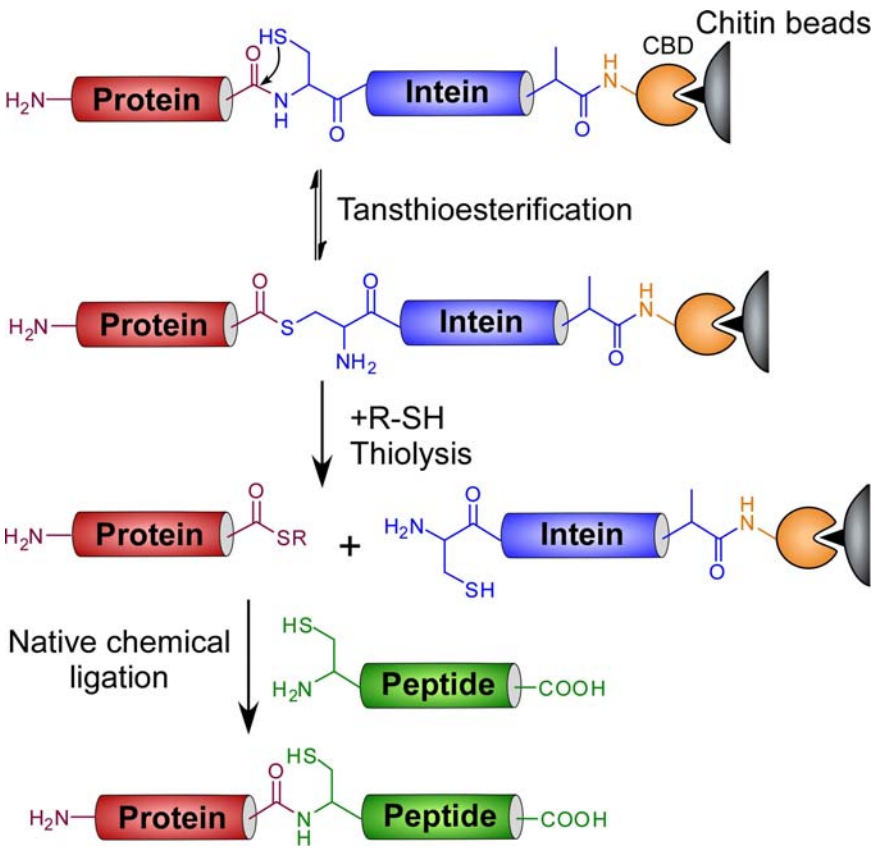

Figure 2-18. Principle of expressed protein ligation. Thioester tagged protein/peptide can be recombinantly produced by C-terminal fusion to and subsequent cleavage of an engineered intein-CBD fusion. Another protein/peptide fragment bearing an N-terminal cysteine can be either chemically synthesized or recombinantly prepared by N-terminal fusion to engineered inteins, or can be prepared by proteolytic cleavage to expose a cysteine.

The recombinant polypeptide α-thioesters can then be ligated with a synthetic peptide or recombinant protein containing N-terminal cysteine. EPL thereby allows site-specific introduction of probes (such as fluorophores and isotopes), posttranslational modifications (such as prenylation, glycosylation, phosphorylation and ubiquitination), incorporation of unnatural amino acids, and immobilization of proteins or peptides onto a chip (reviewed in (Muir et al., 1998)). Moreover, sequential EPL strategies make it possible to introduce modification at any position in a protein (Cotton and Muir, 2000; Cotton et al., 1999). Therefore, EPL provides a platform that makes it possible to apply powerful synthetic chemistry tools to large biomolecules.

2.4.3 Protein trans-splicing

Inteins can also be spliced into two parts that functions only when they bind to each other (Southworth et al., 1998; Mills et al., 1998). The precursor fragments can be fused to a split intein. When these two pieces meet with each other reconstitution

of the intein allows a *tans*-splicing reaction (Figure 2-19). The discovery of the naturally occurring split *Synechocytis (Ssp)* DnaE intein makes it possible to bypass denaturation and renaturation of the isolated precursor fragments (Wu et al., 1998a). Protein *trans*-splicing is a useful approach to selectively ligate two polypeptides, thereby providing a valuable tool for protein engineering (Xu and Evans, Jr., 2005). This approach has been employed to generate head-to-tail cyclic peptides and proteins (Williams et al., 2002; Scott et al., 1999), to selectively incorporate isotopes for NMR analysis (Otomo et al., 1999; Xu et al., 1999b), to fluorescently label proteins *in vivo* (Giriat and Muir, 2003), to assay protein-protein interactions *in vivo* (Kanno et al., 2006b; Paulmurugan et al., 2002; Ozawa et al., 2001; Ozawa et al., 2000), to detect biological events *in vivo* (Kanno et al., 2006a; Kim et al., 2005; Kim et al., 2004), or to selectively immobilize proteins onto a chip (Kwon et al., 2006).

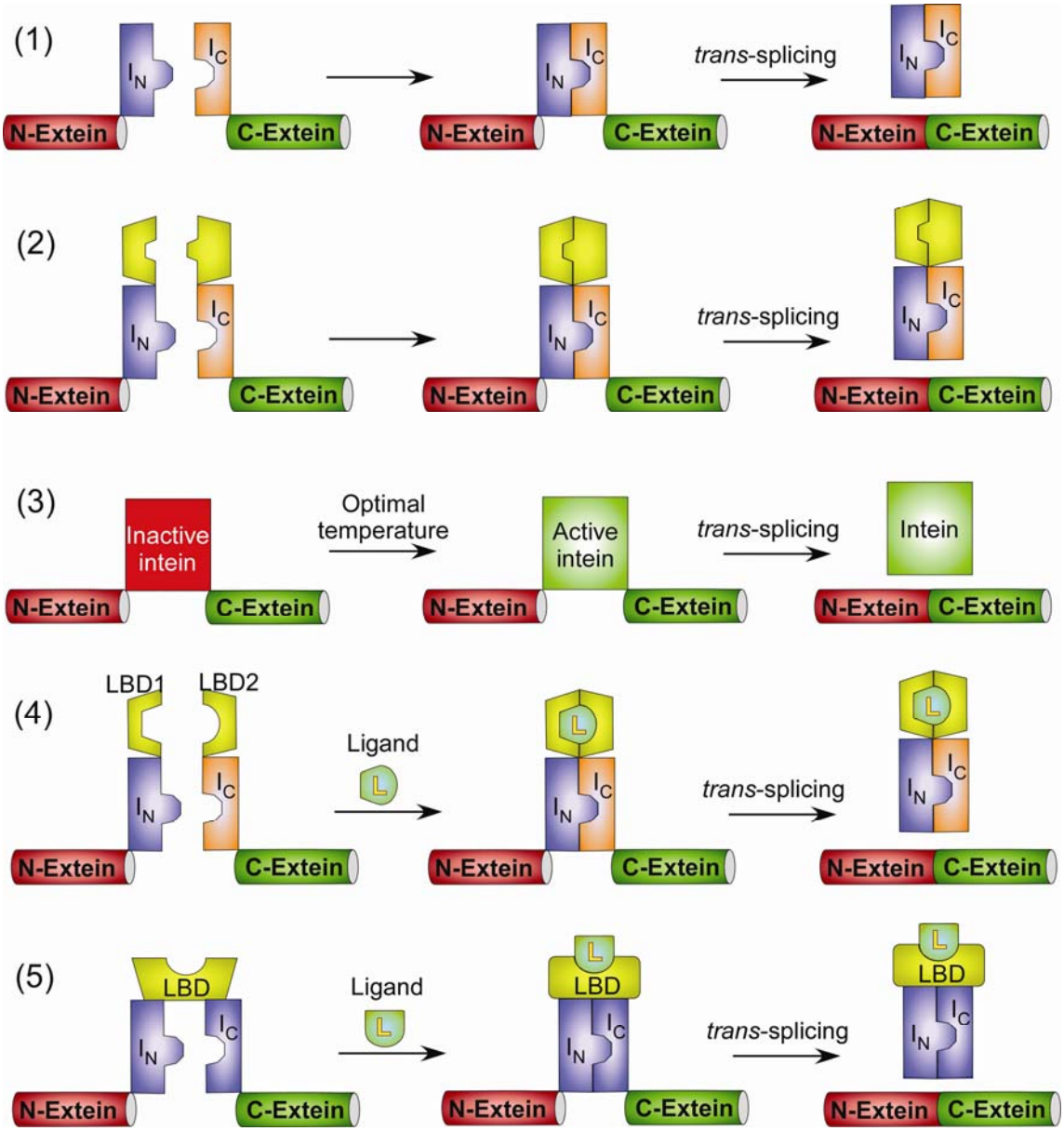

Figure 2-19. Protein *tans*-splicing and conditional protein splicing. (1) Protein *trans*-splicing to ligate two fragments. The split intein N-terminal part (I_N) is fused to the N-extein and the split intein C-terminal part (I_C) is fused to the C-extein. The two pieces of the intein associate to reconstitute splicing activity. (2) Intein association and protein splicing induced by the dimerization of two interacting proteins fused to split intein fragments. This strategy has been used to reconstitute a reporter that can be used for monitoring protein-protein interaction or other biological events *in vivo*. (3) Conditional protein splicing using a temperature-sensitive intein. (4) Split intein association and protein *trans*-splicing induced by ligand (e.g. rapamycin) mediated heterodimerization (LBD, ligand-binding domain; L, ligand). (5) Conditional protein *tans*-splicing controlled by a ligand (e.g. 4-hydroxytamoxifen, thyroid hormone) that binds to a ligand-binding domain engineered into an intein. The activity of the intein is restored by either association of two split intein fragments or activating the engineered intein upon binding of a ligand to LBD.

Recently, the split intein-mediated protein splicing reaction has been extended in a controllable way, leading to conditional protein splicing (Figure 2-19). Several approaches have been explored including the use of temperature or pH-sensitive splicing, inhibition or activation of intein-mediated splicing by small molecule ligands or protein dimerization. Temperature-sensitive splicing based on the vacuolar ATPase subunit intein from *Saccharomyces cerevisiae* has been used to control activation transcription regulators, Gal4 and Gal80 (Zeidler et al., 2004). A small cell-permeable molecule rapamycin was used to trigger splicing mediated by an engineered split VMA intein in mammalian cells (Mootz et al., 2004; Mootz et al., 2003; Mootz and Muir, 2002). The split intein fragments were fused to either the rapamycin receptor or the rapamycin binding domain, which undergoes dimerization upon binding to rapamycin, thereby facilitating the reconstitution of the split intein. A directed evolution approach led to the construction of a chimeric intein with a natural ligand-binding domain inserted. The splicing activity of this intein is triggered by a small cell-permeable molecule, 4-hydroxytamoxifen (Buskirk et al., 2004). Moreover, a chimeric intein containing a thyroid hormone binding domain was rationally designed. Protein splicing can then be regulated by the presence of human thyroid hormone in *E. coli* (Skretas and Wood, 2005). Despite the development of screening platform, a compound that effectively inhibits splicing of a native intein has not yet been found (Gangopadhyay et al., 2003).

3. Aims of this work

This work has used a combination of chemical and biophysical approaches to solve specific biological problems.

The recently developed technology based on intein-chemistry and native chemical ligation, the expressed protein ligation (EPL) approach, facilitates application of powerful synthetic chemistry to the modifications of proteins. Specific features of Rab proteins make them to be suitable targets for a semi-synthetic approach. The C-terminal prenylation motif containing typically two cysteines can be truncated, and thus a fluorophore can be easily introduced to the unstructured C-terminus followed by ligation with a short peptide containing intact cysteines. Alternatively, truncated Rab can be ligated with a compensating peptide bearing a fluorophore.

In addition to Rab proteins, synthetic chemistry and EPL can also be used to make fluorescent analogues of the lipid substrate, GGPP, and prenylated Rab, which may function in a similar way to their native counterparts while containing spectroscopic probes. If applicable, these approaches would be useful in building diversified fluorescent sensors to provide convenient signals for the planned studies.

Since inhibition of RabGGTase emerged as a very promising approach in cancer and osteoporosis therapy, further study of the role of RabGGTase in skeletal disorders and cancer would be facilitated by the development of potent and specific inhibitors for RabGGTase. In addition, although the reaction pathway of Rab prenylation and the structural basis of binary Rab:REP complex and ternary REP:RabGGTase:isoprenoid complex were elucidated, the determinants for Rab prenylation in prenylation machinery are still unclear. Mechanistic studies and the search for inhibitors for Rab prenylation require alternatives to the existing radioactivity-based and HPLC assays for RabGGTase activity, which are both discontinuous, laborious, and poorly amenable to miniaturization and parallelization. Continuous fluorescent assays are much more suitable for high-throughput screening of potential inhibitors and more convenient for characterization of prenylation.

Another purpose of this study is to understand the functional segregation of the two related Rab regulators, REP and GDI, in Rab recycling. For this purpose, absolute affinities of the interaction of prenylated Rab with REP and GDI need to be

determined. However, two technical problems have hampered this kind of study. (a) Geranylgeranylated Rabs are not soluble in the absence of either detergents or their molecular chaperones. Thus, in cells they are found either in the membranes or in complex with REP/GDI. (b) To detect the very tight interaction of prenylated Rab with REP/GDI requires a sensitive sensor that behaves analogously to its native counterpart, since very low concentrations of material have to be applied in the analysis.

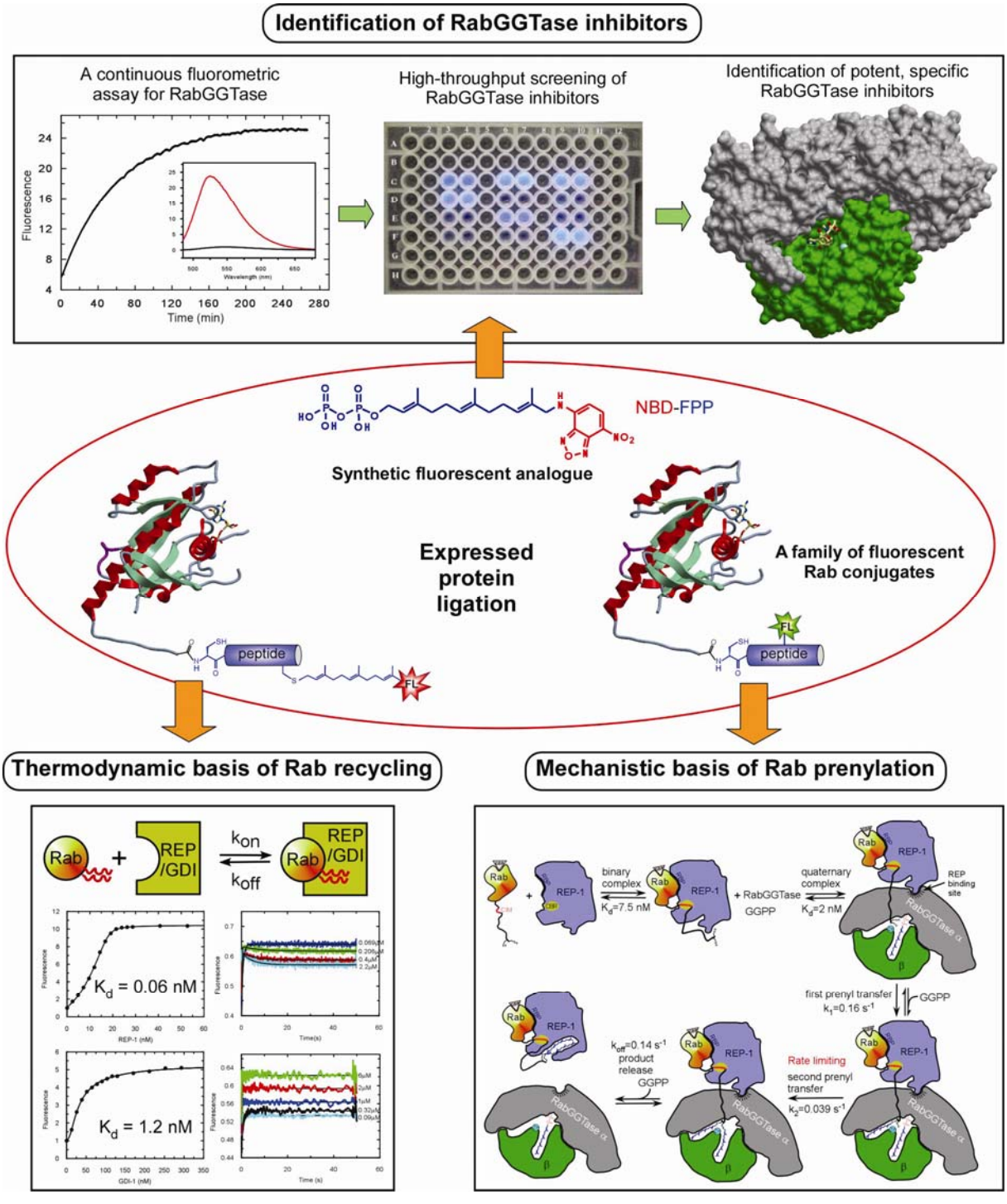

Figure 3-1. Synthetic chemistry and EPL allow the introduction of fluorophores into unprenylated and prenylated Rab proteins and the lipid substrate, phosphoisoprenoid. These sensors were used for the identification of RabGGTase inhibitors, mechanistic studies of Rab prenylation and thermodynamic analysis of prenylated Rab interaction with REP/GDI.

This study aimed at the development of fluorescent sensors and the application of these sensors to identification of RabGGTase inhibitors and mechanistic studies of Rab prenylation and Rab recycling (Figure3-1). The former involves extensive screening and rational design of fluorescent sensors constructed by the approaches described above. These sensors are required to display sensitive fluorescence change upon interactions and prenylation. The latter takes use of a variety of biochemical and biophysical methods, including protein engineering, protein-protein/ligand interaction (fluorescence titration, FRET, stopped-flow transient kinetics, isothermal titration calorimetry), enzyme kinetics and X-ray crystallography.

4. Results and Discussion

4.1 Development of fluorescent sensors for Rab prenylation

Due to their high sensitivity and selectivity, fluorescence techniques stand out among the optical techniques used in the detection, quantitation, identification and characterization of biological structures and processes. These include conformational changes, complex formation, and change of chemical and physical environment during enzymatic reactions. Studies of these processes provide information on proteins that can be related to their function.

In the context of this study, the central aim was to use parallel approaches to generate fluorescent sensors for analysis of protein prenylation. Efficient continuous fluorescence assays for FTase and GGTase-I that utilize the change in fluorescence of a fluorophore attached to a pentapeptide containing the CAAX motif have been reported (Pham et al., 2006; Pickett et al., 1995; Pompliano et al., 1992a). They take advantage of the increase in hydrophobicity of the acceptor peptide following incorporation of an isoprenoid moiety in the vicinity of an environmentally sensitive dye such as the dansyl group. However, this concept of intramolecular fluorescence enhancement cannot be applied directly to RabGGTase which recognizes the Rab:REP complex instead of a short peptide (Anant et al., 1998). Expressed protein ligation (EPL) (Thoma et al., 2001b; Iakovenko et al., 2000) and fluorescence labeling (Alexandrov et al., 2001; Thoma et al., 2001c; Alexandrov et al., 1999) have been used to produce fluorescently labeled Rab7 variants, which have been demonstrated to be valuable tools for spectroscopic interaction studies. Synthetic fluorescent analogues of phosphoisoprenoids have been utilized for monitoring their interaction with protein prenyltransferases (Dursina et al., 2002; Thoma et al., 2000). Moreover, a fluorescence assay for Rab prenylation using semi-synthetic Rab protein substrates with a fluorescent label at the C-terminus was reported (Rak et al., 2004; Durek et al., 2004a), but it only gave a fluorescent decrease not exceeding a factor of 2.

This section will describe the development of two types of fluorescent reporters: a) semi-synthetic Rab GTPase that can function similarly to the native proteins and yet display different spectral properties upon either complex formation with their interacting partners or incorporation of geranylgeranyl groups and b) fluorescent analogues of phosphoisoprenoids that can function as substrates of RabGGTase and display a change in fluorescence upon prenylation.

4.1.1 Strategy for the construction of fluorescent sensors based on Rab proteins

In earlier work, EPL was used to create fluorescent Rab molecules with native biochemical properties. This included incorporation of fluorophores and lipids at different positions of the Rab C-terminus (Alexandrov et al., 2002; Iakovenko et al., 2000). This approach was used to generate the semi-synthetic Rab molecules in which a fluorescent group is conjugated adjacent to the site of prenylation and displays a fluorescence enhancement upon prenylation. This approach was employed to detect differences in the action of REP-1 and REP-2, and provides insights into the molecular mechanism of choroideremia disease (Rak et al., 2004).

This successful example of monitoring prenylation using a Rab protein with a C-terminal fluorescence label prompted us to further persue this concept. Since it is impossible to predict which fluorophore will display a substantial change in fluorescence upon prenylation, we chose to assemble an array of constructs with different fluorophores at different positions. Two strategies can be used to build the sensor family. One is to produce peptides with a variety of fluorophores that are subsequently ligated to Rab proteins. The other is to generate a pool of fluorescently labeled thioester tagged Rab GTPases that can be subsequently ligated with a peptide.

In the first strategy, several aspects about the peptide fragment design should be considered. In the context of choosing the site of ligation, Cys205 of Rab7 appears to be a suitable ligation site for two reasons (Figure 4-1-1): First, the downstream tripeptide ($_{205}$CSC$_{207}$) contains both prenylatable cysteine residues and a compatible N-terminal cysteine that is necessary for ligation. Moreover, residue 206 can be used for coupling fluorescent groups. Second, the amino acid at the C-terminus of the Rab7 α-thioester will be serine, which is neither associated with extremely slow chemical ligation rates (e.g. Ile, Val or Pro) (Hackeng et al., 1999) nor

related to increased levels of premature cleavage of the intein-fusion protein *in vivo* (as for Asp and Gly) (Ayers et al., 1999; Chong et al., 1998).

The synthetic peptide fragment should be short to ensure simple and high yield for synthesis and should resemble the native sequence as closely as possible. Fortunately, the highly diversified Rab C-terminal sequences (CXC, CC, CCX, CCXX, CCXXX, CXXX) provide sufficient room for C-terminal peptide engineering. Positioning of a non-native reporter group requires a compromise between seeking a site that is likely to yield large signal change and, on the other hand, trying to minimize potentially adverse influence of the introduced modification on the process under study. However, the lack of precise information on the molecular basis of Rab recognition by the prenylation machinery precludes a rational positioning of the reporter group. Thus different sites have to be tested, in order to assess the consequences of diverse fluorophores incorporated at each position. In this study the fluorophores were coupled to the ε-amino group on the side chain of lysine to provide a convenient building block for further assembly of a peptide array. Alternatively, fluorophores could also be attached to the C-terminal α-carboxyl group. In this case, the synthetic effort could be reduced to construction of Cys-Cys dipeptide in milligram amounts (Figure 4-1-1).

Although the methods of organic chemistry enable incorporation of virtually any structure into the synthetic peptide fragment, synthesis of a variety of fluorescent peptides is quite laborious and expensive. An alternative would be to produce a range of fluorescently labeled Rab thioesters by chemical labeling, which subsequently can be ligated with a standard peptide containing two prenylatable cysteines or even a single cysteine. If applicable, this strategy would be much more convenient and efficient.

In this approach, site specific fluorescence labeling is the critical issue. Owing to the high selectivity, thiol-reactive reagents often provide a means of selectively modifying a protein at a defined site (Haugland, 2002). There are five cysteines in the Rab7 structure: C83, C84, C143, C207 and C205. C83 and C84 are situated in the core of the molecule, while C143 is on the hydrophobic side of a helix facing towards the core (PDB code 1VG0) (Rak et al., 2004). Thus, only the C-terminal cysteines are able to be labeled by thiol-reactive dyes (Alexandrov et al., 1999). Therefore, a single cysteine engineered at the C-terminus of truncated Rab protein would provide a precise position for coupling of various thiol-reactive dyes. Furthermore this labeling

position can be genetically engineered, potentially allowing rapid production of an array of Rab7 variants containing reporter groups at different positions. (Figure 4-1-1).

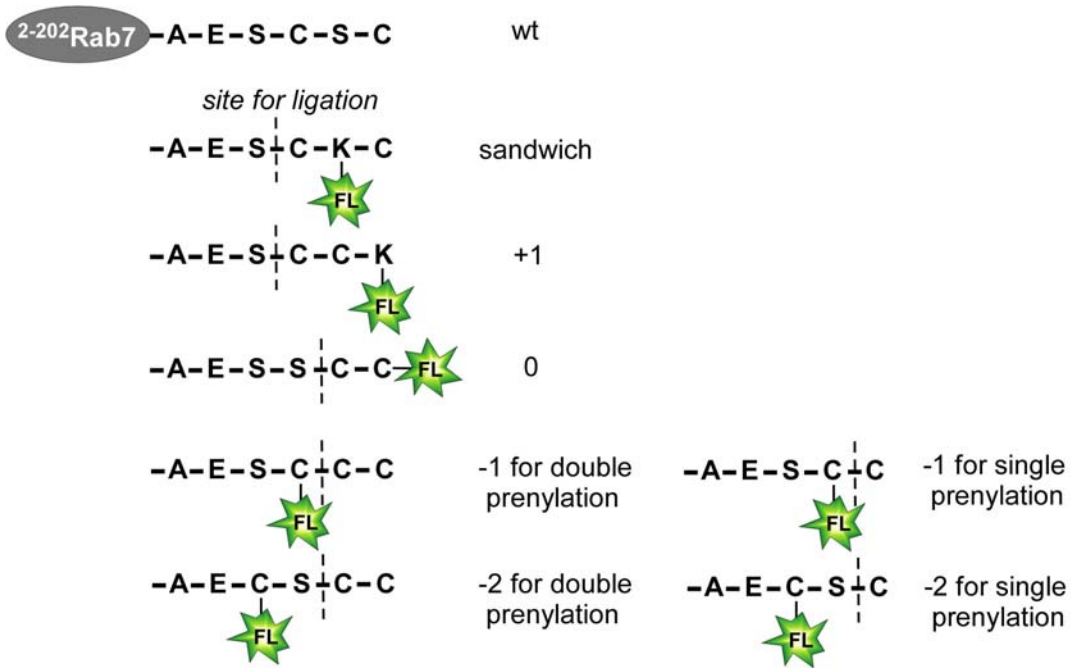

Figure 4-1-1. Construction of Rab7 fluorescent conjugates. The ligation sites were indicated by the dashed lines. FL: fluorophore, wt: wild type, Sandwich, +1, 0, -1and -2 represent different labeling positions according to the modified side chain of amino acid residue away from the first prenylation site, while 0 means that the fluorophore is coupled to the C-terminal α-carboxyl group.

.

4.1.2 Semi-synthesis of Rab7 fluorescent conjugates

4.1.2.1 Expression and purification of Rab7 C-terminal α-thioesters

Figure 4-1-2 shows the cloning and expression strategy for the production of Rab7 C-terminal thioesters truncated by 2 or 3 amino acids. The commercially available pTWIN1 *E. coli* expression vector is used together with the IMPACT™ (Intein Mediated Purification with an Affinity Chitin-binding Tag) System (Xu and Evans, Jr., 2001; Xu et al., 2000). pTWIN vectors are designed for protein purification or for the isolation of proteins with an N-terminal cysteine and/or a C-terminal thioester. Generation of a C-terminal thioester requires the truncated Rab gene to replace the chitin binding domain (CBD)-intein1 (*Ssp* DnaB interin) gene, resulting in a target-intein2 (*Mxe* GyrA intein)-CBD fusion gene. The presence of the chitin binding domain from *Bacillus circulans* (Ikegami et al., 2000) facilitates purification. Expression of the fusion gene is under the control of the T7 promotor/Lac operator (Dubendorff and Studier, 1991) and is regulated by IPTG due to the presence of a Lac repressor gene.

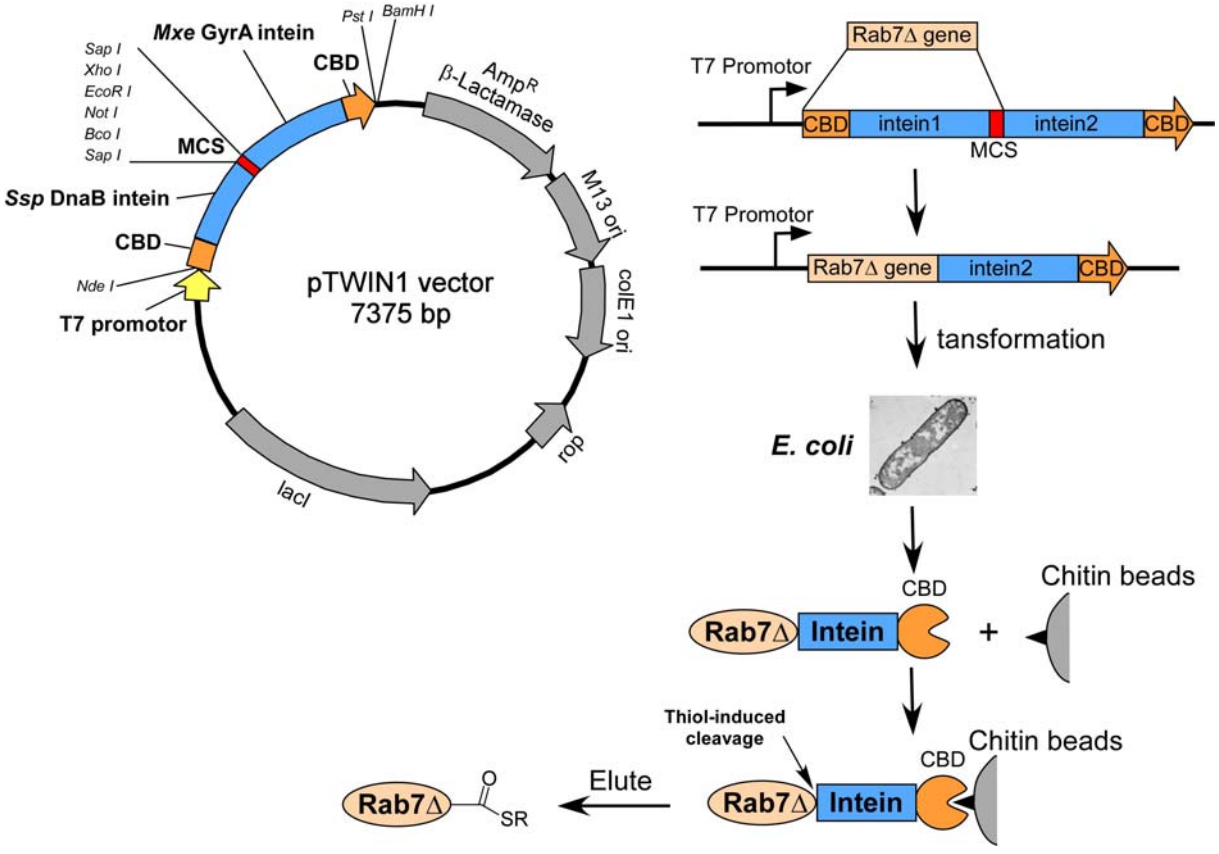

Figure 4-1-2. Production of Rab7 thioesters using IMPACT™ system. MCS: multiple cloning site, Amp^R: ampicillin resistance gene.

Vectors were constructed by PCR amplification of the Rab7 open reading frame with primers containing *NdeI* in the forward primer and synthetic nucleotides corresponding to the engineered C-terminal sequences of the truncated Rab7 and *SapI* restriction sites in the reverse primer. The resulting PCR-products were subcloned into pTWIN1 vector using *NdeI* and *SapI* restriction endonuclease sites. The various expression vectors were then transformed into BL21(DE3) competent cells. Expression conditions, such as IPTG concentration, induction time and temperature were optimized. For soluble Rab fusion protein expression the induction temperature had to be lowered to 20°C (Durek et al., 2004a; Iakovenko et al., 2000; Georgiou and Valax, 1996; Schein and Noteborn, 1988).

The resulting Rab-intein-CBD fusion protein was purified from crude cell lysate using chitin agarose. The binding of CBD to chitin is mediated mainly by hydrophobic interactions, favoring high salt concentration (e.g. 0.5M NaCl) (Hashimoto et al., 2000). This allows non-specifically bound material to be removed by use of stringent wash conditions such as high salt concentration and non-ionic detergents. However, extended storage of the immobilized fusion protein under such conditions led to a significant reduction of the intein mediated cleavage efficiency, which could be due to denaturation of the intein and the fusion protein. Therefore, it is advisable to perform the washing step as quickly as possible and to proceed to the thiol induced cleavage step without intermediate storage in order to improve yields.

To produce Rab7 thioesters, the immobilized fusion protein was induced to undergo intein-mediated cleavage in the presence of a thiol reagent, sodium 2-mercaptoethanesulfonate (MESNA). Trials were performed to identify the optimal thiolysis conditions, i.e. reaction time, temperature and the concentration of MESNA. In addition to MESNA, a variety of molecules have been used to induce the thiolysis of the intein fusion proteins, including the commonly used reductants DTT and β-mercaptoethanol (β-ME) (Chong et al., 1998). Effects of thiol cofactors[*] like ethanethiol, MESNA, 3-mercaptopropanesulfoic acid (MPSNA) and thiophenol on thiolysis and EPL have been systematically investigated (Ayers et al., 1999). The ethyl α-thioester was found to be quite stable but less reactive in EPL reactions, making it ideal for the purification and storage purposes. It is important to note that

[*] After this part of work was performed, Kent and his co-workers (Johnson and Kent, 2006) published a study on the effect of a number of thiol compounds on native chemical ligation (NCL) rate, where they found a new effective thiol cofactor, (4-carboxylmethyl)thiophenol (MPAA), a nonmalodorous, water-soluble thiol. Use of MPAA gave an order of magnitude faster reaction in model studies.

the reactivity of the α-thioester is weaker since the reactivity can be restored by *in situ* transthioesterification during a ligation reaction with a more potent thiol reagent (Xu et al., 1999a; Dawson et al., 1997a). Although phenyl thioester and MPSNA are much more reactive in EPL reactions, they have the disadvantage of a high hydrolysis rate, and are therefore not suitable for storage. Moreover, several practical drawbacks of using thiophenol as the cofactor, i.e. the low solubility in aqueous buffers at neutral pH, precipitation of the symmetrical disulfide derivative of thiophenol during ligation reactions, causing coprecipitation of reactants or products and the unpleasant odor, limits its application in EPL reactions (Ayers et al., 1999). In contrast, MESNA (Evans et al., 1998) is a relatively good cofactor for EPL since its use results in only a 2-fold reduction in the ligation rate as compared to thiophenol. In addition, MESNA thioester displays a relatively slow hydrolysis rate, and it is more suitable for storage (Ayers et al., 1999). Given its superior solubility and handling properties, it is the preferred thiol cofactor in EPL reactions.

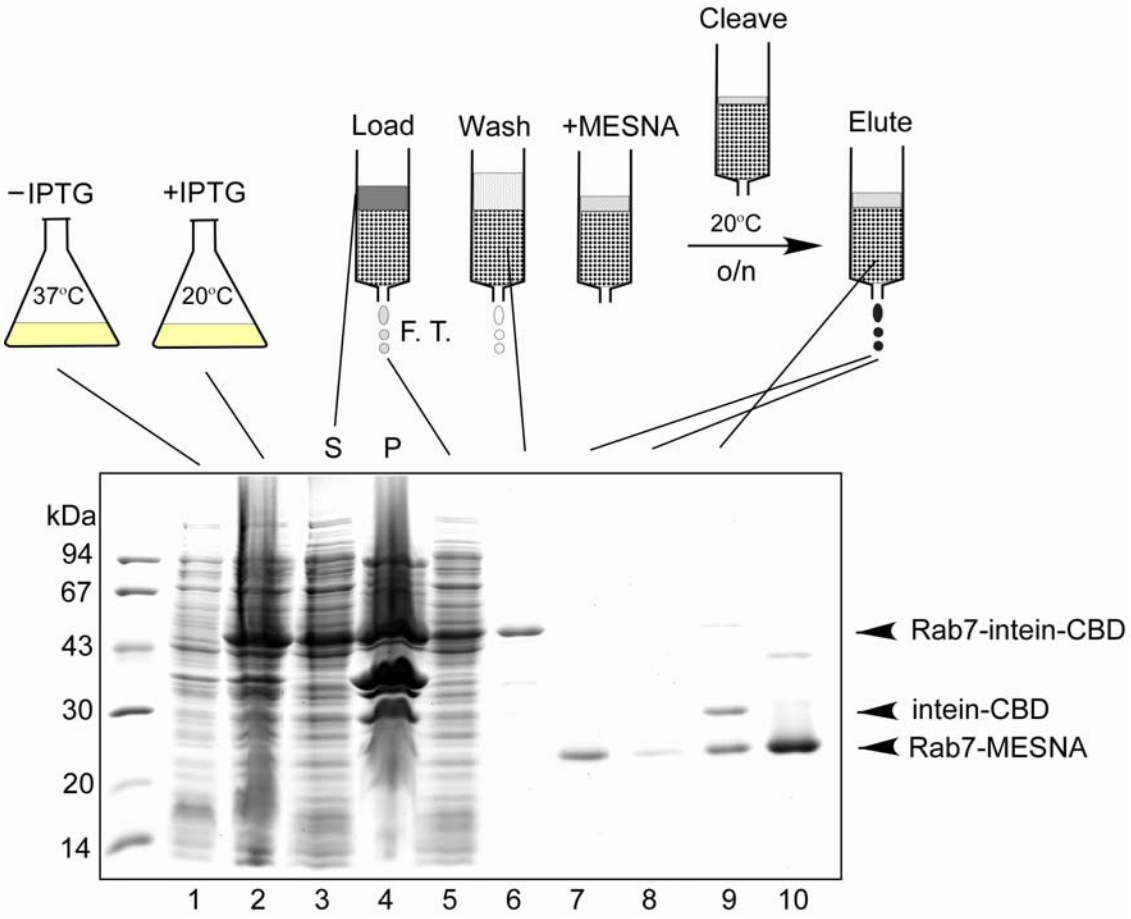

Figure 4-1-3. Expression and purification of Rab7-MESNA thioester. Lane 1: cell lysate before induction, lane 2: cell lysate after induction with IPTG overnight (o/n), lane 3: supernatant of the cell lysate after induction, lane 4: pellet of the cell lysate, lane 5: flow through from the chitin column, lane 6: chitin beads after washing, lane 7 and 8: fractions of the eluted protein after an overnight incubation

with 0.5 M MESNA at 20°C, lane 9: chitin beads after the cleavage, lane 10: concentrated Rab7 thioester.

Thiolysis of Rab-intein-CBD fusion protein with 0.5 M MESNA at room temperature overnight led to quantitative cleavage (Figure 4-1-3). These conditions also resulted in precipitation of part (ca. 50%) of Rab protein on the beads (Figure 4-1-3), which could be a result of denaturation or non-specific attachment to the beads. Using this single chromatographic step, 5-10 mg Rab thioester tagged proteins were typically obtained from a liter of bacterial culture. The soluble Rab protein in the supernatant was present in >95% purity with minor contamination of intein-CBD (<2%) that was eluted from chitin beads together with the Rab thioester. For the purpose of the subsequent fluorescence labeling, the buffer was exchanged using a PD-10 gel filtration column to remove MESNA. At this point, the Rab-MESNA α-thioesters can be stored in a neutral buffer at -80°C for at least one year without any obvious decomposition or loss of ligation reactivity. The resulting Rab thioesters were characterized by electrospray ionization mass spectroscopy (ESI-MS) and ligation reactivity subsequently.

4.1.2.2 Characterization of Rab7 α-thioesters

Since the Rab7 gene is located at the N-terminus of the fusion protein, the expressed Rab7 fusion proteins were processed *in vivo* by the endogenous methionylaminopeptidase (MAP) (Hirel et al., 1989) on account of the nature of the second amino acid residue (Thr2) following Met1. As a result, the starting methionine residue was cleaved in all Rab7 thioesters. Therefore, when the molecular weight of Rab7 thioester was calculated, the Met was left out. Moreover, the presence of thioester could be characterized by its susceptibility to hydrolysis under basic conditions (pH 9-10, see Figure 4-1-4) and its ligation reactivity with cysteine (Figure 4-1-4, 4-1-5).

Figure 4-1-4 shows the LC-ESI-MS analysis of Rab7Δ2CS-MESNA and Rab7Δ2SC-MESNA thioesters. Interestingly, instead of the expected single ESI-MS peak, both of them displayed multiple peaks at ~23 kDa. In order to establish the identities of the conjugates, more experiments had been done to identify these moieties.

In the electrospray ionization mass spectrum of Rab7Δ2CS-MESNA, the molecule with molecular mass of 23328 was identified to be the target thioester

(M_{calc}=23322), which was inferred by the mass reduction of 124 observed upon alkaline hydrolysis (Figure 4-1-4 **B**) and mass reduction of 21 after ligation with cysteine (Figure 4-1-4 **C**).

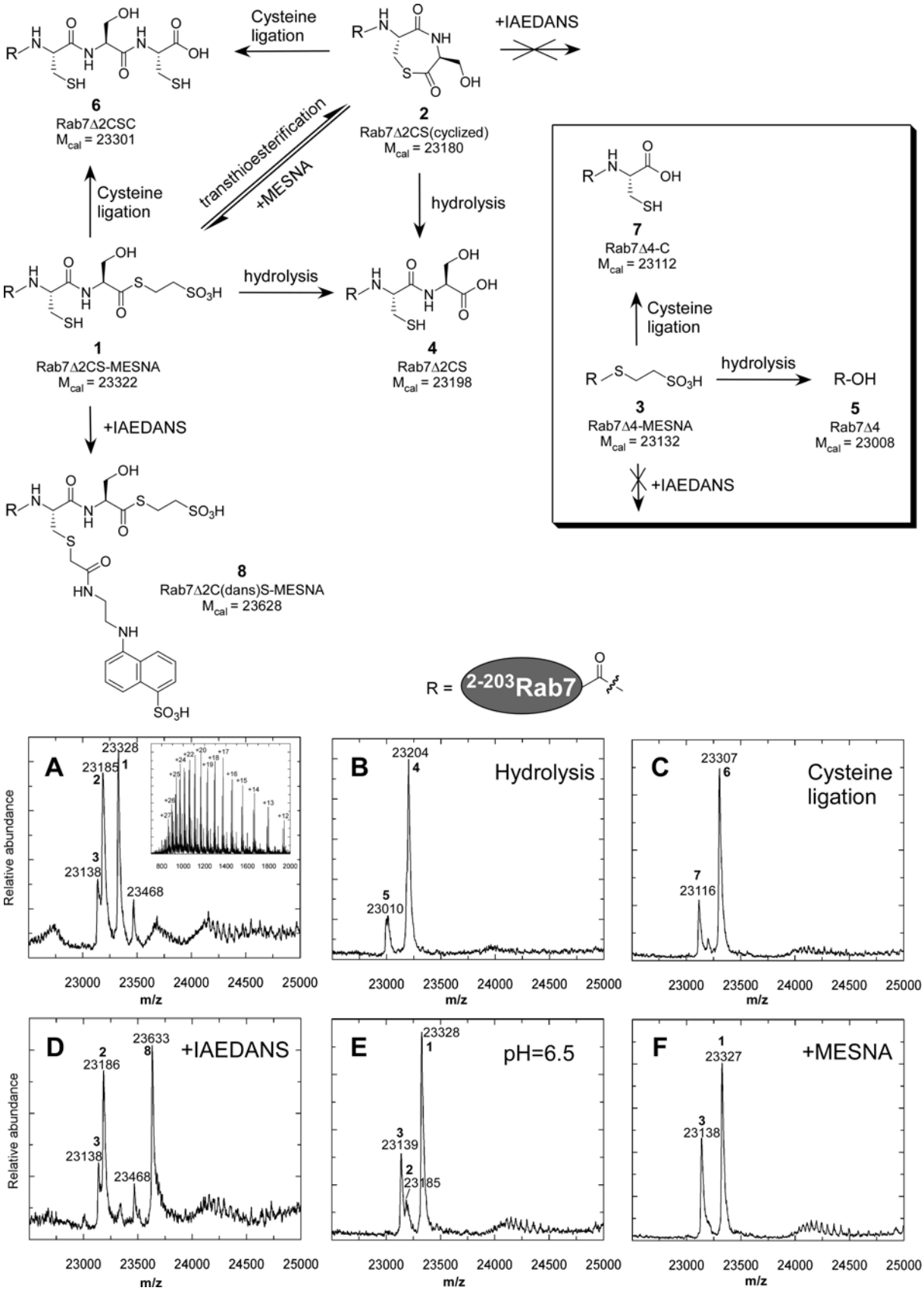

Figure 4-1-4. Reactions scheme of Rab7Δ2CS-MESNA thioester and the ESI mass spectrums of the corresponding reaction products. The mass spectrum of the purified Rab7Δ2CS-MESNA protein (**A**), after hydrolysis of the thioester (**B**), after cysteine ligation (**C**), after reaction with IAEDANS (**D**), after thiolysis at pH 6.5 (**E**), and after incubation with 100 mM MESNA (**F**). The inset of panel A shows the original mass spectrum before deconvolution. The identified mass peaks were marked with bold numbers corresponding to those reaction products shown in the above scheme. IAEDANS: dansyl iodoacetamide, i.e. 5-((((2-iodoacetyl)amino)ethyl)amino) naphthalene-1-sulfonic acid. R: the upstream amino acid residues (2-203) of Rab7.

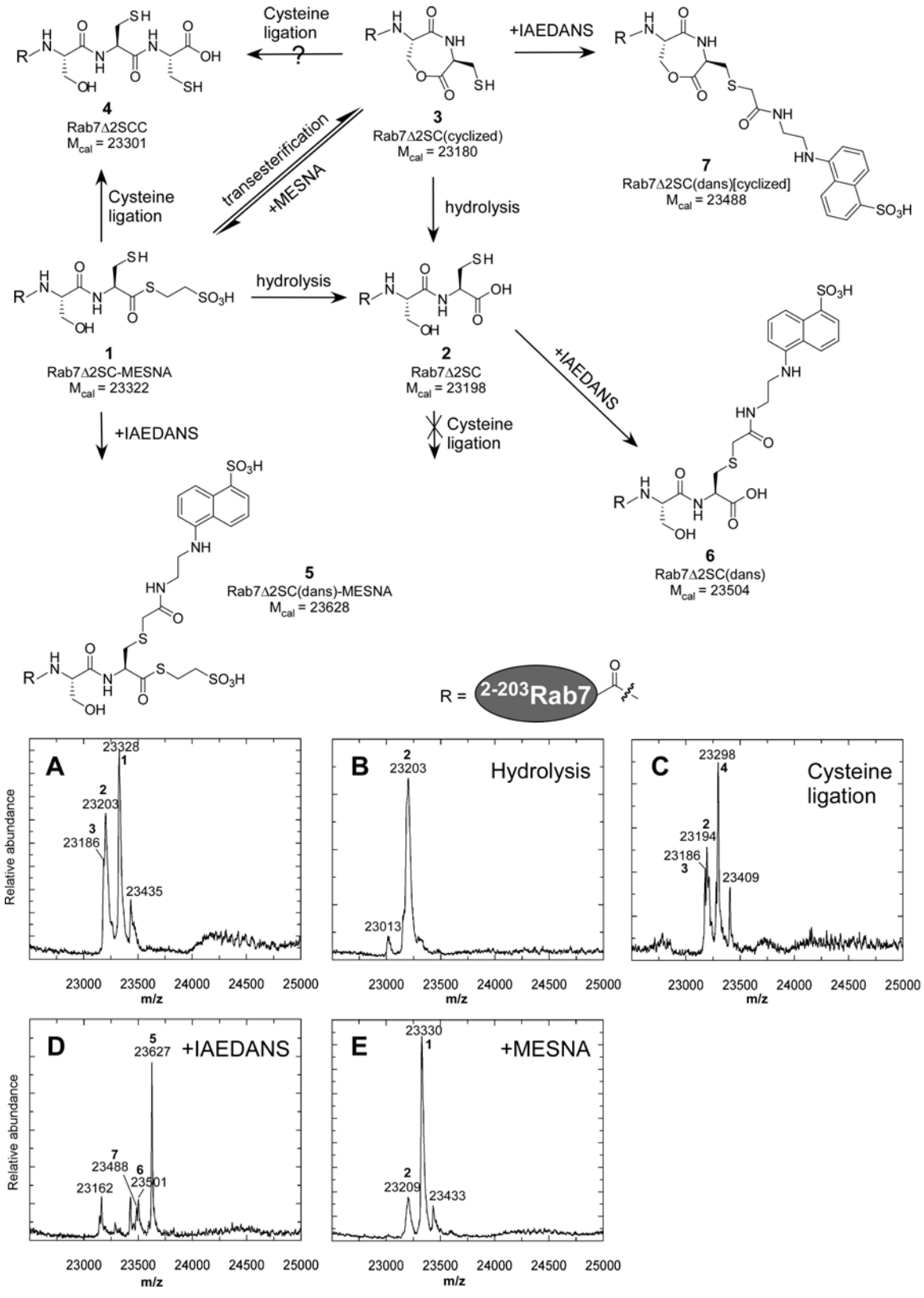

Figure 4-1-5. Reactions scheme of Rab7Δ2SC-MESNA thioester and the ESI mass spectrums of the corresponding reaction products. The mass spectrum of the purified Rab7Δ2SC-MESNA protein (**A**), after hydrolysis of the thioester (**B**), after cysteine ligation (**C**), after reaction with IAEDANS (**D**), and after incubation with 100 mM MESNA (**E**). The identified mass peaks were marked with bold numbers corresponding to those reaction products shown in the above scheme.

The identity of fragment with mass of 23185 was more difficult to establish. It was able to be hydrolyzed to Rab7Δ2CS (Figure 4-1-4 **B**) and remained competent for ligation (Figure 4-1-4 **C**), but was not susceptible to thiol-reactive dyes (Figure 4-1-4 **D**). The most likely explanation for these observations could be an intramolecular transthioesterification resulting in a cyclization between the Cys204 side chain and the carboxyl-terminus, though a seven-member ring (1,4-thiazepane-2,5-dione). This would not be normally a favored structure, but, might have increased likelihood of generation in the tertiary structure of a protein. This conclusion could be further ascertained by the reduction of the cyclization under acidic conditions (pH 6.5) (Figure 4-1-4 **E**) and in the presence of MESNA (Figure 4-1-4 **F**). Most protein thiols have pK_a values in the range of 8.5 ± 0.5 (Gitler et al., 1995). It was shown that the cysteine thiol of the FTase substrate, GCVLS, ionizes with a pK_a of 8 (Hightower et al., 2001). Although the pK_a of the thiol in Rab C-terminal cysteine is not known, the transthioesterification reactivity of the cysteine thiol could be expected to decrease at lower pH. This appears to be indeed the case. Under acidic conditions, the formation of the 1,4-thiazepane-2,5-dione ring was significantly reduced. Furthermore, the presence of excess of MESNA drives the intramolecular transthioesterification reaction equilibrium backward, leading to substitution of the α-thioester. Therefore, the intramolecular cyclization could be a consequence of the remarkable reactivity of the α-thioester or the high reactivity of thiol group of the Rab7 C-terminal cysteine due to reduction of pK_a, resulting from some tertiary structure features of the C-terminus leading to deprotonation at neutral pH, or a combination of both.

The moiety giving a minor peak at 23138 appears to be vulnerable to hydrolysis, reactive in cysteine ligation, and impervious to the thiol-reactive dye. These observations could be associated with Rab7Δ4-MESNA, i.e. when the cleavage occurred at Cys204 instead of at the intein cysteine. To my knowledge, such non-specific splicing has never been reported before. Protein splicing is a highly structured process, where splicing sites are conserved (Klabunde et al., 1998). Most intein sequences start with a cysteine or serine residue that is responsible for an acyl shift at the N-terminal splice junction (Shao et al., 1996). In this case, the cleavage

site has migrated 2 residues upstream to the Rab7 C-terminal cysteines. Nevertheless, this splicing site is not as efficient as the native site, due to the conserved protein splicing mechanism.

The fragments observed in the mass spectrum of Rab7ΔC-MESNA were identified by the same methods as above (see Figure 4-1-5). Interestingly, Rab7ΔC-MESNA behaves quite differently from Rab7ΔCS-MESNA. It was partially hydrolyzed (mass peak of 23203) accompanied by a minor putative intramolecularly cyclized moiety (mass peak of 23186) corresponding to a 1,4-oxazepane-2,5-dione ring. The hydrolysis was not observed in Rab7ΔCS-MESNA under the same conditions, suggesting that it could be triggered by the primary structure or even tertiary structure of the C-terminus of the Rab7ΔC-MESNA thioester. The hydrolysis might be induced by intramolecular transesterification that leads to a dynamic equilibrium between the formation of a 1,4-oxazepane-2,5-dione ring and the hydrolyzed product. To confirm this hypothesis, the resulting Rab7ΔC-MESNA thioester was incubated with 100 mM MESNA, under which conditions a diminished pool of hydrolyzed molecules and no cyclized molecules were observed in the ESI-MS (Figure 4-1-5 **E**).

The cyclization effects can be reversed in the presence of MESNA to restore the thioester, so that they are not detrimental to ligation (Figure 4-1-4 **C**, 4-5 **C**). However, the intramolecular cyclization of Rab7ΔCS-MESNA blocked the cysteine thiol, resulting in a low efficiency of thiol labeling (Figure 4-1-4 **D**). The intramolecular cyclization of Rab7ΔC-MESNA facilitates an essentially irreversible hydrolysis reaction, resulting in a hydrolyzed product that is inaccessible to ligation. In order to minimize the adverse effect on fluorescence labeling, the conjugating reaction could be performed at pH 6.5, where the cyclization is retarded (Figure 4-1-4 **E**) while the C-terminal cysteine thiol is still susceptible for thiol-reactive dyes (data not shown). Alternative solution to this problem was to use ethanethiol in thiolysis of the fusion protein, leading to production of Rab7 ethyl α-thioester (Rab7ΔCS-ET and Rab7ΔC-ET). Not surprisingly, that the decrease in the reactivity of the thioester led to reduction of the cyclization reaction (see Figure 4-1-6). Ethyl α-thioester is much more stable (no observed decomposition after 1-day incubation at 4°C) and enables efficient fluorescence labeling and ligation in the presence of MESNA as a ligation cofactor (data not shown).

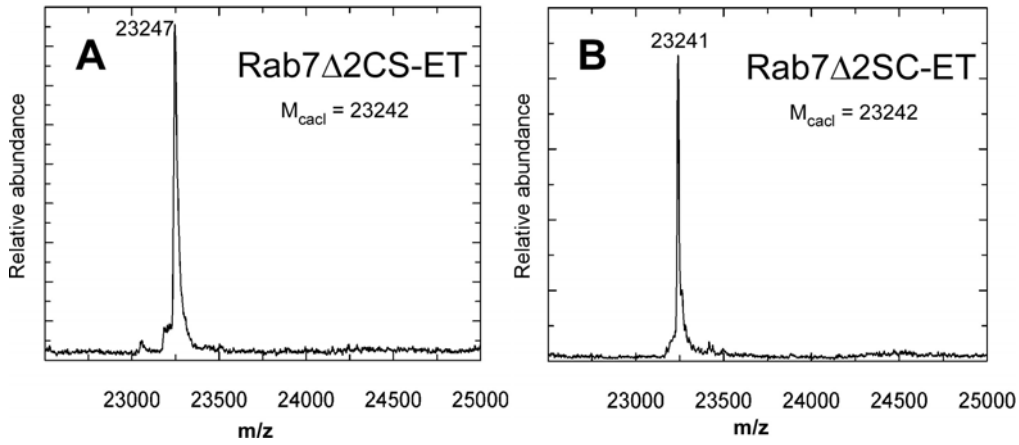

Figure 4-1-6. ESI mass spectra of the purified Rab7Δ2CS-ET thioester (**A**) and Rab7Δ2SC-ET thioester (**B**).

4.1.2.3 Fluorophore conjugation and protein ligation

To obtain fluorescently labeled and thioester tagged Rab7 proteins, thiol-reactive dyes were used to conjugate a fluorophore to the C-terminal cysteine of Rab7 thioesters. The thiol-reactive groups used in this study are alkylating reagents, including iodoacetamides and maleimides. Reaction of any of these functional groups with a C-terminal cysteine of Rab7 thioester usually proceeds quantitatively and rapidly (within half an hour) at or below room temperature in pH range from 6.5 to 8.0, yielding chemically stable conjugates (Scheme 4-1). However, it should be noted that reactions at above pH 8 would increase the risk of non-specific coupling of iodoacetamides with other amino acid residues (methionine, histidine, tyrosine, α-amino group) and hydrolysis of maleimides (Haugland, 2002). Taken together with the considerations on the intramolecular reactions of Rab7 thioesters as mentioned above, the pH for the labeling reaction was set to 6.5-7.2.

Scheme 4-1 Labeling of protein at cysteine side chain with iodoacetamide and maleimide functionalized fluorophores.

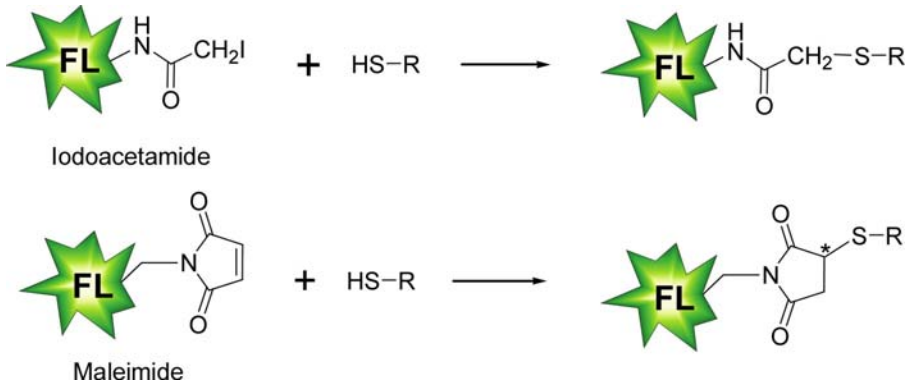

These labeling reactions typically led to specific conjugation of dyes at the C-terminal cysteine, as confirmed by tryptic digestion followed by LC-ESI-MS analysis of the resulting peptide fragments (Figure 4-1-7). Nevertheless, reactions using 5-10 equivalents of maleimide dyes (with respect to protein) resulted in labeling at both C-terminal cysteine and Cys143 (data not shown), which was not observed in conjugation of iodoacetamide dyes even with 20 equivalents. This suggested that maleimide is much more reactive than iodoacetamide in reaction with thiol groups. Thus, 1.5 equivalents of maleimide dyes were applied in labeling reactions. Under such conditions, no labeling at Cys143 was observed.

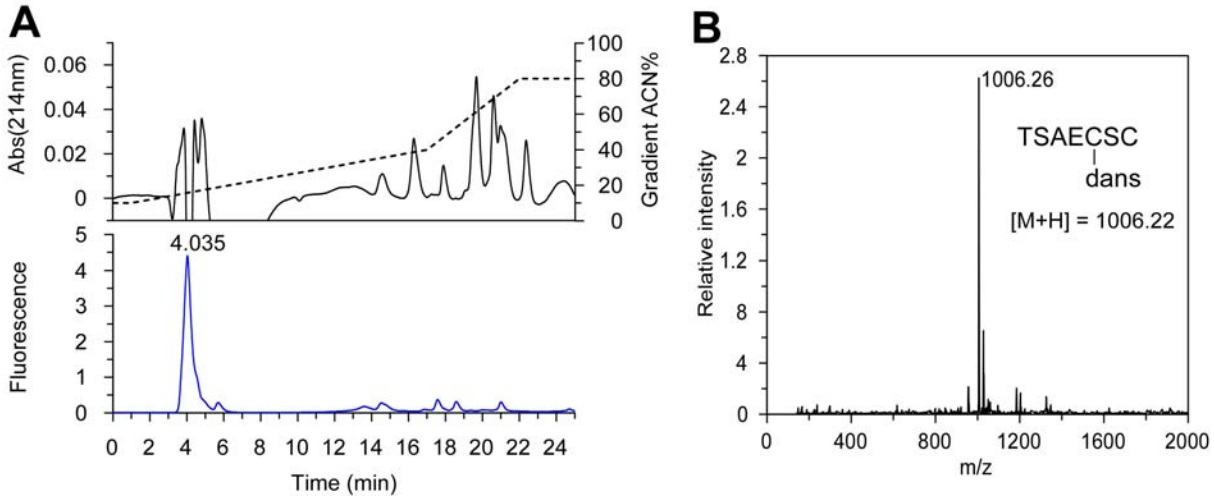

Figure 4-1-7. LC-ESI-MS analysis of the peptide fragments resulted from the trypsin digest of Rab7Δ2C(dans)SC using reverse-phase C18 column. (**A**) The elution profile detected by absorbance at 214nm (upper panel) and by dansyl fluorescence (lower panel, excitation at 340 nm, emission at 480 nm). The dashed line shows the percentage of eluent, acetonitrile, in water. (**B**) The ESI-mass spectrum of the collected fluorescent fraction eluted at 4.0 minutes in the HPLC chromatogram. It was shown to represent the dansyl labeled C-terminal peptide. Rab7Δ2C(dans)SC was produced by conjugation of IAEDANS to Rab7Δ2CS-MESNA thioester followed by ligation to a cysteine.

A set of iodoacetamide or maleimide functionalized fluorophores were used for conjugation, which are structurally diversified and excitable by light from UV to far red (see Figure 4-1-8). I-BA-s-IA and I-SO-s-IA were contributed by Prof. Dr. Klaus Hahn (The Scripps Research Institute, La Jolla, CA, USA) (Toutchkine et al., 2003) while the others were obtained from commercial sources.

Selection of dyes was based on two considerations: First, the dyes should be environmentally sensitive in order to monitor the prenylation reaction. Environmentally sensitive dyes have been covalently attached to proteins to report a diverse array of protein activities *in vitro* (for review see (Giuliano and Taylor, 1998)), including phosphorylation (Wang and Lawrence, 2005; Shults and Imperiali, 2003;

Yeh et al., 2002), conformational changes (Hammarstrom et al., 2001), small ligand binding (Wada et al., 2003; De Lorimier et al., 2002; Morii et al., 2002; Hamachi et al., 2000; Marvin and Hellinga, 1998; Gilardi et al., 1994; Brune et al., 1994), and protein-protein interactions (Nomanbhoy and Cerione, 1999; Daugherty and Gellman, 1999; Sloan and Hellinga, 1998; Cerione, 1994). The typically used environmentally sensitive dyes such as acrylodan (Prendergast et al., 1983), ANS (Cerione, 1994), dansyl, coumarin, NBD, fluorescein, etc., however, have several drawbacks which limit their application in *in vivo* experiments. They fluoresce at short wavelengths which fall inside the range of cellular autofluorescence, resulting in high background. In contrast to dyes commonly used in live cell imaging (e.g. rhodamine, cyanines, Alexa dyes), they show weak absorption, low fluorescence quantum yields, and low photostability. Recent advances in the development of new dyes, such as Dapoxyl™ [5-(4''-dimethylaminophenyl)-2-(4'-phenyl)oxazole] (Wang and Lawrence, 2005; Diwu et al., 1997), BODIPY(as shown in Figure 4-1-8) (Korlach et al., 2004; Isaksson et al., 2003), styryl naphthyl dyes - JPW (De Lorimier et al., 2002), DCDHF (dicyanodihydrofuran) (Willets et al., 2003), merocyanine derivatives (I-BA, I-SO, see Figure 4-1-8) (Toutchkine et al., 2003) and APM (aminophenoxazone maleimide) (Cohen et al., 2005), provide a wider platform for protein activity studies *in vitro* and especially *in vivo* (Nalbant et al., 2004; Hahn et al., 1992). Selected dyes herein (Figure 4-1-8) included the traditional small environmentally sensitive dyes (e.g. dansyl, coumarin, NBD, fluorescein) and bright dyes such as rhodamine and its derivatives - ATTO 520, 565, coumarin derivative - ATTO 425, acriflavine derivative - ATTO 465, and merocyanine derivatives - Dyomics dyes.

Second, the dyes should be suitable for protein modification. Besides thiol-reactivity, good aqueous solubility is required for protein labeling, since proteins usually cannot tolerate high concentrations of organic solvents. However, only relatively hydrophobic dyes tend to be good reporters, presumably because interaction with protein hydrophobic regions is necessary to substantially alter the dye's environment (Toutchkine et al., 2003). Moreover, multiply charged dyes can perturb local structure and motion as well as inhibit labeling at certain positions. Therefore, selection of dyes on the basis of hydrophobicity is a trade-off between the compatibility with protein modification and its capability as a reporter. Another encountered problem is the self-aggregation of hydrophobic dyes in aqueous solvents, which was observed for fluorescein in this study. Aggregation leads to self-

fluorescence quenching and difficulties during protein labeling and separation of the noncovalently attached dyes (Toutchkine et al., 2003). It was shown that the inclusion of charged groups (Soper and Mattingly, 1994) and out-of-plane groups (Toutchkine et al., 2003) prevents aggregation. The length of linker between probe and protein could also be a concern. On the one hand, short linkers would reduce the accessibility of dyes to protein due to steric hindrance, as was observed in this study (see below). On the other hand, long, flexible linkers may raise the question about whether the probe motions faithfully mirror the motions of the residue to which it is attached (Cohen et al., 2005). Because of lack of knowledge in this aspect, the length of linker between probe and protein ranged from 3 to 10 atoms in this study.

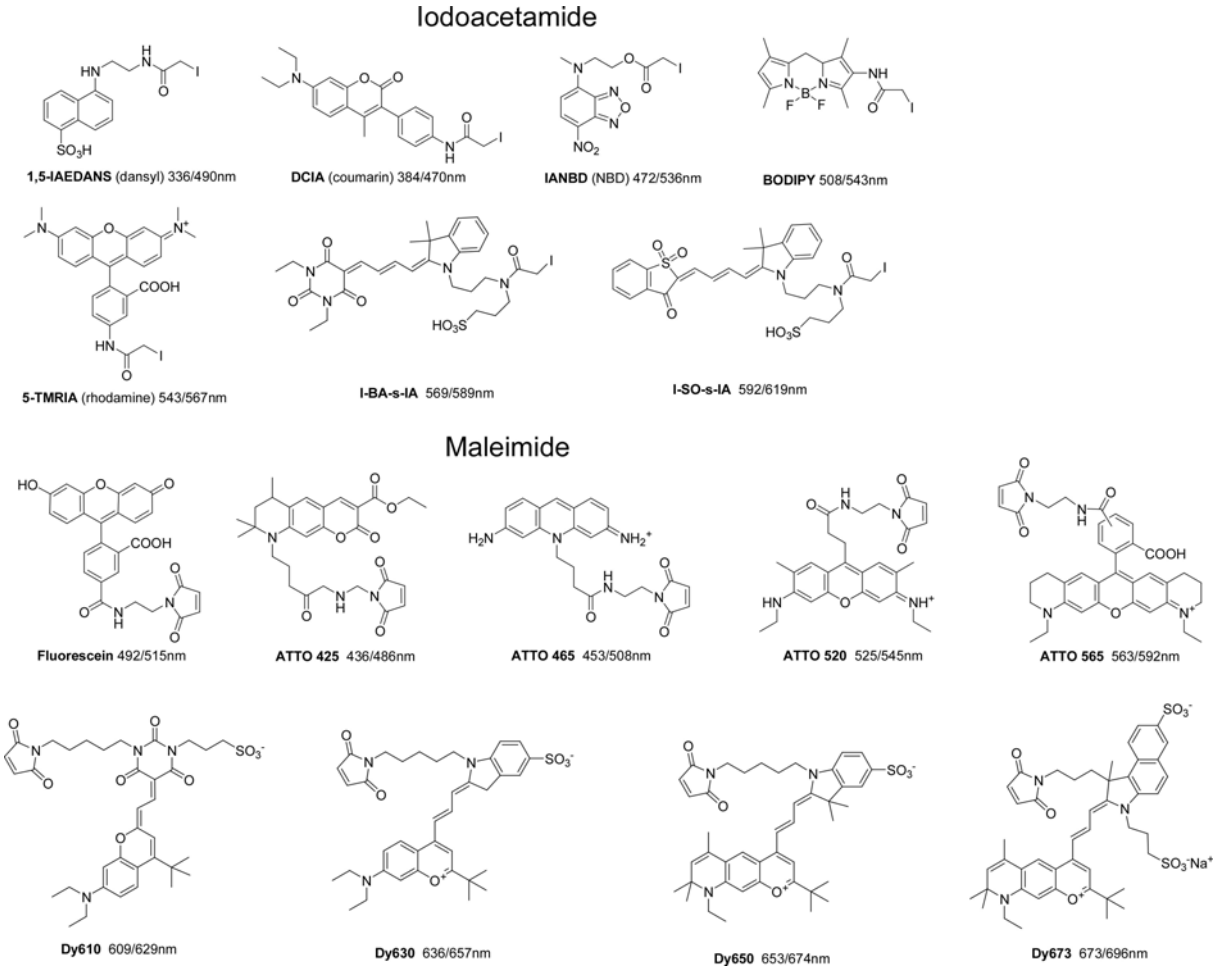

Figure 4-1-8. Structural formulae of thiol-reactive fluorophores used in this study. Excitation and emission wavelength are indicated. For I-BA and I-SO, I = indolenine, BA = barbituric acid, SO = benzothiophen-3-one-1,1-dioxide. IAEDANS: 5-((((2-iodoacetyl)amino)ethyl)amino)naphthalene-1-sulfonic acid, DCIA: 7-diethylamino-3-((4'-(iodoacetyl)amino) phenyl)-4-methylcoumarin, IANBD: N-((2-(iodoacetoxy)ethyl)-N-methyl)amino-7-nitrobenz-2-oxa-1,3-diazole, BODIPY: N-(4,4-difluoro-1,3,5,7-tetramethyl-4-bora-3a,4a-diaza-s-indacene-2-yl)iodoacetamide, 5-TMRIA: tetramethylrhodamine-5-iodoacetamide dihydroiodide.

In most cases, conjugation of iodoacetamide functionalized dyes to Rab7 proceeded without observed influence on the thioester group under neutral conditions (examples see Figure 4-1-4 **D**, 4-5 **D**). Interestingly, conjugation of maleimide dyes to Rab7Δ2SC-MESNA thioester promoted hydrolysis of the thioester. The resulting maleimide conjugates lost their reactivity for cysteine ligation (data not shown). However, this was not observed in the maleimide conjugates of Rab7Δ2CS-MESNA thioester, nor was this dependent on the type of dye coupled. Taken together, this suggests that attachment of maleimide to the side chain of cysteine residue in the vicinity of thioester specifically induced its hydrolysis in the context of the Rab7Δ2SC-MESNA protein. To this end, a series of tests were performed to study the kinetics of the conjugation of maleimide and the hydrolysis of thioester in order to reveal the reason for such a phenomenon. Since both reactions are sensitive to pH, the pH and time for conjugation and subsequent incubation were manipulated in the tests.

Table 4-1-1-1. Conjugation of ATTO 425-maleimide to Rab7Δ2SC-MESNA thioester. Reactions were performed for 30 or 5 minutes at different pH. After reaction, the excess dye was removed and the buffer was changed using a spin column. The resulting conjugates were analyzed by ESI-MS, displaying two major mass peaks corresponding to the labeled thioester (expected 23722) and the labeled hydrolyzed molecule (expected 23846).

Conjugation		pH after conjugation	ESI-MS relative abundance (%)	
pH	Time (min)		Rab7Δ2SC(425) observed 23720	Rab7Δ2SC(425)-MESNA observed 23844
7.2	30	7.0-7.5	100	10
6.5	30	7.0-7.5	100	15
6.5	5	7.0-7.5	100	40
5.0	30	7.0-7.5	100	0
6.5	30	5	20	100
6.5	5	5	10	100
5.0	30	5	10	100

The data summarized in the Table 4-1-1 indicates that (i) the conjugation of the maleimide functionalized dye to Rab7 is rapid (reaction completes within 5 minutes at pH 6.5-7.5); (ii) it was the formation of maleimide adduct but not the coupling reaction that induced the hydrolysis of the C-terminal thioester; (iii) the hydrolysis was relatively slow at pH 7.0-7.5, and was impeded at pH 5.0. Without further investigation, it is unclear how the maleimide adduct induces the hydrolysis of α-

thioester. In a previous report, the conjugation of *N*-(1-pyrene)maleimide with cysteine and protein where primary amino groups were also present led to spectral shift of the fluorescence. This spectral change was postulated to be a consequence of an intramolecular nucleophilic attack on the succinimido ring of the adduct by the primary amino group (Wu et al., 1976). However, no 3-D structure of full length Rab7 is available due to the highly flexible C-terminus (Rak et al., 2004). The connection between maleimide adduct induced possible intramolecular aminolysis and induced thioester hydrolysis could not be established. Despite these puzzles, the resulting fluorescently labeled α-thioester tagged proteins are able to be ligated with cysteine and peptides at pH 5.0 (data not shown).

Table 4-1-2. Fluorescence labeling efficiency.

Dyes	Rab7Δ2CS-MESNA	Rab7Δ2SC-MESNA	Rab7wt
IAEDANS	~90%	~95%	Mono-label ~42% Di-label ~29%
IANBD	~85%	~90%	
DCIA	<10% ~50%[a]	<10% ~70%[a]	<10%
Fluorescein	~10%[a]	~25%[a]	
BODIPY	<10%	~10%	<10%
5-TMRIA	<10% <10%[a]	<10% <10%[a]	<10% <10%[a]
ATTO425	~70%	~95%	
ATTO465	~60%	~95%	
ATTO520	~30%	~95%	
ATTO565	~65%	~90%	
Dy610	~40%	~90%	
Dy630	~50%	~90%	
Dy650	<10% ~30%[a]	~50%	
Dy673	<10% ~30%[a]	~90%[a]	
I-BA-s-IA	~60%	~90%	
I-SO-s-IA	~70%	~90%	

Labeling efficiency was estimated from the ratio of ESI-MS signals. [a] in the presence of detergent DDMAB.

The summary of conjugation efficiencies of the fluorescent dyes is shown in Table 4-1-2. Not surprisingly, as a result of the intramolecular cyclization at the C-

terminus of Rab7Δ2CS-MESNA, it appears less susceptible for the dyes than Rab7Δ2SC-MESNA. Although most of the labeling reactions were rapid and quantitative, some hydrophobic dyes, e.g. 5-TMRIA, BODIPY, DCIA and fluorescein, with short linkers displayed very poor reactivity for Rab7 (see Table 4-1-2). This could be due to a combination of steric clashes, the unfavorable electrostatic interactions and poor solubility of bulky fluorescent groups and protein conjugates. In order to increase the labeling efficiency, either longer linkers could be introduced or an optimization of reaction conditions should be further performed.

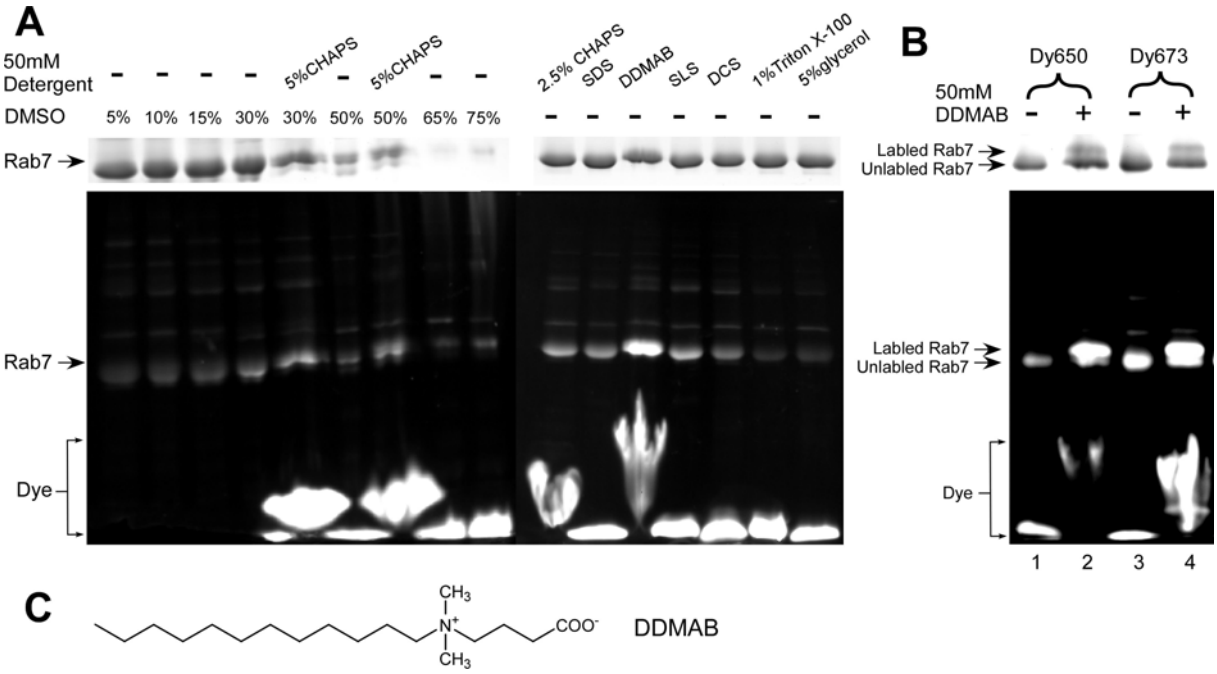

Figure 4-1-9. Identification of detergents facilitating dye conjugation to Rab7 thioesters by SDS-PAGE analysis. (**A**) Conjugation of DCIA to Rab7Δ2SC-MESNA thioester in the presence of various detergents at concentrations above the critical micelle concentration (CMC). The gels were imaged using UV illumination (lower panel) and then stained with Coomassie blue (upper panel). (**B**) Conjugation of Dy650-maleimide (lane 1, 2) and Dy673 (lane 3, 4) to Rab7Δ2CS-ET thioester in the presence and the absence of 50 mM DDMAB. (**C**) Structure of DDMAB. SDS: sodium dodecyl sulfate, SLS: sodium lauryl sarcosine, DCS: Deoxycholic acid sodium salt, CHAPS: 3-[(3-Cholamidopropyl)dimethylammonio]-1-propanesulfonate, DDMAB: *N*-dodecyl-*N*,*N*-(dimethylammonio)butyrate.

Given the hydrophilic nature of the protein, conditions had to be identified under which both molecules (i.e. protein and dye) could be maintained in solution. To make dyes soluble, DMSO (up to 30%) was included as a cosolvent that can be tolerated by Rab7. The conjugation of dyes to the proteins was assayed by means of ESI-MS as well as SDS-PAGE, where the intensity of the fluorescent Rab7 band indicates the formation of the conjugate. Although the organic dyes were soluble under these conditions, the labeling efficiency was still very low (Figure 4-1-9 **A**). It should be

noted that conjugation of TMRIA and DCIA to Rab7 led to partial precipitation of the protein conjugates (data not shown), which could be one of the reasons for the low labeling efficiencies with these dyes. Previous work in our lab showed that detergent can facilitate the ligation of hydrophobic geranylgeranylated peptide to Rab7 thioester (Durek et al., 2004a). This encouraged us to search for detergents supporting the conjugation reaction. After screening a small set of detergents, we identified *N*-dodecyl-*N*,*N*-(dimethylammonio)-butyrate (DDMAB) as a compound efficiently supporting the conjugation of DCIA to Rab7 thioesters (Figure 4-1-9 **A**, Table 4-1-2).

Although all detergents were able to mediate solubilization of the organic dyes and the protein conjugates, only a few of them were able to support efficient protein labeling, suggesting that solubilization is not sufficient for conjugation (Figure 4-1-9 **A**). Moreover, conjugation of the soluble dyes Dy650 and Dy673 with long linker to Rab7Δ2CS-ET can be significantly improved by supplementing the reaction with 50 mM DDMAB (Figure 4-1-9 **B**). In addition to supporting fluorophore conjugation, DDMAB is able to assist fluorescent peptide ligation toRab7 thioester (Figure 4-1-10 **A**). However, DDMAB as well as other detergents tested in this study did not play a critical role in the conjugation of some other dyes, like TMRIA and fluorescein, to Rab7 protein.

DDMAB has been found to support the ligation of geranylgeranylated peptide with Rab7 thioester (Thomas Durek, PhD thesis, MPI-Dortmund). It is a zwitterionic detergent with a critical micelle concentration (CMC) of 4.3 mM (Chevalier et al., 1991), which was successfully used for solubilization of membrane proteins (Welling-Wester et al., 1998; Brenner et al., 1995; Tanford and Reynolds, 1976). T. Durek et al. proposed that the observed ligation improvement is a result of concentration of both reactants into a small micelle, resulting in an increase of the frequency of molecular collisions, consequently improving the prenylated peptide ligation. Such a proximity effect is often the main factor responsible for the catalysis of reactions in micellar solutions (Tascioglu, 1996). Besides concentrating the reactants in a small volume, micelles stabilize substrates, intermediates or products, and orient substrates so that ionization potentials and oxidation-reduction properties, dissociation constants, physical properties and reactivities are changed. Thus, they can alter reaction rate, mechanism, and regio- and stereochemistry (Dwars et al., 2005).

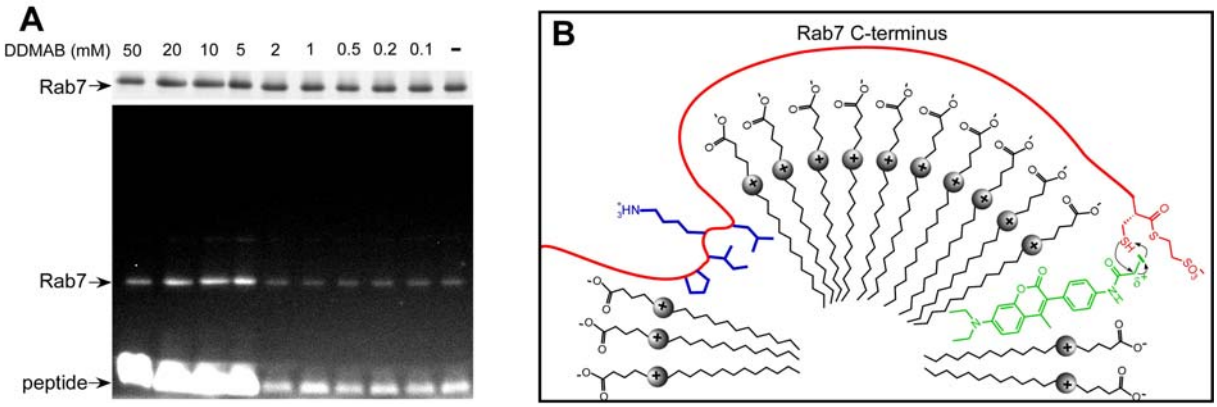

Figure 4-1-10. (**A**) Ligation of C(S*t*Bu)C(S*t*Bu)-dans to Rab7Δ2SC-MESNA thioester in the presence of DDMAB at various concentrations. The gels were imaged using UV illumination (lower panel) and then stained with Coomassie blue (upper panel). (**B**) A model of the DDMAB micelle mediated fluorophore conjugation. The C-terminus of Rab7Δ2SC-MESNA thioester is depicted in red ribbon and the side chains of amino acid residues (Pro189, I190, K191, L192) colored in blue. While the labeling reagent DCIA is shown in green.

In order to understand the function of DDMAB in conjugation and ligation reactions, a series of concentrations of DDMAB were used for fluorescent peptide ligation. This showed clearly that only at concentrations above the CMC was the ligation efficiency significantly enhanced (Figure 4-1-10 **A**). The frontier of the fluorescent gel corresponding to the unreacted peptides shows enhanced fluorescent intensity and reduced mobility in the presence of DDMAB of concentration above CMC, which could be due to the micelle bound peptides. The formation of micelles was also observed in fluorescence labeling reactions (see Figure 4-1-9 **A**, **B**). Therefore, micelle formation could play an important role in the improvement of the labeling and ligation reactions. In the present case, the observed micellar catalysis effects could arise from two major factors (Figure 4-1-10 **B**): (i) an increase in the local concentration of both reactants; (ii) denaturation of the Rab7 C-terminus, resulting in exposure of the buried thiol group (Gitler et al., 1995). In addition, the high charge density at the micelle surface could enhance the polarization of the carbonyl thioester, thereby increasing its reactivity for ligation. A cationic detergent (cetyltrimethylammonium bromide; CTAB), was proposed to increase the thiol ionization and reduce the pK_a of dyes bound to the micelles, thereby enhance the reactivity of protein to a thiol-reactive dye labeling (Gitler et al., 1995; Montal and Gitler, 1973). Nevertheless, the analysis of the exact contribution of these effects on the conjugation and ligation efficiencies is quite speculative.

The lack of response of other dyes to the micelle mediated labeling reactions could be due to low affinity to the micelle, determined by the physical properties of

both dyes and detergents. To increase the labeling efficiencies of these dyes would require more extensive screening for detergents.

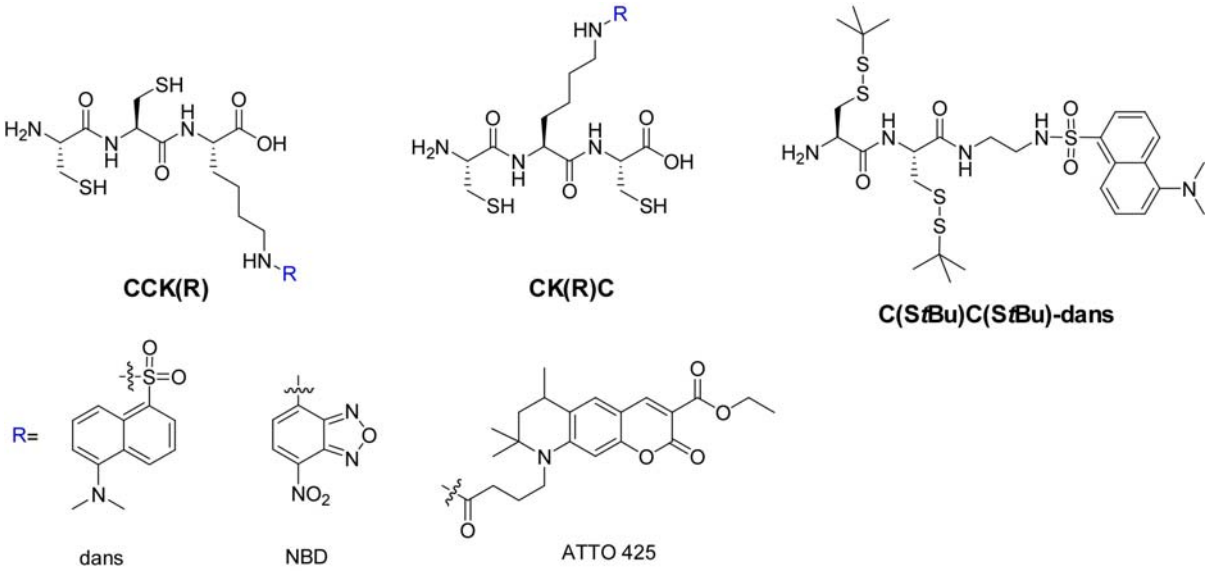

Figure 4-1-11. Fluorescent peptides. Fluorophores were linked to the peptides via either ε-amino group of lysine or C-terminal α-carboxyl group.

The resulting fluorescently labeled Rab7 thioester protein conjugates were ligated with either cysteine or Cys-Cys dipeptide synthesized by standard solid-phase peptide synthesis. Ligation of fluorescent conjugates with 40-50 equivalents of cysteine or Cys-Cys dipeptide proceeded quantitatively under standard ligation conditions, resulting in a fluorescent Rab7 conjugate family applicable for prenylation. Those fluorescent groups conjugated to Rab7 that give positive fluorescent signal changes upon Rab prenylation were selected for further investigation. Subsequently these fluorophores were coupled to a peptide containing two cysteine residues (see Figure 4-1-11, obtained from Novabiochem, EMD and Thermo Hybaid GmbH) via either ε-amino group of lysine or C-terminal α-carboxyl group. The ligation of a cluster of fluorescent peptides with Rab7 thioester further enriched the Rab cojugate family (see Table 4-1-3). The extent of ligation was typically 80-95% under standard ligation conditions, while the inefficient ligations were improved from 30% to 80% in the presence of the detergent micelle (see Figure 4-1-10 **A**).

S-*tert*-butyl protecting groups were cleaved *in situ* by excess MESNA during ligation (Durek et al., 2004a; Alexandrov et al., 2002; Tolbert and Wong, 2000). Upon completion of the labeling and ligation reaction, excess dye, peptide, detergents and additive (MESNA) were removed by dialysis and gel filtration. However, the purification of the labeled and ligated protein from unlabeled and unligated protein

turned out to be highly challenging. It was not possible to separate them by gel filtration and dialysis due to their close molecular weights. However, we assumed that the minor unlabeled and unligated protein would not significantly affect the activity of the sensors. This indeed turned out to be the case, as will be shown in the following section. Thus, in the initial screening for the sensors these contaminants were not removed.

4.1.2.4 Characterization of Rab7 fluorescent conjugates

Table 4-1-3. List of Rab7 fluorescent conjugates used in screening for prenylation sensors.

λ_{ex}/ nm	Rab7 conjugate C-terminus for single prenylation		Rab7 conjugate C-terminus for double prenylation			
	-2	-1	-2	-1	Sandwich	+1
340	C(dans)SC	SC(dans)C	C(dans)SCC	SC(dans)CC		SCCK(dans) SCCC-dans
379	C(Coum)SC	SC(Coum)C				
437	C(425)SC	SC(425)C	C(425)SCC	SC(425)CC	SCK(425)C	SCCK(425)
458	C(465)SC	SC(465)C				
490	C(NBD)SC	SC(NBD)C	C(NBD)SCC	SC(NBD)CC	SCK(NBD)C	SCCK(NBD)
506	C(BO)SC*	SC(BO)C*				
524	C(520)SC	SC(520)C				
552	C(Rhod)SC*	SC(Rhod)C*				
567	C(565)SC	SC(565)C				
569	C(I-BA)SC	SC(I-BA)C	C(I-BA)SCC	SC(I-BA)CC		
592	C(I-SO)SC	SC(I-SO)C	C(I-SO)SCC	SC(I-SO)CC		
615	C(610)SC	SC(610)C				
633	C(630)SC	SC(630)C				
648	C(650)SC	SC(650)C				
667	C(673)SC	SC(673)C				

dans: dansyl, Coum: coumarin, BO: BODIPY, 425: ATTO 425, 465: ATTO 465, 520: ATTO 520, 565: ATTO 565, Fluo: fluorescein, Rhod: rhodamine, 610: Dy610, 633: Dy 633, 648: Dy 648, 667: Dy 667. * Yield < 10%. The conjugates that were not reactive in *in vitro* prenylation are shown in blue. The conjugates that displayed florescence changes upon prenylation are shown in red.

The constructed Rab7 conjugate family is listed in Table 4-1-3. Their activities for prenylation were measured by a quantitative HPLC assay (Thoma et al., 2001c), which took advantage of the different mobilities of un-, mono- and doubly prenylated Rab7 on a reverse-phase C4 column. The Rab7 conjugates can be selectively and sensitively detected via their fluorescence, even in the case of co-elution with other components of the Rab prenylation reaction. Figure 4-1-12 shows an example of this

assay quantifying the activity of Rab7Δ3CCK(NBD). The shift of the elution peak to longer retention time after prenylation (Figure 4-1-12 **A**) indicates formation of prenylated products that were confirmed by mass spectroscopy (data not shown). As a control, the fluorescently labeled Rab7 thioesters that do not contain the prenylatable cysteines cannot be prenylated, and thus do not display a shift of mobility after the prenylation reaction (Figure 4-1-12 **B**).

Most of the Rab7 fluorescent conjugates could serve as substrates of RabGGTase, albeit with different efficiencies. However, Dy673 conjugates were not able to undergo prenylation (Table 4-1-3). These conjugates contain bulky fluorescent groups in the vicinity of the prenylation sites, which might influence the accessibility of the C-terminal cysteines to the geranylgeranyl moieties.

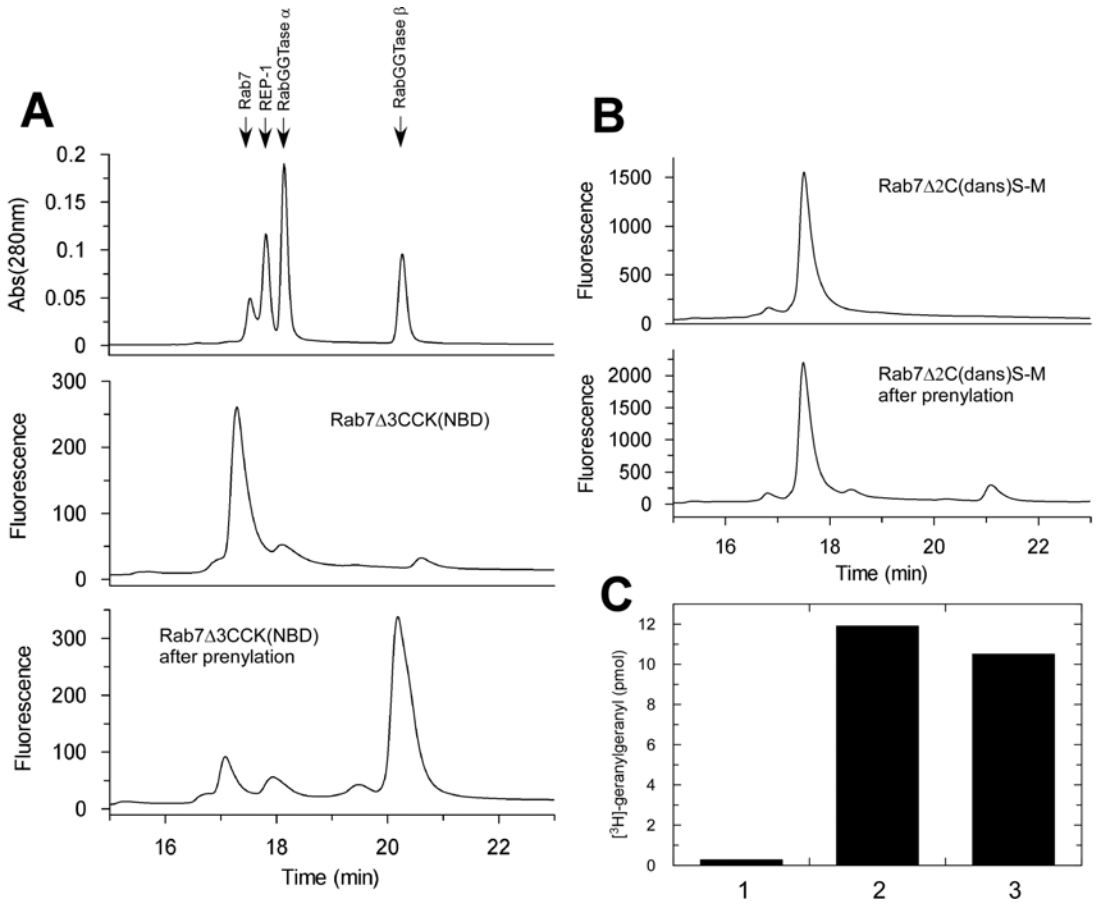

Figure 4-1-12. (**A**) The elution profile of a mixture of Rab7wt, REP-1 and RabGGTase resolved on the C-4 reversed phase column detected by absorption at 280 nm (top panel), the elution profile of a mixture of Rab7Δ3CCK(NBD) (17.3 min), RabGGTase and GGPP resolved on the same column using a fluorescence detector (Ex: 490 nm, Em: 535 nm) (middle panel), and the elution profile of an identical sample supplemented with REP-1 and incubated for 30 min at room temperature. The peak of Rab7Δ3CCK(NBD) shifted to 20.2 min was assigned as the doubly prenylated Rab7Δ3CCK(NBD) (bottom panel). (**B**) The elution profile of Rab7Δ2C(dans)S-M before and after prenylation detected by dansyl fluorescence (Ex: 340 nm, Em: 480 nm) (**C**) In vitro prenylation isotopic assay using (^{3}H) labeled GGPP. Incorporation of (^{3}H)-geranylgeranyl into wild-type Rab7 protein (lane 2) and Rab7Δ3CCK(NBD) (lane 3) catalyzed by RabGGTase. The reactions contained 100 pmol (^{3}H)-labeled

GGPP (2652 cpm/pmol), 10 pmol of Rab7:REP-1 complex and 10 pmol of mammalian RabGGTase. REP-1 was omitted in the control reaction (lane 1) containing wt Rab7.

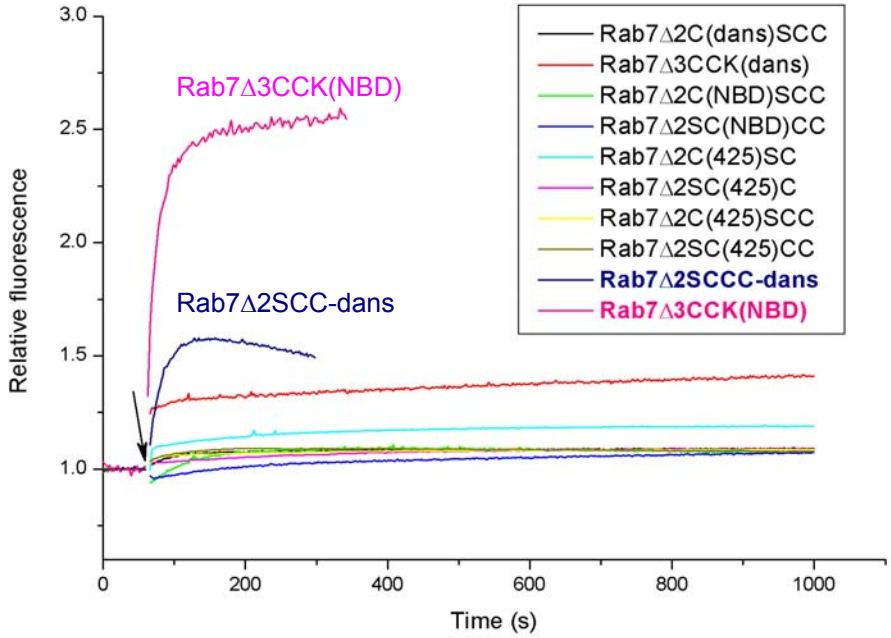

Figure 4-1-13. Time course of change in fluorescence seen upon mixing 100nM Rab7 fluorescent conjugates, REP-1 and RabGGTase with 10μM GGpp (the time point indicated by the arrow). Reactions were run at 20°C in prenylation buffer: 50 mM Hepes, pH7.2, 50 mM NaCl, 5 mMDTE, 2mM $MgCl_2$, 100μM GDP.

Only a small subset of the fluorescent conjugates that are capable of reporting prenylation was identified. These conjugates bear fluorescent groups such as dansyl, NBD and coumarin derivatives that are known to be environmentally sensitive, while some conjugates constructed from other fluorophores such as coumarin, BODIPY, I-BA and I-SO which have been used as sensitive reporters in protein studies did not display significant change in fluorescence upon prenylation. Interestingly, for a given fluorescent group some attachment sites are more effective in sensing prenylation than others. Among NBD conjugates, placing NBD at the +1 (with respect to the prenylation site) lysine side chain resulted in the highest sensitivity to prenylation, yielding a 2-fold fluorescence increase. Within the dansyl modified proteins, the conjugate compromising a dansyl group linked to the C-terminal α-carboxyl exhibits the best fluorescence enhancement (1.5-fold) upon prenylation. Other conjugates show only moderate changes in fluorescence upon prenylation (Figure 4-1-13).

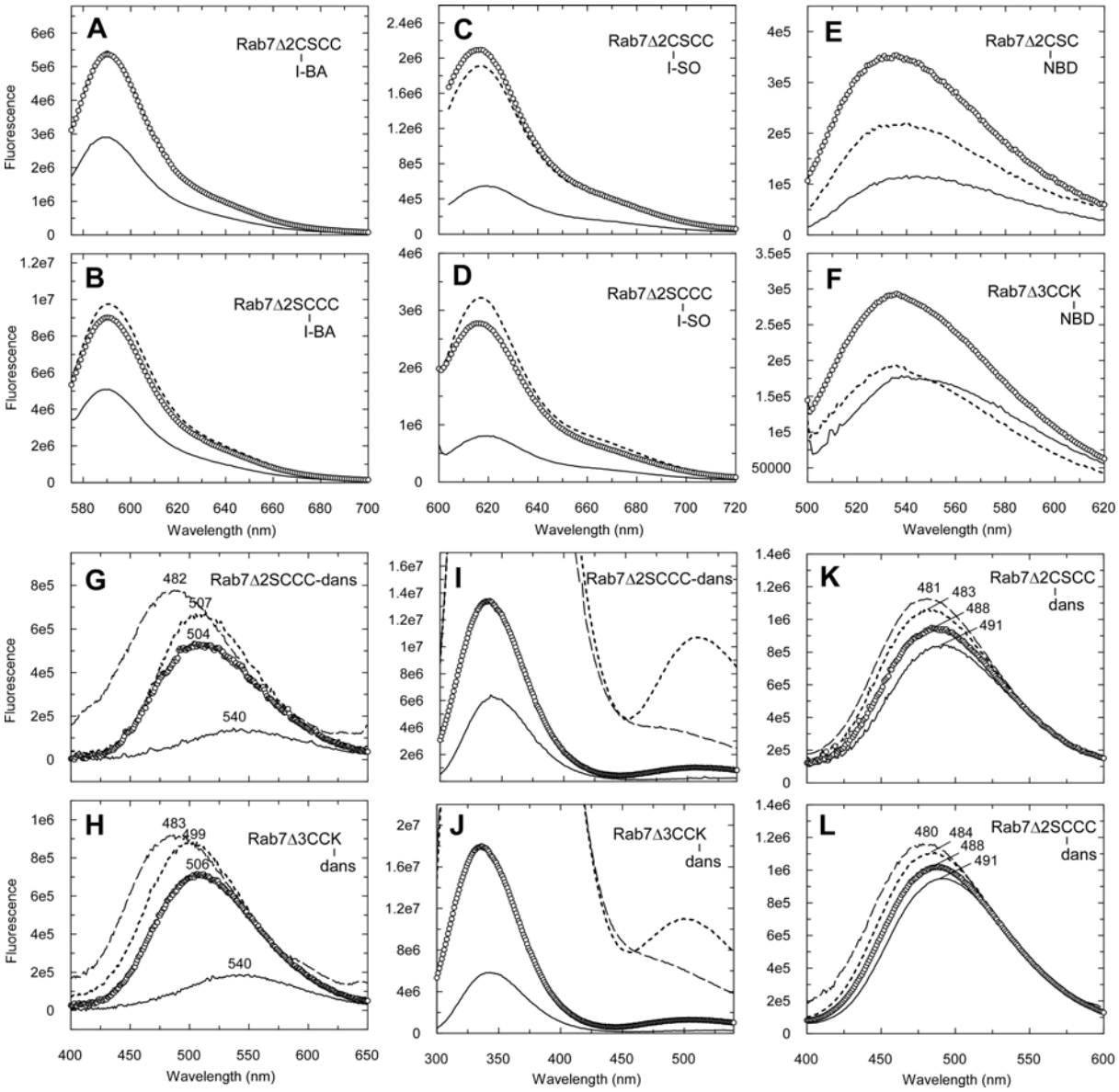

Figure 4-1-14. Emission spectra of Rab7 fluorescent conjugates (solid lines), the binary complexes with REP-1(open circles), and the ternary complexes with RabGGTase (dotted lines), and emission scan after prenylation (dashed lines, shown only in G-L). (**A**) Rab7Δ2C(I-BA)SCC, λ_{ex}=570nm. (**B**) Rab7Δ2SC(I-BA)CC, λ_{ex}=570nm. (**C**) Rab7Δ2C(I-SO)SCC, λ_{ex}=595nm. (**D**) Rab7Δ2SC(I-SO)CC, λ_{ex}=595nm. (**E**) Rab7Δ2SC(NBD)CC, λ_{ex}=495nm. (**F**) Rab7Δ3CCK(NBD), λ_{ex}=490nm. (**G**) Rab7Δ2SCCC-dans, λ_{ex}=333nm. (**H**) Rab7Δ3CCK(dans), λ_{ex}=340nm. (**I**) Rab7Δ2SCCC-dans, λ_{ex}=280nm. (**J**) Rab7Δ3CCK(dans), λ_{ex}=280nm. (**K**) Rab7Δ2C(dans)SCC, λ_{ex}=340nm. (**L**) Rab7Δ2SC(dans)CC, λ_{ex}=340nm.The concentration of each fluorescent protein conjugate was ca. 100 nM.

Despite the relatively low sensitivity to prenylation, some of the fluorescent conjugates were capable of sensitively reporting interactions between Rab, REP and RabGGTase. I-BA and I-SO Rab7 conjugates displayed 200% and 350% increase in fluorescence intensity, respectively, upon binding to REP-1, but only a limited change in fluorescence intensity upon assembly of the ternary Rab7:REP-1:RabGGTase complex (Figure 4-1-14 **A**-**D**). All NBD conjugates constructed here were able to

report on both binary Rab7:REP-1 and ternary Rab7:REP-1:RabGGTase complex formation, which typically resulted in 2-3 fold increase and 2-fold quenching in the NBD fluorescence, respectively (two examples are shown in Figure 4-1-14 **E**, **F**). The dansyl conjugates could respond to both interactions when either directly excited at 340 nm or via fluorescence resonance energy transfer (FRET) from tryptophan at 280 nm (Figure 4-1-14 **G**-**L**). Whereas several dansyl conjugates showed only a minor change in the emission spectra (Figure 4-1-14 **K**, **L**), the two with dansyl linked to the side chain of +1 lysine [Rab7Δ3CCK(dans)] and to α-carboxyl group (Rab7Δ2SCCC-dans) displayed dramatic enhancements in fluorescence intensity accompanied by a spectral shift upon interactions (Figure 4-1-14 **G**, **H**). Upon interaction with REP-1, Rab7Δ3CCK(dans) exhibited a 6-fold increase in the dansyl fluorescence at 504 nm as well as a blue shift of emission maximum from 540 nm to 506 nm. Binding of Rab7Δ2SCCC-dans to REP-1 resulted in a 5-fold fluorescence enhancement at 504 nm accompanied by a blue shift of λ_{max} from 540 nm to 504 nm. In contrast, only 130% increase in fluorescence intensity as well as minor emission shift was observed on binding of RabGGTase to REP-1 complexed with Rab7Δ3CCK(dans) or Rab7Δ2SCCC-dans, however, 10-fold fluorescence enhancement was observed in both cases using the FRET signal (Figure 4-1-14 **I**, **J**; 4-16 **F**). After prenylation, both Rab7Δ3CCK(dans) and Rab7Δ2SCCC-dans exhibited an 8-nm blue shift of the emission maximum as compared with those of ternary complexes (Figure 4-1-14 **G**, **H**).

The labeling position of I-SO, I-BA and NBD in the Rab7 conjugates did not significantly influence the character of their emission spectra as well as their sensitivity for the interactions (Figure 4-1-14 **A**-**F**). Nevertheless, when dansyl group was attached to Rab7 via the *N*-(2-sulfonylamino)alkyl group [ligation with DNS labeled peptides, CCK(dans) and CC-dans] instead of *N*-(2-aminoethyl)acetamido group (coupling with IAEDANS) (Figure 4-1-15), the emission maxima of the resulting conjugates shift from 490 nm (Figure 4-1-14 **K**, **L**) to 540 nm (Figure 4-1-14 **G**, **H**) with a concomitant decrease in fluorescence intensity. As a result, the former can report interactions and prenylation much more efficiently via either direct fluorescence or FRET.

The utility of the merocyanine dyes has been demonstrated by using them to build a biosensor that reported activation of camodulin in living cells (Hahn et al., 1992; Hahn et al., 1990) and an endogenous GTPase, Cdc42, *in vitro* (Toutchkine et

al., 2003) and *in vivo* (Nalbant et al., 2004). The S-SO (benzothiazole - benzothiophen-3-one-1,1-dioxide) labeled Wiskott Aldrich Syndrome Protein (WASP) molecule showed a 300% increase in fluorescence intensity without a change of emission maximum upon binding to GTP bound Cdc42. I-SO and I-BA biosensors that respond to the interactions with REP showed a similar character of fluorescent response to those of Cdc42 activation. The minimal change in the fluorescence maxima was supposed to be a result of the cyanine limit structure of the dyes by experimental and theoretical studies (Toutchkine et al., 2003; Han et al., 2003). The change in fluorescence intensity could be interpreted as the variation in hydrogen bonding of the dyes, which has been shown in cyanine (Soper and Mattingly, 1994), merocyanine (Liu et al., 2004; Onganer et al., 1993) and Nile Red (Cser et al., 2002). The properties of I-SO and I-BA biosensors, i.e. excitation at long wavelength, high quantum yield, high photostability and 2-3 fold increase in fluorescence intensity upon binding to REP make them suitable for *in vivo* applications.

The NBD and dansyl moieties are characterized by a high sensitivity of the emission to the polarity of the surrounding solvent, enabling their use as reporters in biophysical studies on proteins (Lakowicz, 1999). The increase in the fluorescent intensity as well as the blue shift of emission maximum observed upon interactions shown in Figure 4-1-14 **E**-**H** could be interpreted in terms of decrease in polarity of the microenvironment around the NBD (Gether et al., 1995) and dansyl (Hudson and Weber, 1973) group caused by a reduction in solvent accessibility. In NBD-conjugated maltose binding protein (Gilardi et al., 1997), ligand binding induced differences in spectral properties have been explained by a twisted intramolecular charge transfer (TICT) mechanism (Grabowski et al., 2003), wherein the NBD group is constrained into a conformation that prevents efficient relaxation of the excited state.

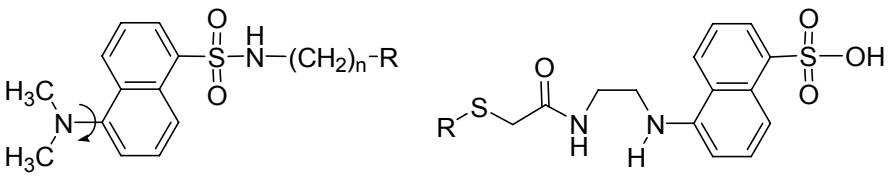

DNS **AEANS**

Figure 4-1-15. Two types of dansyl conjugates. R: other part of protein

As mentioned above, the linking format between dansyl and protein determined the sensitivity of the dansyl conjugates. Figure 4-1-15 shows two types of dansyl

conjugates dependent on the linkage through either tertiary amino group (AEANS) or sulfonyl group (DNS). The AEANS conjugate is a result of IAEDANS attachment to a cysteine thiol, while the DNS conjugate is typically generated by coupling dansyl chloride to a primary amino group on the side chain of a peptide. The observed much higher sensitivity of the DNS conjugates as compared with that of the AENS conjugates could be rationalized in terms of a TICT mechanism. DNS has been suggested to relax from the excited state via TICT, where a pair of charge transfer groups, donor and acceptor, are present (Ren et al., 1999) (Grabowski et al., 2003). In this case the donor is the tertiary amino group and the acceptor is the sulfonyl group (Figure 4-1-15). In Rab7-DNS, the dimethylamino group is relatively free to rotate and hence the relaxation of the excited state of DNS through TICT is efficient, representing emission at low energy (λ_{em}=540nm, A* state). While in Rab7-AEANS, the conjugated protein molecule increases the viscous drag and is sufficient to inhibit the rotation of the amino group of AEANS during its excited state lifetime, thus AEANS conjugates exhibit fluorescence at high energy (λ_{em}=490nm, B* state) as compared with that of free IAEDANS in the same solution (λ_{em}=520nm). The subsequent interaction of Rab7-DNS with REP and RabGGTase could result in a restriction of the rotational mobility of DNS so as to bring about an increase in the emission energy characterized by a blue shift of emission maximum.

In the light of this idea, DNS would be more useful as a reporter that AEANS, leaving aside the concern of the facility in chemical modification. Besides the observation in this study, DNS has been widely used in the construction of highly sensitive biosensors for Zn^{2+} binding (Walkup and Imperiali, 1996), farnesylation (Pompliano et al., 1992a), DNA interaction (Barawkar and Ganesh, 1995), etc. In contrast, AEANS conjugates display relatively low sensitivity in their applications (Hammarstrom et al., 2001; Post et al., 1994).

On account of the photophysical properties of NBD and dansyl, their usefulness for *in vivo* studies is limited. However, NBD and dansyl conjugates respond to REP and RabGGTase binding by undergoing highly sensitive spectral shifts and changes in fluorescence intensity, making them useful in the characterization of the interactions of the prenylation machinery *in vitro* (see Chapter 4.3).

The sensitive change in fluorescence upon the formation of complexes can be used to quantitatively analyze the interactions of the binary and the ternary complexes. As shown in Figure 4-1-16, titration of REP-1 to a fixed concentration of

the Rab7 fluorescent conjugates or titration of RabGGTase to the Rab7:REP-1 complexes resulted in a dose-dependent change in fluorescent intensity or FRET signal, which could be utilized to determine the equilibrium constants of the interactions.

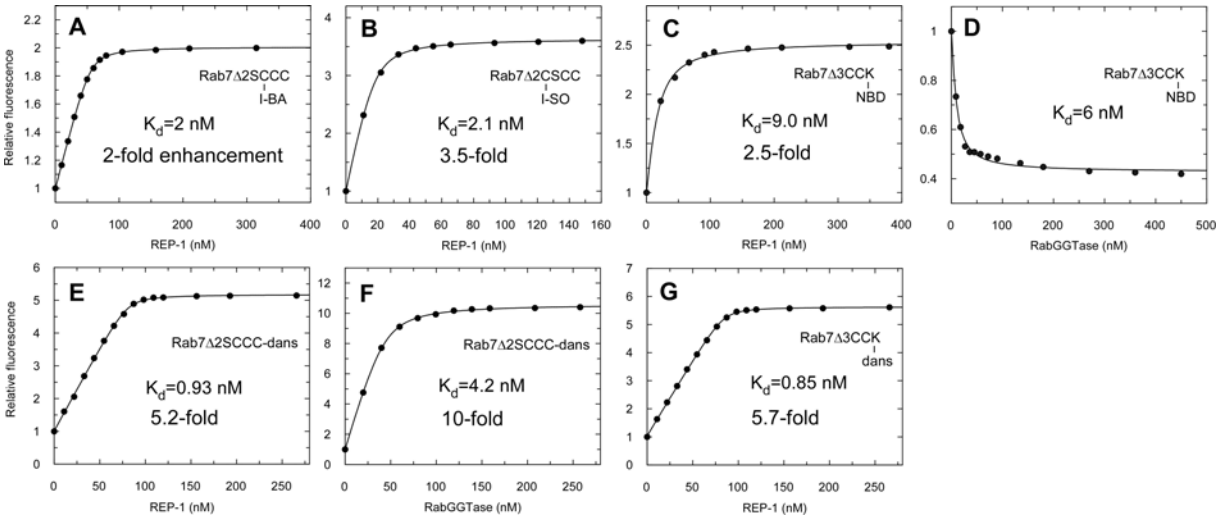

Figure 4-1-16. (**A**) Titration of REP-1 to Rab7Δ2SC(I-BA)CC (λ_{ex}=570 nm, λ_{em}=590 nm). (**B**) Titration of REP-1 to Rab7Δ2C(I-SO)SCC (λ_{ex}=595 nm, λ_{em}=615 nm). (**C**) Titration of REP-1 to Rab7Δ3CCK(NBD) (λ_{ex}=490 nm, λ_{em}=535 nm). (**D**) Titration of RabGGTase to the Rab7Δ3CCK(NBD):REP-1 complex (λ_{ex}=490 nm, λ_{em}=535 nm). (**E**) Titration of REP-1 to Rab7Δ2SCCC-dans (λ_{ex}=333 nm, λ_{em}=504 nm). (**F**) Titration of RabGGTase to the Rab7Δ2SCCC-dans:REP-1 complex using the FRET signal (λ_{ex}=280 nm, λ_{em}=508 nm). (**G**) Titration of REP-1 to Rab7Δ3CCK(dans) (λ_{ex}=340 nm, λ_{em}=504 nm). The solid lines show the fits to a quadratic equation as described in Chapter 8.1.1 to give K_d values. To each fluorescence titration, corrections were made for background signal from Rayleigh scattering of the buffer and the non-specific background fluorescence of titrating components. All reactions were performed at 20°C in titration buffer (50 mM Hepes, pH7.2, 50 mM NaCl, 5 mM DTE).

The dissociation constants, K_d, extracted from the binding curves are summarized in Table 4-1-4. Because there is a thermodynamic linkage between the protein binding and the interaction of the coupled fluorophore with the protein, the fluorophore is expected to change the intrinsic dissociation constant. The change in affinity imparted by the fluorophore is dependent on its nature and its location in the protein. The two DNS conjugates Rab7Δ2SCCC-dans and Rab7Δ3CCK(dans) display higher affinity to REP-1 than wild type Rab7. The others exhibit lower affinity to REP-1 than the wild type, with the ATTO425 conjugates showing the lowest affinity. However, the conjugation of fluorophores to Rab7 increases the affinities of the ternary complexes, which might result from the interaction of the conjugated fluorophore with RabGGTase. Interestingly, among these conjugates the most sensitive sensors (i.e. showing the highest fluorescence change, Figure 4-1-13) for

prenylation, Rab7Δ3CCK(NBD) (2-fold) and Rab7Δ3CCK(dans) (1.5 fold), show the highest affinity to REP and RabGGTase, presumably coincidently.

Table 4-1-4 K_d values of binary and ternary complexes of Rab7 fluorescent conjugates determined by fluorescence titration as shown in Figure 4-1-16.

Construct	K_d (Rab:REP-1) /nM	K_d (Rab:REP-1:RabGGTase) /nM
Rab7wt*	1	121
Rab7Δ2C(dans)SC	14	44
Rab7Δ2SC(dans)C	2.4	14
Rab7Δ2SCCC-dans	0.94	3.9
Rab7Δ3CCK(dans)	0.85	ND
Rab7Δ2C(NBD)SC	2.2	63
Rab7Δ2SC(NBD)C	9.5	33
Rab7Δ3CCK(NBD)	9.0	6.8
Rab7Δ2C(425)SC	16	ND
Rab7Δ2SC(425)C	83	ND
Rab7Δ2SC(I-BA)CC	2.0	ND
Rab7Δ2C(I-SO)SCC	2.1	ND

* see ref (Alexandrov et al., 1999; Alexandrov et al., 1998), ND: not determined

4.1.3 NBD-FPP as a sensitive fluorescent sensor for Rab prenylation

In spite of the limited success in the prenylation sensors based on Rab proteins, several useful lessons could be extracted: first, the modified set-up for the concept of intramolecular fluorescence enhancement, i.e. introduction of a fluorophore in the vicinity of the Rab prenylation sites, yielded only moderately efficient sensors for Rab prenylation, which only gave fluorescence intensity changes not exceeding a factor of 2. This can be rationalized in terms of the probability that the hydrophobic geranylgeranyl groups are already buried deeply in REP in order to increase the solubility of the prenylated Rab proteins (Rak et al., 2004). Second, among constructed fluorescent sensors, semi-synthetic Rab with a small environmentally sensitive fluorescent group like NBD or DNS conjugated in the proximity of the C-terminal cysteine showed the best fluorescence enhancement upon prenylation. This indicates that NBD or DNS could be good candidates for the construction of other types of fluorescent sensor in the context of the prenylation machinery. In addition, construction of Rab protein conjugates required labor-intensive screening for fluorophores and labeling positions, and moreover, this kind of sensor is based on such a specific Rab construct that it cannot be a versatile reporter for prenylation of other Rab GTPases. Hence, we devised an alternative strategy in which a fluorophore is incorporated into the soluble isoprenoid donor which is expected to undergo marked changes of hydrophobicity during the prenylation reaction. Towards this goal we prepared a fluorescent analogue of geranylgeranyl pyrophosphate, {3,7,11-trimethyl-12-(7-nitro-benzo[1,2,5]oxadiazo-4-ylamino)-dodeca-2,6,10-trien-1} pyrophosphate (NBD-FPP) in collaboration with Prof. Dr. Waldmann in MPI Dortmund and demonstrated that it serves as a sensitive sensor for Rab prenylation.

4.1.3.1 A sensitive, real-time fluorometric assay for RabGGTase activity

NBD-FPP with an NBD group coupled to a C-15 farnesyl moiety approximately mimics the length of a C-20 native lipid substrate, GGPP (see Figure 4-1-17 **A**). As shown in Figure 4-17 **B**, addition of RabGGTase to a solution of NBD-FPP resulted in fluorescence quenching by 70% with a concurrent 8-nm blue shift of emission maximum (from 547 to 539nm). Addition of an excess of GGPP to the mixture

resulted in a reversal of the signal change and return of the fluorescence to the original level, indicating that the fluorescence change indeed reflected specific interaction of the developed compound with the active site of the enzyme (data not shown). The sensitive changes in fluorescence allowed us to determine the affinity of the GGPP analogue for RabGGTase. Titration of NBD-FPP with RabGGTase is shown in Figure 4-1-17 **C** to give K_d = 73 ± 2 nM.

The titration was subsequently carried out under competitive conditions to determine the K_d for the interaction of RabGGTase with its natural substrate GGPP. In this experiment, 200 nM NBD-FPP was mixed with 100 nM GGPP and the resulting mixture was titrated with increasing concentrations of RabGGTase. As shown in Figure 4-1-17 **D**, there is an initial lag in the fluorescence decrease. This is explained by GGPP binding more strongly than NBD-FPP to the enzyme, initially resulting in the formation of a fluorescently silent complex. However, at higher RabGGTase concentrations, the enzyme forms a complex with NBD-FPP, causing a decrease in fluorescence intensity. The data were fitted numerically using the program SCIENTIST^{TM} and led to a K_d value of 0.85 nM (for competitive titration model see Appendix 6.2). The K_d value of 0.83 nM for GGPP interaction with RabGGTase was also determined using another fluorescent isoprenoid mant-FPP, which displays fluorescene enhancement upon binding to RabGGTase. This shows that RabGGTase bound its lipid substrate 10 times more tightly than was previously determined using mant-FPP as a reporter [K_d(GGPP:RabGGTase) = 8 nM] (Thoma et al., 2000). The discrepancy could arise from the systematic errors.

The fluorescence titrations show that RabGGTase binds NBD-FPP ca. 70-fold more weakly than it binds GGPP. This is not surprising, since the fluorescent reporter group often impairs binding of the modified substrate molecule, as also observed in fluorescently labeled Rab proteins (see section 4.1.2.4). NBD-FPP binds RabGGTase (K_d=73nM) with a affinity similar to that FPP does (K_d=60nM) (Thoma et al., 2000), suggesting that NBD does not significantly compensate for the affinity of phosphoisoprenoid, in other words, the phosphoisoprenoid plays a dominant role in the contact with the RabGGTase site. It has been suggested that the length of the isoprenoid correlates with the affinity to RabGGTase (Thoma et al., 2000). Therefore, it is the shortening of the isoprenoid chain in NBD-FPP that probably leads to the decrease of affinity.

Following the observation that NBD-FPP can bind to prenyltransferases in a mode similar to that of native phosphoisoprenoids, we set out to determine whether these compounds could also serve as lipid donors for these enzymes. To this end, we performed an *in vitro* prenylation reaction in which enzyme was mixed with its corresponding fluorescent isoprenoid substrate and Rab7 GTPase. Control samples were supplemented with an excess of GGPP that would compete with the fluorescent analogues and thus yield nonfluorescent prenylated GTPases. The reaction was allowed to proceed for 1 h at room temperature and was quenched by addition of SDS-PAGE sample buffer, after which the samples were resolved on a 15% SDS-PAGE gel and scanned for fluorescence using a laser fluorescent image reader followed by Coomassie blue staining. As can be seen in Figure 4-1-17 **E**, under these conditions incubation of RabGGTase with its protein substrate led to emergence of a fluorescent band corresponding to the prenylated Rab7. No fluorescent product was generated when REP-1 was omitted. As expected, the reaction was strongly inhibited by excess GGPP (Figure 4-1-17 **E**). The resulting product was further confirmed by HPLC and mass spectroscopy (not shown). Therefore, we conclude that the observed fluorescent Rab7 GTPase does indeed represent the specific product of the prenylation reaction. NBD-FPP and NBD-GPP, the fluorescent analogue of FPP (farnesyl pyrophosphate), were also found earlier to be efficient lipid donors for GGTase-I and FTase, respectively (Dursina et al., 2006).

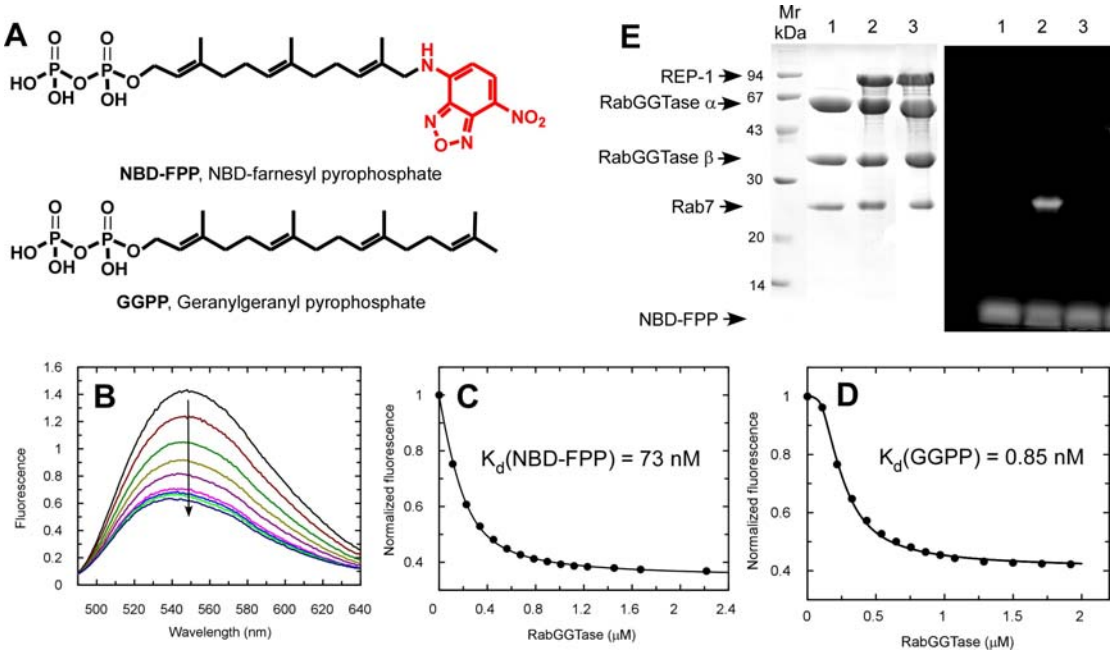

Figure 4-1-17. (**A**) Fluorescent analogue of GGPP, NBD-FPP. (**B**) Emission spectra of 400nM NBD-FPP in the absence (black line) and the presence of increasing concentrations of RabGGTase as

indicated by arrow. λ_{ex}= 479 nm. (**C**) Titration of 200nM of NBD-FPP with increasing concentrations of RabGGTase (exciation at 479 nm, emission at 547 nm). The data were fitted to a quadratic equation as described in Chapter 8.1.1, during the simulation the concentration of NBD-FPP was kept constant at 0.2 µM to give K_d value. (**D**) Co-titration of a mixture of 200nM NBD-FPP and 100 nM GGPP with RabGGTase. The K_d value for GGPP was obtained by simulation with a competitive titration model where the K_d for NBD-FPP determined in C was fixed. (**E**) Incorporation of NBD-FPP to Rab7 upon in vitro prenylation resolved by SDS-PAGE (left panel: Coomassie blue staining, right panel: fluorescence scan). Lane 2, prenylation in the presence of 5 µM Rab7, REP-1 and RabGGTase initiated with 15µM NBD-FPP for 1h; lane1, control reaction where REP-1 was omitted; lane3, control reaction where 25 µM GGPP was added to compete with the fluorescent lipid substrate.

To assess the sensitivity of this method, decreasing amounts of the prenylation mixture were loaded onto the SDS-PAGE gel and analyzed by fluorescent scanning. The highly sensitive fluorescent signal excited by the laser makes it possible to detect as little as 6 fmol of fluorescent protein, indicating that the developed methods could be significantly scaled down (data not shown). Fluorescent scanning and quantification of the SDS-PAGE gels loaded with increasing amounts of NBD-FPP showed that the fluorescence intensity of the NBD-FPP bands is a linear function of the concentration up to 400 pmol (Figure 4-1-22 **A**), indicating no “inner filter effect” (for details, see section 4.1.3.3) over the range of fluorescent conjugate concentrations used in the reactions. This suggests that NBD-FPP can be used in an SDS-PAGE assay for RabGGTase activity, which will be discussed in section 4.1.3.3.

Although very sensitive, the SDS-PAGE assay using NBD-FPP as a fluorescent substrate is discontinuous, laborious, and poorly amenable to parallelization. Continuous fluorescence assays are much better suited for high-throughput screening and characterization of potential inhibitors. Therefore, we sought to develop a continuous fluorometric assay for Rab prenylation based on NBD-FPP.

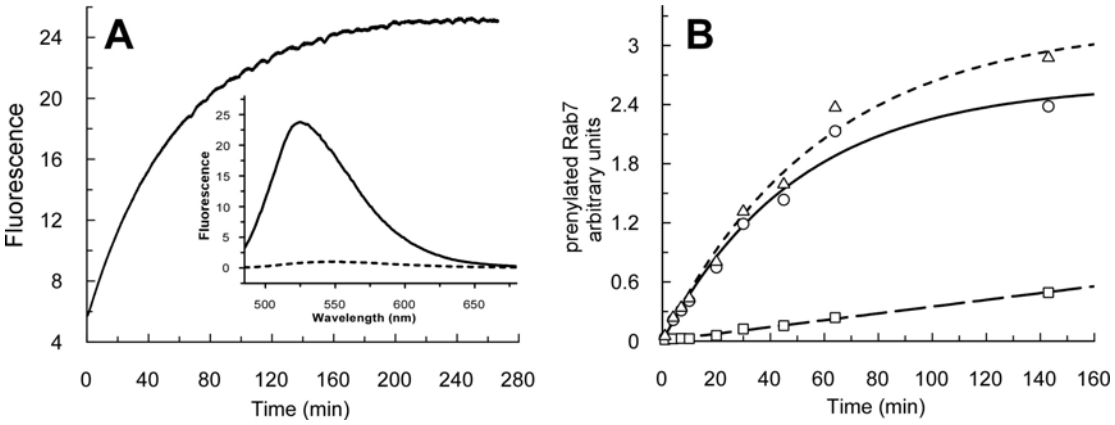

Figure 4-1-18 (**A**) Time-course of fluorescence change upon prenylation catalyzed by RabGGTase (0.02µM) on Rab7:REP-1 complex (6 µM) in the presence of NBD-FPP (4 µM) at 37°C. Fluorecence was recorded at 520 nm. Assay buffer: 50 mM Hepes, pH7.2, 50 mM NaCl, 5mM DTE, 2mM $MgCl_2$, 10µM GDP. Inset: Emission spectra (λ_{ex}= 479 nm) of 1 µM substrate NBD-FPP (dashed line) and 1 µM product mono-NBD-farnesylated Rab7:REP-1 complex (solid line). (**B**) HPLC assayed time-

dependent generation of mono-NBD-farnesylated Rab7 (open circles), doubly NBD-farnesylated Rab7 (open square) and total NBD-farnesylated Rab7 (open triangles) in the prenylation reaction catalyzed by RabGGTase (0.02μM) using the Rab7:REP-1 complex (1 μM) in the presence of NBD-FPP (4 μM) at 37°C.

To this end, we analyzed the fluorescence changes of the *in vitro* prenylation reaction supplemented with NBD-FPP. As can be seen in Figure 4-1-18 **A**, upon incorporation of the NBD-farnesyl group into Rab proteins, an increase in fluorescence intensity over time with excitation at 479 nm and emission at 520 nm was observed. The correlation of the reaction progress with the fluorescence increase was confirmed by HPLC analysis (Figure 4-1-18 **B**). Fluorescence emission spectra taken before and after the reaction showed a shift of the emission maximum from 547 to 525 nm. To determine the extent of fluorescence enhancement, mono-NBD-farnesylated Rab7 (Rab7_NF):REP-1 was prepared by *in vitro* prenylation essentially as described before but using the Rab7C207S single cysteine mutant and NBD-FPP as an isoprenoid donor (Kalinin et al., 2001). The product was characterized by MALDI-TOF and fluorescence scanning (Chapter 6.4.3). Rab7_NF:REP displays an emission maximum at 525 nm, i.e. the same as that of the products after multi-turnover NBD-farnesylation reactions. A 23-fold enhancement of fluorescence intensity at 525 nm was observed when the same concentration of Rab7_NF:REP and NBD-FPP were used (Figure 4-1-18 **A** inset).

This dramatic increase in fluorescence can be interpreted as a consequence of the Rab-conjugated NBD-farnesyl group's binding into the lipid binding pocket of REP. This interpretation was ascertained by the finding that Rab7-NBD-farnesyl displays a 10-fold enhancement in fluorescence upon binding to REP-1 accompanied by a blue shift of emission maximum from 545 nm to 525 nm (see Chapter 4.4, Figure 4-1-40 **A**). In this case, REP would play a dual role as both Rab chaperone and conjugated fluorescent isoprenoid trapper, in the process enhancing its fluorescence (Rak et al., 2004; Pylypenko et al., 2003; Thoma et al., 2001b). This idea is indirectly supported by the observation that GGTase-I mediated prenylation of RhoA with NBD-FPP resulted in only a moderate fluorescence increase (data not shown).

4.1.3.2 Characterization of NBD-farnesyltation

In order to gain insight into the details of the NBD-farnesylation reaction, a previously established HPLC based method was used to simultaneously measure the absolute amounts of unprenylated, mono- and di-NBD-farnesylated Rab7 (Thoma et al., 2001c), which was also used in characterization of prenylation of fluorescent Rab7 conjugates (see section 4.1.2.4).

For investigation of single turn-over reaction kinetics, at different time intervals, a constant amount (40 μl) of the reaction mixture was withdrawn and mixed with an equal volume of quenching buffer containing 0.4% TFA and 10% glycerol. Addition of TFA reduced the pH to 2-3, which is sufficient to stop enzyme activity and quench the reaction. The presence of glycerol is to prevent the protein from aggregation and precipitation under acidic conditions. The quenched reaction samples were subjected to reverse-phase chromatography. Identification of the elution peaks corresponding to Rab7 and its NBD-farnesylated products was carried out using purified standards and ESI-mass spectroscopy. Rab7, REP and RabGGTase were detected by absorbance at 280 nm. As can be seen in Figure 4-1-19 **A**, **B**, mono-NBD-farnesylated Rab7 (Rab7_NF) at 17.7 min co-eluted with REP-1 and di-NBD-farnesylated Rab7 (Rab7_NFNF) at 18.4 min co-eluted with the RabGGTase alpha subunit, but they can be specifically detected by fluorescence.

The primary HPLC data (Figure 4-1-19 **A**, **B**) analysis was performed by integrating the peak areas of absorbance at 280 nm for Rab7 and the fluorescence intensity for mono- and di-NBD-farnesylated Rab7. The data at each individual time point were subsequently processed by normalizing against an internal standard. In this case, the beta subunit of RabGGTase (retention time: 20.1 min) that gave a strong enough signal and did not co-elute with any other molecule in the system was used as an internal standard.

To obtain individual prenylation rate constants, the experiments were carried out using concentrations of Rab7, REP, RabGGTase, NBD-FPP far above their respective K_d values (Alexandrov et al., 1999; Alexandrov et al., 1998). Thus, even if dissociation of substrate and intermediate is mandatory, re-association should be fast enough not to be rate limiting, ensuring that the observed rate constants represent the prenylation reaction steps. Essentially identical observed rate constant for the decay of Rab7 during prenylation were observed when 4 μM Rab7:REP, RabGGTase and 20 μM NBD-FPP were used (k_{obs} = 0.12 min^{-1} or 0.0021 s^{-1}) instead of 1 μM Rab7:REP, RabGGTase and 2 μM NBD-FPP (k_{obs} = 0.11 min^{-1} or 0.0018 s^{-1}),

indicating that prenyl transfer is slower than binding of substrate to RabGGTase. In a typical pseudo first order consecutive reaction S→I→P (S: substrate, I: intermediate, P: product), the substrate decays with a transient increase and then decay of the intermediate and the emergence of the product (see model in Scheme 4-2).

Scheme 4-2.

$$Rab7{:}REP{:}RabGGTase + NBD\text{-}FPP \xrightarrow{k_1} Rab7\_NF{:}REP{:}RabGGTase$$

$$Rab7\_NF{:}REP{:}RabGGTase + NBD\text{-}FPP \xrightarrow{k_2} Rab7\_NFNF{:}REP{:}RabGGTase$$

However, in the reaction system containing 1 μM protein substrate - Rab7:REP-1 complex, 2 μM lipid substrate - NBD-FPP and 1 μM enzyme - RabGGTase, substrate Rab7 decayed accompanied by a saturable increase of both mono- and di-NBD-farnesylated Rab7 (Figure 4-1-19 **C**). This indicated that NBD-FPP was so limited as to be consumed before Rab7 and Rab7_NF were fully transformed to Rab7_NF and Rab7_NFNF respectively. Therefore, the pseudo first order treatment cannot be applied in the model, and the reversible equilibrium between substrates and enzyme should be taken into account between the prenylation reaction steps, as described in Scheme 4-3.

Scheme 4-3.

$$Rab7{:}REP + RabGGTase \underset{k_{-1}}{\overset{k_1}{\rightleftharpoons}} Rab7{:}REP{:}RabGGTase$$

$$Rab7{:}REP{:}RabGGTase + NBD\text{-}FPP \underset{k_{-2}}{\overset{k_2}{\rightleftharpoons}} Rab7{:}REP{:}RabGGTase{:}NBD\text{-}FPP$$

$$Rab7{:}REP{:}RabGGTase{:}NBD\text{-}FPP \xrightarrow{k_3} Rab7\_NF{:}REP{:}RabGGTase$$

$$Rab7\_NF{:}REP{:}RabGGTase \underset{k_{-4}}{\overset{k_4}{\rightleftharpoons}} Rab7\_NF{:}REP + RabGGTase$$

$$Rab7\_NF{:}REP{:}RabGGTase + NBD\text{-}FPP \underset{k_{-5}}{\overset{k_5}{\rightleftharpoons}} Rab7\_NF{:}REP{:}RabGGTase{:}NBD\text{-}FPP$$

$$Rab7\_NF{:}REP{:}RabGGTase{:}NBD\text{-}FPP \xrightarrow{k_6} Rab7\_NFNF{:}REP{:}RabGGTase$$

$$Rab7\_NFNF{:}REP{:}RabGGTase \underset{k_7}{\overset{k_{-7}}{\rightleftharpoons}} Rab7\_NFNF{:}REP + RabGGTase$$

Based on this model, rate constants were extracted from the time traces of Rab7, Rab7_NF and Rab7_NFNF using a global-fitting approach through numerical

integration according to a set of differential equations (see Appendix 6.4). Since the equilibrium constants between Rab7:REP and RabGGTase (Alexandrov et al., 1999), NBD-FPP and RabGGTase (Figure 4-1-17 **C**), Rab7_NF:REP and RabGGTase (Figure 4-1-21) have been determined independently, during simulation these parameters were kept constant to allow the rate constants of prenylation to be fitted.

This model resulted in an excellent fit using the program Scientist^{TM} (MicroMath Software) giving k_3 = 0.11±0.0089 min^{-1} (0.0019 s^{-1}) for the first prenyltransfer step, k_6 = 0.12±0.012 min^{-1} (0.0021 s^{-1}) for the conversion of mono-NBD-farnesylated Rab7 into doubly NBD-farnesylated Rab7, and an effective (i.e. fitted) NBD-FPP concentration of 0.93 µM (Figure 4-1-19 **C**). It is not surprising that the effective NBD-FPP concentration is 2-fold lower than the nominal concentration. TLC (silica gel Thin Layer Chromatography) analysis of NBD-FPP showed that storage of NBD-FPP in ammonium carbonate buffer for long periods led to partial hydrolysis (data not shown). Moreover, REP expressed in the baculovirus system has been found to have some phosphatase contamination resulting in degradation of pyrophosphate (Pylypenko et al., 2003). Thus, it is possible that NBD-FPP was partially degraded during the course of the reaction.

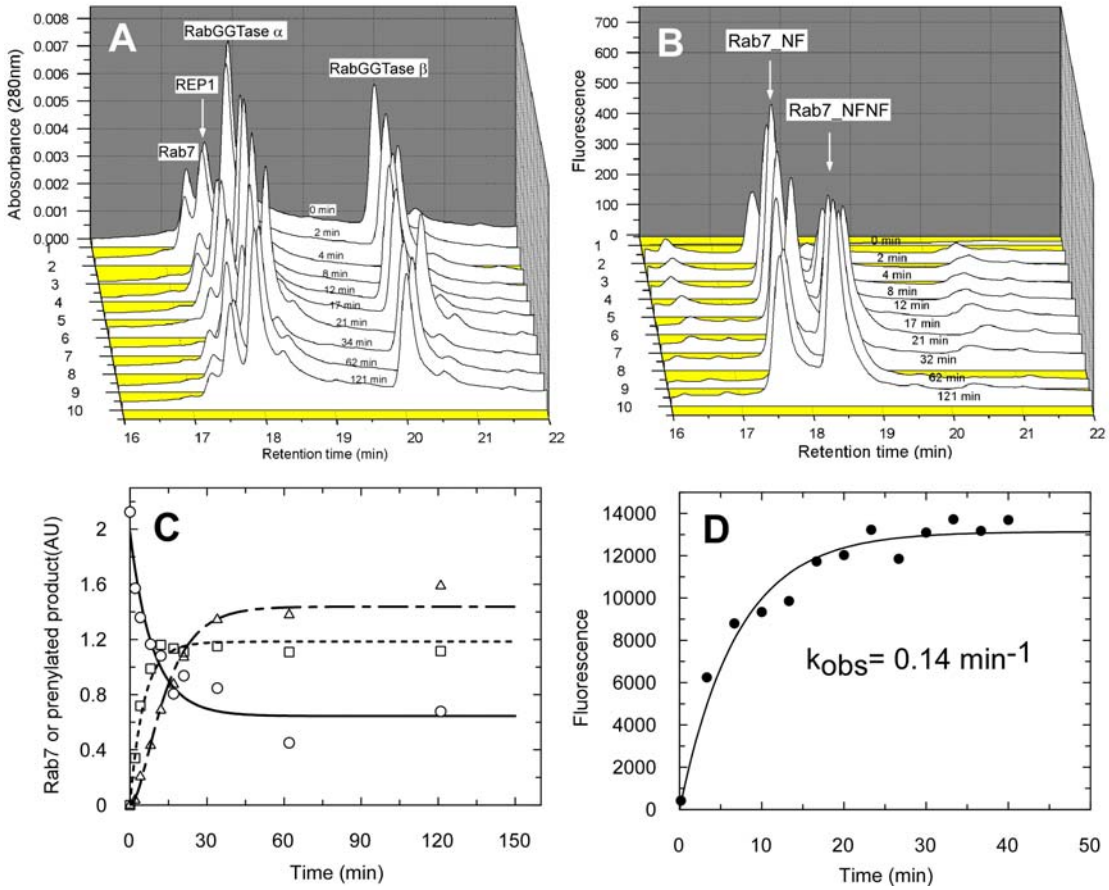

Figure 4-1-19. HPLC elution profile of the *in vitro* NBD-farnesylation reaction at defined time intervals detected by absorbance at 280 nm (**A**) and fluorescence with λ_{ex}=490nm, λ_{em}=535nm (**B**). Reaction was performed using 1 μM Rab7, REP-1 and RabGGTase, and 2 μM NBD-FPP at 25°C. As indicated, the peak for Rab7 at 17.4 min decreases, while the peaks for Rab7_NF at 17.7 min and Rab7_NFNF at 18.4 min increase and eventually saturate. (**C**) Kinetics and global fitting of unprenylated Rab7 (open circle), mono-prenylated Rab7 (open square), and doubly prenylated Rab7 (open triangle) in the *in vitro* NBD-farnesylation reaction. Data were processed based on peak intensity shown in **A** and **B**. The fits (solid, doted, and dashed line respectively) shown are based on numerical simulation using the model shown in Scheme 4-3, giving k_3 = 0.11±0.0089 min^{-1} for the first prenyltransfer step, k_6 = 0.12±0.012 min^{-1} for the conversion of Rab7_NF into Rab7_NFNF. (**D**) SDS-PAGE based assay for *in vitro* NBD-farnesylation (2 μM Rab7:REP-1, 3 μM RabGGTase, 40 μM NBD-FPP) at 25°C gives an observed rate constant. The solid line showed the fit to a single exponential function.

To determine the NBD-farnesylation reaction rate using an independent method, a quantitative SDS-PAGE based assay as shown in 4.1.3.1 was utilized, where at different time intervals an aliquot of reaction mixture was withdrawn, quenched by SDS-sample buffer and resolved by SDS-PAGE. Quantitative scanning of the gel by laser fluorescence reader led to the profile of time-dependent incorporation of NBD-farnesyl into Rab7, giving the observed rate constant (k_{obs} = 0.14±0.016 min^{-1}, or 0.0024±0.0003 s^{-1}) (Figure 4-1-19 **D**). This result is consistent with those determined by HPLC assay.

The kinetic data revealed that NBD-farnesylation of Rab7 is ca. 84-fold slower for the prenylation of the first cysteine and 19-fold slower for the prenylation of the second cysteine than in the case of native substrate (Thoma et al., 2001c). Since these rate constants represent the prenyl transfer step of the reaction, the reduced affinities of lipid substrate and intermediate do not contribute to the lower rate constants for prenyl transfer. However, the method used here does not distingusih the sub-steps in prenyl transfer, such as conformational changes before and/or after prenylation chemistry (condensation of the cysteine thiol with the prenyl group). So the critical step responsible for the reduced rate of prenyl transfer is still unclear. As proposed by a molecular ruler mechanism for prenyltransferases (Liang et al., 2002), FTase transfers only FPP efficiently but not GGPP, because the C1 of 20-carbon GGPP is out of reach of the catalytic center Zn^{2+}, while FPP still serves as a moderately effective substrate of GGTase-I because its diphosphate moiety can be located in the vicinity of Zn^{2+}. Conjugation of FPP to peptide substrates catalyzed by GGTase-I occurs 37-fold slower (0.015 s^{-1}) than the analogous geranylgeranylation reaction (0.56 s^{-1}) (Yokoyama et al., 1997). In contrast, FPP is transferred by RabGGTase with a similar observed rate constant to that of GGPP (Thoma et al., 2000). The identical rate for the first and the second NBD-farnesyl transfer indicates

that the impaired rates could be due to the change of geometry of NBD-FPP, which also alters the prenylation preference of two C-terminal cysteines.

The observed NBD-farnesylation reaction rate of the single cysteine mutant Rab7C207S (Rab7CSS, k_{obs}=8.4±0.1×10^{-4} s^{-1}) is ca. 3-fold faster than that of Rab7C205S (Rab7SSC, k_{obs}=2.8±0.1×10^{-4} s^{-1}) (Figure 4-1-20). Essentially the same rate constants were obtained when saturating concentrations of protein substrate and NBD-FPP were used in the SDS-PAGE assay (Figure 4-1-20 **B**), which indicates that NBD-farnesyl transfer is rate limiting, and thus the rate of NBD-farnesyl transfer from the ternary complex being measured is not limited by both substrates binding, consistent with the double NBD-farnesylation reaction assayed by HPLC (Scheme 4-3 and Figure 4-1-19). In other words, the observed rate constants for NBD-farnesylation reactions of Rab7CSS and Rab7SSC represent rates of prenyl transfer. This suggests that the N-terminally located cysteine is somewhat preferred for the first NBD-farnesylation. This contrasts with the previous observations made with native lipid substrates, which indicate no strict order of first isoprenoid addition, where a preference for one of the residues can be influenced by the sequence of the Rab C-terminus or the geometry of the lipid substrate.

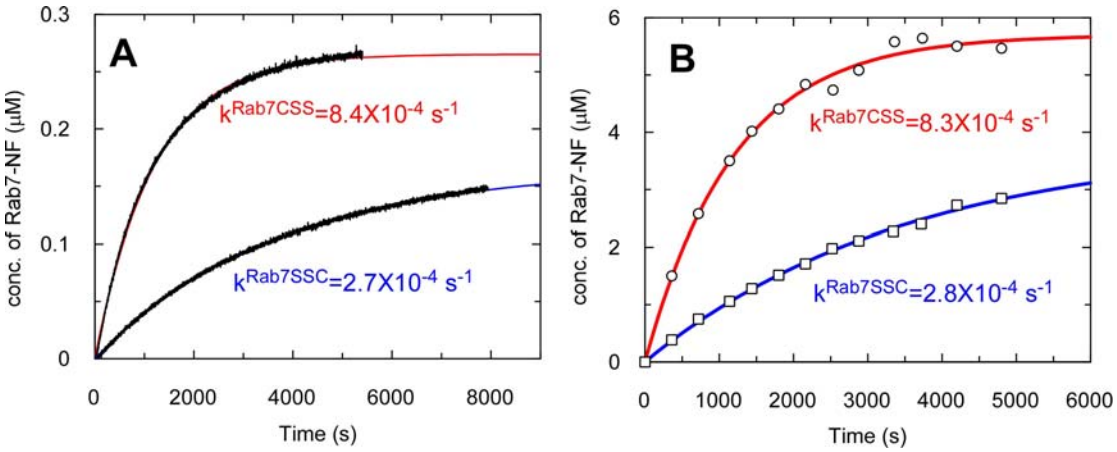

Figure 4-1-20. Single turnover NBD-farnesylation reactions of Rab7C207S (Rab7CSS) and Rab7C205S (Rab7SSC) monitored by continuous fluorometric and SDS-PAGE assays. (**A**) In the fluorometric assay, the reaction contained 200nM of REP-1, RabGGTase and 4 μM NBD-FPP and was initiated by adding 200 nM Rab7 in assay buffer (50 mM Hepes, pH7.2, 50 mM NaCl, 5 mMDTE, 2mM $MgCl_2$, 10μM GDP) at 25°C. (λ_{ex}=479nm, λ_{em}=521nm) The solid lines represent fits to single-exponential functions for Rab7C207S in red (k_{obs}= 8.4X10^{-4} s^{-1}) and for Rab7C205S in blue (k_{obs}= 2.7X10^{-4} s^{-1}). The fluorescence intensity was quantified as described in Materials and Methods (Chapter 6.4.3). (**B**) In the SDS-PAGE assay, 4 μM Rab7 and 4 μM REP-1 were incubated with 4 μM of RabGGTase and 50 μM NBD-FPP in the same prenylation buffer at 25°C. The solid lines represent fits to single-exponential functions for Rab7C207S in red (k_{obs}= 8.3X10^{-4} s^{-1}) and for Rab7C205S in blue (k_{obs}= 2.8X10^{-4} s^{-1}). The fluorescence incorporation was quantified as described in Materials and Methods (Chapter 6.4.3)

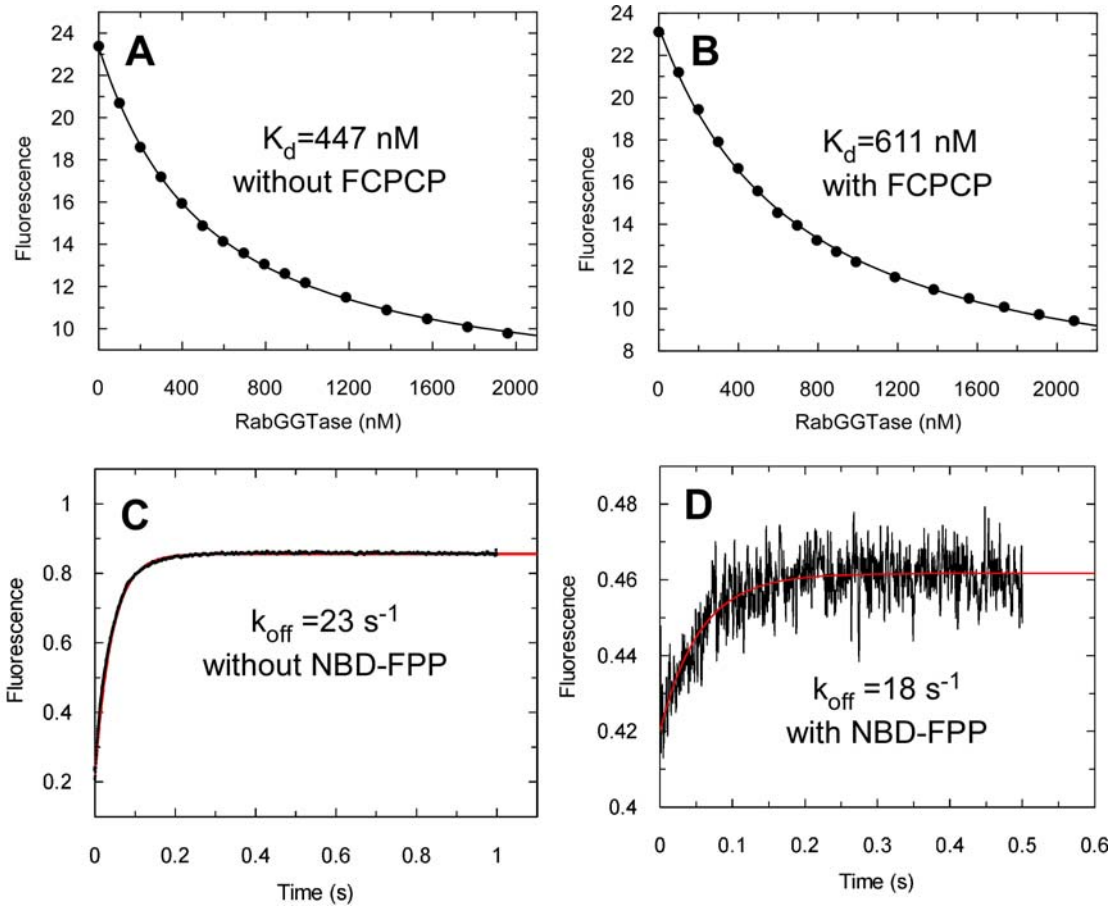

Figure 4-1-21. (**A** and **B**) Titration of RabGGTase to 100 nM Rab7CSS_NF:REP-1 complex (excitation wavelength 479 nm, emission 525 nm) in the presence (**A**) and the absence (**B**) of 30 µM FCPCP. Conditions: 25°C, 50 mM Hepes, pH7.2, 50 mM NaCl, 5 mM DTE. The solid line shows the fit to a quadratic equation giving values of 447±10 nM and 611±23 nM for K_d, respetively. (**C** and **D**) Stopped-flow measurement of the dissociation rate of Rab7_NF:REP1 from RabGGTase. (**C**) 385nM of Rab7CSS_NF:REP-1 complex were premixed with 3.3µM RabGGTase and then dissociated by addition of 9.5µM Rab7:REP-1. (**D**) 35nM of Rab7_NF:REP-1 complex were mixed with 35nM RabGGTase complex and was dissociated by addition of 400 nM Rab7:REP-1 in the presence of 2 µM NBD-FPP; The interaction was monitored from the increase in fluorescence of the NBD group with excitation at 479nm and the fluorescence recorded through a 530nm cut-off filter. Mixing and measuring chambers were thermostated at 25°C. The transients were fitted to a single exponential function, resulting in the observed rate constants.

It has been previously demonstrated that during the prenylation reaction the mono-geranylgeranylated Rab7:REP complex remained bound to RabGGTase very tightly and the second prenylation step occurs without dissociation of the catalytic ternary complex (Thoma et al., 2001b; Thoma et al., 2001c). Prompted by the apparent accumulation of Rab7_NF during the multi-turnover reaction (Figure 4-1-18 **B**), we decided to analyze the interaction of Rab7_NF:REP-1 complex with RabGGTase. Titration and dissociation experiments were preformed in the presence and the absence of a non-hydrolysable analogue of FPP, (hydroxy((3*E*,7*E*)-4,8,12-trimethyltrideca-3,7,11-trienyl)phosphoryl)methylphosphonic acid (i.e. farnesyl-C-P-C-P, FCPCP), showing that the isoprenoid has no influence on the interaction of

Rab7_NF:REP with RabGGTase. The data shown in the Figure 4-1-21 indicate that the interaction of the reaction intermediate, Rab7_NF:REP-1 complex, with RabGGTase (K_d= 447±10 nM) is weakened by a factor of ca. 500 when the conjugated prenyl moiety is NBD-farnesyl instead of geranylgeranyl. This is a surprising finding, which suggests that the intermediate Rab7_NF:REP-1 complex is bound even more loosely to the RabGGTase than the Rab7:REP-1 substrate making the release of the mono-NBD-farnesylated intermediate mandatory (Scheme 4-4). The reduced affinity arises from the increase of dissociation rate (k_{off} = 18±0.4 s^{-1})(Figure. **C**,**D**) that is much faster than the second prenylation step. As a consequence, more than 99% of the mono-NBD-farnesylated Rab7 molecules would dissociate and must reassociate before they become prenylated with the second lipid. This explains the accumulation of the mono-prenylated intermediate in the multi-turnover NBD-farnesylation reaction (Figure 4-1-18 **B**). Since the fluorescent trace (Figure 4-1-18 **A**) is correlated with the accumulation of mono-prenylated Rab7 (Figure 4-1-18 **B**), we conclude that the first prenylation step is predominantly responsible for the observed fluorescence enhancement.

Scheme 4-4. The kinetic and equilibrium constants of the Rab7 prenylation reaction using geranylgeranyl pyrophosphate (black) or NBD-farnesyl pyrophospahte (red in brackets) as a substrate.

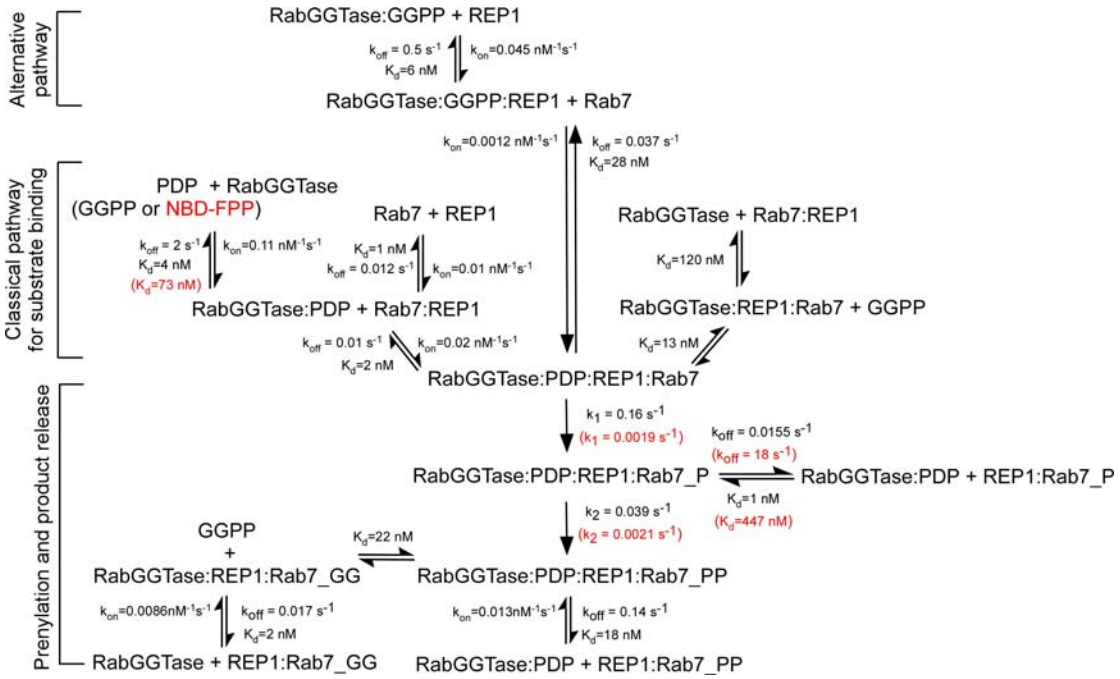

From the mechanistic point of view this observation can be rationalized in the following way. The affinity of REP:RabGGTase interactions vary over a broad range. Unliganded REP binds to RabGGTase with an affinity of several micromolar via a

compact protein:protein interface formed by α helices in the vicinity of the lipid binding site on the domain II of REP and α-subunit of RabGGTase (Pylypenko et al., 2003). The affinity is dramatically increased by either binding of GGPP to RabGGTase (K_d=6 nM) or by binding of a Rab molecule to REP-1 (K_d=120nM) (Thoma et al., 2001a; Alexandrov et al., 1999). The affinity of the Rab7:REP-1 complex towards RabGGTase increases from ca. 120 nM to ca. 2 nM in the presence of GGPP. The mono-geranylgeranylated Rab7:REP complex binds to RabGGTase with an affinity of ca. 1 nM indicating that binding of a conjugated geranylgeranyl moiety to the lipid binding site does not destroy the interaction of Rab7:REP complex with RabGGTase (Thoma et al., 2001c). Doubly prenylated Rab:REP complex remains tightly associated with RabGGTase (K_d= 2 nM) until the latter binds another molecule of GGPP which leads to a reduction in affinity (K_d= 18 nM) and product release (Thoma et al., 2001b). In contrast, the presence of excess non-hydrolysable FPP analogue, FCPCP, as well as GGPP (data not shown) had no significant influence on the affinity of Rab7_NF:REP to RabGGTase, and the presence of NBD-FPP had essentially no effect on the dissociation rate either, possibly indicating that the observed affinity represents the upper limit of affinities for the interaction between Rab7_NF:REP complex and RabGGTase (Figure 4-1-21). The kinetic and equilibrium constants of the Rab7 prenylation reaction pathway, the substrate binding and product release are shown in Scheme 4-4. We propose that binding of the bulky isoprenoid NBD-farnesyl moiety into the lipid binding pocket of REP leads to allosteric distortion of the REP:RabGGTase binding interface and simulates the release of mono-NBD-farnesylated intermediate.

Based on the above observations, we propose a mechanistic model of the developed prenylation assay (Scheme 4-5).

Scheme 4-5. Schematic illustration of the proposed function model of the prenylation sensor.

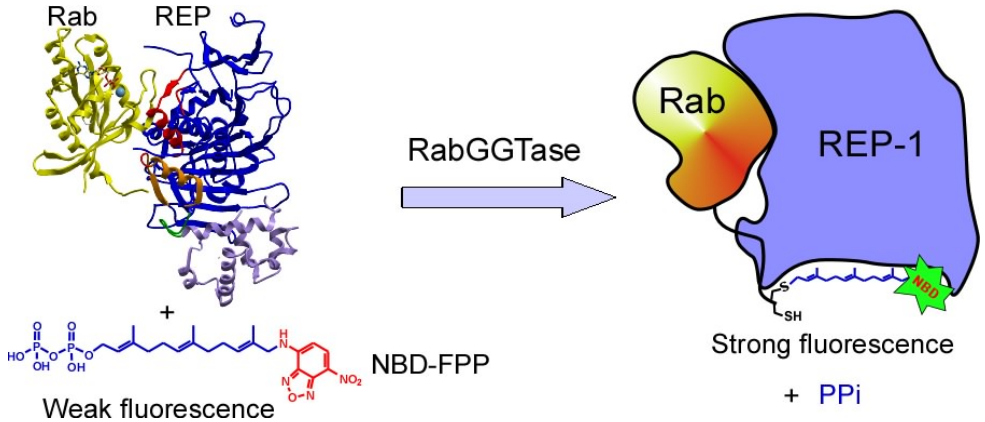

4.1.3.3 Steady-state kinetics of the NBD-farnesylation reaction

With both the SDS-PAGE assay and the continuous fluorometric assay for *in vitro* Rab prenylation, we were able to collect statistically relevant data on initial reaction rates. To make a comparison, the steady-state kinetic studies of Rab NBD-farnesylation reaction were performed by both assays.

Recombinant RabGGTase and Rab7 used here were expressed in *E. coli.*, while recombinant REP-1 was produced from infected SF9 cells. However, it was shown before that recombinant REP-1 has some phosphatase activity most likely from contaminants (Pylypenko et al., 2003). Anant J.S. et. al. (Anant et al., 1998) found that an excess of REP inhibits the prenylation reaction. This effect was assigned to the free REP's competition for Rab:REP prenylation by forming nonproductive complexes with RabGGTase. It is a possible explanation, since REP-1 with the affinity of ca. 6 nM to RabGGTase in the presence of GGPP is sufficient to compete with the Rab:REP complex for binding to RabGGTase (K_d =ca. 2 nM). However, it cannot be ruled out that the inhibition comes from phosphatase activity present in the recombinant REP-1.

Since Rab is recognized by RabGGTase through REP, the Rab:REP complex is the true substrate for RabGGTase, and REP should be regarded as a component of the substrate but not as a component of the enzyme (Pylypenko et al., 2003; Anant et al., 1998). To reduce REP inhibition, a limited amount of REP (1 eq. to Rab) was applied in the reaction. It is known that Rab7 binds to REP-1 with a very high affinity of K_d =1 nM (Alexandrov et al., 1998). Thus, the Rab7:REP-1 complex could be treated as one substrate component, since the concentrations of Rab7 and REP-1 applied in the reaction are far above the K_d value.

For routine measurements of RabGGTase activity, various concentrations (0.5 - 10 μM) of the protein substrate, Rab7:REP-1 complex, and 1 - 18 μM of the lipid substrate, NBD-FPP, provide an adequate signal to noise ration for both measurements on the fluorometer and the laser scanner. Velocities were derived from the initial 10 minutes of the reaction, typically corresponding to less than 2% prenyl transfer of the total substrate, which would in principle provide a good estimation of the initial velocity. Here we assumed that REP-1 associated phosphatase activity does not significantly influence the prenylation rates at the initial short time.

For quantification of the fluorometric assay and the SDS-PAGE assay, samples were tested for an “inner filter effect”, i.e. the absorption of the exciting light and/or the absorption of the emitted radiation, which cause non-linearity between fluorescence intensity and fluorophore concentration. Inner filter effects are observed in samples where the optical density (OD = log I_0/I) of a solution at the excitation wavelength is sufficiently high that the intensity of exciting light in the cuvette is significantly less than at the front face of the cuvette. Because fluorescence intensity is proportional to the intensity of exciting light, the inner filter effect causes a deviation from linearity in the relationship between concentration and fluorescence intensity. If there is an inner filter effect, fluorescence intensities must be corrected at every lipid concentration used (Lutz and Luisi, 1983).

To determine whether a significant inner filter effect is present, the observed fluorescence intensities of NBD-FPP measured under the same conditions (bandpass, emission and excitation wavelengths) as those under which reaction velocity measurements are made was plotted against concentration (Figure 4-1-22 **D**). No inner filter effect was observed for the fluorescent lipid concentrations up to 10 μM used in this study.

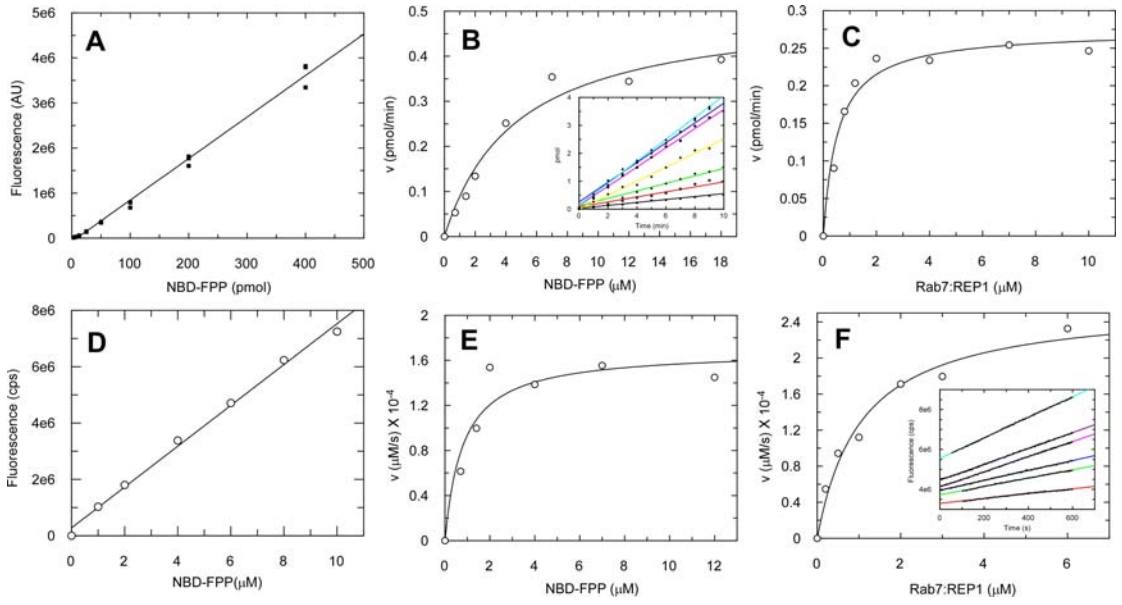

Figure 4-1-22. (**A**) Plot of the fluorescence versus the amount of NBD-FPP samples resolved on SDS-PAGE. The fluorescence of the fluorescent isoprenoid was determined by scanning of the gels as described in Chapter 6.4.3. (**B** and **C**) In the SDS-PAGE assay, determination of initial velocities versus increasing concentrations of NBD-FPP (**B**) and Rab7:REP-1 complex (**C**) catalyzed by 0.2 pmol RabGGTase at 30°C. Reaction mixture contained 6 μM Rab7:REP-1 and 20 μM NBD-FPP, respectively. (**D**) Plot of the fluorescence intensity versus the concentration of NBD-FPP in the cuvette. Fluorescence was recorded in a Fluomax-3 fluorometer with λ_{ex}= 479 nm (slit width = 1nm) and λ_{em}= 520 nm (slit width = 5nm). (**E** and **F**) In the fluorometric assay, determination of initial velocities of prenylation reaction catalyzed by 0.02 μM RabGGTase at 37°C as a function of NBD-FPP (**D**) and the

protein substrate concentrations (**F**). Reaction mixture contained 2 μM Rab7:REP-1 complex and 4 μM NBD-FPP respectively. Hyperbolic lines show the fits to the Michaelis-Menten equation. (**Inset**) Initial phase of the prenylation at different concentrations of substrates used for prenylation rate determinations.

According to the model proposed for the NBD-farnesylation reaction, for the k_{cat} calculation the transfer of one NBD-farnesyl group to Rab should be assumed rather than two NBD-farnesyl groups. Under the standard assay conditions, Michaelis-Menten kinetic parameters were determined by the fluorometric assay at 37°C and SDS-PAGE assay at 30°C. Typical reaction velocity versus substrate concentration profiles for the transformation of Rab7 and NBD-FPP by RabGGTase are presented in Figure 4-1-22.

Table 4-1-5. Steady-state kinetic parameters for protein and lipid substrates of RabGGTase determined by two assays.

Assay	Substrate	K_m (μM)	k_{cat} (s^{-1})
SDS-PAGE assay	NBD-FPP	4.7±1.1	0.043[ab]
	Rab7:REP-1	0.54±0.11	
Continuous assay	NBD-FPP	0.8±0.34	0.013[b]
	Rab7:REP-1	1.1±0.23	

[a] Quantitation with NBD-FPP.
[b] k_{cat} values are calculated assuming transfer of one NBD-farnesyl group to Rab7.

From Table 4-1-5, it can be seen that both assays give comparable steady-state parameters. The significant difference between the K_m values for NBD-FPP could be due to the use of different batches of reagents, and the partially hydrolyzed phosphoisoprenoids would lead to substrate inhibition that can be observed at high concentrations of NBD-FPP (data not shown). The difference in the of k_{cat} values could result from distinct activities of different batches of the recombinant enzyme and/or systematic error from two quantitation methods.

The availability of a continuous fluorometric assay with a large dynamic range prompted us to test whether it can be used for identification and characterization of RabGGTase inhibitors. As a test example we used NE10790 - the first reported specific but weak biphosphonate analogue inhibitor of RabGGTase (Coxon et al., 2001). Using the fluorometric assay, we determined an IC_{50} value of 502±113 μM which is identical to that determined by a radioactive assay, and it was shown to be essentially non-competitive to NBD-FPP with a K_i of 176±18 μM according to the Lineweaver-Burk plot (Figure 4-1-23).

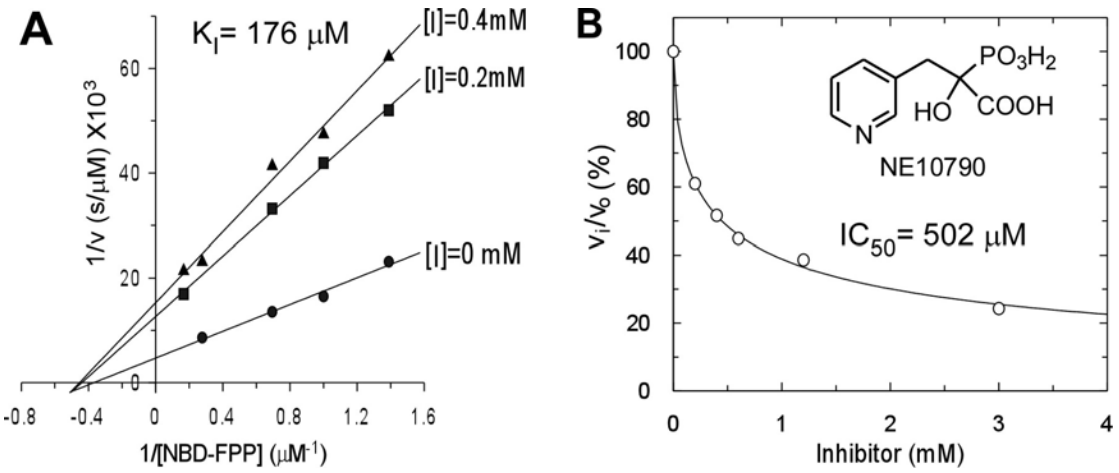

Figure 4-1-23. Inhibition of RabGGTase by NE10790. (**A**) Lineweaver-Burk plot. The reaction mixture contained 2 μM Rab7:REP-1 complex, 0.02 μM RabGGTase and varying concentrations of NBD-FPP in the absence and the presence of the indicated concentrations of inhibitor. (**B**) Concentration dependent inhibition of RabGGTase by NE10790.

4.2 Identification of RabGGTase inhibitors

4.2.1 High-throughput screening for RabGGTase inhibitors

Having developed a continuous fluorometric assay for RabGGTase activity, we sought to miniaturize and parallelize the assay to make it suitable for high-throughout screening and characterization of potential inhibitors. We adapted the assay for 96-well and 384-well plate formats, with improved efficiency with respect to both time and reagents.

Fluorescence intensities of the substrate NBD-FPP and the product Rab7-NBD-farnesyl:REP-1 complex were measured using a Fluoroskan plate reader (Thermo BioAnalysis) (Figure 4-2-1 **B**). A 21-fold enhancement of fluorescence was observed, which is quite similar to what was observed in the cuvette assay described in section 4.1.3 (Wu et al., 2006).

A typical 96-well assay to identify RabGGTase inhibitors is shown in Figure 4-2-1. The fluorescence intensity increased upon reaction in the positive control, whereas there was a decrease in the negative control where the protein substrate Rab7:REP was omitted. We assumed that the decrease of fluorescence intensity could be the result of photo-bleaching of the NBD. As shown in Figure 4-2-1 **A**, the reaction in the presence of various concentrations of inhibitor showed a time-dependent fluorescence change between the positive control and the negative control, from which an inhibition profile could be extracted as shown in Figure 4-2-1 **C**. In order to obtain an estimate of a genuine IC_{50}, a set of corrections were performed, where the velocity of the inhibited reaction was corrected by the velocity of the negative control (no substrate) in the presence of the corresponding concentration of inhibitor, while the velocity of the positive control was corrected by subtraction of the velocity of the negative control in the absence of inhibitor. The IC_{50}s were calculated using a 2 parameter equation using GraFit 5.0 (Erithacus Software Limited)(Figure 4-2-1 **D**).

$$v_i/v_0 = \frac{100\%}{1+\left(\frac{[I]}{IC_{50}}\right)^s}$$

where v_i is the inhibited velocity minus the background, i.e. the negative control in the presence of the corresponding concentration of inhibitor, v_0 is the uninhibited velocity (positive control) minus the background (the negative control in the absence of

inhibitor), [I] is the concentration of inhibitor, *s* is a slope factor and IC_{50} is the concentration of the inhibitor that produces 50% inhibition.

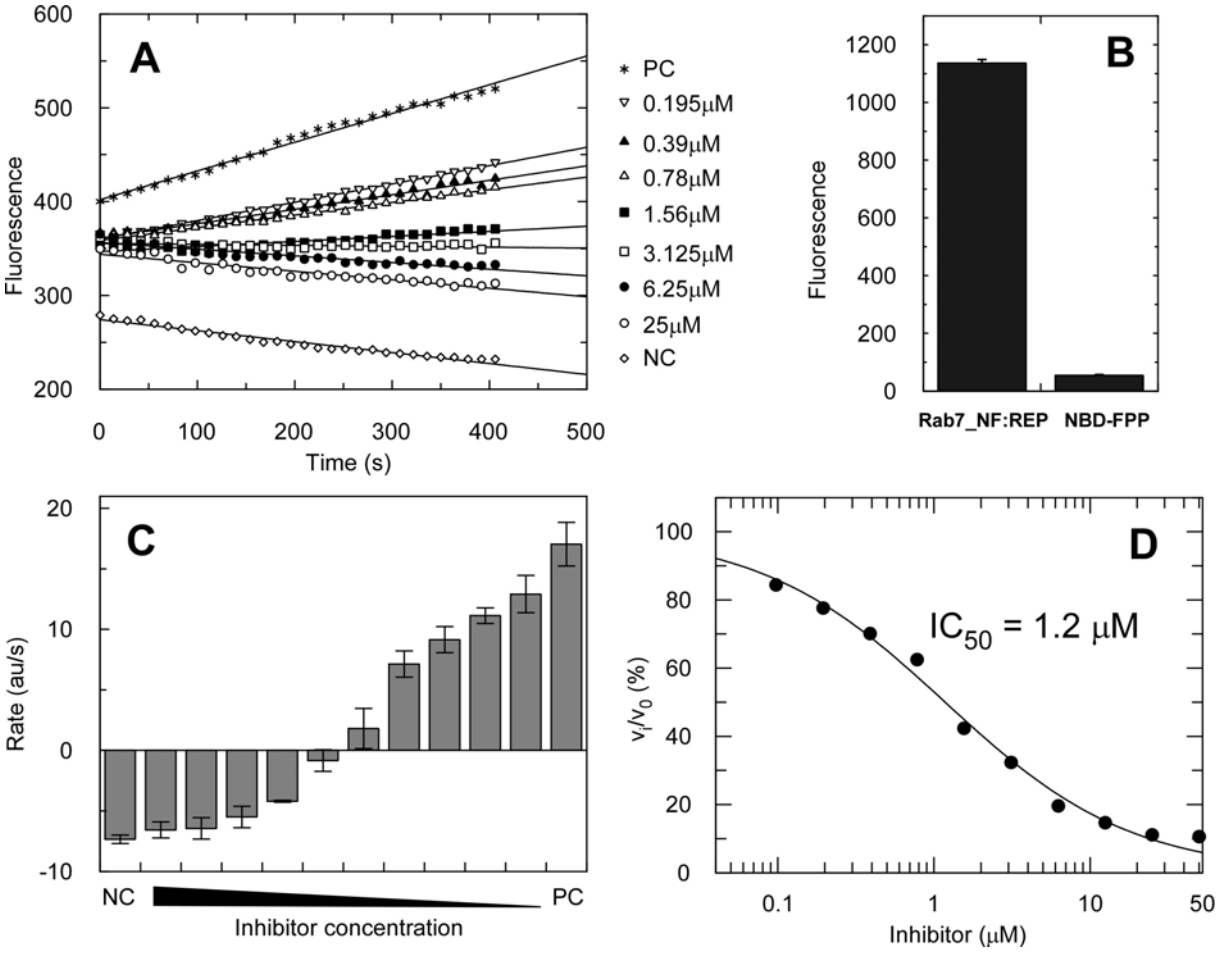

Figure 4-2-1. (**A**) Time-course of fluorescence change upon prenylation of 2 μM Rab7:REP-1 complex and 2 μM NBD-FPP catalyzed by RabGGTase (0.02 μM) in the absence (PC) and the presence of various concentrations of inhibitor at 37°C and time-dependent decrease of 2 μM NBD-FPP fluorescence in the presence of 0.02 μM RabGGTase (NC). Solid lines show the linear fits. Fluorecence was recorded on Fluoroskan with exitation cut-off filter 485 nm and emission cut-off filter 538nm. Buffer: 50mM Hepes, pH 7.2, 50mM NaCl, 2mM $MgCl_2$, 5mM DTE, 0.01% Triton-X100. (**B**) The fluorescence intensity of 100 μl of 1 μM fluorescent substrate NBD-FPP and the fluorescent product Rab7-NBD-farnesyl:REP-1 in a 96-well plate recorded in the same conditions. The fluorescence intensities shown in the graph are subtracted the background of buffer, and a 21-fold fluorescence enhancement was observed. Buffer: 50mM Hepes, pH 7.2, 50mM NaCl, 2mM $MgCl_2$, 5mM DTE. (**C**) Inhibition profile of the inhibitor. Observed rates were obtained by linear regressions of the traces shown in panel A. (**D**) Determination of IC_{50} of the inhibitor using the equation as described in the text.

High-throughput screening (HTS) is a major technique used in early-stage drug discovery. A key problem in HTS is the prevalence of nonspecific or promiscuous inhibitors (Rishton, 1997). A major cause of this is aggregation, especially when compounds are screened at high concentrations (>10 μM). Some organic molecules tend to form large colloid-like aggregates that sequester and thereby inhibit enzymes (McGovern et al., 2003; McGovern et al., 2002). Screening at high concentration of

compounds would also lead to false-negatives, since at high concentration compounds with low solubility would precipitate, resulting in a decrease of actual concentration and possibly an influence on fluorescence read-out. False-positive and false-negative hits from HTS may make the SAR analysis flat and mislead the discovery optimization of lead compounds. Addition of detergent in the high-throughput assays largely or completely attenuated the nonspecific inhibition in a library composed of random drug-like molecules (Feng et al., 2005). In order to reduce promiscuous inhibitors in the high-throughput screening, 0.01% Triton X-100 was included in our assay buffer. The presence of detergent on the one hand increases the solubility of compounds on the other hand reduces aggregation of compounds that could lead to promiscuous inhibition

4.2.2 In silico screening of RabGGTase inhibitors

In recent years, the need for acceleration of the drug development process has inspired the advance of a large number of new methods aimed at a more efficient and rapid lead structure discovery process. Recent advances in combinatorial chemistry enable rapid synthesis of large compound libraries with diversified structures. High-throughput screening (HTS) allows considerable reduction of the time required for the discovery of new active molecules which modulate a particular biomolecular pathway. However, the experimental screening of millions of compounds is prohibitively expensive. Therefore, in silico screening of compound databases for potential new lead compounds, referred to as virtual screening (VS), has emerged as a promising tool for decreasing both the time and cost of drug discovery (Jalaie and Shanmugasundaram, 2006).

Virtual ligand screening (VLS) can be used for screening as many compounds as desired depending on the amount of computer power available. Internal coordinate mechanics (ICM) is the software product from Molsoft LLC (La Jolla, CA, USA). ICM-Pro contains an all atom internal coordinate force field and efficient algorithm to perform local and global energy optimization of small or large molecules with respect to an arbitrary subset of variables. In addition, ICM contains MMFF94 force field for energy optimization in Cartesian space for any organic molecule. ICM-VLS is an add-on product to ICM-Pro. It has been successfully used by the pharmaceutical industry and academia for identifying drugs and inhibitors for a wide variety of diseases (Cavasotto et al., 2006; Cavasotto and Abagyan, 2004). Virtual

ligand screening using Molsoft-ICM is performed by docking a database of ligands to a receptor structure followed by an evaluation of the docked conformation with a binding-score function.

The crystal structure of a truncated version of RabGGTase in complex with an inhibitor, MT650 (Dursina et al., 2006; Thutewohl et al., 2002), which has recently been solved by Zhong Guo in our group, enables us to perform a VLS using ICM platform (this work was done during a visit to the Scripps Research Institute, La Jolla, CA). ICM pocket finder function in the ICM-Pro was used to predict the binding pockets that drugs could potentially target. Three of them are located in the active site of RabGGTase (pocket 1, 2 and 3, Figure 4-2-2 **A**). Pocket 1 is mainly in the beta subunit, overlapping with the GGPP binding site (Figure 4-2-2 **A**, **C**) and the MT650 binding site (Figure 4-2-2 **B**). Thus, pocket 1 is a well-defined pocket for the VLS, since its volume and area fall into the range of drug targets. Pocket 2 is situated between the alpha and beta subunit. Pocket 3 (displayed in dark gray in Figure 4-2-2 **A**) is located at the beta subunit, resembling a balcony projecting from the GGPP binding cavity.

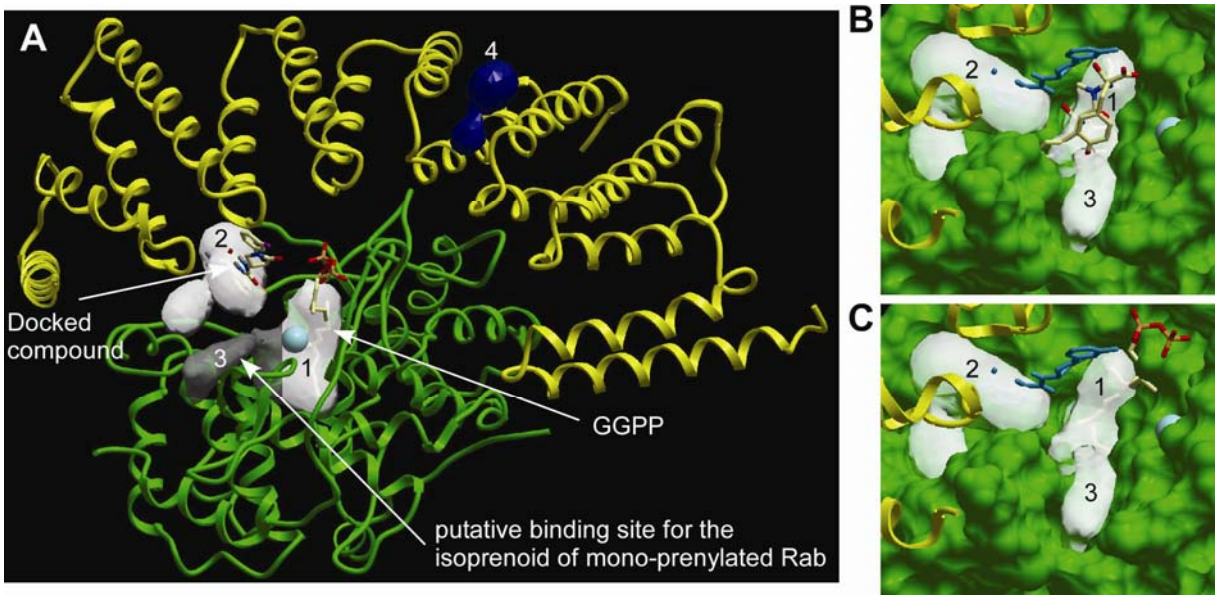

Figure 4-2-2. Binding pockets and virtual ligand screening of RabGGTase. (**A**) Ribbon representations of RabGGTase α subunit (yellow) and RabGGTase β subunit (green) in complex with MT650 (not shown in the panel), while the Zn^{2+} is shown as a turquoise ball. The binding pockets are shown in gray and blue meshes. One of the docked compounds to the pocket is in stick representation colored by atom type. The crystal structure of the RabGGTase:GGPP complex was superimposed with that of RabGGTase:MT650 to show the GGPP in stick representation colored by atom type. (**B**) Surface representations of the active site of RabGGTase. RabGGTase β subunit is in green surface representations, and the α subunit is in yellow ribbon representations. MT650 is in stick representation colored by atom type. The docked compound is shown in blue stick representation. Zn^{2+} is shown as a turquoise ball. (**C**) The same as B, but the superimposed GGPP is shown instead of MT650.

However, the location of the putative binding site for the isoprenoid of mono-prenylated Rab is still unclear, which would be expected to exist in RabGGTase since the mono-prenylated Rab intermediate has to associate with RabGGTase for the second prenyl transfer (Thoma et al., 2001b; Thoma et al., 2001c). Many processive enzymes feature two product-binding sites as those observed for CaaX prenyltraseferases, FTase (Long et al., 2002) and GGTase-I (Taylor et al., 2003). In the last step of reaction pathway of FTase and GGTase-I, binding of a fresh FPP/GGPP substrate molecule leads to translocation of the prenyl group of prenylated CaaX to a new binding site, termed the “exit groove”. The exit groove observed in CaaX prenyltransferases is a conserved structural feature of RabGGTase. In apo-RabGGTase (1DCE), a 7.5 Å diameter hydrophobic tunnel that originates from a shallow groove analogous to the exit groove in FTase (1KZO) and GGTase-I (1N4S) extends through the beta subunit (residues $_{\beta}$Tyr30, $_{\beta}$Tyr39, $_{\beta}$Arg46, $_{\beta}$Gly49, and $_{\beta}$Pro288 line the tunnel). This tunnel was proposed to be the binding site for the geranylgeranyl moiety of the mono-prenylated Rab intermediate (Long et al., 2002). Pocket 3 extends along the putative binding site for the isoprenoid of mono-prenylated Rab (Figure 4-2-2 **A**), and could be an important pocket for drug targeting.

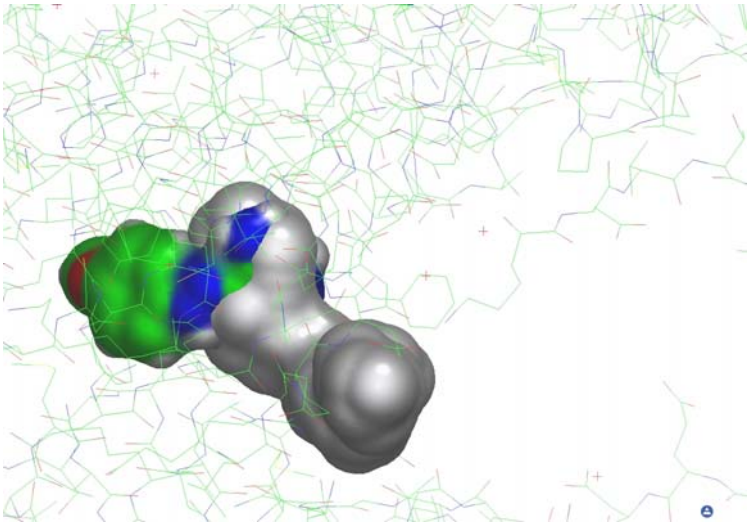

Figure 4-2-3. The docked compound in the REP binding interface of RabGGTase. The compound is in surface representation, RabGGTase in stick representation.

Another small pocket (pocket 4, Figure 4-2-2 **A**) located at the REP binding interface (Pylypenko et al., 2003), though too small to qualify as a classical drug target site, could be promising for the purpose of design of a specific inhibitor for RabGGTase. A compound binding to pocket 3 would be able to disrupt the REP:RabGGTase interaction, so that Rab cannot be processed by RabGGTase.

Since this mechanism is only present in RabGGTase, an inhibitor targeting the interface of REP:RabGGTase would be expected to inhibit RabGGTase with high specificity. Based on the crystal structure of REP:RabGGTase (PDB code 1LTX), an in silico screening of ligands targeted to the REP binding interface of RabGGTase was performed by Mahesh Kulharia in our group (Figure 4-2-3) (see Ph.D. Thesis, Dortmund University, 2008). One of nine virtual hits was identified to be a real inhibitor for RabGGTase (Table 4-2-6, MK21986).

A virtual library of 3263807 compounds was docked into pocket 1 and 2 of RabGGTase using the Molsoft ICM-VLS platform, and ca. 500 hits were identified. These hits were further reduced by the Lipinski rule of five (Lipinski et al., 2001) to give 62 potential hits. These commercially available compounds were further evaluated by the 96-well plate assay for RabGGTase. Two of them (AG205/33152020 and AH487/41653773) were identified as actual hits, as shown in Table 4-2-6.

4.2.3 Structure and activity relationship (SAR) analysis of peptide inhibitors for RabGGTase

The high-throughput screening assay allows for the rapid identification and characterization of RabGGTase inhibitors. To this end, a large compound library (ca. 7000 species) composed of commercially available compounds and the compounds synthesized in Prof. Dr. Waldmann's department was screened on a TECAN™ Freedom EVO® automation platform using this assay. A diverse library of around 400 Pepticinnamin E derivatives prepared using a hydrazine linker and 2-chlorotrityl chloride resin (synthesized by Kui-Thong Tan and Dr. Ester Guiu-Rozas) together with 50 previously identified FTase inhibitors (Dursina et al., 2006; Thutewohl et al., 2002) was screened for inhibition of RabGGTase both manually in the 96-well plate assay and in the robot-assisted 384-well plate assay.

The synthesis of the peptide inhibitors is decribed and discussed in detail in the thesis of Kui-Thong Tan (Ph.D. Thesis, Dortmund University, 2007). Figure 4-2-4 shows the building blocks used in the combinatorial Fmoc-solid phase peptide synthesis (Fmoc-SPPS).

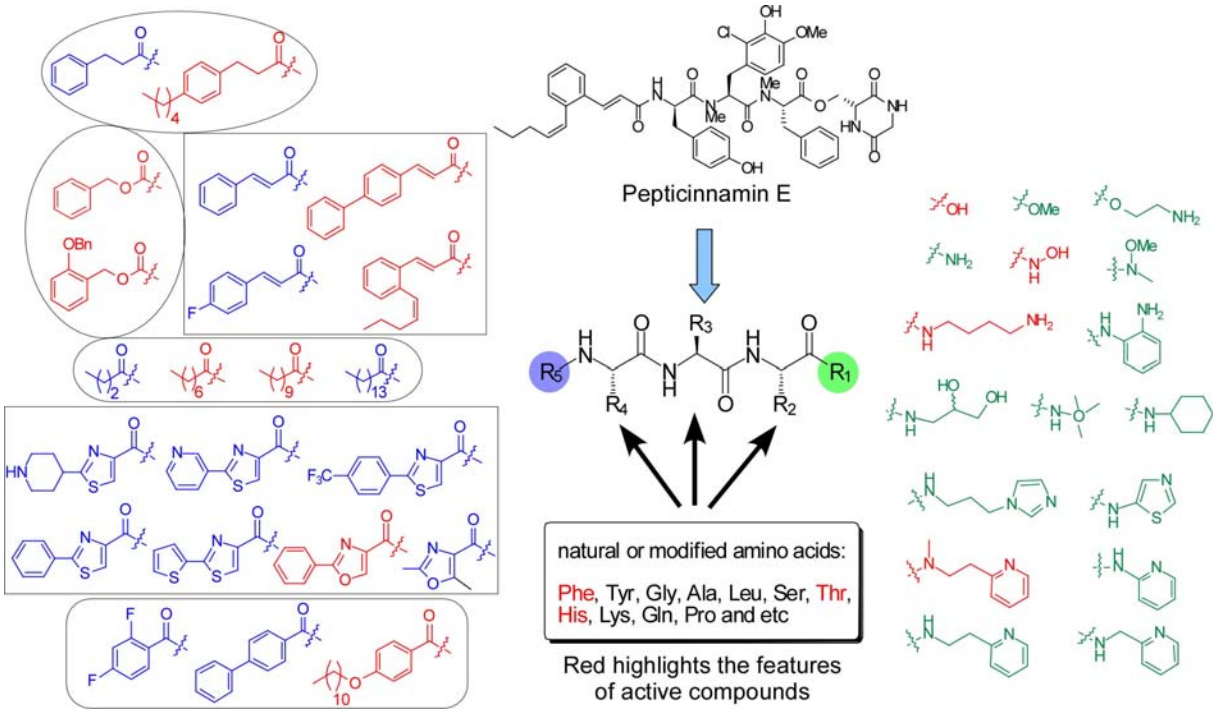

Figure 4-2-4. Representative building blocks used in the Fmoc-SPPS.

The 450 peptides can be divided into two categories based on the modification of the N-terminus (R^5 position). Type-I consists of around 200 peptides with lipid chains at their N-terminus (R^5 position), whereas 250 peptides in Type-II carries an aromatic functionality at the N-terminus. Table 4-2-1 and 4-2-2 list the IC_{50} values for selected Type-I and Type-II inhibitors.

Table 4-2-1. IC_{50} values of the Type-1 inhibitors with a lipid chain at the R^5 position

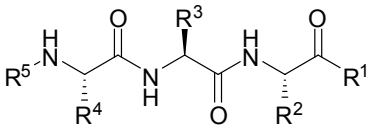

Entry	Peptide	R^5	R^4	R^3	R^2	R^1	IC_{50} (μM)[a]
1	**5**		L-His	L-Phe	L-Tyr	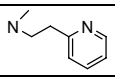	4.7 ± 0.1
2	**6**		L-Tyr	L-His	L-Tyr	OMe	3.9 ± 0.2
3	**7**		L-Tyr	L-His	L-Tyr	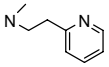	6.3 ± 0.6
4	**8**		L-Tyr	L-His	L-Tyr	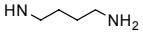	7.1 ± 0.3
5	**9**		L-His	L-His	L-Tyr	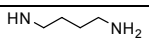	5.2 ± 0.7
6	**10**		L-His	L-His	L-Tyr	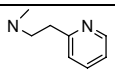	11.0 ± 1.2
7	**11**		L-His	L-Phe	L-Tyr	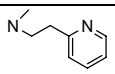	2.8 ± 0.4
8	**12**		L-His	L-Phe	L-Tyr	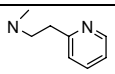	26 ± 0.3

9	**13**		L-His	L-Phe	L-Tyr	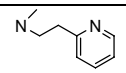	> 100
10	**14**	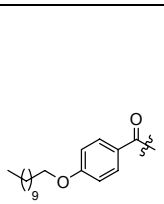	L-Tyr	L-Tyr	L-Tyr	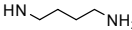	11.6 ± 1.2
11	**15**		L-His	L-His	L-His	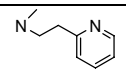	12.1 ± 0.8
12	**16**		L-His	L-His	L-His	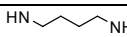	24.0 ± 1.4
13	**17**		L-His	L-Tyr	L-Phe	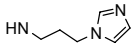	12.3 ± 0.6

[a] the IC_{50} values were calculated from 3 independent measurement

Table 4-2-2. IC_{50} values of the Type-II inhibitors with an aromatic functionality at R^5 position

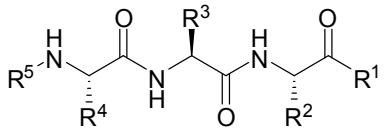

Entry	Peptide	R^5	R^4	R^3	R^2	R^1	IC_{50} (μM)
1	**31**	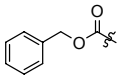	D-Tyr	L-Phe	L-Tyr	OH	4.1 ± 0.2
2	**32**		L-His	L-(Me)Phe	L-Trp	NH-OH	5.2 ± 0.6
3	**33**		L-His	L-(Me)Phe	L-Tyr	NH-OH	9.0 ± 1.0
4	**34**		L-His	L-(Me)Phe	D-Tyr	NH-OH	13.6 ± 1.1
5	**35**		L-His	L-(Me)Phe	L-Tyr	OH	22.7 ± 1.7
6	**36**	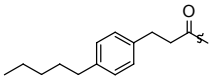	D-Tyr	L-Tyr	L-Phe	OH	11.0 ± 1.4
7	**37**		D-Tyr	L-Tyr		OH	19.1 ± 2.4
8	**38**		D-His	L-(Me)Phe	L-Phe	OH	19.0 ± 3.8
9	**39**	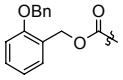	D-His	L-Tyr	L-Phe	OH	15.6 ± 1.3
10	**40**		L-His	L-Tyr	L-Phe	OH	19.3 ± 3.6
11	**41**	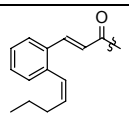	D-His	L-Tyr	D-Phe	OH	15.2 ± 2.2
12	**42**	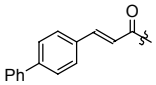	D-His	L-Tyr	L-Tyr	OH	22.7 ± 2.9
13	**43**	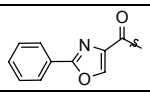	L-His	Gly	L-His(Trt)	OH	8.1 ± 1.0

SAR analysis of the sequence and nature of amino acid residues in the peptide central core of both types of inhibitors reveals that aromatic amino acids, namely

histidine, phenylalanine and tyrosine are essential for give good inhibitory activity towards RabGGTase (Table 4-2-1 and 4-2-2). For example, in Type-I inhibitors, changing the L-tyrosine at the R^2 position (Table 4-2-1, entries 5 and 6) to L-serine increases the IC_{50} values of peptides **9** and **10** from 5 μM and 11 μM to over 100 μM. Type-II peptides with alanine, leucine, proline, serine, threonine, glutamine, glutamic acid and lysine in the peptide central core did not give pronounced inhibitory activity for RabGGTase. For example, by substituting phenylalanine with glycine and β-alanine at the R^3 position, the inhibitory activity of peptide **35** decreases dramatically from an IC_{50} value of 22 μM to no detectable inhibitory activity at 100 μM. The non-tolerance of aliphatic amino acid residues in the two types of RabGGTase peptide inhibitors may be due to the large and deep active site of RabGGTase, which requires rigid and bulky amino acids to fill the binding pocket. SAR analysis reveals that a central core consisting of histidine at the R^4 position, tyrosine and phenylalanine residues at the R^2 and R^3 positions is important for the inhibitory activity of Type-II peptide inhibitors against RabGGTase.

The length of the lipid chain of Type-I compounds is critical for the inhibitory activity. It appears that the optimal length of lipid chain is between 7 and 10-carbon (Table 4-2-1, entry 1-7). Peptide **11** with a heptyl chain (IC_{50} = 2.8 μM) is the most potent inhibitor for RabGGTase in this compound collection (Table 4-2-1, entry 7). Extending the chain length to 14 carbons (Table 4-2-1, entry 8) or reducing the lipid chain to 3 carbons (Table 4-2-1, entry 9) significantly decrease the inhibitory activity.

All the peptides except compounds **6** and **17** listed in Table 4-2-1 contain a pyridine ring or an amine group at the R^1 position. In order to understand the effect of C-terminal groups on the inhibitory activity, different moieties were used to substitute the R^1 group of peptide **5**, which is one of the most potent inhibitors in this peptide collection. As can be seen in Table 4-2-3, chemical moieties at R^1 position play a decisive role in influencing the potency of inhibitors. In general, only those containing potential Zn^{2+} coordinating group such as *N*-methyl 2-ethyl pyridine (Table 4-2-3, entry 1) gave better inhibitory activity. Although the hydroxylamine group of peptide **26** (Table 4-2-3, entry 10) is a better zinc ion binding group, **26** does not show inhibition to RabGGTase at 100 μM, which might be attributed to the short chain length of the hydroxylamine group. Reducing the 2-carbon chain connecting amine and pyridine of *N*-methyl 2-ethyl pyridine group resulted the peptide **28** and **29** (Table 4-2-3, entry 12 and 13) that show no inhibitory activity towards RabGGTase at 100

μM. In addition, the *N*-methyl moiety of *N*-methyl 2-ethyl pyridine group is very important for keeping the inhibitory activity towards RabGGTase (Table 4-2-3, entry 14).

Table 4-2-3. Inhibitory activity of various substituents at R^1 position of peptides **5**.

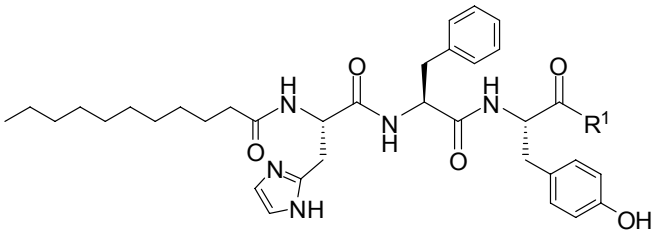

Entry	Peptide	R^1	IC_{50} (μM)[c]
1	**5**	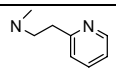	4.7±0.1
2	**18**[b]	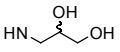	n.a.
3	**19**		n.a.
4	**20**[b]	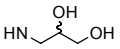	> 50
5	**21**	NH_2	> 50
6	**22**	OMe	n.a.
7	**23**		n.a.
8	**24**	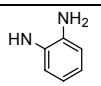	> 50
9	**25**	OH	n.a.
10	**26**	NH-OH	n.a.
11	**27**		n.a.
12	**28**	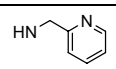	n.a.
13	**29**		n.a.
14	**30**	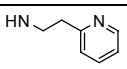	n.a.

n.a.: not active at 100 μM (<50% inhibition). [b] Inhibitors **18** and **20** are diastereoisomers with the variable stereochemistry at the C-terminal secondary alcohol. [c] The screening was performed at 100 μM.

Table 4-2-4. IC_{50}s of the Type-II peptides with or without trityl protecting group (Trt)

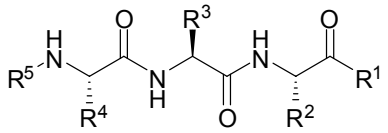

Entry	Peptide	R^5	R^4	R^3	R^2	R^1	IC_{50} (μM)[a]
1	**43**	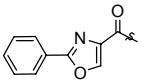	L-His	Gly	L-His(Trt)	OH	8.1 ± 1.0
2	**44**		L-His	Gly	L-His	OH	> 50
3	**45**		L-His(Trt)	Gly	L-His	OH	38 ± 8.7
4	**46**	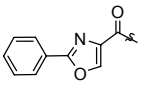	His	Gly	L-Phe	OH	> 50
5	**47**		L-His(Trt)	Gly	L-Phe	OH	30 ± 1.8
6	**48**	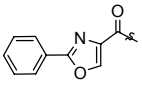	Gly	L-Phe	L-His	OH	45 ± 21
7	**49**		Gly	L-Phe	L-His(Trt)	OH	25 ± 8.0
8	**50**		Gly	L-Phe	L-His(Bn)	OH	> 50
9	**51**		Gly	L-Phe	L-His(Boc)	OH	> 50
10	**52**	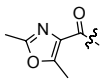	Gly	L-Phe	L-His	OH	> 50
11	**53**		Gly	L-Phe	L-His(Trt)	OH	46 ± 5.4
12	**54**	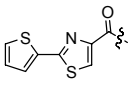	Gly	L-Phe	L-His	OH	41 ± 6.2
13	**55**		Gly	L-Phe	L-His(Trt)	OH	36 ± 5.7
14	**56**	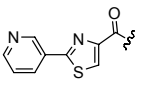	Gly	L-Phe	L-His	OH	> 50
15	**57**		Gly	L-Phe	L-His(Trt)	OH	37 ± 2.0

[a] The IC_{50} was determined manually using 96 well-plate assay.

Interestingly, Type-II compounds with a trityl protecting group (Trt) showed higher activity than the corresponding unprotected compounds (Table 4-2-4), suggesting that the binding is enhanced by hydrophobic interactions. This is consistent with the crystal structure of RabGGTase in complex with one of the Type-II compounds (Figure 4-2-2 **A**), where the interaction between RabGGTase and compound **35** is mainly hydrophobic. This also correlates with the finding from the interaction analysis that compound **43** associates with the prenyl binding site (Figure 4-2-2 **B**). Therefore, introduction of hydrophobic groups to the peptides may improve the activity of the peptide inhibitors.

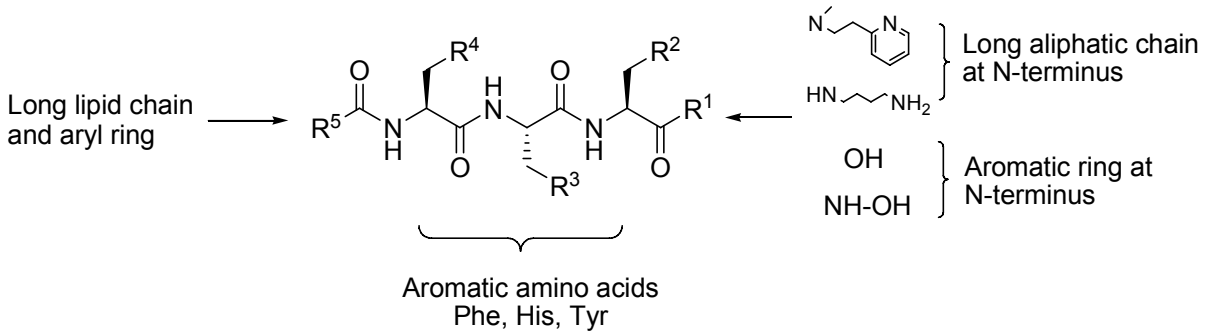

Figure 4-2-5. Features of the active compounds in the peptide library.

4.2.4 Quantitative analysis of the interaction of identified inhibitors with prenyltransferases

The obtained IC_{50} values provide an indication of the inhibitory activity of the identified compounds under the chosen conditions but do not provide direct information on either their mode of action or their affinity for prenyltransferases. To gain insights into the mechanisms of action of the compounds, a series of fluorescence titrations and enzyme kinetic studies were performed with two Type-I inhibitors, **5** and **10,** and a Type-II inhibitor, **43**.

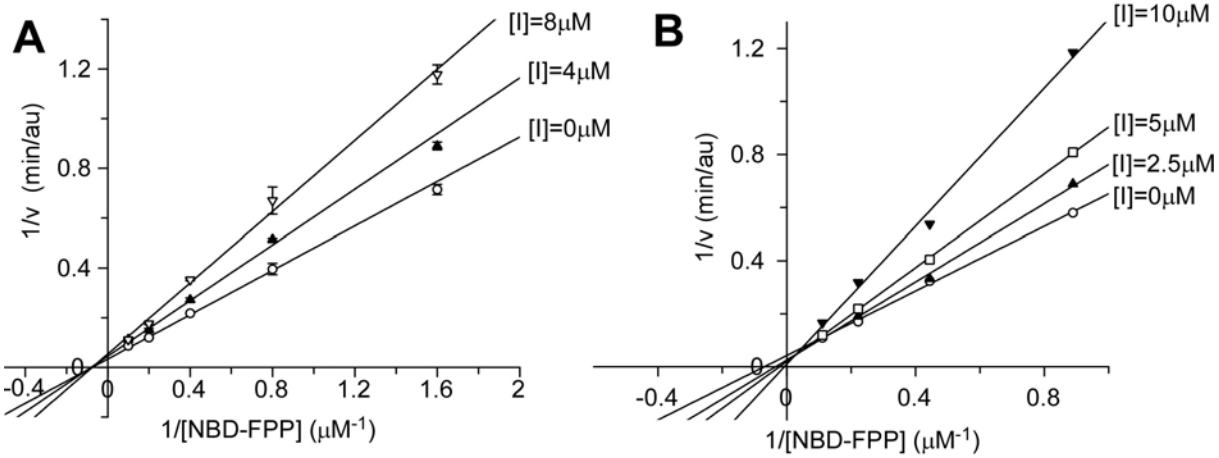

Figure 4-2-6. Lineweaver-Burk plot against NBD-FPP in the presence and the absence of **5** (**A**) and **43** (**B**). The concentration of Rab7:REP-1 (1.2 μM) and RabGGTase (0.03 μM) were kept constant, while the concentration of NBD-FPP varied. The concentrations of inhibitor **5** and **43** were indicated in the plot.

Classic enzyme catalyzed reactions follow the Michaelis-Menten equation {$v=V_{max}/(1+K_m/[S])$}. Transformations of the equation to other mathematical forms provide useful methods of analysis. A double-reciprocal plot constructed from 1/v and 1/[S], both measurable variables, referred to as a Lineweaver-Burk plot, has most commonly been used for presenting inhibition patterns (Engel, 1996). Figure 4-2-6

shows the double-reciprocal plots of the initial velocity against the NBD-FPP concentration in the absence and presence of inhibitor. The plots intersect at the x-axis in Figure 4-2-6 **A**, indicating that **5** is non-competitive with respect to NBD-FPP. In contrast, the plots do not exactly intersect at the y-axis in Figure 4-2-6 **B**, suggesting mixed inhibition with a competitive component.

To further assess the compounds' interactions with RabGGTase, we took advantage of the fluorescence change of NBD-FPP upon its binding to RabGGTase. Using this signal change, a K_d value for the NBD-FPP:RabGGTase interaction of around 160 nM was obtained (Figure 4-2-5 **C**, **F**). To test the effects of **5** and **10** on this interaction, two titration strategies were adopted. In one, the inhibitor was titrated to a mixture of RabGGTase and NBD-FPP. As shown in Figure 4-2-7 **A** and **C**, the fluorescence intensity decreased significantly after addition of RabGGTase to NBD-FPP, indicating binding of NBD-FPP to RabGGTase. On titration of **5** to the solution, there was a modest but dose-dependent and saturable increase in fluorescence intensity (Figure 4-2-7 **A**). In contrast, titration of **10** into RabGGTase:NBD-FPP resulted in a dose-dependent increase in fluorescence intensity that saturated until the recovery of NBD-FPP fluorescence (Figure 4-2-7 **D**). This indicates that **10** competes with NBD-FPP resulting in full displacement of NBD-FPP. In a control experiment where the enzyme was omitted no fluorescence change was observed, suggesting that the fluorescence change upon titration of **5** and **10** was specific for binding of the compounds to the enzyme. The observed fluorescence increase data could be fitted as described above to give an apparent K_d value of 645±137 nM for **5**. As shown in Figure 4-2-7 **A**, the fluorescence recovery was not complete at the concentrations where addition of **5** did not lead to further fluorescence change. At this point an excess of GGPP was added to the reaction mixture, resulting in fluorescence increase to the level of unbound NBD-FPP, indicating the full displacement of NBD-FPP from RabGGTase. This can be interpreted as either **5** induced partial displacement of NBD-FPP from RabGGTase or that simultaneous binding of **5** to the enzyme allosterically induces fluorescence change of the associated NBD-FPP.

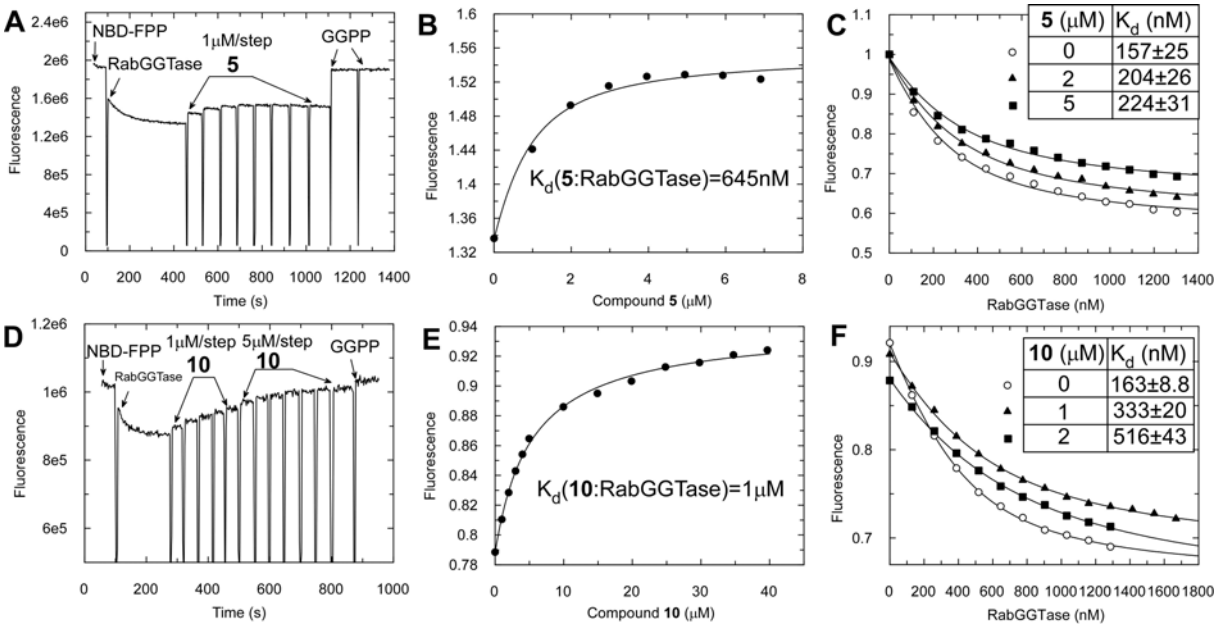

Figure 4-2-7. Analysis of the interaction of compound **5** (**A**-**C**) and **10** (**D**-**F**) with RabGGTase. (**A**) Raw data for a titration of **5** into the solution of RabGGTase complexed with NBD-FPP followed by addition of GGPP. The initial level of the fluorescence signal represents the fluorescence of free NBD-FPP (400 nM). In the first titration step RabGGTase were added to a final concentration of 550 nM. Subsequently, **5** was titrated into the cuvette in 1 μM steps. Finally, GGPP was added to a final concentration of 4 μM. (**B**) The same process as in (A), the data was fitted by numerical simulation to a non-competitive model to give a genuine K_d of 645±153 nM for the interaction of **5** with RabGGTase. (**C**) Titration of a 200 nM solution of NBD-FPP with RabGGTase in the absence of **5** (open circles) and in the presence of 2 μM (filled triangles) and 5 μM (filled squares) of **5**. The data were fitted with a quadratic equation to obtain the apparent K_d values as shown in the inset table. (**D**) Raw data for a titration of NBD-FPP:RabGGTase with **10** followed by addition of GGPP. The initial level of the fluorescence signal represents the fluorescence of free NBD-FPP (400 nM). In the first titration step RabGGTase was added to a final concentration of 650 nM. Subsequently, **10** was titrated into the cuvette in 1 μM and 5 μM steps. Finally, GGPP was added to a final concentration of 4 μM. (**E**) The same process as in (D), the data were fitted by numerical simulation to a competitive model leading to the dissociation constant of **10** from RabGGTase (K_d=1.0±0.078 μM). (**F**) Titration of a 400 nM solution of NBD-FPP with RabGGTase in the absence of **10** (open circles) and in the presence of 1 μM (filled triangles) and 2 μM (filled squares) of **10**. The data were fitted with a quadratic equation to obtain the apparent K_d values as shown in the inset table. The fluorescence of NBD was excited at 479 nm, and the data were collected at 547 nm.

To distinguish between these two scenarios for the binding of **5** to RabGGTase and to confirm the binding mode of **10**, an independent co-titration experiment was performed, in which RabGGTase was titrated to NBD-FPP in the presence of 2 and 5 μM of **5** (Figure 4-2-7 **C**), 1 and 2 μM **10** (Figure 4-2-7 **F**). No significant change was observed in the apparent K_d values in the presence of **5** (Figure 4-2-7 **C** inset table), suggesting that binding of **5** has no, or very little influence on the affinity of NBD-FPP to RabGGTase. This is consistent with the observation from the Lineweaver-Burk plot (Figure 4-2-6 **A**), which shows that **5** is non-competitive with respect to NBD-FPP. Taken together, the titrations shown in Figure 4-2-7 **C** suggest that **5** and NBD-FPP concurrently bind at two independent but weakly communicating sites of the enzyme. In contrast, the presence of **10** reduced the affinity between NBD-FPP and

RabGGTase in a dose-dependent manner (Figure 4-2-7 **F** inset table), indicating that **10** is competitive to NBD-FPP. From these data, the K_I value was calculated to be 0.94±0.025 μM from the relationship, $K^{app}=K_d(1+[I]/K_I)$.

Fitting the competitive titration data shown in Figure 4-2-7 **B** by numerical simulation to a non-competitive model led to a K_d value of 645±153 nM for the interaction of **5** with RabGGTase. This represents the genuine K_d value for **5** with RabGGTase. Since **5** binds in a non-competitive site with respect to the NBD-FPP binding site, the apparent K_d value is the same as the genuine one. In this situation, NBD-FPP acts essentially as a tracer that monitors the interaction between **5** and RabGGTase. Simulation of the competitive titration and co-titration data shown in Figure 4-2-7 **E** and **F** through a competitive model gave K_d values of 1.0±0.078 μM (Figure 4-2-7 **E**) and 1.1±0.042 μM, respectively, for the binding of **10** to RabGGTase. These results are in good agreement with the obtained K_I value estimated by the competitive inhibition equation as described above. Hence **10** competes with NBD-FPP for the prenyl binding site of RabGGTase.

Compounds **5** and **10** differ in only one amino acid residue (R^3). Replacing phenylalanine to a histidine residue at R^3 leads to a significant change of the binding mode of the compound. The crystal structure of the RabGGTase:**10** complex (Figure 4-2-8) shows that the R^3 histidyl side chain coordinates to Zn^{2+} and the N-terminal decyl chain extends into the GGPP binding cavity. This suggests that **10** competes with NBD-FPP mainly via the decyl chain. Coordination of the peptide side chain of **10** with Zn^{2+} could bring the molecule to the entrance of the cavity, facilitating insertion of the N-terminal decyl chain into the lipid binding cavity. However, based on the interaction analysis of **5** interaction with RabGGTase, it is possible to postulate that changing the R^3 amino acid residue of the peptide core may change the orientation of the decyl chain of **5** that could now possibly bind to the putative binding site for the isoprenoid of mono-prenylated Rab (Figure 4-2-2 **A**), which is expected to be located between the reactive center (Zn^{2+}) and the rim of the β subunit. The crystal structure of RabGGTase complexed with **10** as well as the interaction analysis of **5** and **10** with RabGGTase suggest that the peptide core determines the geometry of the molecule bound with RabGGTase, while the lipid chain further enhances the interaction.

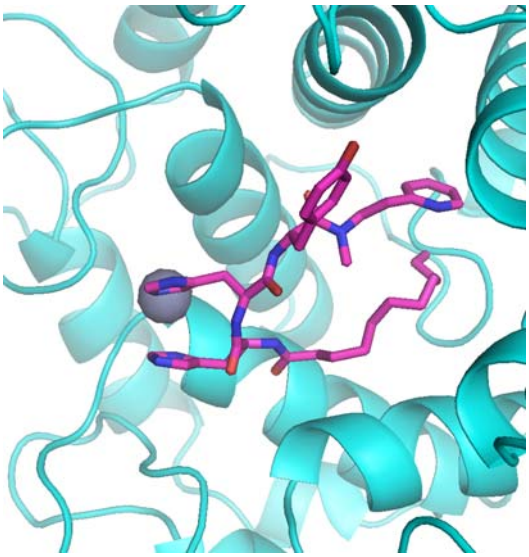

Figure 4-2-8. Crystal structure of the RabGGTase:**10** complex. RabGGTase is in ribbon representation (cyan), Zn^{2+} is shown as a gray ball, while **10** is in stick representation. The histidyl side chain of peptide backbone coordinates to Zn^{2+} and the N-terminal decyl chain overlaps with the GGPP binding site. (Crystal structure determinated by Zhong Guo)

The same analysis was applied to Type-II inhibitor **43** to reveal the mechanism of inhibition of RabGGTase. The Lineweaver-Burk plot for compound **43** suggests that it is essentially a competitive inhibitor for RabGGTase with respect to NBD-FPP. The competitive titration of **43** into the RabGGTase:NBD-FPP complex revealed that compound **43** has a K_d value of 9.2 μM for the interaction with RabGGTase. Fitting of the co-titration data by numerical simulation to a competitive model led to a genuine K_d value of 5.3 μM for the interaction of compound **43** with RabGGTase. The action of **43** towards RabGGTase appears to be quite similar to that of another Type-II inhibitor, **35** (Dursina et al., 2006). The crystal structure of RabGGTase:**35** complex reveals that **35** competes with the lipid substrate mainly through hydrophobic association with the prenyl binding site (Figure 4-2-2 **B**). It would be expected that **43** also associates with the prenyl binding site via the hydrophobic moieties.

The interaction and SAR analysis of the two types of inhibitors for RabGGTase suggest that the hydrophobic residues play a predominant role in the association of inhibitor with RabGGTase. This is determined by the nature of the active site of RabGGTase, which consists of the prenyl binding site and the putative binding site for the isoprenoid of mono-prenylated Rab. Both sites are promising target pockets for inhibitors. In addition to the hydrophobic interactions, the presence of hydrogen-bonding and Zn^{2+} coordination groups would provide additional interaction free energy of the inhibitor with RabGGTase.

The interactions of some inhibitors with RabGGTase were also investigated by isothermal titration calorimetry (ITC), and the results are summarized in Table 4-2-5. Interaction analyses of PA with RabGGTase and other inhibitors from VLS with FTase (Table 4-2-5) have been discussed in detail in the Diploma thesis of Weiyun Zhou (Diplom Thesis, Dortmund University, 2007).

Table 4-2-5. K_d values of inhibitor interaction with RabGGTase and FTase.

Compound	Inhibition type with respect to NBD-FPP	K_d (μM) for RabGGTase		
		Co-titration	Competitive titration	ITC
5	non-competitive		0.645	
10	competitive	1.1	1.0	
43	competitive	5.3	9.2	
PA	competitive	0.122	0.053	0.543
MK21986	non-competitive		13.8	
AG205/33152020	mixed inhibition			

Compound	Inhibition type with respect to peptide	Inhibition type with respect to FPP	K_d (μM) for FTase		
			Co-titration	Competitive titration	ITC
MK21986	competitive	non-competitive	1.4	1.3	2.4
AG205/33152020	mixed inhibition	mixed inhibition			

4.2.5 Selectivity of inhibitors towards RabGGTase, FTase and GGTase-I

In order to identify selective inhibitors for prenyltransferases, some of the identified active compounds were evaluated for their inhibitory activity towards RabGGTase, FTase and GGTase-I by an SDS-PAGE end-point assay. A typical SDS-PAGE end-point assay for characterization of prenyltransferase inhibitors is shown in Figure 4-2-9. In FTase and GGTase-I reactions, protein substrates GST-KiRas and GST-RhoA, and fluorescent lipid substrate NBD-GPP and NBD-FPP were used, respectively. Reactions were carried out in the presence and the absence of various concentrations of inhibitor for the same period of time and quenched by adding SDS sample buffer. The reaction mixtures were resolved by 15% SDS-PAGE, and the fluorescence bands corresponding to the formation of the prenylated product were quantified. The data were processed in the same way as the plate assay (section 4.2.1).

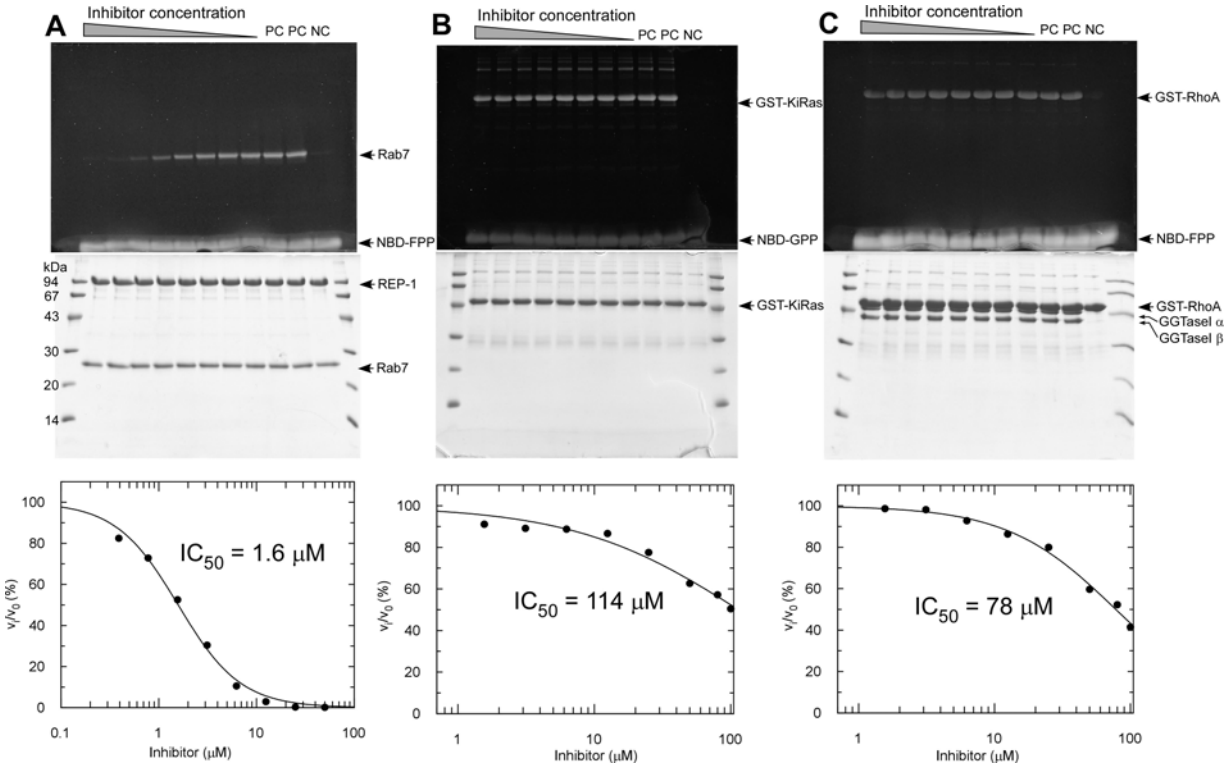

Figure 4-2-9. Determination of IC_{50} of PA for RabGGTase (**A**), FTase (**B**) and GGTase-I (**C**) by SDS-PAGE end-point assay. The top panels show the fluorescence scan of the gel, the middle panels show the Coomassie blue stained gel as a loading control, the bottom panels show the inhibition profile by quantification of the prenylation reaction shown in the top panels. In PC (positive control) no inhibitor was added. In NC (negative control) both inhibitor and enzyme were omitted.

The SDS-PAGE end-point assay (further referred to as a gel assay) enables us to evaluate of the inhibitory activity of the inhibitor towards the three prenyltransferases systematically. Table 4-2-6 shows the IC_{50} values of inhibitors for FTase, GGTase-I and RabGGTase determined by the gel assay. The IC_{50} values determined using the gel assay were comparable to those obtained using the plate assay as decribed in section 4.2.1, suggesting that both assays were able to provide comparable and consistent estimation of the inhibitory activity of the compounds.

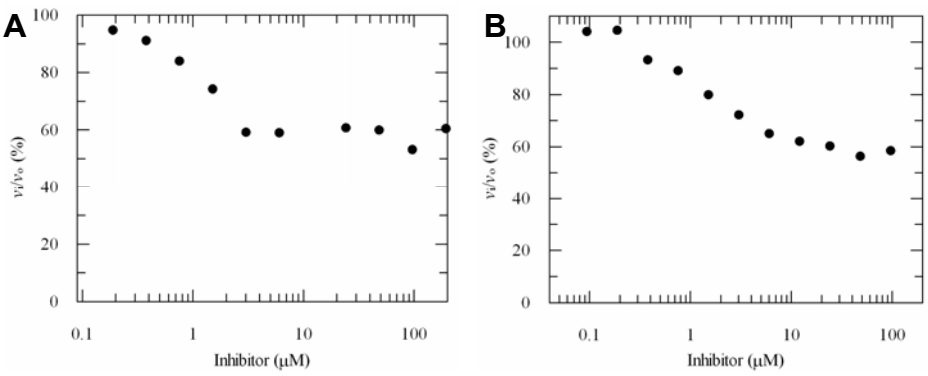

Figure 4-2-10. Inhibition profiles of compounds **5** (A) and **7** (B) against FTase. vi/v0 represents the remaining activity in the presence of inhibitor.

Table 4-2-6. IC_{50} values of inhibitors using 96-well format continuous fluorescence assay (plate assay) and SDS-PAGE assay (gel assay).

Entry	Compound	R^5	R^4	R^3	R^2	R^1	IC_{50} (μM) for RabGGTase		IC_{50} (μM) for FTase (gel assay)	IC_{50} (μM) for GGTase-I (gel assay)
							Plate assay	Gel assay		
1	**5**		L-His	L-Phe	L-Tyr	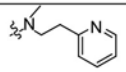	0.97 ± 0.1	2.8 ± 0.1	>100	>100
2	**7**		L-Tyr	L-His	L-Tyr	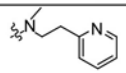	2.4 ± 0.7	4.3 ± 0.4	>100	>100
3	**10**		L-His	L-His	L-Tyr	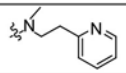	4.9 ± 0.6	10 ± 0.9	35 ± 5.8	60 ± 5.3
4	**11**		L-His	L-Phe	L-Tyr	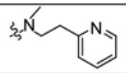	2.8 ± 0.4	8.8 ± 0.7	98 ± 4.7	97 ± 31
5	**43**	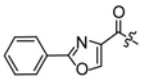	L-His	Gly	L-His(Trt)	OH	21 ± 4.5	14 ± 1.3	13 ± 1.0	6.9 ± 2.3
6	**45**		L-His(Trt)	Gly	L-His	OH	38 ± 8.7	41 ± 4.0	14 ± 2.6	2.6 ± 1.0
7	**49**		Gly	L-Phe	L-His(Trt)	OH	25 ± 8.0	31 ± 8.3	3.4 ± 0.7	5.6 ± 2.0
8	**58**		Gly	L-Phe	L-His	OH	50 ± 5.9	141 ± 12	6.8 ± 0.7	5.1 ± 0.4
9	**50**		Gly	L-Phe	L-His(Bn)	OH	79 ± 5.0	> 50	19	> 50
10	**53**	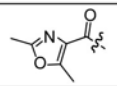	Gly	L-Phe	L-His(Trt)	OH	46 ± 5.4	50	15	> 50
11	PA						1.7± 0.5	1.6	114	78
12	MK21986						7.0± 1.5	9.4 ± 1.5	21.5 ± 12	11 ± 3.2
13	AG205/33152020						5.3	9.9	19	17
14	AH487/41653773						34	nd	37	75

[a] nd: not determined. PA is identified from a random library. MK21986 is from a small virtual library identified by Mahesh Kulharia. AG205 and AH487 are from the hits of Molsoft ICM-VLS.

The IC_{50} values of **5** and **7** (Table 4-2-6, entry 1 and 2) for FTase were not extractable. Although the compounds showed dose-dependent inhibition of FTase, the inhibition saturated at less than 50% (Figure 4-2-10), which was not observed in the cases of the other two prenyltransferases. This suggests that both compounds partially inhibit FTase with a complex inhibition mode, i.e. neither classicially non-competitive nor competitive to both substrates. Compounds **5** and **7** exhibit more than 50- and 20-fold selectivity for RabGGTase over FTase and GGTase-I. Peptide **11** (Table 4-2-6, entry 4) with a three-carbon shorter N-terminal lipid chain than peptide **5**, displays an 11-fold selectivity for RabGGTase over FTase and GGTase-I. Peptide **10** (Table 4-2-6, entry 3) is only 3 and 6 times more specific towards RabGGTase over FTase and GGTase-I, respectively. The inhibition profile of these 4 inhibitors for FTase exhibits a similar trend as observed for GGTase-I. Thus, Type-I compounds, **10**, **11** ,**7** and **5**, show moderate to very good selectivity for RabGGTase and can be regarded as the first low micromolar RabGGTase inhibitors that do not show significant cross-activity for FTase and GGTase-I.

Certain Type-II compounds shown in Table 4-2-4, which do not show very high inhibitory activity for RabGGTase, were chosen for selectivity studies with the other two prenyltransferases. As shown in Table 4-2-6, in contrast to **43** (Table 4-2-6, entry 5) that extensively inhibits three prenyltransferases, the compounds, **45**, **49** and **58** (Table 4-2-6, entry 6, 7 and 8)**,** exhibit 5-20 fold inhibitory selectivity for FTase and GGTase-I over RabGGTase.

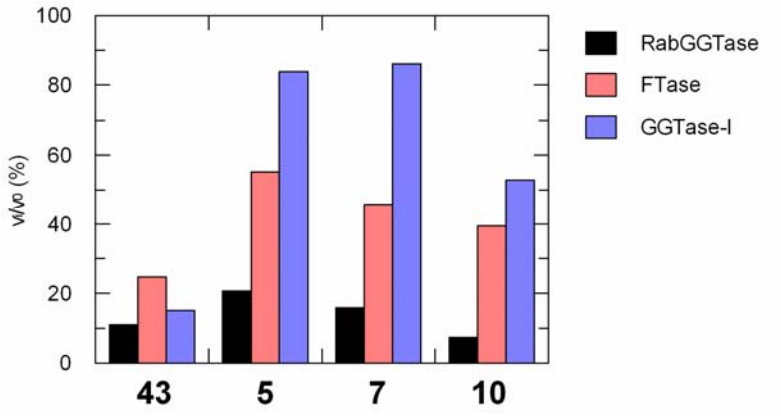

Figure 4-2-11. Initial velocity of prenyltransferases-mediated reactions in the presence of 50 μM of the indicated compounds as a percentage of that in the absence of the compounds.

A potent RabGGTase inhibitor, PA, was identified, which shows 70- and 50-fold selectivity for RabGGTase over FTase and GGTase-I, respectively. To compare the selectivity of the compounds in another manner, the same concentration of **5**, **7**, **10** and **43** were analyzed for their ability to inhibit prenylation mediated by the three

prenyltransferases. From Figure 4-2-11, we can see that the selectivity of compounds **5**, **7** and **10** for inhibition of RabGGTase is indeed much better than that of **43**.

Since the prenyl binding sites in RabGGTase, FTase and GGTase-I are conserved, compounds with a lipid chain would be expected to universally inhibit the three prenyltransferases. However, these compounds showed significantly higher inhibitory activity towards RabGGTase than towards FTase and GGTase-I, suggesting that the lipid chain does not determine the binding mode of the compound. Together with the findings from the interaction analysis, we concluded that the peptide core of the inhibitors is the key determinant of the geometry of the bound molecule, whereas the lipid chain is directed by binding of the peptide core and further strengthens the protein-inhibitor interaction. It should be noted that the not-competitive* inhibitor **5** with respect to NBD-FPP showed better selectivity for RabGGTase than the competitive inhibitor **10**. This is not surprising, since a compound with a lipid chain that associates with the conserved prenyl binding site of prenyltransferases would be more likely to display cross-activity for the three prenyltransferases. As mentioned above, the not-competitive inhibitor may bind to the putative binding site for the isoprenoid of mono-prenylated Rab, which is structurally different from the analogous exit grooves in FTase and GGTase-I. This suggests that the putative binding site for the isoprenoid of mono-prenylated Rab represents an important binding pocket for rational design of selective RabGGTase inhibitors. Compound **5** would be a good starting point for the design of not-competitive and selective inhibitors.

The variation in the structures of the peptides with very good inhibitory selectivity for one of the three prenyltransferases suggests that selectivity of the inhibitors in this compound class can be attenuated to yield specific prenyltransferase inhibitors. In this peptide library, the R^5 position appears to be critical for selectivity among the three prenyltransferases. A long lipid chain at R^5 position was found to improve selectivity of the compounds, with the preference towards RabGGTase. These observations provide guidance for design of new selective prenyltransferase inhibitors.

* Since non-competitive and uncompetitive have distinct definitions, we use the term ‘not competitive’ here.

4.2.6 Inhibition of RabGGTase *in vivo* by peptide inhibitors

To evaluate the cellular activity of the identified peptide inhibitors of RabGGTase, a cellular assay for RabGGTase activity was performed (Figure 4-2-12). Briefly, COS-7 cells were transfected with a construct mediating overexpression of a EYFP-Rab7 fusion protein. Transfected cells were treated with the compounds, incubated for 24h, then harvested and lysed. The resulting cell lysate was assayed for presence of unprenylated Rabs by incubation with excess RabGGTase, REP1 and BiotinGPP. Subsequently cell lysates were then resolved by SDS-PAGE, Western blotted and probed with steptavidin-horse radish peroxidase to detect Rab-geranyl-biotin conjugates (Figure 4-2-13). The emergence of blot bands of Rab GTPases indicates the presence of unprenylated Rabs and therefore inhibition of Rab prenylation in cells. (*In vivo* evaluation was performed by Dr. Christine Delon)

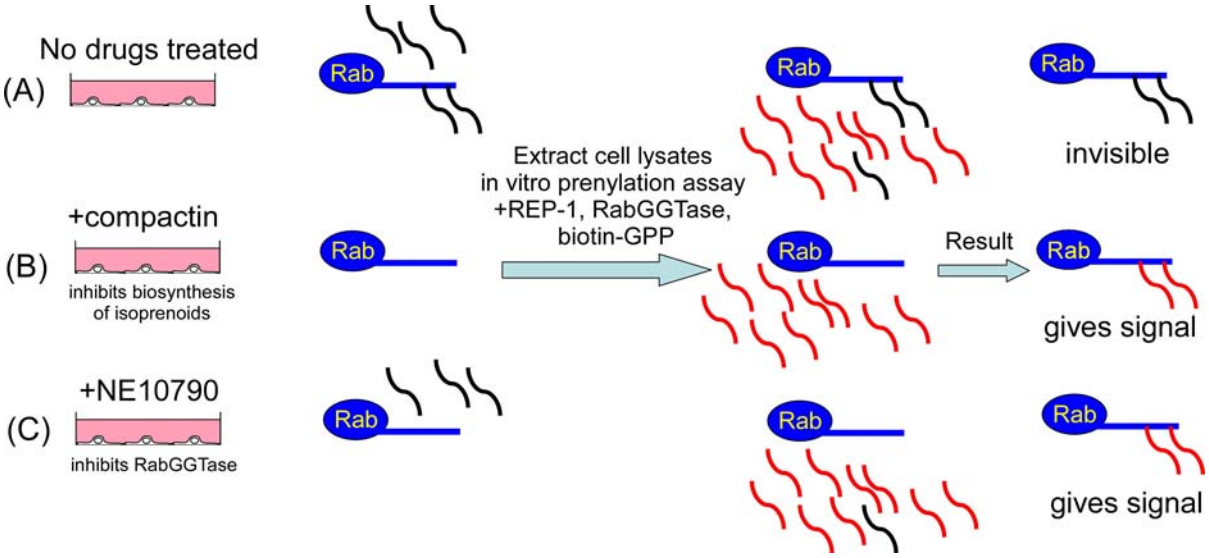

Figure 4-2-12. Schematic illustration of the principle of the *in vitro* prenylation assay. Black lines represent GGPP and red lines represent biotin-GPP. (**A**) No drug is added to the cell assay. The Rab proteins are prenylated by endogenous GGPP, therefore subsequent *in vitro* prenylation by RabGGTase, REP1 and biotin-GPP gives no signal. (**B**) Compactin is added as a positive control for the inhibition of the biosynthesis of isoprenoids. Rab proteins are not prenylated in the cell and therefore subsequent *in vitro* prenylation by RabGGTase, REP1 and biotin-GPP gives signal. (**C**) A known RabGGTase inhibitor, NE10790, is added to the cell assay. Rab proteins are not prenylated in the cell and therefore subsequent *in vitro* prenylation by RabGGTase, REP1 and biotin-GPP gives a signal.

The test compounds **5, 7, 10, 32, 33** and **43**, were observed to be non-cytotoxic to the cells at 100 μM. Although the inhibitors did not significantly affect the endogenous pool of Rab proteins, they all caused increased incorporation of biotin-GPP to YFP-Rab7 (Figure 4-2-13 **A**), indicating that these compounds were able to

inhibit the prenylation of over-expressed EYFP-Rab7 *in vivo* to an extent comparable to inhibition by compactin (which prevents formation of GGPP by inhibiting the mevalonate pathway) (Woo et al., 2000; Brown et al., 1978) or NE10790, a selective inhibitor of RabGGTase (Coxon et al., 2001).

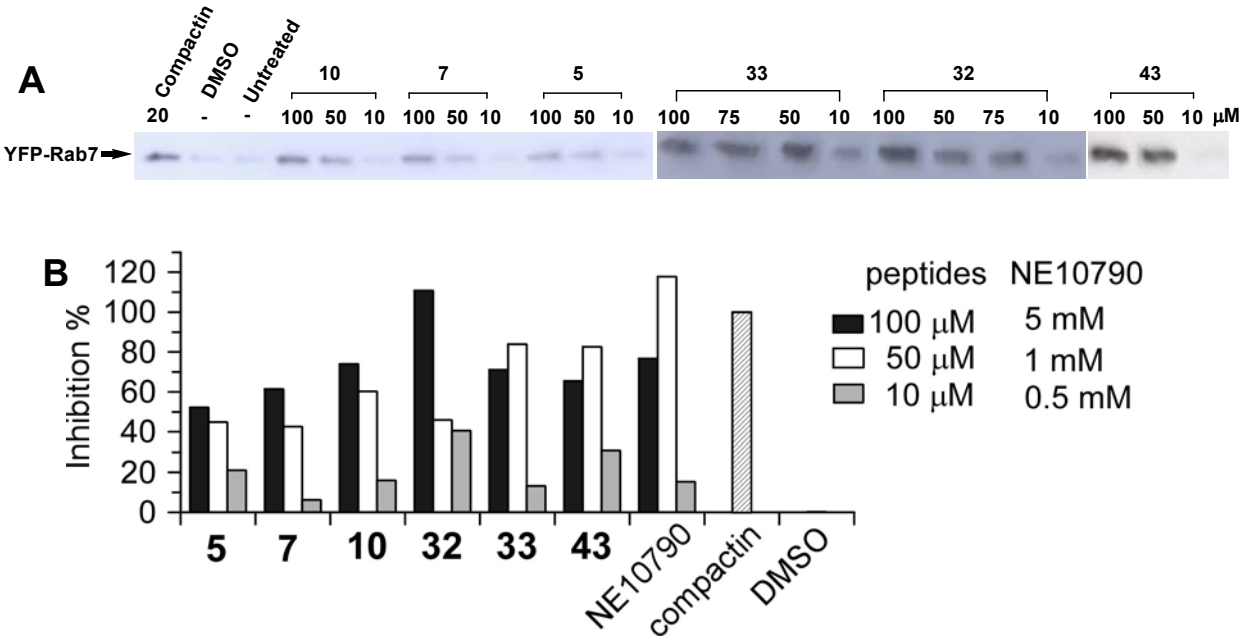

Figure 4-2-13. *In vivo* inhibition of RabGGTase by peptide inhibitors. COS-7 cells transiently over-expressing EYFP-Rab7 were treated with 20 μM compactin as a positive control, with 1% (v/v) DMSO as a negative control, with the inhibitors of three different concentrations, 100 μM, 50 μM and 10 μM, and with 5mM, 1mM and 0.5 mM NE10790. The cells were lysed and the resulting cell lysates were collected and prenylated *in vitro* with 0.5μM RabGGTase and REP1 and 5μM BiotinGPP for 1h at 25°C. The *in vitro* prenylated cell lysate was resolved by SDS-PAGE followed by Western blotting with Streptavidin-HRP. Western blot (**A**) and the *in vivo* inhibition profile of inhibitors (**B**) are shown here. The *in vivo* inhibition profile was obtained by quantification of the band intensity and subsequent normalization of the intensity against the positive control (compactin) and negative control (DMSO).

The six inhibitors show concentration-dependent inhibition of RabGGTase in the cellular assay (Figure 4-2-13 **B**). The intensity of the blot bands were quantified and data were processed in the same way as described in section 4.2.1, assuming 100% inhibition by 20 μM compactin and 0% inhibition by 1% DMSO. All inhibitors show more than 50% inhibition of RabGGTase at 100 μM. The peptide inhibitors identified in this assay are 10 times more potent than the previously validated RabGGTase inhibitor, NE10790. In general, the peptide inhibitors show higher inhibitory activity at 50 μM than NE10790 at 500 μM. Moreover, peptide **32** exhibits an *in vivo* inhibition at 100 μM comparable to that induced by NE10790 at 1 mM.

In conclusion, a building block strategy equipped with the hydrazine linker and the 2-chlorotrityl chloride resin led to generation of a peptide library derived from Pepticinnamin E with different chemical functionalities at the N- and C-terminus and incorporation of various amino acids at the peptides central core. Several potent RabGGTase inhibitors with low micromolar IC_{50}s have been identified from a screening of 450 peptides. The SAR analysis of the peptide library has revealed several functional groups which are essential for the inhibitory activity of the peptides for RabGGTase. Figure 4-2-5 outlines the important features of the active RabGGTase inhibitors from the peptide library. Aromatic amino acid residues at the peptide central core (R^2-R^4), phenylalanine, histidine and tyrosine, are essential for the inhitory activity of the peptide inhibitors towards RabGGTase. The Type-I inhibitors with a combination of a long lipid chain at the N-terminus (R^5) and a potential zinc binding group, such as *N*-methyl 2-ethyl pyridine, at the C-terminus (R^1) have shown good inhibitory activity for RabGGTase, whereas the active Type-II inhibitors contain an aryl ring at the N-terminus (R^5) and a carboxylic acid at the C-termunus (R^1).

The quantitative analyses and selectivity studies of the peptide inhibitors with RabGGTase, FTase and GGTase-I suggest that changes of the chemical structures of the peptides lead to different modes of inhibition, binding sites and selectivity profiles. The peptide central core (R^2-R^4) determines the binding configuration of the compound and the R^1 residue strongly influences the activity of the peptide. However, the chemical moiety at R^5 position appears to be critical for the selectivity among the three prenyltransferases. The large volume of the active site of RabGGTase makes the rational design of potent and selective inhibitors challenging. However, targeting the putative binding site for the isoprenoid of mono-prenylated Rab in RabGGTase would be a very promising approach for future identification of specific RabGGTase inhibitors. Compound **5** can be a suitable starting point for this purpose. Furthermore, the interesting selectivity of the inhibitors for the three prenyltransferases found here may lead to a better understanding and interpretation of the extensive inhibition of three prenyltraseferses by FTIs (farnesyltransferase inhibitors). The identification of cellularly active peptides, in particular highly specific inhibitors, would open up the opportunity for Pepticinnamin E derivatives as small and selective molecular probes for the *in vivo* investigation of prenyltransferases via a chemical genetic approach (Lackner et al., 2005).

4.3 The mechanistic basis of Rab prenylation

4.3.1 Simulation of the Rab C-terminus in the ternary protein complex

The mechanism of the Rab prenylation pathway including the lipid substrate binding and specificity (Thoma et al., 2000), binary (Rak et al., 2004; Pylypenko et al., 2003) and catalytic ternary complex assembly (Thoma et al., 2001a; Alexandrov et al., 1999), the process of double prenylation (Thoma et al., 2001c), and product release (Thoma et al., 2001b), have been systematically investigated in our group by kinetic and structural methods (see the summary of kinetic and thermodynamic studies in Scheme 4-4, and for a review see (Goody et al., 2005)). In brief, there are two pathways for assembly of the prenylation machinery. One of them, referred to as the 'classical' pathway, involves initial binding of Rab and REP molecules with variable affinity. Subsequently REP presents Rab to the RabGGTase:GGPP complex in a high-affinity interaction (K_d = ca. 2 nM). The contact between the protein substrate Rab and enzyme RabGGTase is believed to occur via REP, since Rab and RabGGTase have no detectable affinity, but the crystal structure of the Rab:REP:RabGGTase ternary complex is not available yet. REP has low affinity for RabGGTase in the absence of Rab and of GGPP, but both entities have a positive effect on this affinity. Binding of GGPP to the active site of RabGGTase appears to induce long-range (36 Å) structural changes that are transduced from the core of β subunit to the outer helices of the α subunit of RabGGTase in order to accommodate the side chain of $_{rep}$F279 of REP-1, resulting in a K_d of 6 nM for the REP interaction with RabGGTase. Since Rab can now bind with high affinity to form the quaternary complex (K_d = 28 nM), this order of binding represents an 'alternative' pathway of the catalytic complex formation. After assembly of the prenylation machinery, double prenylation proceeds without dissociation of the mono-prenylated intermediate, with a preference of the C-terminal cysteine in Rab7 for the first prenyl transfer. After prenylation, the prenylated Rab:REP remains tightly associated with RabGGTase (K_d = ca. 2 nM). This high affinity would result in product inhibition as well as a problem for Rab membrane delivery. However, this situation appears to be relieved by binding of an additional phosphoisoprenoid substrate (i.e. GGPP) molecule, since this binding leads to a decrease in the affinity of RabGGTase to the prenylated Rab:REP

complex by an order of magnitude (K_d = 18 nM). The crystal structures of the prenylated Rab:REP complex and REP:RabGGTase complex led to a proposal for the a mechanism for product release. After prenylation, binding of a further isoprenoid molecule expels the conjugated geranylgeranyl moieties from the active site on RabGGTase. After release, they must migrate towards their binding site on domain II of the REP molecule. Creation of a lipid-harboring cavity to generate the binding pocket for the conjugated isoprenoids leads to displacement of $_{rep}$F279 and $_{rep}$R290 from their binding interface on RabGGTase, resulting in dissociation of the RabGGTase.

The ternary protein complex has so far not proven amenable to structural analysis, although it has been generated and crystallized (Rak et al., 2002). The availability of the prenylated Rab7:REP complex and REP:RabGGTase complex structures allows modeling of the Rab:REP:RabGGTase ternary complex (Rak et al., 2004). However, electron density in the prenylated Rab7:REP complex can only be traced until D193 of Rab7, with the remaining 14 residues being invisible in the electron density map, probably due to high flexibility in the structure. Based on the structures of the prenylated Rab7:REP complex (PDB access code, 1VG0) and REP:RabGGTase complex (PDB access code, 1LTX), internal coordinate mechanics (ICM) methodology (Molsoft) was used to simulate of the disordered C-terminus of Rab7 in the ternary complex, leading to a lowest energy conformation shown in Figure 4-3-1 (this work was done together with Prof. Dr. Ruben Abagyan during a visit to the Scripps Institute, La Jolla, CA). In the resulting model, the Rab molecule is located above the α subunit of RabGGTase and the last visible residue of Rab7 C-terminus is positioned ca. 35 Å above its active site (Figure 4-3-1 **A**). The flexible Rab7 C-terminus is long enough to reach the active site on the β subunit (Figure 4-3-1 **A** and **B**).

As shown in Figure 4-3-1 **C**, the simulated C-terminus of Rab7 extends on the surface of REP and RabGGTase and protrudes into the active center, where the cysteine thiol coordinates the Zn^{2+} ion. However, no interaction could be detected between a Rab7 C-terminal 10-mer peptide and RabGGTase by isothermal titration calorimetry (ITC) (data not shown). This suggests that the contact of the disordered C-terminus with the protein surface is weak and probably non-specific, in keeping with the idea that the Rab C-terminus needs to be flexible for movement in later events, including prenylation of the second cysteines and translocation of the

conjugated geranylgeranyl moieties from RabGGTase to REP, and also in keeping with the fact that both the sequence and length of this reagion vary highly. The low specificity of the contact also ensures that RabGGTase and REP can process all Rab proteins with their highly variable C-termini. Nevertheless, it is still unclear what the critical determinants for Rab prenylation are.

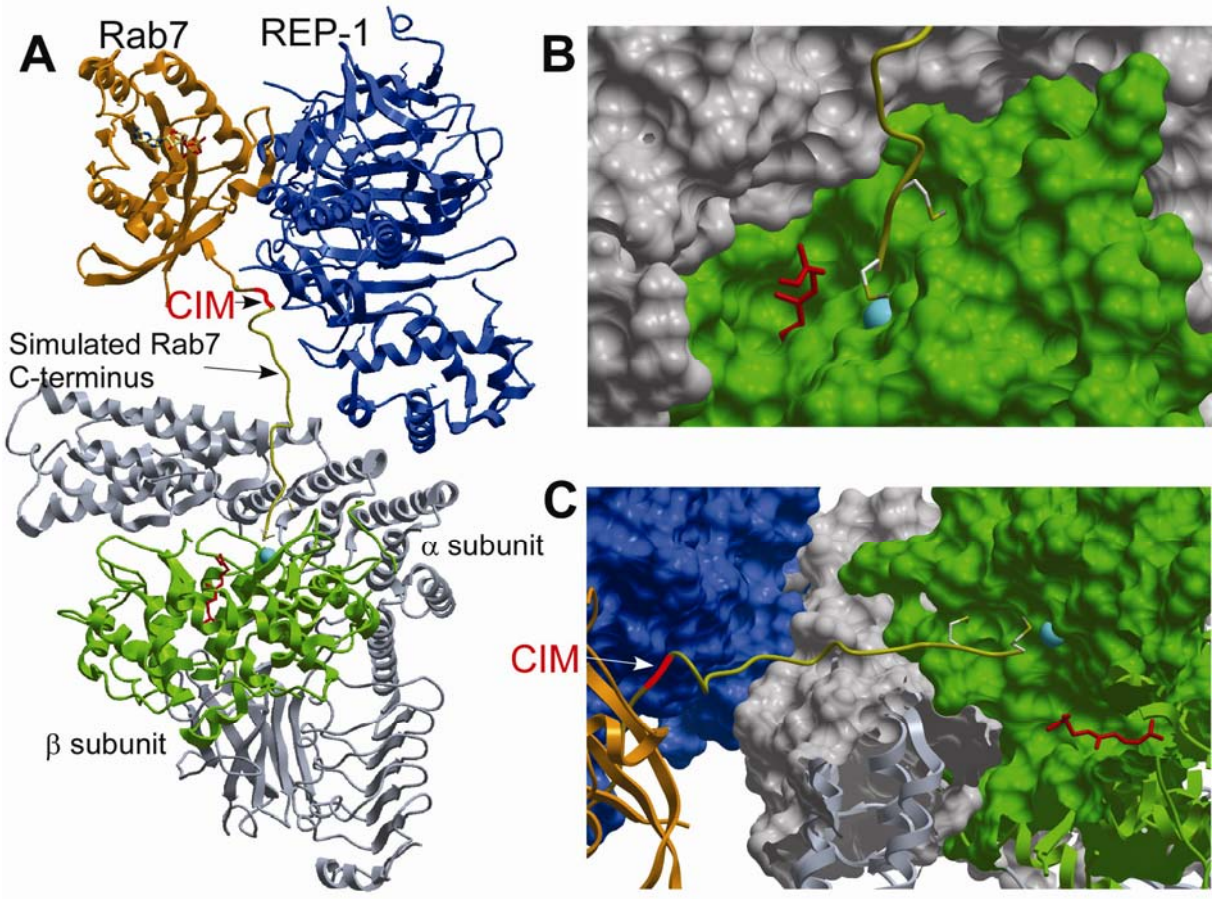

Figure 4-3-1. Simulation of the Rab7 C-terminus in the ternary complex base on structures of prenylated Rab7:REP complex (1VG0) and REP-1:RabGGTase (1LTX). (**A**) Ribbon representations of Rab7 (orange) with CIM highlighted in black, REP-1 (blue), RabGGTase α subunit (gray), RabGGTase β subunit (green), and simulated Rab7 C-terminus (gold). The farnesyl group is show in stick representation in red, and Zn^{2+} as a turquoise ball. (**B**) Surface representations of RabGGTase with the C-terminus of Rab7 protruding into the active site. The colors of all species are the same as in A. The residues of the two cysteines at Rab7 C-terminus are show in stick representation. (**C**) Ribbon representation of simulated C-terminus of Rab7 on the surface of REP and RabGGTase. All species are colored the same as in A. RabGGTase is sliced to show the active site.

4.3.2 Rab C-terminus plays multiple roles in Rab prenylation

4.3.2.1 Engineering of the Rab C-terminus based on simulation and binary complex structures

The structures of mono-prenlyated Rab7:REP-1 as well as mono- and di-prenylated Ypt1:GDI complexes (Pylypenko et al., 2006; Rak et al., 2003) provided

detailed information on the interaction mechanism of RabGTPases with REP and GDI. Both REP and GDI interact with Rab proteins through two binding sites designated the Rab Binding Platform (RBP) and the C-terminal binding region (CBR). The Rab Binding Platform interacts via a complex network of primarily polar interactions with the switch regions I and II of RabGTPases forming both a specific and conformation sensitive protein:protein interface. In contrast to the RBP, the CBR of both REP and GDI molecules interacts with the C-terminus of Rab molecules via primarily hydrophobic interactions formed by a patch of two or three hydrophobic amino acid residues (I, L and P) located within the last 10-20 residues of Rab molecules (Figure 4-3-2). As shown in Figure 4-3-3, sequence analysis of Rab proteins revealed that this cryptic motif is identifiable in most RabGTPases and binding this motif to the hydrophobic CBR on the surface of REP/GDI molecules appears to be required for proper fixation of the long unstructured C-terminus of RabGTPase (Rak et al., 2004). This coordination was assumed to be required for the proper positioning of the C-terminal cysteine residues in the active center of the RabGGTase and the positioning of the conjugated geranylgeranyl moieties in the lipid binding site of REP/GDI, as shown in the simulation (Figure 4-3-2). Moreover, the hydrophobic C-terminal motif, termed the CBR Interacting Motif (CIM), is in the hypervariable part of Rab's C-terminus that is believed to be largely or at least partially responsible for their targeting to specific membranes. This idea is indirectly supported by the fact that, being bound to the CBR via the CIM motif, the hypervariable part of the C-terminus is located in the immediate proximity of the so-called mobile effector loop of REP/GDI molecules, which is believed to be a second component required for the membrane delivery of prenylated Rab proteins (Sakisaka et al., 2002). However, it remains unclear whether the CIM is strictly required for Rab prenylation since it cannot be identified with certainty in all RabGTPases. Moreover, its contribution to overall affinity and specificity of the REP/GDI interaction is unclear since Rab7 lacking 22 C-terminal residues retains the ability to stably associate with REP (Rak et al., 2004).

In addition, the simulation of the Rab C-terminus in the ternary protein complex reveals that the length of the C-terminus downstream of the CIM could be important for Rab prenylation. If we assume that the geometry of the overall Rab:REP:RabGGTase ternary complex is rigid as we have in our simulation, the appropriate length of the chain after CIM would determine the proper targeting of the

C-terminal cysteine to the active site for its prenylation, i.e. the downstream C-terminal chain must be long enough to bridge the CBR of REP and the active site of RabGGTase. The length of the C-terminus after the CIM should also be enough to ensure the positioning of conjugated geranylgeranyl moieties in the lipid binding site of REP. Furthermore, the exact nature of the C-terminal residues after the CIM may or may not play a role in Rab prenylation. As already mentioned, this region is hypervariable in Rab proteins.

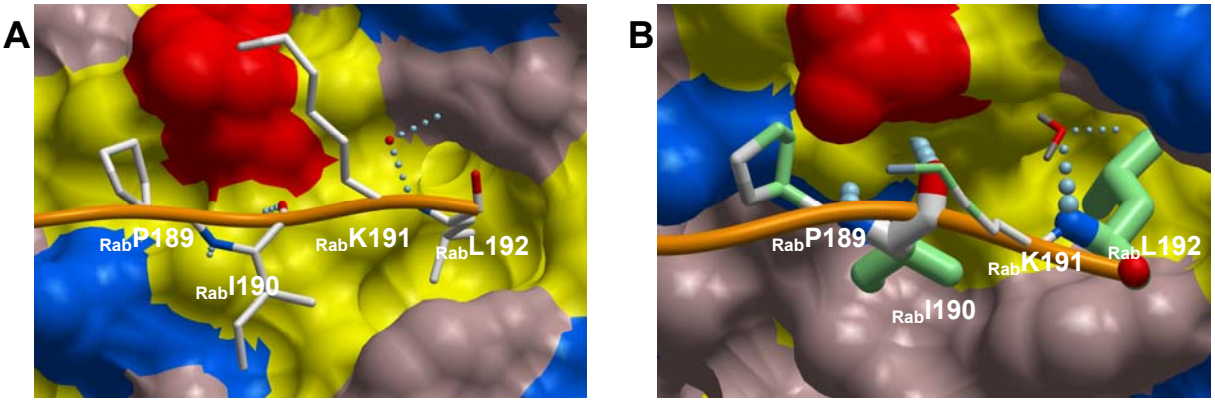

Figure 4-3-2. Interaction of the Rab7 CIM with the CBR of REP-1. (**A**) The hydrophobic patch of REP-1 is displayed in surface representation and hydrophobic residues are colored in yellow, polar and charged residues are colored in pink, blue (+) and red (-). The main chain atoms involved in hydrogen bonding are displayed in atomic colors. The C-terminus of Rab7 is displayed as an orange worm and the residues $_{Rab}$P189-$_{Rab}$L192 are displayed in stick format. The hydrogen bonds are displayed as strings of tiny cyan balls. The water molecule involved in H-bonding is displayed as a red ball. (**B**) Calculation of the contact area of these residues with REP displayed and colored as in (A). The atoms involved in hydrophobic interactions are colored green. The more they are involved in the interaction with REP, the bolder is the residue stick. The order of contact area for these residues is: L192>I190>P189>K191.

In the light of this idea, we designed a series of Rab7 mutants with engineered C-termini (Figure 4-3-4). To identify cryptic CIMs in other Rab proteins, mutations at the putative CIM motif of different Rab proteins were generated. The established and versatile reporter NBD-FPP (Chapter 4.1.3) enables us to study the prenylation of a large number of Rab proteins and Rab mutants. The fluorescent Rab conjugates described in Chapter 4.1 were used as sensors for the interaction of Rab proteins and mutants with REP and RabGGTase. These analyses will be described in a later section.

```
hRAB6A          --------------D-RSREDMID-----IKLEKPQEQPVS-EGGCS---C---- 27
hRAB6B          --------------E-KSKEGMID-----IKLDKPQEPPAS-EGGCS---C---- 27
hRAB7           -------------Q-ETEVELYNEFPEPIKLDKNDRAKAS-AESCS---C---- 32
hRAB39          -----GEICIQDGWE-GVKSGFVP-----NTVHPSEEAVKP-RKECS---C---- 36
hRAB39B         -----GEITIQEGWE-GVKSGFVP-----NVVHSSEEVVKS-ERRCL---C---- 36
hRAB11A         -----KQMSDRRENDMSPSNNVVP-----IHVPPTTE-NKP-KVQC----CQNI- 38
hRAB11B         -----KQIADRAAHDESPGNNVVD-----ISVPPTTDGQKPNKLQC----CQNL- 40
hRAB9           --------------TEDRSDHLIQ-----TDTVNLH-RKPKPSSSC----C---- 27
rRAB29          ------------NSREDIMSSSTQ-----GNYINLQ-TKPSPGWTC----C---- 29
rRAB12          ---------VLRSELSNSILSLQP-----EPEIPPELPPPRPHVRC----C---- 33
mRAB33B         ------------SHKPLMLSQLP-----DNRISLK-PETKPAVTCW---C---- 29
hRAB27A         -----MERCVDKSWIPEGVVRSN------GHASTDQLSEEKEKGACG---C---- 37
hRAB27B         -----MEQCVEKTQIPDTVNGGNS-----GNLDGEKPPEKK----CI---C---- 34
HRAB35          ----KKDNLAKQQQQQQNDVVKLT-----KN--------SKRKKRC----C---- 30
bRAB34          -------ELEKSGSRRIGDVVRIN-----SDDSNLYLTASKKKPTC----CP--- 36
hRAB1A          ----------MGPGA---TAGGAEK----SNVK-IQSTP-VKQSGGG---CC--- 30
rRAB1B          ----------MGPGA---ASGG-ER----PNLK-IDSTP-VKSASGG---CC--- 29
cRAB21          ---AQVDERAKGNGS---SQPGAAR----RGVQIIDDEPQAQSSGGG---CCSSG 42
rRAB26          ------------STK---APSEPRF----RLHDYVKREG--RGVSC----CRL-- 28
mRab37          ------------AGR---QPDEPSF----QIRDYVESQK--KRSSC----CSFV- 29
rRAB3C          -----MS-ESLETDP---AITAAK-----QSTRLKETPP-PPQPNCG---C---- 33
hRAB3B          -----MS-DSLDTDP---SMLGSS-----KNTRLSDTPP-LLQQNCS---C---- 33
rRAB16          IICDKMN-ESLEPSS---SPGSNG-----KGPSLGDTPP-PQPSSCG---C---- 38
hRAB3D          -----MN-ESLEPSS---SSGSNG-----KGPAVGDAPA-PQPSSCS---C---- 33
hRAB4A          ---GELDPERMGSGI---QYGDAAL----RQLRSPRRTQAPNAQECG---C---- 38
rRAB4B          ---GELDPERMGSGI---QYGDISL----RQLRQPRSAQAVAPQPCG---C---- 38
rRAB14          ---GSLDLNAAESGV---QHKPSAP----QGGRLTSEPQ-PQREGCG---C---- 37
hRAB5B          --------EPQNLGG---AAGRSR------GVDLHEQSQ-QNKSQC----CSN-- 31
hRAB5C          --------EPQNATG---APGRNR------GVDLQENNP-ASRSQC----CSN-- 31
hRAB5A          --------EPQNPGA---NSARGG------GVDLTEPTQ-PTRNQC----CSN-- 31
hRAB8           -------DKKLEGNS----PQGSN-----QGVKITPD-Q-QKRSSFFR--CVLL- 34
rRAB8B          -------NRKMNDSN----SSGAG-----GPVKITE-SR-SKKTSFFR--CSLL- 34
hRAB40A         ARMMHGGSYSLTTSS---THKRSSL----RKVKLVRPPQ-SPPKNCTRNSCKIS- 46
hRAB40B         ARMMRGLSYSLTTSS---THKRSSL----CKVKIVCPPQ-SPPKNCTRNSCKIS- 46
hRAB40C         --------YSLASGAGGGGSKGNSL----KRSKSIRPPQ-SPPQNCSRSNCKIS- 41
cRAB22          -----------DANP----PSGGK------GFKLRRQPS-EPQRSC----C---- 25
hRAB3A          -----MSESLDTADP---AVTGAK-----QGPQLSDQQV-PPHQDCA---C---- 34
rRAB10          ------------PVK---EPNSEN-----VDISSGGGVT-GWKSKC----C---- 26
mRAB20          --------MIMRQRA---EESDQT-----VDIASCKTPK-QTRSGC----CA--- 31
mRAB24          -----------AAFQ---VMTEDK------GVDLSQKAN-PYFYSC----CHH-- 28
mRAB17          ---------AGDTGS---SRPQEG-----EAVALNQEPP-IRQRQC----CAR-- 31
mRAB23          ---VFNASVGSHLGQNSSSLNGGD----VINLRPNKQRTKRTRNPFSS--CSVP- 45
hRAB22B         -----------DPHE-----NGNN------GTIKVEKPTMQSSRRC----C---- 25
hRAB32          -------NHQSFPNE---ENDVDK-----IKLDQETLRA-ENKSQC----C---- 31
rbRAB25         --------KQIQNSP---RSNAIAL----GSAQAGQEPGPGQKRAC----CINL- 35
rRAB15          -------GLRTCASN---ELALAEL----EEDEGKTEGPANSSKTCW---C---- 34
hRAB33A         ----AQKSLLYRDAE---RQQGKV-----QKLEFPQEAN--SKTSCP---C---- 34
hRAB41          ---YNVKKLFRRVASALLSTRTSPPPK--EGTVEIELESFEESGNRS--YC---- 44
mRAB19          ----ARNSLHLYGES---AQQGLSQ----DSSPVLVAQVPNESTRCT---C---- 37
mRAB18          ----------LWESE-----NQNK------GVKLSHREESRGGGACGG-YCSVL- 32
hRAB2           ---GVFDINNEANGIKIGPQHAAT-----NATHAGNQGGQQAGGGC----C---- 39
hRAB36          ------DLERQSSAR--LQVGDGDLIQMEGSPPETQESKRPSSLGC----C---- 39
hRAB30          ----------ARQNT---LVNNVS-------SPLPGEGKSISYLTC----CNFN- 30
hRAB13          -----------GGRR---SGNGNK-----PPSTDLKTCDKKNTNKCS---LG--- 30
rRAB38          -----------NECD---FIESIE-----PDIVKPHLTS-PKVVSCSG--CAKS- 32
hRAB28          --------IKLNKAEIEQSQRIVR-----AEIVKYPEEENQHTTSTQSRICSVQ- 41
```

Figure 4-3-3. Sequences of the Rab C-terminus. The non-polar residues (I, L, V, P) shown in bold typeface and highlighted are the putative CBR interacting motif (CIM). In some Rab proteins, it is difficult to assign this motif.

```
                      190  195  200  205
Rab7wt              EFPEPIKLDKNDRAKTSAESCSC
Rab7Δ204            EFPEPIKLDKNDRAKTSAECSC
Rab7Δ203-204        EFPEPIKLDKNDRAKTSACSC
Rab7Δ202-204        EFPEPIKLDKNDRAKTSCSC
Rab7Δ201-204        EFPEPIKLDKNDRAKTCSC
Rab7Δ200-204        EFPEPIKLDKNDRAKCSC
Rab7Δ199-204        EFPEPIKLDKNDRACSC
Rab7Δ198-204        EFPEPIKLDKNDRCSC
Rab7Δ197-204        EFPEPIKLDKNDCSC
Rab7Δ3              EFPEPIKLDKNDRAKTSAES
Rab7Δ14             EFPEPIKLD
Rab7Δ22             E
Rab7-7A             EFPEPIKLAAAAAAASAESCSC
Rab7-5A             EFPEPIKLDKNDRAAAAAACSC
Rab7-11A            EFPEPIKLAAAAAAAAAAACSC
Rab7_ASA            EFPEPIKLDKNDRAKTSAESCSCASA
Rab7_NLYFQ          EFPEPIKLDKNDRAKTSAESCSCNLYFQ
Rab7_WFY            EFPEPIKLDKNDRAKTSAESCSCWFY
Rab7I190H           EFPEPHKLDKNDRAKTSAESCSC
Rab7L192S           EFPEPIKSDKNDRAKTSAESCSC
Rab7I190HL192S      EFPEPHKSDKNDRAKTSAESCSC

                          200       210       220
Rab27             KSWIPEGVVRSNGHTSTDQLSEEKEKGLCGC
Rab27_Rab7_Cter   KSWIPEPIKLDKNDRAKTSAESCSC
```

Figure 4-3-4. The upper panel shows sequences of the C-terminus of a series of Rab7 mutants. The lower panel shows the C-terminal sequences of Rab27 and a Rab27_Rab7 chimera, where part of the C-terminus of Rab27 was replaced by Rab7 CIM and downstream sequence (shown in red). *Note: expression of Rab7-7A and Rab7-11A in E. coli was not successful, resulting in a protein with 13 C-terminal residues truncated (reason unknown).*

4.3.2.2 CBR interacting motif is essential for Rab prenylation in vitro

As described above, the Rab7 C-terminus is mounted to REP-1 via the interaction of I190 and L192 with the CBR of the latter (Figure 4-3-2). In order to understand the effect of this interaction on Rab prenylation, we prepared mutants of Rab7 where either or both of the residues were mutated to polar amino acids. The resulting mutants were purified and subjected to *in vitro* prenylation analysis using a fluorescent analogue of geranylgeranyl pyrophosphate, NBD-FPP (see Chapter 4.1.3). As can be seen in Figure 4-3-5 A and Table 4-3-1, individual mutations led to a reduction in the rate and total yield of the prenylation reaction. The Rab7 L192S mutant displayed more significant inhibition of prenylation than Rab7 I190H, suggesting that L192 is the more critical residue in the CBR:CIM interaction. This finding is consistent with the structure of the CBR:CIM interface, where L192 protrudes deeply into the hydrophobic cavity on the REP-1 surface while I190

contacts the outer edge of the CBR. Calculation of the contact area of these residues also shows that L192 has a higher contact area with REP than I190 (Figure 4-3-2 **B**).

The mutations appear to have more than an additive effect since the double mutant Rab7 I190HL192S showed no detectable prenylation. While single mutatants showed reduction in prenylation efficiency. This indicats that the CIM motif is strictly required for Rab prenylation (Figure 4-3-5 **A**, Table 4-3-1).

Analysis of Rab:REP and Rab:GDI structures shows that the CIM motif functions as a hydrophobic anchor which in principle can be composed of different amino acid residues. Moreover, the C-terminus of Rab GTPases can differ significantly in length. These situations complicate the unambiguous identification of the CIM motif in Rab proteins. While some Rab proteins contain a clearly identifiable CIM motif resembling that of Rab7, others do not (Figure 4-3-3). To test experimentally whether CIM sequences are present in other RabGTPase, we chose Rab2, Rab13 and Rab16 proteins for detailed analysis. As shown in Figure 4-3-6, Rab13 and Rab16 have an obvious CIM motif in their C-terminus. But Rab2 has two putative CIM motifs in the C-terminal region, if we assumed that the CIM motif would highly likely be located in the unstructured domain of apo-Rab GTPase. In Rab2, I185 and I187 appear to more resemble a CIM motif.

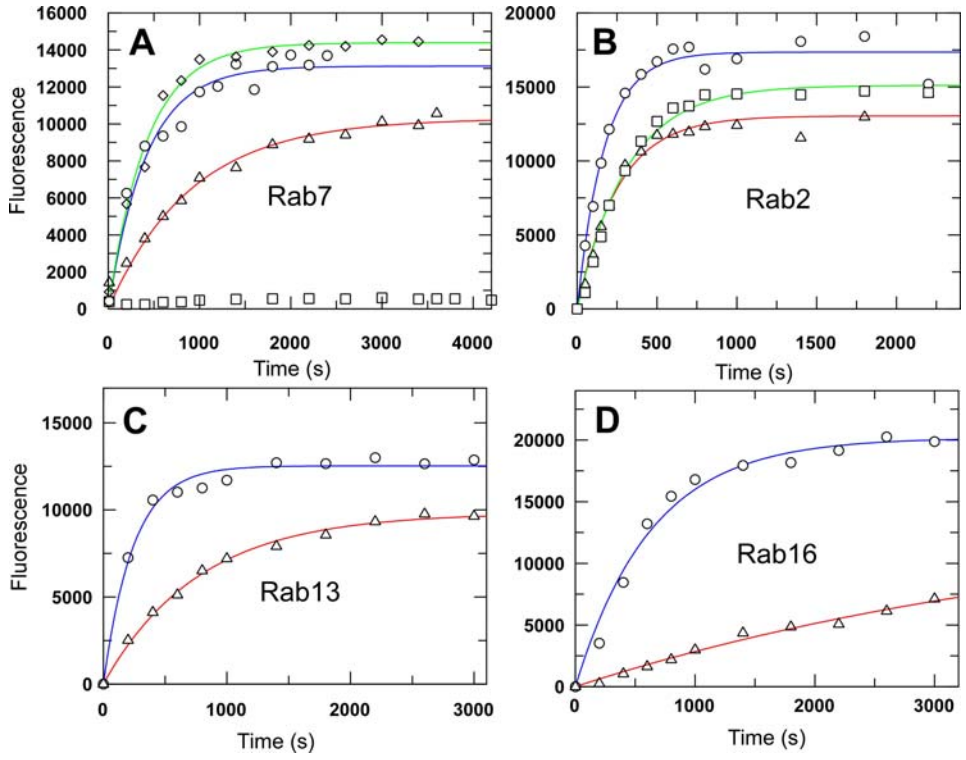

Figure 4-3-5. In vitro prenylation of wild type and CIM mutants of Rab7, Rab2, Rab13 and Rab16 with NBD-FPP. The reaction was started by addition of NBD-FPP to a mixture of RabGTPase, RabGGTase and REP and aliquots were withdrawn at indicated time points quenched and resolved on 15% SDS-PAGE gel. Fluorescent scanning of the gels and data analysis was performed as

described under the Chapter 6.4.3. (**A**) ○ Rab7 wt, ◇ Rab7 I190H, △ Rab7 L192S and □ Rab7 I190HL192S. (**B**) ○ Rab2 wt, △ Rab2 I185S and □ Rab2 I185SI187S. (**C**) Wild type (○) and L189S mutant (△) of Rab13. (**D**) Wild type (○) and L185S mutant (△) of Rab16. The solid lines show the fits to single exponential functions.

Table 4-3-1. Observed in vitro prenylation rate of wild type and CIM mutants of Rab proteins.

Protein	Rate X10^{-3} (s^{-1})	Protein	Rate X10^{-3} (s^{-1})
Rab7wt	2.39±0.28	Rab2wt	5.80±0.46
Rab7I190H	2.36±0.15	Rab2I185S	3.91±0.33
Rab7L192S	1.09±0.10	Rab2I185SI187S	3.20±0.21
Rab7I190HL192S	-		
Rab13wt	4.11±0.32	Rab16wt	1.57±0.14
Rab13L189S	1.30±0.06	Rab16L185S	0.22±0.07

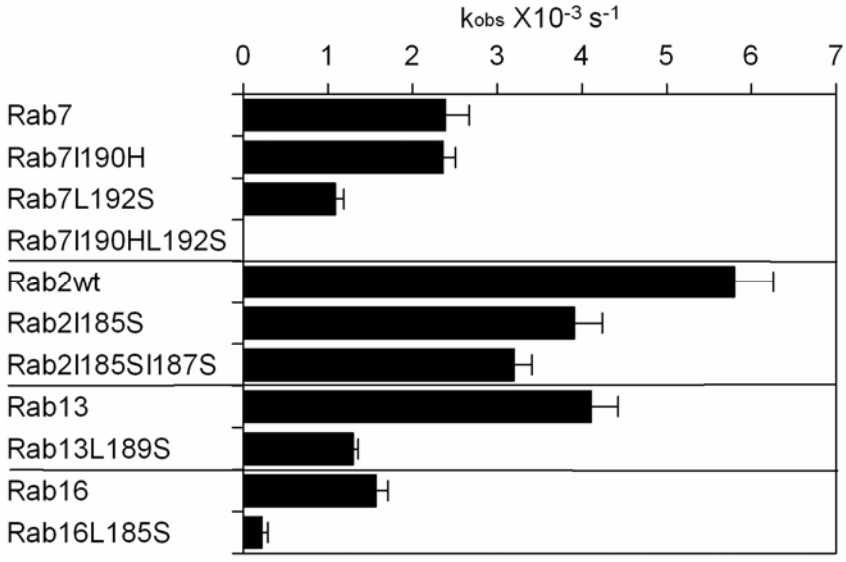


```
hRAB2       AFINTAKEIYEKIQEGVFDINNEANGIKIGPQHAATNATHAGNQGGQQAGGGCC 212
hRAB7       AFQTIARNALKQETE--------VELYNEFPEPIKLDKNDRAKASAESCSC--- 207
rRAB13      AFSSLARDILLKTGG-------RRSGNSSKPSS--TDLKVSDKKNSNKCSLG-- 203
rRAB16      VFERLV-DIICDKMN-------ESLEPSSSPGSNGKGPSLGDTPPPQPSSCGC- 198
              .*   . :   .                .  *     .     .   : ..

                    170       180       190       200       210
hRAB2       INTAKEIYEKIQEGVFDINNEANGIKIGPQHAATNATHAGNQGGQQAGGGCC
hRAB7       NVEQAFQTIARNALKQETEVELYNEFPEPIKLDKNDRAKASAESCSC
rRAB13      AFSSLARDILLKTGGRRSGNSSKPSSTDLKVSDKKNSNKCSLG
rRAB16      IICDKMNESLEPSSSPGSNGKGPSLGDTPPPQPSSCGC
```

Figure 4-3-6. C-terminal sequence alignment and residue number in each pr
otein. The putative CIM motifs (I, L, V, P) are shown in bold typeface and highlighted in yellow, the regions highlighted in pink are α-helixes observed in the crystal structures.

First we produced recombinant wild type and I187S and I185SI187S mutants of Rab2 and assessed their ability to undergo prenylation *in vitro*. The results shown in Figure 4-3-5 **B** and Table 4-3-1 demonstrate that I185S mutation slightly reduced the

prenylation of Rab2 protein. Unlike in the case of Rab7, the activity of the Rab2 I185SI187S double mutant for prenylation only decreased by a factor of 2. This indicates that I185 and I187 may not be the correct CIM motif for Rab2 protein. Another putative CIM motif of Rab2, V175 and I178, should be tested further.

To analyse the CIM motifs of Rab13 and Rab16 we introduced a single point L to S mutation in each of these proteins at the position that would correspond to I190 or L192 in Rab7. As shown in the Figure 4-3-5 **C**, **D** and Table 4-3-1, in both cases the mutations led to a substantial reduction in the rate and the total amount of GTPase prenylation. This indicates that the CIM is functionally important for Rab prenylation across the Rab family.

4.3.2.3 Effects of sequence downstream CIM on Rab prenylation

As shown in the simulation (Figure 4-3-1), the length of the chain after CIM has to be long enough to deliver the C-terminal cysteine residues to the active center of the RabGGTase. Nevertheless, it is the most divergent part of Rab proteins and no specific sequence could be identified in this domain across the Rab family. In order to understand the effect of the sequence downstream CIM on Rab prenylation, we truncated sequentially 1 to 8 amino acid residues located before the first prenylatable cysteine. This resulted in shortening of the length of the linker between CIM and the active site. In other constructs, the length of the linker was kept but either (193)DKNDRAKT(198), (199)KTSAES(204) or the whole linker, (193)DKNDRAKTSAES(204), was replaced by a poly-alanine chain to verify whether specific residues in this domain are required for Rab prenylation (Figure 4-3-4).

The continuous fluorometric assay as described in section 4.1.3 was used to evaluate the prenylation rate of these Rab constructs. The chosen concentrations of the individual components were far above the respective K_d values. Under such conditions the dissociation and association would not be rate limiting so as to ensure a single turnover reaction. The obtained time traces (Figure 4-3-7 **A**) upon reaction could be fitted to the double exponential functions, giving two rate constants (Table 4-3-2). This indicated that at least two steps give rise to fluorescence changes. Because the fluorescence time trace exactly correlates with reaction progress assayed by HPLC and SDS-PAGE (section 4.1.3, Figure 4-1-18, Figure 4-1-20), this type of experiment can still be used to derive prenylation rate constant, although such fits do not have a direct physical meaning.

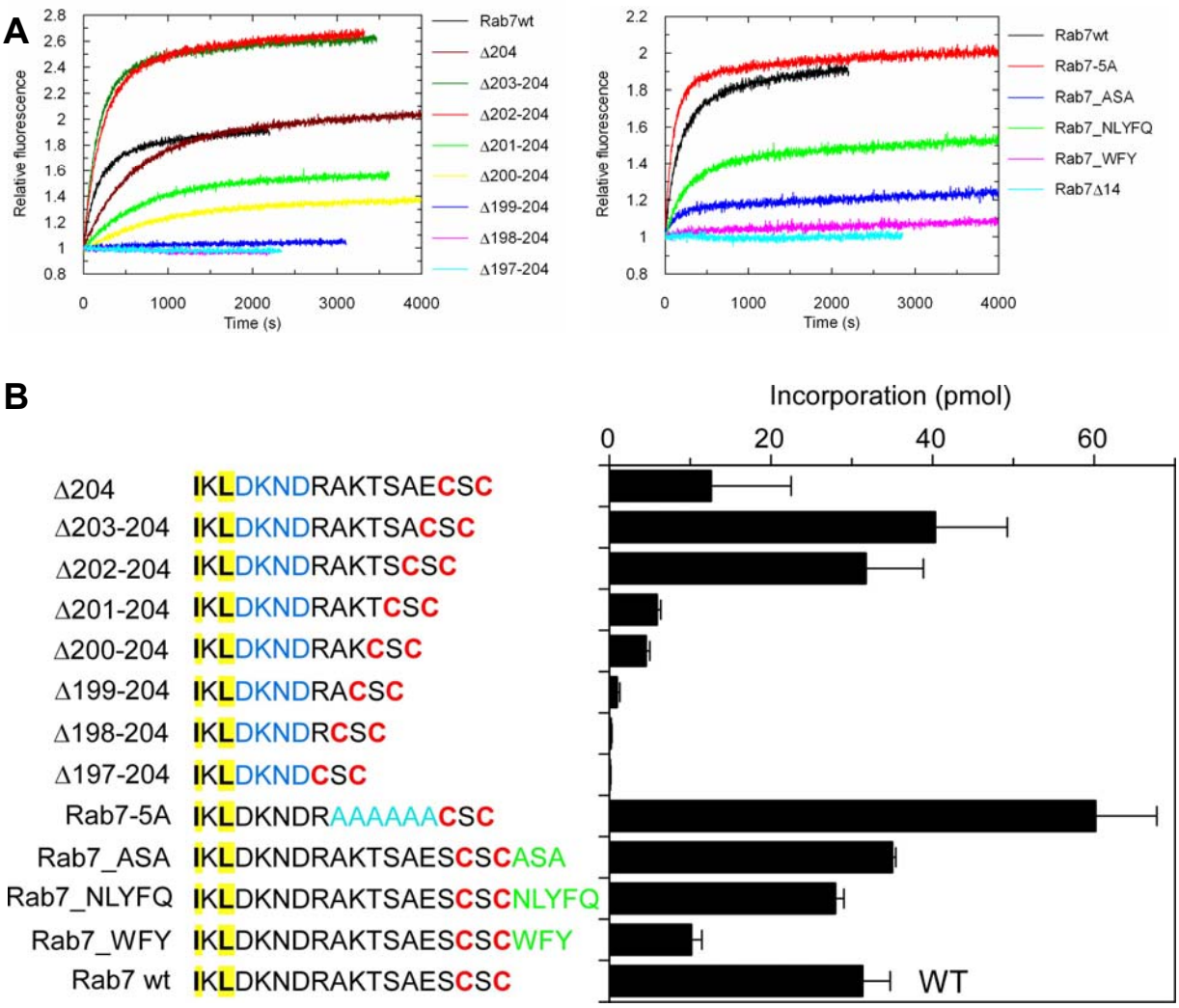

Figure 4-3-7. (**A**) Time-course of in vitro prenylation of Rab7wt and its mutants at 25°C. Reaction mixture contains 1 μM Rab, REP-1 and RabGGTase, and 4 μM NBD-FPP. (**B**) Quantification of prenylated products after saturation of the reaction by SDS-PAGE analysis. The reaction mixture contains 6 μM Rab protein (totally 61 pmol), 10 μM REP-1 and 6 μM RabGGTase, and 40 μM NBD-FPP. The fluorescence of the bands corresponding to the prenylated Rab was quantified using AIDA densitometry software and the values were corrected using Coomassie blue staining of the same bands

Table 4-3-2. Observed in vitro prenylation rates of Rab7wt and its mutants

Species	C-terminus of Rab7wt and mutants	Amp1	Rate1 (s^{-1})	Amp2	Rate2 (s^{-1})
Rab7wt	IKLDKNDRAKTSAESCSC	0.61	0.0068	0.31	0.0010
Rab7Δ204	IKLDKNDRAKTSAECSC	0.82	0.0018	0.41	0.00018
Rab7Δ203-204	IKLDKNDRAKTSACSC	1.3	0.0062	0.34	0.00083
Rab7Δ202-204	IKLDKNDRAKTSCSC	1.3	0.0050	0.40	0.00070
Rab7Δ201-204	IKLDKNDRAKTCSC	0.5	0.0015	0.18	0.00012
Rab7Δ200-204	IKLDKNDRAKCSC	0.32	0.0013	0.19	0.00011
Rab7Δ199-204	IKLDKNDRACSC	0.015	0.0014	0.04	0.00048
Rab7Δ198-204	IKLDKNDRCSC	0	0	0	0
Rab7Δ197-204	IKLDKNDCSC	0	0	0	0
Rab7-5A	IKLDKNDRAAAAAACSC	0.79	0.0096	0.19	0.00057
Rab7_ASA	IKLDKNDRAKTSAESCSCASA	0.14	0.0079	0.17	0.00018
Rab7_NLYFQ	IKLDKNDRAKTSAESCSCNLYFQ	0.38	0.0039	0.21	0.00030
Rab7_WFY	IKLDKNDRAKTSAESCSCWFY	0.019	0.0082	0.082	0.0003

As shown in Figure 4-3-7 and Table 4-3-2, the length of the linker between CIM and first prenylatable cysteine is critical. Truncation of the linker from 12 residues to 9 residues did not lead to significant influence on both prenylation rate and total amount of prenylated Rab (Rab7Δ204 to Rab7Δ202-204). However, truncation of the linker peptide to less than 8 amino acid residues resulted in significant reduction of prenylation efficiency (Rab7Δ201-204 to Rab7Δ197-204). The replacement of (199)KTSAES(204) with a poly alanine sequence even slightly improved Rab prenylation. These observations indicate that there is a strict criterion for the bridge between the CBR on REP and the active site on RabGGTase. This criterion is based on the length, but not the sequence of the bridging. It appears that the length between CIM and first prenylatable cysteine should not be too short (no less than 9 amino acids), and the length varies among different Rab proteins. Indeed a truncation of 10 amino acids in the C terminus (adjacent sequences in the upstream of cysteine motif) of Rab5 renders the protein cytosolic despite the presence of intact cysteine motif (Chavrier et al., 1991). It also suggests that another anchor within the linker is not required for proper Rab prenylation, correlating with the simulation results, which shows the downstream C-terminal chain non-specifically extends on the surface of REP and RabGGTase. This is further supported by the fact that Rab family possesses a diverse array of C-terminus. An additional anchor might actually be disadvantageous, since it might adversely influence translocation of the conjugated geranylgeranyl moieties from RabGGTase to REP, which would require a large movement of C-terminus.

An additional random sequence with 3-5 residues following prenylatable cysteine did not reduce Rab prenylation, consistent with the fact that 1-3 residues occur after C-terminal cysteine in some Rab proteins. However, addition of a group of aromatic amino acid residues (WFY) after the prenylatable cysteine considerably inhibits Rab prenylation. These aromatic residues may contact with the active site so as to influence prenylation, as will be discussed in a later section.

4.3.2.4 Rab C-terminus modulates affinity of Rab:REP binary complex and Rab:REP:RabGGTase ternary complex

There are two most obvious explanations for the effect of CIM motif mutations on Rab prenylation. Since the CIM motif provides an additional contact between REP and Rab proteins it may contribute to the overall affinity of the complex and thereby

modulate the ability of RabGGTase to recruit and process the Rab protein. It is also possible that it is required for the coordination of Rab C-terminus and the observed reduction in prenylation of CIM mutants reflects the failure of the C-terminus to associate with the active site of RabGGTase efficiently. To discriminate between these possibilities, we quantitatively analysed the role of the Rab C-terminus in the interaction of Rab:REP binary complex and Rab:REP:RabGGTase ternary complex.

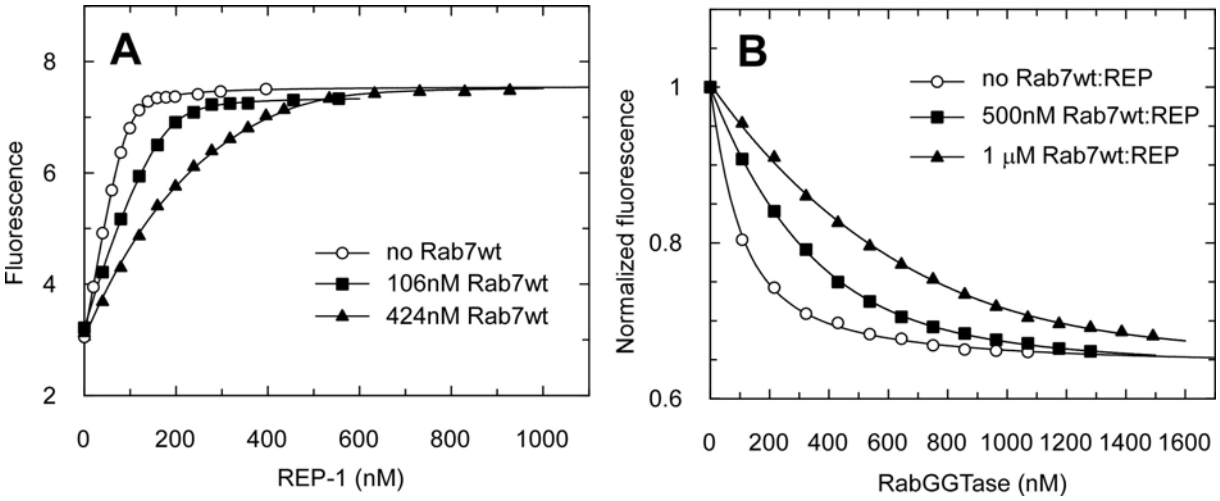

Figure 4-3-8. (**A**) Titration of REP-1 into 100 nM Rab7C(NBD)SCC in the absence (open circle) and the presence of 106 nM (filled square) and 424 nM (filled triangle) Rab7wt. Free titration data were fitted to a quadratic equation giving K_d of 3 nM. The co-titration data were fitted by numerical simulation with a competitive model to obtain K_d of 5.6 nM and 9.4 nM for Rab7wt:REP-1, during which the K_d of 3 nM for the reporter was fixed. (**B**) Titration of RabGGTase into 65 nM Rab7C(NBD)SC:REP-1 in the absence (open circle) and the presence of 500 nM (filled square) and 1000 nM (filled triangle) Rab7wt:REP-1. Data fitting was performed as in A to give K_d of 66 nM for Rab7C(NBD)SC:REP-1:RabGGTase, K_d of 137 nM and 124 nM for Rab7wt:REP-1:RabGGTase.

Since the affinity of the Rab7:REP interaction is very high (K_d~1nM) it can be accurately measured only when the titration experiment is performed at low concentrations of the reactants (Thomä and Goody, 2003). This in turn requires an assay with a sensitive fluorescence change and good quantum yield that enables reliable monitoring of the interactions at low concentrations. The Rab biosensor construction efforts performed before provided us with such a platform. As described in Chapter 4.1, we used the expressed protein ligation (EPL) approach to generate a Rab7 protein C-terminally modified with NBD group (Figure 4-1-1). Addition of REP-1 protein to a solution of Rab7C(NBD)SC or Rab7C(NBD)SCC (termed Rab7-NBD) resulted in 4-fold increase in NBD fluorescence, while association of RabGGTase with Rab7-NBD:REP-1 binary complex led to 2-fold fluorescence quenching (Figure 4-1-14 **E**). We used this sensitive signal change to monitor the interaction of a 50 nM solution of Rab7–NBD and Rab7-NBD:REP-1 with increasing concentrations of REP-

1 and RabGGTase respectively (Figure 4-3-8). The fit of the data to the quadratic equation led to a K_d value of 2.8±0.8 nM for Rab7-NBD:REP-1 and 61±7 for Rab7-NBD:REP-1:RabGGTase.

In order to obtain the values for interaction of Rab7 wild type and mutants with REP and RabGGTase, we performed co-titration experiments in which a mixture of Rab7-NBD and Rab7wt/mutant, or Rab7-NBD:REP-1 and Rab7wt/mutant:REP-1 were titrated with increasing concentrations of REP or RabGGTase. Typical co-titration experiments were shown in Figure 4-3-8. In the presence of non-fluorescent Rab7 protein, a "lag" of fluorescence increase or decrease during the titration was observed, indicating that the non-fluorescent molecule competes with the fluorescent molecule in binding to REP or RabGGTase. The resulting data was processed with a set of differentiation equations for a competitive model using program SCIENTIST™ (Thoma et al., 2000), resulting in the dissociation constants for binary and ternary complex summarized in Table 4-3-3.

Table 4-3-3. Summery of dissociation constants for interaction between Rab7wt/mutants and REP and RabGGTase.

Rab wt/mutants	C-terminal sequence	K_d of the binary complex (REP-1) [nM]	K_d of the ternary complex (RabGGTase) [nM]
Rab7C(NBD)SC	EFPEP**I**K**L**DKNDRAKTSAE**C**(**NBD**)S**C**	2.8±0.8	61±6.9
Rab7C(NBD)SCC	EFPEP**I**K**L**DKNDRAKTSAE**C**(**NBD**)S**CC**	3.2±0.9	nd
Rab7wt	EFPEP**I**K**L**DKNDRAKTSAES**C**S**C**	7.5±2.7	130±9.3
Rab7Δ3	EFPEP**I**K**L**DKNDRAKTSAES	16.1±1.0	191±22
Rab7Δ14	EFPEP**I**K**L**D	15.8±2.1	321±11
Rab7Δ22	E	381±37	491±31
Rab7-5A	EFPEP**I**K**L**DKNDRAAAAAA**C**S**C**	21.5±1.1	188±45
Rab7_WFY	EFPEP**I**K**L**DKNDRAKTSAES**C**S**C**WFY	nd	107±16
Rab7I190H	EFPEPHK**L**DKNDRAKTSAES**C**S**C**	228±59	nd
Rab7L192S	EFPEP**I**KSDKNDRAKTSAES**C**S**C**	341±74	nd
Rab7I190HL192S	EFPEPHKSDKNDRAKTSAES**C**S**C**	547±46	nd

nd: not determined.

As shown in Table 4-3-3, the determined K_d values for Rab7wt binary and ternary complex are very close to the affinity values extracted previously from the kinetic experiments (Alexandrov et al., 1999; Alexandrov et al., 1998), indicating that this assay is suitable for monitoring Rab7:REP and Rab7:REP:RabGGTase interactions. Mutation of residues of the CIM motif results in ca. 30-70 fold reduction in Rab7:REP affinity, suggesting that interactions of the CIM with the CBR makes a significant contribution to the overall affinity of the binary complex. The order of the affinity of the CIM mutants with REP correlates with the calculation results of the contact area between the CIM residues and the CBR shown in Figure 4-3-2 and the observed effects of CIM mutations on the efficiency of the prenylation shown in Figure 4-3-5 **A**. To further verify our findings we prepared three mutants of Rab7 truncated by 3, 14 and 22 amino acids (Figure 4-3-4). Rab7Δ3 lacks the C-terminal cysteines, Rab7Δ14 keeps the CIM motif intact while Rab7Δ22 removes C-terminus including the CIM motif. Analysis of Rab7Δ3, Rab7Δ14 interaction with REP reveals that the deletion of the prenylation motif and (Rab7Δ3) even the whole downstream residues after CIM (Rab7Δ14) motif does not dramatically influence the affinity of the interaction. However, deletion of the 22 residues including the CIM motif resulted in 50-fold decrease in the affinity for binary complex. This observation indicates that in accord with the structural data, the CIM motif is the only site in the Rab7 C-terminus that contributes significantly to Rab7:REP interaction. K_d for Rab7Δ22 is quite close to that of the double mutant Rab7I190HL192S, suggesting that I190 and L192S play a central role in coordination of the Rab C-terminus on the surface of REP molecule. This is also consistent with the calculation results of contact area for the CIM motif (Figure 4-3-2).

Next we wanted to confirm our observations using an independent and preferably direct method. We chose the isothermal titration calorimetry (ITC) to measure the influence of CIM mutation on the Rab:REP interactions. The results of the titration experiments, in which a fixed amount of wild type or mutant Rab7 were titrated with increasing concentrations of REP are shown in the Figure 4-3-9. The fit of the ITC data to the binding constant equation via an iteration method resulted in a K_d value of 476 ± 8nM and 21 ± 185nM for Rab7L192S and Rab7wt, respectively. The high error for the K_d value determined for wild type Rab7 is due to the limitation of the ITC method for monitoring of the interaction with low nanomolar affinities.

Nevertheless this experiment clearly confirms the results obtained using fluorescence co-titration approach.

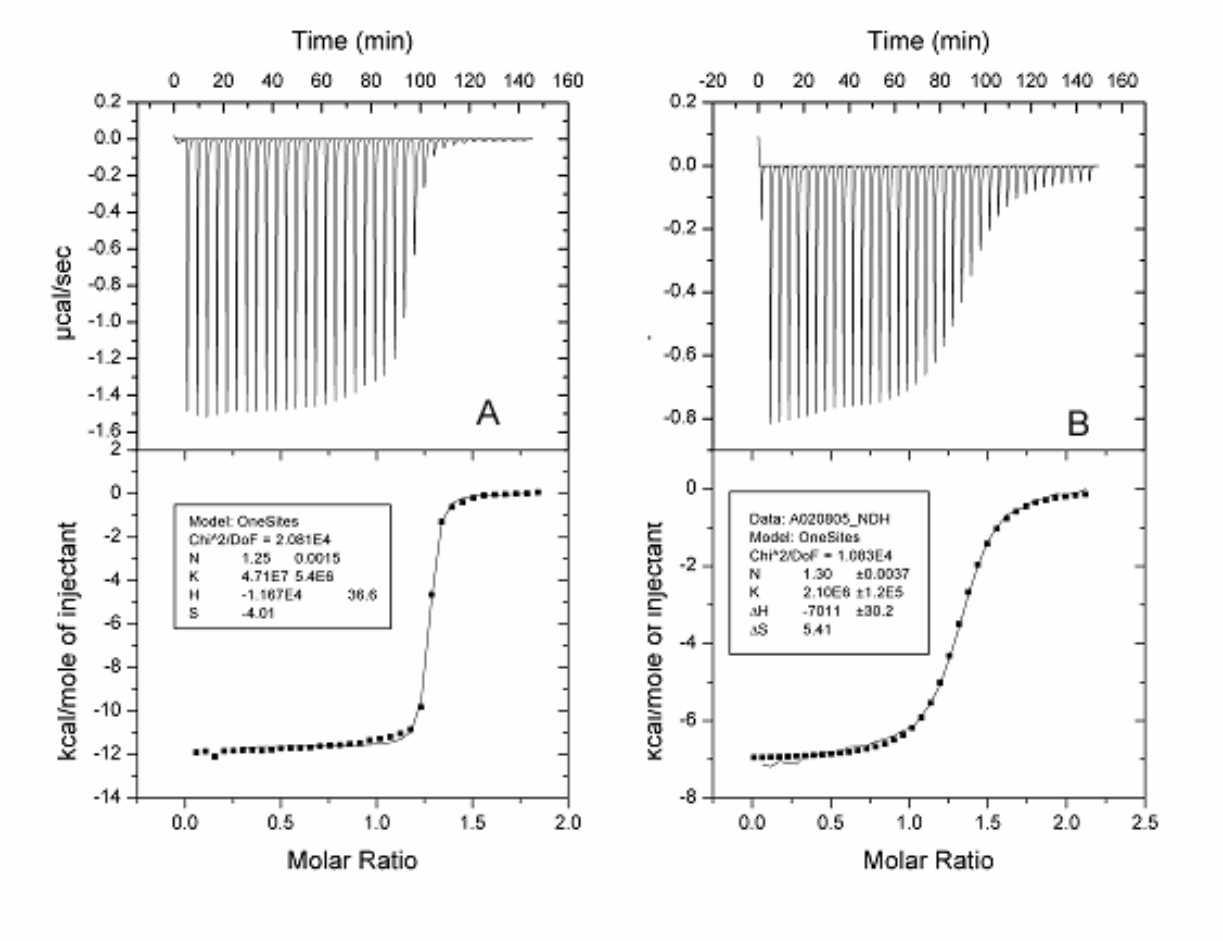

Figure 4-3-9. Isothermal titration calorimetry titration of the wild type Rab7 (**A**) and Rab7L192S (**B**) with REP-1. The best values for stoichiometry, binding constant, and enthalpy are shown in the box.

As can be seen in Table 4-3-3, interaction of Rab:REP:RabGGTase ternary complex of Rab7wt, Rab7Δ3, Rab7Δ14 and Rab7Δ22 displays a trend of slight decrease in affinity with truncation of C-terminal residues. Replacement of (199)KTSAES(204) of Rab7 by poly alanine (Rab7-5A) and additional aromatic amino acid residues at the Rab7 C-terminus (Rab7_WFY) result in minor reduction and enhancement in ternary complex affinity, respectively. These observations demonstrate that the amino acids of the C-terminus make only a limited contribution of the overall affinity of the Rab:REP complex interaction with RabGGTase, which is consistent with previous finding (Alexandrov et al., 1999). However, the C-terminus is obviously involved in the association of ternary complex, from the evidence of quantitative analyses shown here. The disordered Rab C-terminus must weakly associate with REP:RabGGTase for prenylation instead of freely hanging outside, as can also be seen in the simulation (section 4.3.1). Interestingly, Rab7_WFY leads to

increased affinity of the ternary complex, whereas its prenylation was inhibited. This suggests that aromatic WFY residues may bind to the active site of RabGGTase. There could be two possible explanations for the inhibition effect. First, the interaction of WFY with the active site changes the orientation of C-terminal cysteines so that it is not able to coordinate Zn^{2+}. Second, WFY disrupts the proximity effect between prenyl and cysteines thiol groups, resulting in inhibition of reaction between these two moieties.

Analysis of the K_d values for binary and ternary complexes shown in Table 4-3-3 enables us to conclude that the CIM motif, though is shown to be an important contributor to Rab:REP binding, is not so significant for ternary complex assembly as GTPase domain functions. This excludes the first possibility for the effect of CIM mutations on Rab prenylation, as mentioned at the beginning of this section, i.e. the CIM motif does not significantly influence the recruitment of the Rab:REP complex by RabGGTase. As shown in section 4.3.2.2, the in vitro prenylation experiments (Figure 4-3-5) were performed under conditions where all components were present at concentrations far above the respective K_d values, incomplete complex formation should not be rate limiting. Moreover, further increase of the concentration of each component does not lead to a change in the observed rate constant, thus the observed rate reflects the single turnover reaction rate. Although CIM mutations lead to considerable reduction in the stability of the binary complex, Rab7 CIM mutants still associate with REP in affinity high enough, and it would not be expected the significant decrease in affinity of ternary complex. In principle, at the sufficiently high concentration of prenylation components, the observed rate would not change upon CIM mutations. However, it turned out not to be the case. Therefore, we conclude that the CIM mutation changes the micro-environment within the ternary protein complex rather than the assembly of the whole complex. It appears that loss of coordination of the C-terminus reduces the likelihood of its proper association with the catalytic site of RabGGTase. To an extent one can view CIM fairy like an AAX motif of CAAX box in the case of FTase and GGTase-I working from a remote location. From this perspective the primary purpose of the CIM motif is to provide an anchor facilitating extension of downstream C-terminal residues on the surface of REP and RabGGTase so as to position cysteines in the vicinity of the active site of RabGGTase for conjugation with prenyl groups. Taking into account the diversity of the Rab C-terminal sequence and the variation in length of the C-terminal fragments

among Rab proteins, the fact that the C-terminus of Rab proteins is dispensable for assembly of high affinity Rab:REP:RabGGTase ternary complex supports this model.

In conclusion, the interaction of the CIM motif of RabGTPases with the CBR on REP-1 makes a significant contribution to the overall affinity of the binary complex. But the trigger for the assembly of Rab:REP:RabGGTase is mostly contributed from the GTPase domain of Rab, while the Rab C-terminus donates only a minor fraction of the binding energy of Rab:REP interaction with RabGGTase. However, mutation of the CIM motif considerably reduces both single turnover prenylation rate and the final amount of prenylated Rab. This effect arises from the change of micro-environment inside the ternary complex rather than disrupted assembly of the complex. Based on the simulation of the disordered Rab C-terminus in the ternary protein complex, we propose a model (Scheme 4-6) for Rab prenylation. In this model, the CIM:CBR interaction functions as a anchor to support weak and non-specific association of Rab C-terminus on the REP and RabGGTase surface in order to position C-terminal cysteines in the active site of RabGGTase. During reaction, there must be large motions of the Rab C-terminus for the purpose of double prenylation and translocation of conjugated prenyl moieties. In addition to these objectives, specific coordination of the Rab C-terminal fragment downstream the CIM does not exist, which might be an explanation for the fact that RabGGTase can process Rab proteins containing C-terminal peptides with diverse sequences and varied lengths. It appears that the proper length of this fragment rather than the sequence is critical for Rab prenylation. This in turn suggests that the overall configuration of the ternary protein complex is more of less rigid, but some degree of internal flexibility is required during prenylation. Hence, we could divide the interactions within the ternary complex into three parts, one of which is the interaction between the GTPase domain of Rab and the RBP on REP, the second is binding of the CIM with the CBR, and the last is the formation of the interface between RabGGTase and REP. The first and the third determine the assembly of the ternary protein complex, while the second serves as a coordinator within the micro-environment of the machinery for communication between the Rab C-terminus and the active site of RabGGTase. Once the communication is established, prenylation occurs in a dynamic way where flipping of the first conjugated prenyl group and translocation of the doubly conjugated prenyl moieties might be triggered by binding of phosphoisoprenoids (Thoma et al., 2001b; Thoma et al., 2001c).

Scheme 4-6. A model for assembly of Rab prenylation machinery and subsequent Rab prenylation. RBP: Rab binding platform, CBR: C-terminal binding region. CIM: CBR interacting motif.

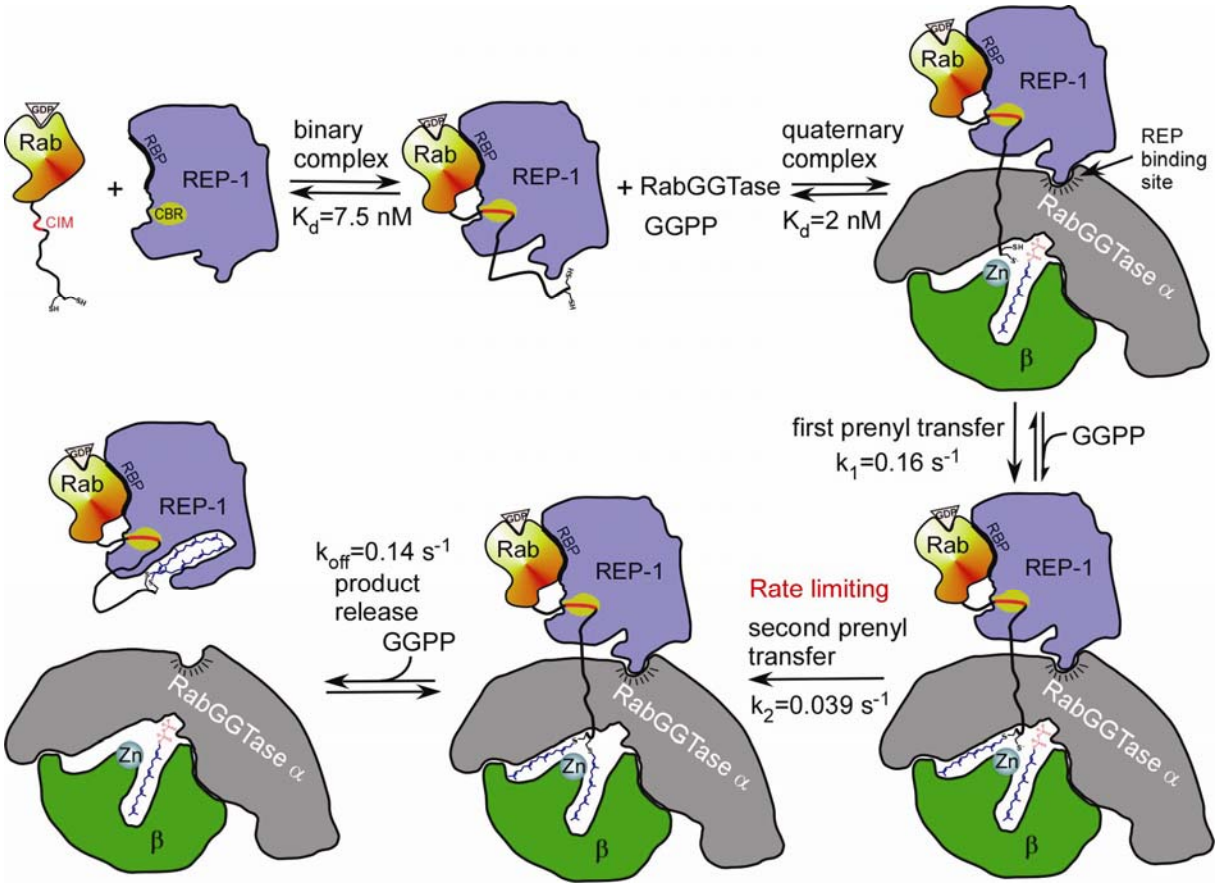

4.4 The thermodynamic basis of Rab recycling

4.4.1 The functional segregation of REP and GDI

As described in Chapter 4.3, REP is a multifunctional protein that recruits a newly synthesized RabGTPase and presents it to the RabGGTase by binding to its α subunit (Pylypenko et al., 2003). After addition of, in most cases, two geranylgeranyl moieties onto C-terminal cysteines of Rab, the catalytic ternary complex dissociates and the prenylated Rab:REP complex travels to the destined membrane organelle (Alexandrov et al., 1994). Insertion of geranylgeranyl moieties into lipid bilayers ensures stable association of RabGTPases with membranes (Ghomashchi et al., 1995; Shahinian and Silvius, 1995). Membrane-bound Rabs are activated by nucleotide exchange and mediate processes of vesicular transport, docking and fusion. Eventually Rab proteins are converted into the GDP bound form and become available for extraction by GDP dissociation inhibitor (GDI) (Araki et al., 1990). Similar to REP, GDI is a tightly packed molecule composed of two domains (Figure 4-4-1), the larger of which forms an extended protein:protein interface with the catalytic domain of the GTPase, while the smaller one harbors conjugated isoprenoids (Rak et al., 2004; Rak et al., 2003; Schalk et al., 1996). GDI is able to extract prenylated Rab proteins from membranes and mediate their reinsertion into donor membranes. The process of extraction is believed to be thermodynamically favored and can occur spontaneously, but additional factors were proposed to be involved in its regulation (Chen and Balch, 2006; Goody et al., 2005). Remarkably, the structurally and functionally related REP is inefficient in extracting Rab proteins from membranes despite its high affinity for these molecules (Pylypenko et al., 2006; Rak et al., 2004).

As mentioned above, the overall structure of REP-1 shows high similarity with that of RabGDI (Figure 4-4-1). Comparative structural and functional analysis of REP and GDI revealed that the Rab binding site of REP is more extensive than that of GDI and allows it to bind unprenylated RabGTPases with nanomolar affinity. In contrast, GDI binds unprenylated Rab proteins with micromolar or worse affinity and prenylation of Rabs is strictly required for stable complex formation as discussed in Chapter 4.3. Moreover, residues correspondingly to F279 and R290 in REP, whereas the key residues in REP:RabGGTase interaction that are essential for prenylation of

Rab proteins revealed by crystal structure of REP-1:RabGGTase and mutational analysis, are not present in GDI (Pylypenko et al., 2003; Alory and Balch, 2000). These observations explain why it is REP but not GDI can support Rab prenylation.

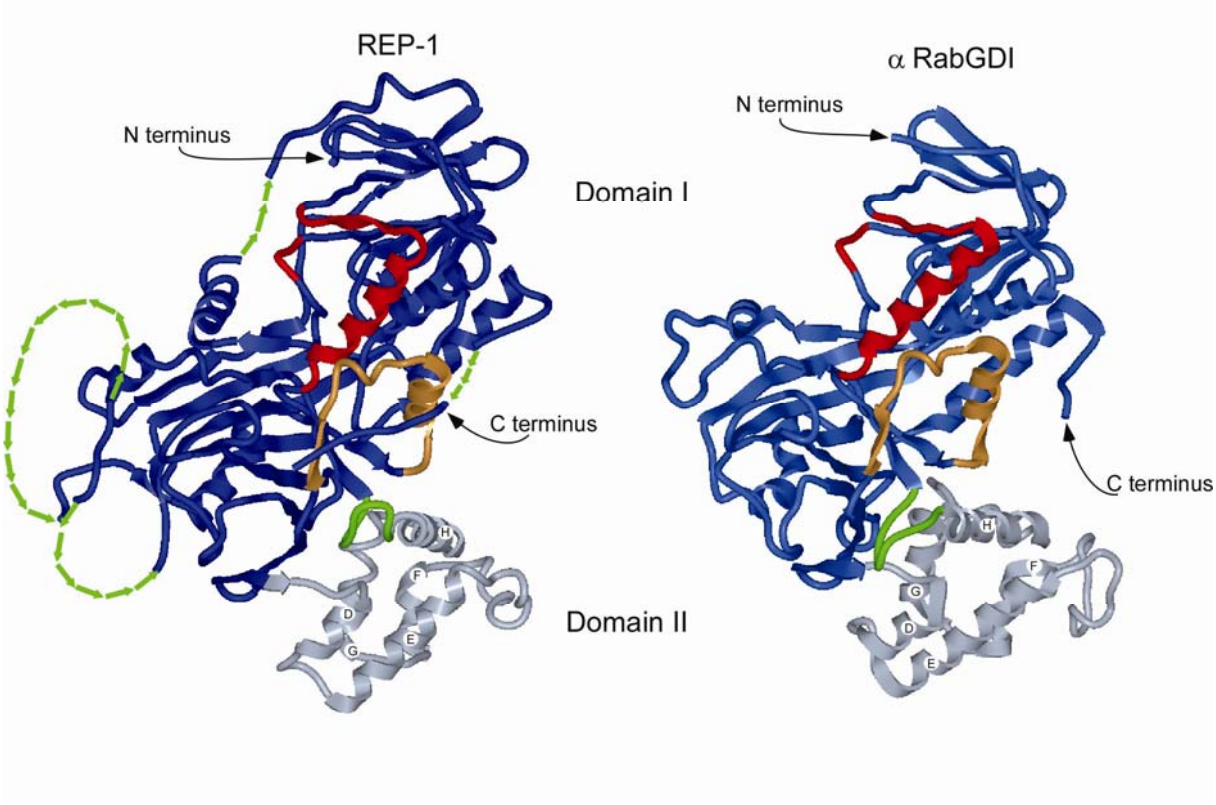

Figure 4-4-1. Structural comparison of REP-1 (left) and αRabGDI (right). Domain I of REP-1 and RabGDI is shown as a blue ribbon, domain II is displayed in light blue, the Rab-binding platform in red, the C-terminal binding region (CBR) in pale orange and the mobile effector loop (MEL) in green. The lime dashed arrow ribbon shown in REP-1 represents the unstructured part.

In order to understand the functional segregation of these two molecules in Rab recycling, recently, we proposed a model that postulated that the affinity difference in the REP/GDI interaction with prenylated and unprenylated forms of Rab proteins determines and distinguishes their role in the Rab cycle (Goody et al., 2005). Although formally consistent, this model was based on very approximate estimates of the prenylated Rab affinities for GDI and REP, due to technical difficulties associated with handling prenylated proteins. Geranylgeranylated proteins aggregate in aqueous solutions and require the presence of detergents to compensate for the hydrophobicity of the lipid moieties. Classical experiments used low concentrations of detergent to keep prenylated Rab9 in solution and estimate its affinity to GDI by measuring the influence of the GDI concentration on the rate of nucleotide release from the former (Shapiro and Pfeffer, 1995). This study concluded that prenylated Rab9 has a nanomolar affinity for GDI while also demonstrating that concentration of

detergent strongly influences Rab:GDI interactions. The affinity of REP for prenyated Rab is still unknown, making it impossible to develop a quantitative comparative model of REP/GDI mediated Rab cycling. This is a shared problem in the analysis of geranylgeranylated proteins and is exemplified, for instance, by Rho and RhoGDI interactions, where no reliable affinity estimates are available. In this work, to address that perplexing question we used novel techniques that enable us to get the absolute affinities and study the kinetics of interaction of GDI and REP with prenylated RabGTPase.

4.4.2 Development of a fluorescent sensor for the interaction of prenylated Rab with REP and GDI

In order to gain insight into the interaction of prenylated Rab GTPase with its regulatory proteins or membranes, two interconnected technical issues need to be addressed. First, an efficient and if possible time-resolved method for monitoring the interaction of prenylated Rab with REP and GDI needs to be devised. Secondly, a way needs to be found to apply this assay to monitor the interaction of prenylated Rab with REP and GDI in the absence of detergent, which is known to strongly influence the properties of the prenylated proteins (Shapiro and Pfeffer, 1995).

As already shown in Chapter 4.1.3, we have developed an *in vitro* Rab prenylation assay that takes advantage of a 20-fold increase in the fluorescence intensity of a geranylgeranyl pyrophosphate (GGPP) analogue, NBD-FPP (Scheme 4-7), upon its utilization as lipid substrate by RabGGTase (Wu et al., 2006). In the case of NBD-FPP, a monoprenylated reaction intermediate could dissociate from RabGGTase and needed to rebind to acquire the second prenyl moiety, in stark contrast to the native reaction (Wu et al., 2006; Thoma et al., 2001c). This increased tendency to dissociate is a consequence of reduced hydrophobicity of the fluorescent analogue compared with the native isoprenoid. We conjectured that the NBD-farnesylated Rab molecule would on the one hand have the features of geranylgeranylated Rab proteins and on the other hand be more soluble than natively prenylated protein. However, to produce NBD-farnesylated Rab by enzymatic approach turned out to be impractical, since it binds to REP too tightly to be efficiently separated. Since we have established a platform for production of fluorescent Rab conjugates as described in Chapter 4.1, we chose an expressed protein ligation approach for construction of NBD-farnesylated Rab (Durek et al.,

2004a; Muir, 2003; Muir et al., 1998). To this end, we synthesized a tripeptide Cys-Ser-Cys(NBD-farnesyl) and ligated it *in vitro* to sodium 2-mercaptoethanesulfonate (MESNA) thioester-tagged Rab7 lacking three C-terminal amino acids (Scheme 4-7). The Rab7Δ3-MESNA thioester is produced using the same approach as described in section 4.1.2.1.

Scheme 4-7. Construction of prenylated fluorescent Rab7. (**A**) The fluorescent analogue of geranylgeranyl, NBD-farnesyl. (**B**) Synthesis of the fluorescent analogue of mono-geranylgeranylated Rab, Rab7-NBD-farnesyl.

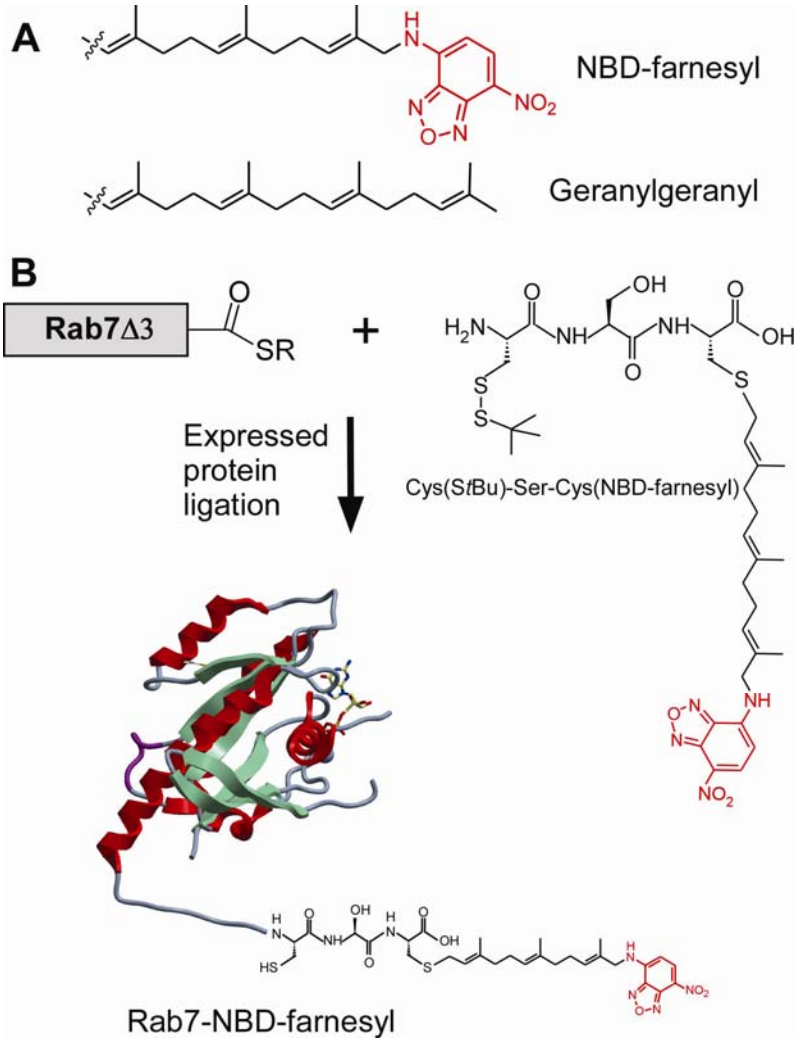

Ligation of soluble Rab thioester with aqueously non-soluble prenylated peptide meets a problem of inhomogeneous reaction, which makes the typical ligation condition not applicable. Our group has identified detergents that are able to mediate the ligation of Rab with prenylated peptide. Only few of them are functional, like DDMAB (*N*-dodecyl-*N*,*N*-(dimethylammonio)butyrate) and CTAB (Cetyltrimethylammonium bromide), which are also observed facilitating the conjugation of fluorescent dye with Rab (section 4.1.2.3, Figure 4-9).

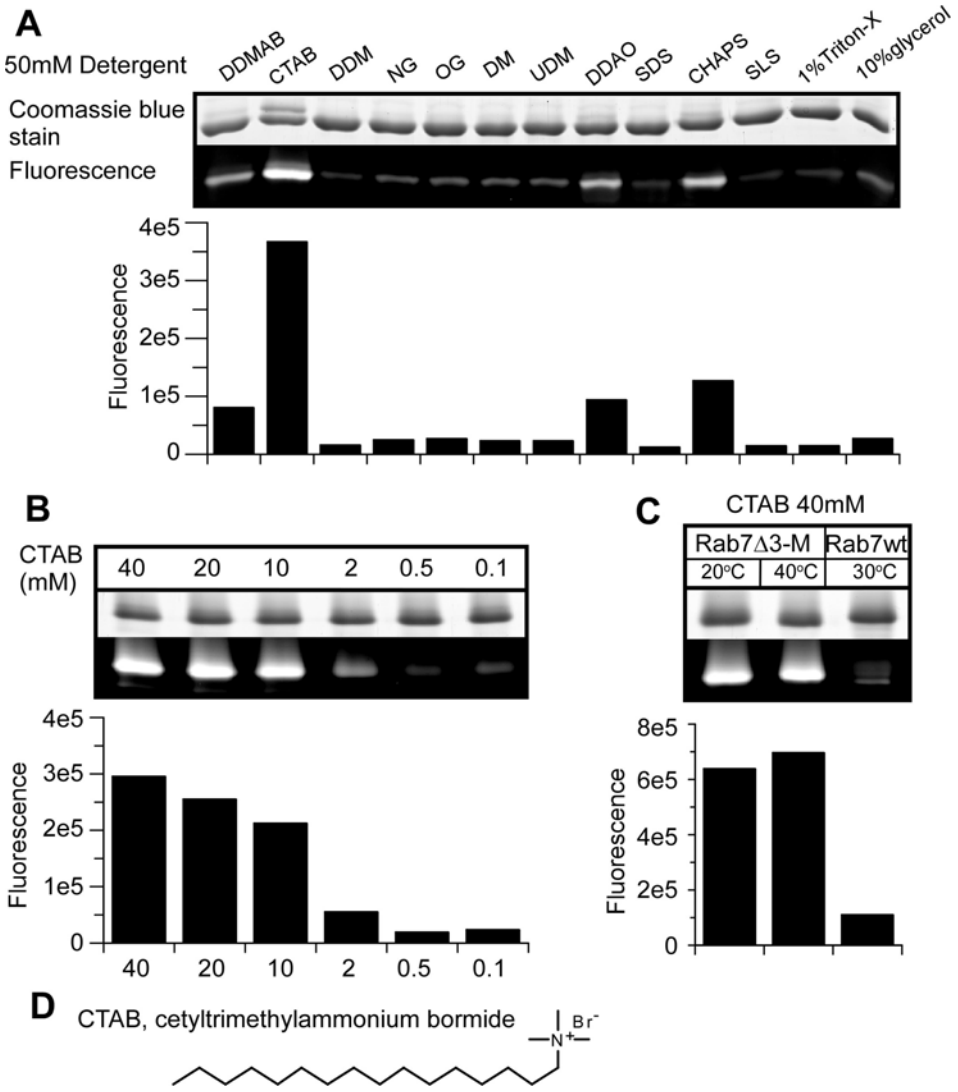

Figure 4-4-2. Optimization of the reaction conditions for the ligation of Rab7Δ3-MESNA with Cys(StBu)SerCys(NBD-farnesyl). (**A**) Screening of detergent for ligation. Reaction was run overnight at 30°C in the presence of 50mM detergent in buffer: 25mM Na-Pi, pH 7.5, 25mM NaCl, 2mM $MgCl_2$, 100μM GDP, 100mM MESNA. The concentrations of protein and peptide are 0.21 mM and 2 mM, respectively. (**B**) Ligation in the presence of various concentrations of CTAB at 30°C. Other conditions are the same as in A. (**C**) Ligation in the presence of 40 mM CTAB at different temperatures. Other conditions are the same as in A. As a control Rab7wt was present in the reaction instead of Rab7Δ3-MESNA thioester. The lower columns in each panel show the quantification of the corresponding fluorescent bands. (**D**) The structure of CTAB.

In the effort to create Rab7-NBD-farnesyl conjugate, we encounter the same problem as the synthesis of geranylgeranylated Rab. Based on previous experience, we sought to identify an additive that would facilitate synthesis of NBD-farnesylated Rab. The fluorescently labeled peptide allows convenient assay of the ligation efficiency by means of SDS-PAGE where the ligated product can be quantified by a fluorescence reader as described in section 4.1.3. A small set of detergents including CTAB and DDMAB were screened for their abilities to support ligation reaction. Although all of detergents can facilitate solubilization of the prenylated peptide, only CTAB is able to efficiently support the ligation (Figure 4-4-2 A). We then sought to

find out at what concentration CTAB can catalyze the ligation reaction. As can be seen in Figure 4-4-2 B, reducing the concentration of CTAB lower than 10mM led to significant decrease of ligation efficiency, suggesting that the concentration of CTAB above CMC is essential for the ligation (CMC of CTAB is 0.9mM in aqueous solution). As discussed in section 4.1.2.3, this effect might be a result of micelle catalyzed reaction (Figure 4-1-10).

Figure 4-4-2 **C** shows that the level of ligation after 12 h was essentially independent of reaction temperature above 20°C. In a control experiment, Rab7wt lacking the thioester, thereby would be expected not to undergo ligation, showed only residual fluorescence incorporation, which might be resulted from non-specific binding and coupling with peptide through disulfide bonds. This result confirms the specificity of the chemical ligation reaction (Dawson et al., 1994) and reliability of the SDS-PAGE assay.

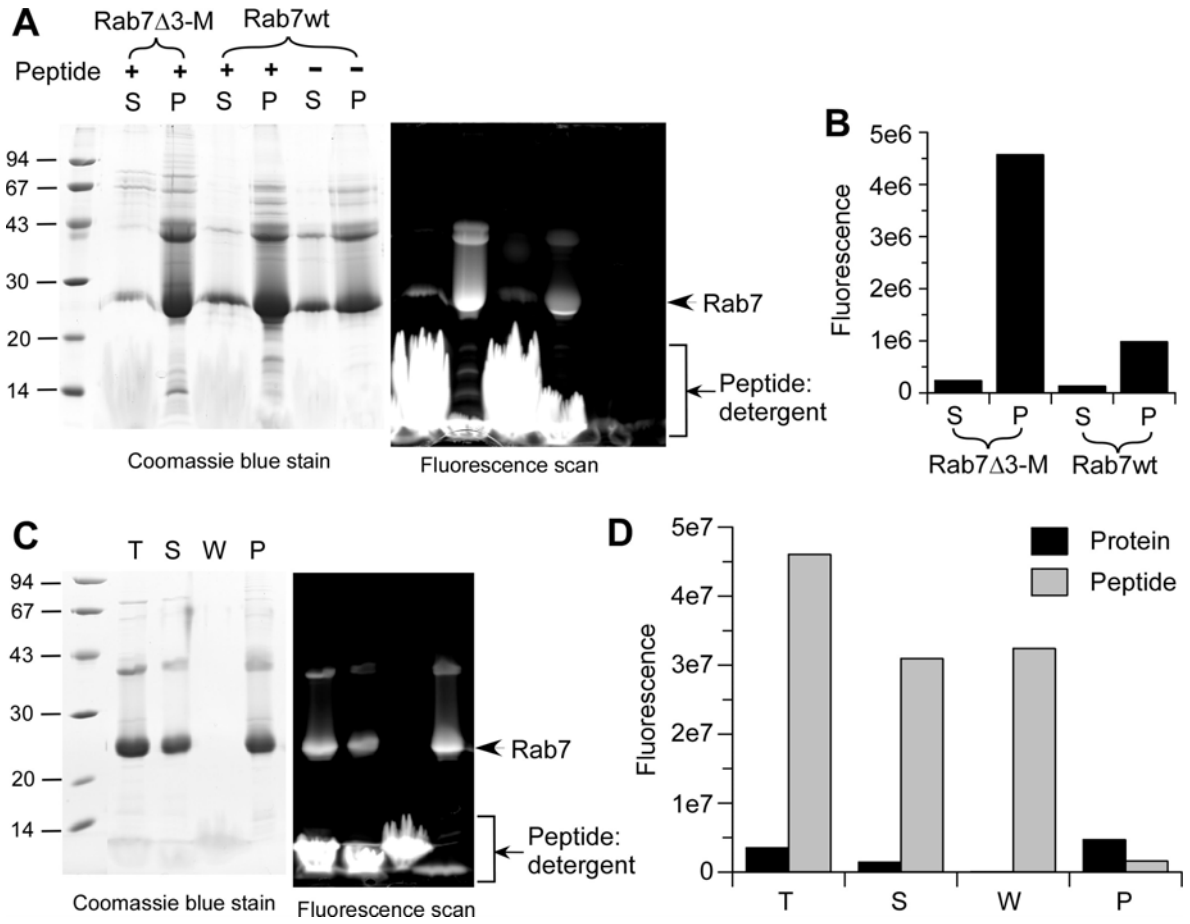

Figure 4-4-3. Purification of NBD-farnesylated Rab7. (**A**) After reaction, supernatant (S) and pellet (P) were separated. In the control experiments, Rab7wt was used instead of Rab7Δ3-MESNA thioester in the presence of peptide and the absence of peptide. (**B**) Quantification of the fluorescence of the protein bands shown in A. (**C**) Separation of protein and unligated peptide by washing with organic solvents. T: mixture after reaction, S: supernatant after reaction, W: MeOH solution after washing the

pellet, P: pellet after washing. (**D**) Quantification of the fluorescence of the corresponding protein and peptide bands shown in C.

As expected under such harsh reaction conditions both ligated and unligated protein were denatured and formed precipitate. As can be seen in Figure 4-4-3 **A** and **B**, protein was found mostly in the pellet, while the majority of unligated peptide remained in the supernatant. A crude purification of the ligated protein from unligated peptide and detergent can be achieved simply by separation of the supernatant and the pellet. Subsequent washing of the ligation mixture with organic solvent, such as methanol and dichloromethane, led to extraction of the peptide and detergent to the organic phase but left protein in the pellet (Figure 4-4-3 **C** and **D**). Some residual contaminating peptide and detergent could be removed in a later refolding, dialysis and gel filtration step.

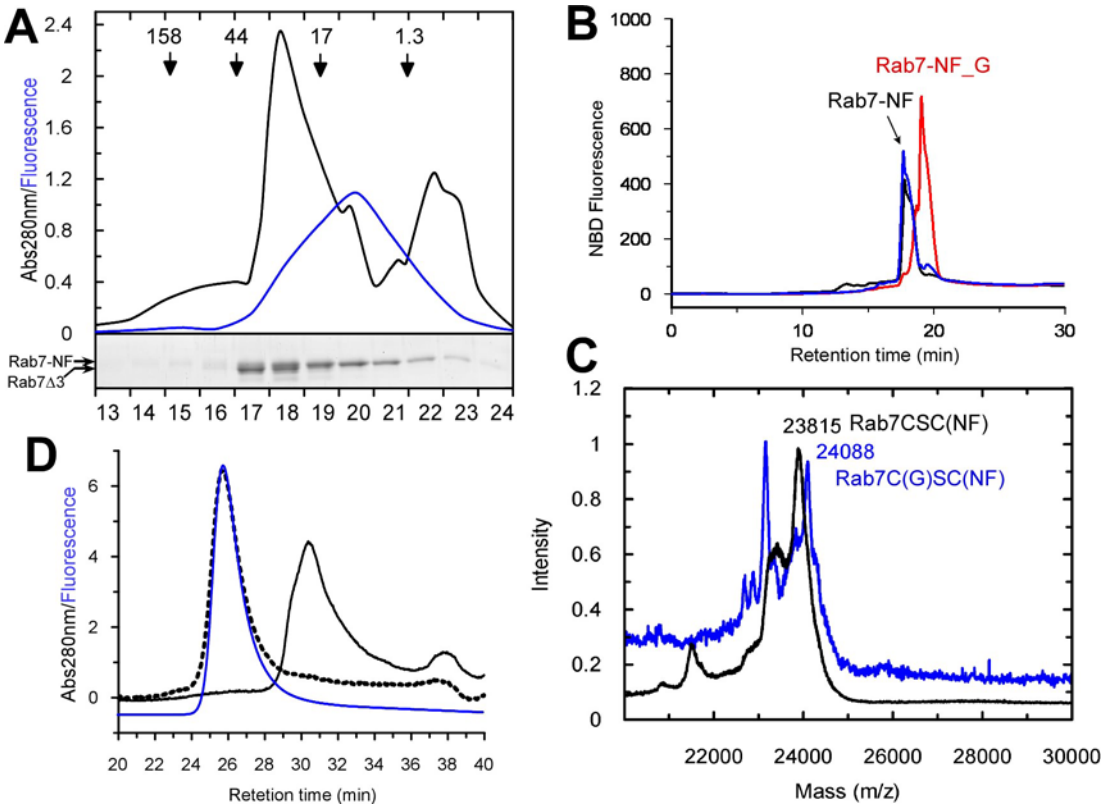

Figure 4-4-4. Gel filtration chromatography of semi-synthetic Rab7-NF and confirmation of its correct folding. (**A**) Elution profile of Rab7-NF resolved on a Superdex-200 column and analysis of the resulting fractions by SDS-PAGE followed by Coomassie blue staining (inset). The black lines represent absorbance at 280 nm while the blue line represents fluorescence detection. The arrows on the top panel indicate elution position of molecular weight standards in kDa. Fractions 19-21 containing Rab7-NF were collected with >80% purity and used for further analysis. (**B**) HPLC elution profile of Rab7-NF alone (17.8 min, black line) or in vitro prenylated with GGPP (19.1 min, red line). The control reaction where REP was omitted is shown as a blue line (17.8 min.). The HPLC fluorescence detector was set to $\lambda_{ex/em}$ values of 490 and 535 nm. (**C**) MALDI-MS analysis of Rab7-NF (black, M_{calc} = 23,770 Da) and its in vitro geranylgeranylated form (blue, M_{calc} = 24,043 Da), i.e., Rab7C(geranylgeranyl)SC(NBD-farnesyl). (**D**) Gel filtration chromatography of Rab7-NF (black solid line) and Rab7-NF in the presence of GDI. The samples were resolved by a Superdex-200 gel

filtration column and eluted proteins were detected both by absorbance at 280 nm (black dashed line) and by fluorescence (blue solid line) of NBD.

Subsequent resolubilization and renaturation steps follow the protocol developed for geranylgeranylated Rab (Durek et al., 2004b). The denatured ligated product was resolubilized in 6 M GdmHCl buffer containing reductant DTE and detergent CHAPS. Renaturation of the denatured protein was achieved by pulse-refolding approach in which the denatured protein was titrated into refolding buffer of typical 30-fold dilution in pulses (Clark et al., 1999). Addition of CHAPS, arginine, trehalose and cofactors (e.g. GDP or GTP) in the refolding buffer has been shown to improve yields of renaturation.

The resulting Ra7-NF protein remained in solution after removal of detergent present during protein ligation and purification - an atypical behavior for geranylgeranylated protein that tends to form aggregates under these conditions. The ligated protein eluted from a size exclusion column at a position corresponding to a molecular mass <10 kDa whereas unligated protein eluted at the expected position corresponding to 28 kDa (Figure 4-4-4 **A**), suggesting that the protein does not form multimers and that its migration is retarded on the column probably by hydrophobic interaction with the matrix. Distinct character of ligated and unligated protein allows convenient separation of both species by gel filtration.

The solubility of Rab7-NF is not surprising, since the reduction in the length of the isoprenoid chain is known to decrease the hydrophobicity of the prenylated protein, for example, farnesylated RasGTPases per se is soluble (Jügen Kulmann, personal communication), and the introduction of polar NBD group to farnesyl moiety could also reduce its hydrophobicity (Nguyen et al., 2007; Dursina et al., 2005; Chehade et al., 2002).

Semisynthetic Rab7-NBD-farnesyl (Rab7-NF) displayed the expected molecular mass (Figure 4-4-4 **C**) and was correctly folded as judged by its ability to form a stoichiometric complex with GDI (Figure 4-4-4 **D**). The formation of the complex gives a first indication that the NBD-farnesyl group contributes to assembly of the Rab:GDI complex. To further assess the extent to which the semisynthetic Rab7-NF emulates the monoprenylated Rab protein we subjected it to *in vitro* prenylation by RabGGTase by using geranylgeranyl pyrophosphate (GGPP) as a substrate. In this case, the isoprenoid should be incorporated onto the C-terminal cysteine that was used as a ligation site (Scheme 4-7). The in vitro prenylation reaction was analyzed both by reversed phase HPLC (Figure 4-4-4 **B**) and MALDI-TOF (Figure 4-4-4 **C**),

confirming that the geranylgeranyl group was conjugated to the previously free C-terminal cysteine. Therefore, the constructed semisynthetic protein closely mimics monoprenylated Rab7 in this respect.

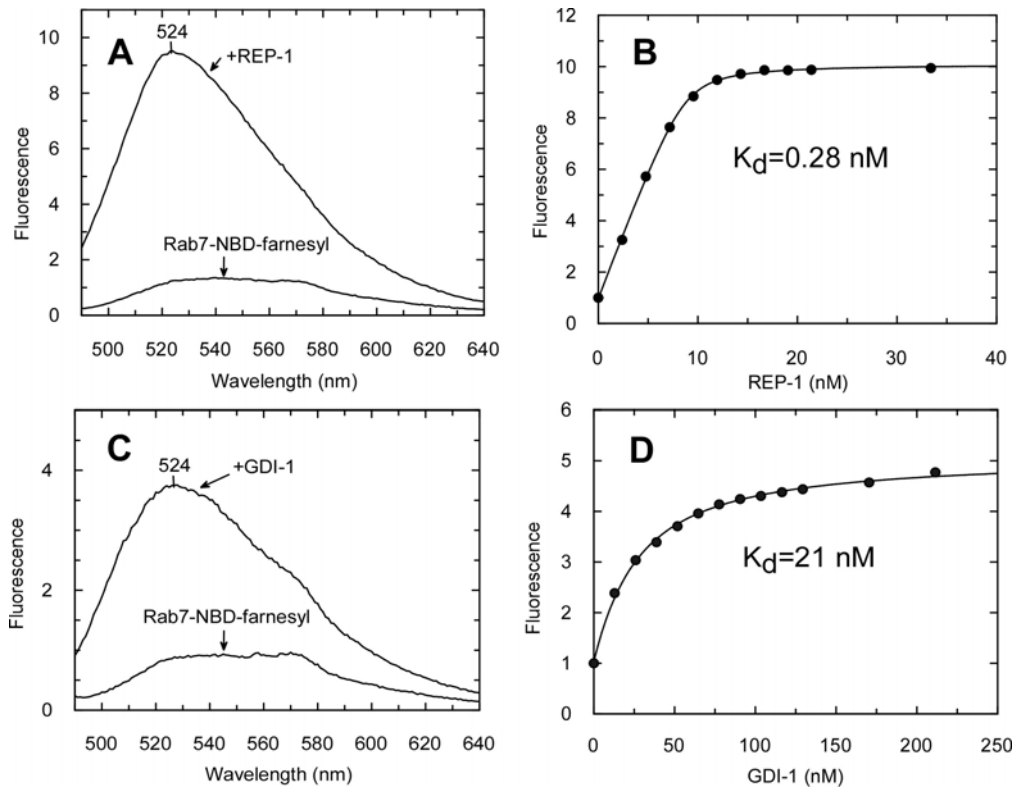

Figure 4-4-5. Analysis of interaction of Rab7-NF with RPE and GDI. (**A**, **C**) Emission spectra of Rab7-NF in the absence and in the presence of REP-1 (**A**) and αRabGDI (**C**). (**B**, **D**) Titration of REP-1 (**B**) and RabGDI (**D**) to a 10 nM solution of Rab7-NF. (D) Titration of GDI to a 10 nM solution of Rab7-NF. The fluorescence of NBD was excited at 479 nm, and the emission was collected at 525 nm. K_d values were obtained by fitting the data to a quadratic equation (see section 8.1.1).

Since semi-synthetic Rab7-NF is both soluble and active, we attempted to use the fluorescence of the conjugated NBD-farnesyl group to monitor its interaction with REP and GDI. As shown in Figure 4-4-5 **A**, addition of REP-1 to a solution of Rab7-NF resulted in a 10-fold increase of fluorescence and a blue shift from 545 to 525 nm. Similar behavior was observed on addition of GDI, albeit with a 5-fold fluorescence increase (Figure 4-4-5 **C**). The large fluorescence change enabled us to perform titration experiments to determine the affinity of the Rab7-NF:REP interaction, which is expected to be in the low nanomolar range and hence must be assayed at very low concentrations of the reactant. The dramatic enhancement in fluorescence is presumably a consequence of the Rab-conjugated NBD-farnesyl group binding in the hydrophobic lipid binding site on REP and GDI, as proposed in the model of fluorescence enhancement in the NBD-farnesylation (Wu et al., 2006; Pylypenko et al., 2006; Rak et al., 2004). Titration of 10 nM Rab7-NF with REP-1 yielded a K_d

value of 0.28 nM (Figure 4-4-5 **B**). A similar experiment using GDI yielded a K_d value of 21nM (Figure 4-4-5 **D**). These data indicate that the Rab7-conjugated NBD-farnesyl group increases the affinity of Rab7:REP complex by a factor of ca. 5 compared with unprenylated Rab (K_d= ca. 1 nM, ref (Alexandrov et al., 1998)), while its effect on the Rab7:GDI interaction is much more pronounced. Unprenylated RabGTPases interact with GDI with micromolar affinities implying that the presence of NBD-farnesyl increases the affinity of the complex by >100 fold (Pylypenko et al., 2006).

4.4.3 Construction and solubilization of semi-synthetic geranylgeranylted Rab7

The data described above reflects the different effects prenylation has on Rab:REP and Rab:GDI interactions. However, this is an artificial system and thus the data may be only an approximation of the native situation. Thus, we sought a way to repeat some of these experiments with natively geranylgeranylated Rab7. Geranylgeranyl modified Rab proteins are soluble in the presence of detergents, however their presence significantly affects the interaction between prenylated Rab and GDI (Shapiro and Pfeffer, 1995). Ideally, a chaperone would be needed that on the one hand would prevent aggregation of prenylated Rab but on the other hand not interfere with its protein:protein interactions.

To make geranylgeranylated Rab soluble but exclude detergent, we searched for a chaperone that can stabilize the prenylated Rab and can deliver it to REP and GDI. Yeast GDI (yGDI) and yeast homologue of REP, MRS6, which can be expressed in *E coli.*, bind with Rab7-NF in a high affinity (K_d=4.3±0.49nM and 0.94±0.46nM, respectively). This prompted us to choose the relative low affinity chaperone, yGDI, for protein engineering, in order to idenfity yGDI mutants that could solubilize prenylated Rab but display much lower affinity for it. Analysis of crystal structure of prenylated Ypt1:yGDI complex (PDB code 1URV) (Rak et al., 2003) reveals that Y44, E241 and R248 are important residues in Rab binding platform of yGDI. Mutation of these residues would be expected to reduce the affinity between yGDI and GTPase domain of Rab. Quantitative analyses of the interactions between Rab7-NF and yGDI mutants show that the mutations indeed lead to significant decrease in affinity, and this effect correlates with the contribution of these residues to the interaction of the complex (Table 4-4-1).

Table 4-4-1. Affinity of Rab7-NF to MRS6 and yGDI.

Protein	K_d (nM)	Fluorescence enhancement (fold)	Contact area[a]
MRS6	0.91±0.46	6	
yGDI	4.0±0.49	7	
yGDI Y44A	670±72	6	47
yGDI E241A	114±7.5	6.5	29.6
yGDI R248A	2505±220	8	60

[a] Contact area involved for the corresponding residue in Ypt1-G:yGDI complex (PDB code 1URV)

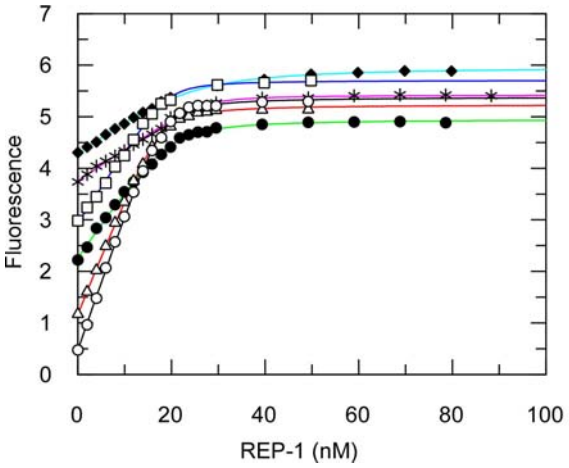

Symbol	Concentration of yGDI E241A (nM)	K_d^{app} (nM)	Effective [Rab7-NF] (nM)
◆	510	3.0	23.7
✳	292	0.49	26.8
□	140	0.35	19.6
●	73	0.88	19.9
△	10	0.43	17.8
○	0	0.36	18.3

Figure 4-4-6. Analysis of interaction of Rab7-NF:REP-1 in the absence and the presence of indicated concentrations of yGDI E241A. The graph shows the titration profiles and fittings. Results are summarized in the table. Effective concentration of Rab7-NF is the concentration fitted.

Gel filtration analysis shows that yGDI E241A is able to form a complex with Ypt1Δ3CC(geranylgeranyl)C(geranylgeranyl), so that it can be used as a chaperone to solubilize the doubly geranylgeranylated Ypt1 protein (data not shown). The relative low affinity between prenylated Rab and yGDI mutant enables delivery of prenylated Rab to REP as can be seen in Figure 4-4-6. The starting fluorescence of Rab7-NF before titration of REP increased with the increase of concentration of yGDI E241A, indicating the formation of complex between Rab7-NF and yGDI E241A. Titration of REP led to further increase of the fluorescence, suggesting competition between REP and yGDI in binding to Rab7-NF, since REP binds Rab-NF much tighter and gives higher enhancement (10-fold) in fluorescent intensity. The presence of increasing concentration of yGDI E241A resulted in enlargement of apparent K_d values but constant effective concentration of Rab7-NF. This further confirmed that yGDI E241A is competitive with REP in binding to Rab7-NF and was fully displaced by REP at the end.

Although we achieved our objective of creating a chaperone capable of solubilization and release of prenylated Rab, it displayed several drawbacks that rendered its usefulness for our purpose. First, binding of Rab7-NF to yGDI and mutants saturates the fluorescence enhancement (Table 4-4-1), resulting in reduction of the fluorescence sensitivity upon binding of Rab7-NF to REP and GDI. Moreover, and most importantly, yGDI mutant also functions as a good competitor for the interaction of prenylated Rab with REP/GDI. To make geranylgeranylated Rab (especially doubly geranylgeranylated Rab) stable in solution, a high concentration of the chaperone has to be applied. This would cause significant inhibition of the interaction of prenylated Rab with REP/GDI (Figure 4-4-6).

The limited success of engineered specific chaperone drove our attention to unspecific chaperone that would not influence the fluorescent signal and interaction of the system. Since the hydrophobic geranylgeranyl moiety is the primary cause for the insolubility of prenylated Rab, we speculated that the β-subunit of RabGGTase, which contains a geranylgeranyl lipid binding site, might function as an unspecific isoprenoid chaperone. To prevent interactions of RabGGTase with REP we chose to work with the β-subunit only (Pylypenko et al., 2003).

In the light of this idea, semi-synthetic mono-geranylgeranylated Rab7 (Rab7-G) was prepared as described before and was renatured in the presence of an equimolar amount of recombinant β-subunit of RabGGTase (βGGT). The mixture was subjected to size exclusion chromatography. Both proteins coeluted at a position corresponding to a molecular weight of ca. 45kDa, which is deviated from the elution position of the mixture of unprenylated Rab7 and βGGT from gel filtration (Figure 4-4-7 **A**). This and the fact that no Rab7-G was recovered in the void volume indicate that prenylated Rab7 was stabilized in solution in the absence of detergent by forming a stoichiometric complex with βGGT. This finding is not surprising considering the fact that prenyltransferases typically remain in complex with their products and that these are eventually released by the binding of new lipid substrate molecules (Thoma et al., 2001b; Tschantz et al., 1997). We believe that the presented method will be applicable to all prenylated polypeptides and should enable quantitative analysis of their interactions with proteins and membranes.

The native folding and functionality of stabilized monoprenylated Rab7 was assessed by *in vitro* prenylation and analyzed by SDS-PAGE in which the incorporation of NBD-farnesyl to Rab7-G was quantified (Figure 4-4-7 **C**). The βGGT

stabilized Rab7-G complex could be efficiently prenylated by RabGGTase, confirming that the protein was fully functional and that the presence of βGGT did not significantly influence its ability to interact with REP. Its functionality was assayed by the conjugation of the second geranylgeranyl group resolved on MALDI-TOF as well (data not shown). Prenylated Rab proteins could also be stabilized in solution using delipidated BSA (Dirac-Svejstrup et al., 1994), but required higher molar excess of the later.

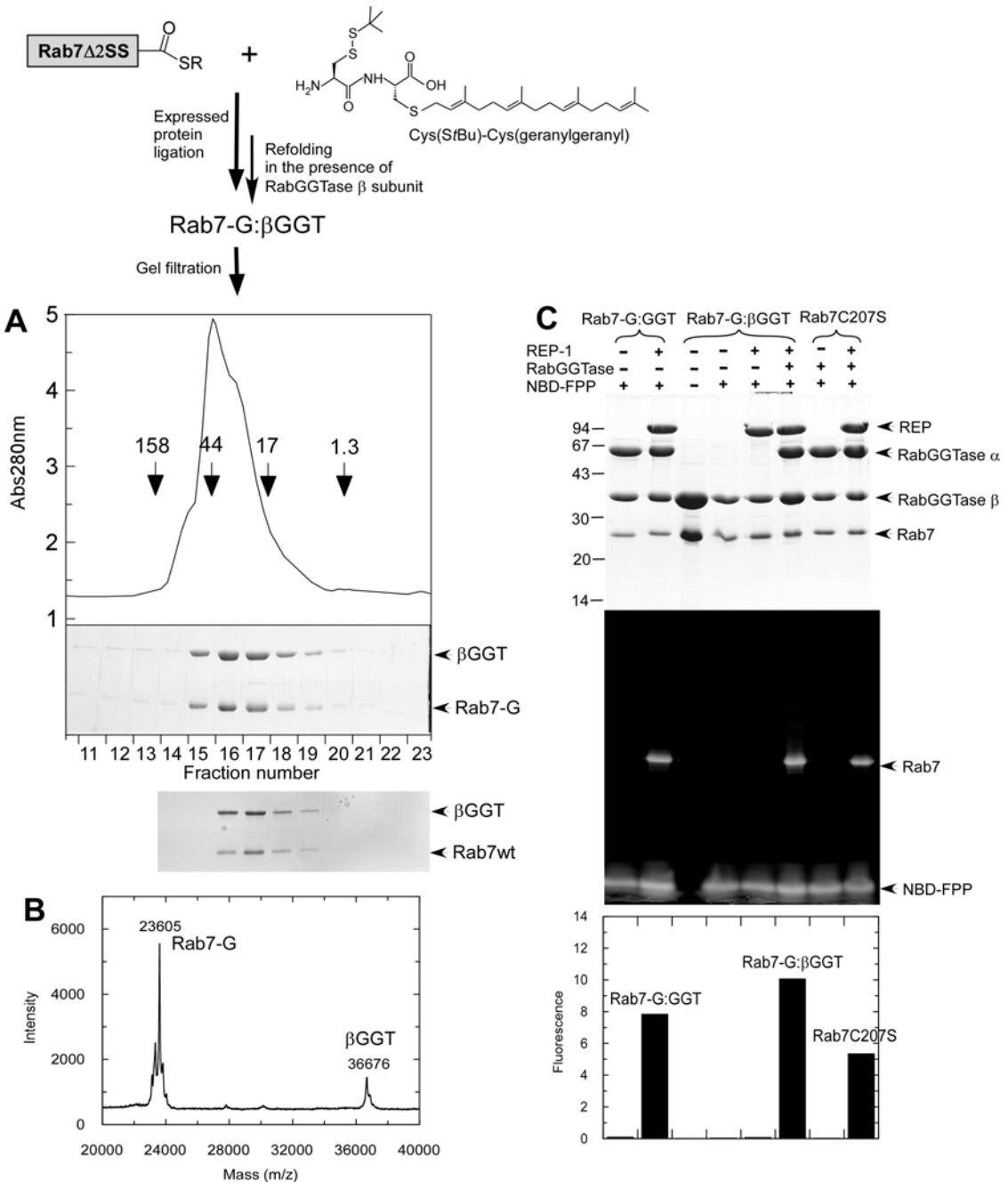

Figure 4-4-7. The construction of soluble mono-geranylgeranylated Rab7 stabilized with the β subunit of RabGGTase. (**A**) Gel filtration chromatography of Rab7-G:βGGT on a Superdex 200 column and SDS-PAGE analysis of resulting fractions (upper). As a control, the same process applied to a mixture of Rab7wt and βGGT gave SDS-PAGE analysis of the same fractions as above (lower). (**B**) MALDI-MS analysis of Rab7-G:βGGT complex (M_{calc}=23660Da for Rab7-G). (**C**) The activity of Rab7-G in

complex with RabGGTase (Rab7-G:GGT) and βGGT (Rab7-G:βGGT) was confirmed by in vitro prenylation assay resolved by SDS-PAGE. The same amount of single C-terminal Cys mutant Rab7C207S was run as a positive control. The middle panel represents the fluorescent scan of the gel, while the top panel shows the same gel stained with Coomassie blue. The bottom panel shows the quantification of incorporation of NBD-farnesyl to Rab7 in the corresponding reactions.

Our group previously reported synthesis of a semi-synthetic doubly prenylated fluorescent variant, Rab7-A202C-E203K(dans)SC(GG)SC(GG) termed Rab7d-GG. This protein was produced using ligation of Rab7Δ6-MESNA thioester with a peptide CK(dans)SC(GG)SC(GG). The molecule displayed near native properties and was used earlier as a fluorescent sensor for analysis of the interaction of the prenylated Rab7:REP complex with RabGGTase (Durek et al., 2004a).

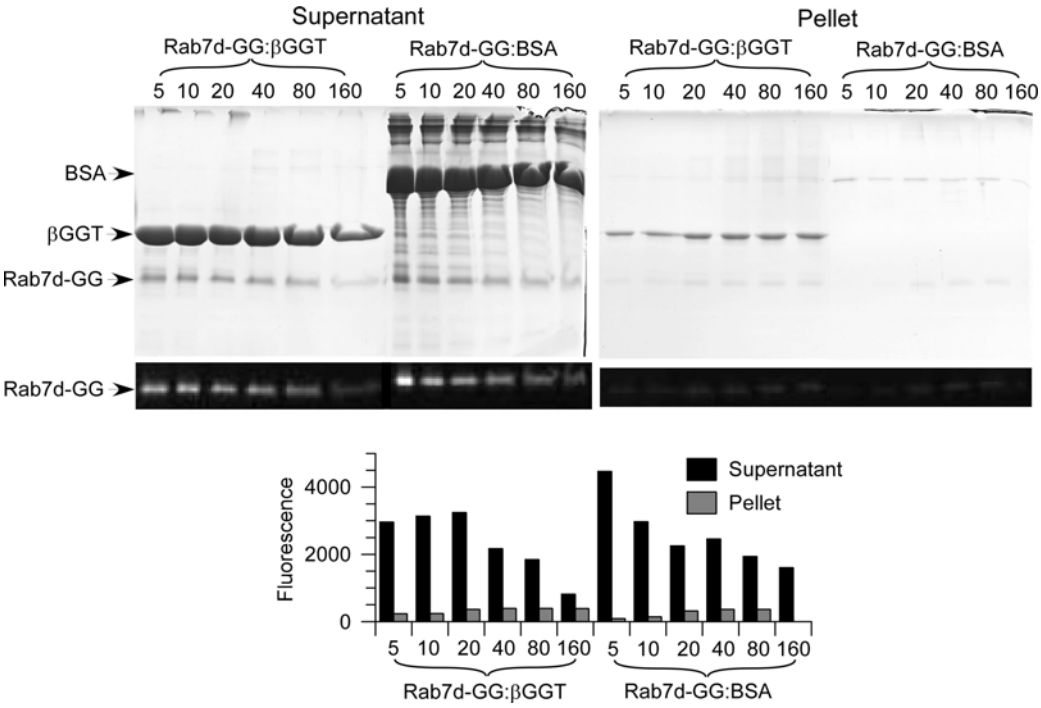

Figure 4-4-8. Analysis of stability of Rab7d-GG:βGGT and Rab7d-GG:BSA by SDS-PAGE. 28 μM Rab7d-GG were present in 10.3 mg/ml βGGT and 15.6 mg/ml delipidated BSA, respectively. The protein mixture was diluted 5, 10, 20, 40, 80 and 160 times, and incubated in room temperature for 1h. Mixture was ultracentrifuged for 10 min to separate the supernatant and pellet, and subsequently resolved by SDS-PAGE followed by fluorescent scanning. The fluorescence of dansyl was quantified by Quantity One software.

However, not like in case of mono-geranygeranylated Rab7, the stoichiometric complex of Rab7d-GG with βGGT could not be detected by gel filtration chromatography. After dialysis of detergent at the presence of low concentration (nanomolar) of βGGT, most of digeranylgeranylated protein precipitated, which can be judged by the fluorescence of the protein in the supernatant and the pellet (data not shown). We interpreted this as a consequence of the relative low affinity of

digeranylgeranylated Rab7 from βGGT and the higher hydrophobicity of digeranylgeranylated molecules that tend to aggregate. Nevertheless, this molecule could be stabilized in solution in the absence of detergent with higher concentration (micromolar) of βGGT or dellipidated BSA (Figure 4-4-8). Most of the digeranylgeranylated protein remained soluble even after the hundred times dilution with buffer.

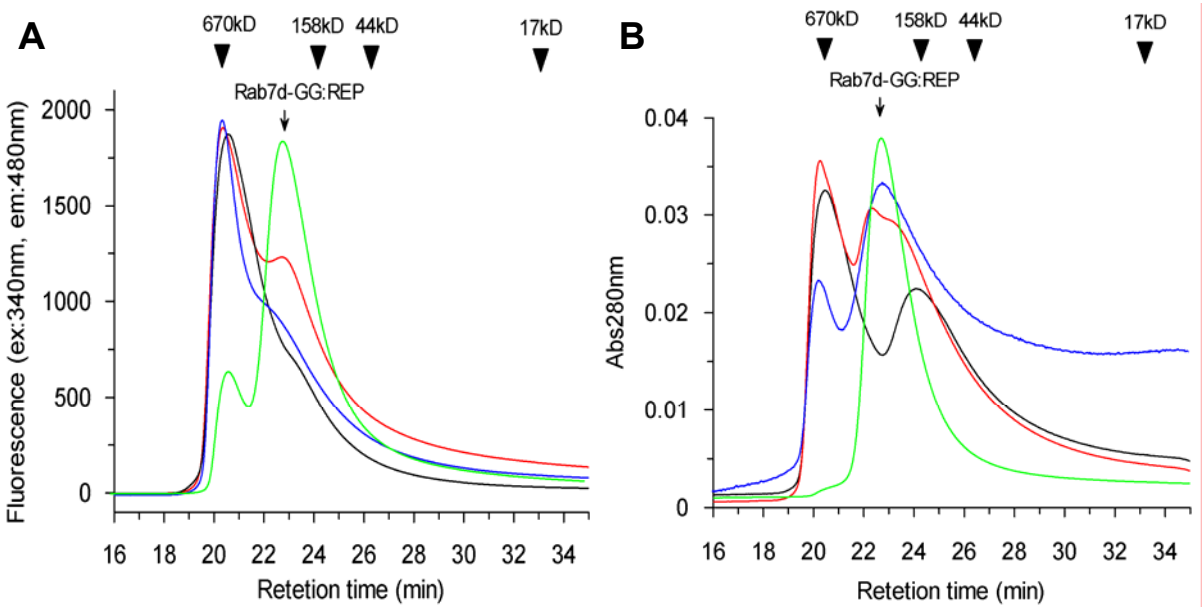

Figure 4-4-9. (**A**) Elution profile of a Superdex 200 gel filtration chromatography loaded with Rab7d-GG refolded in the presence of BSA (black line), Rab7d-GG:BSA in the presence of REP (red line), Rab7d-GG refolded by REP (blue line) and Rab7d-GG:REP low molecular mass fractions from gel filtration (lime line), detected by fluorescence with excitation at 340 nm and emission at 480 nm. (**B**) The same as A, elution profile was recorded by absorbance at 280 nm.

Both approaches yielded native, correctly folded Rab7 GTPase that could form a binary complex with REP and GDI as confirmed by gel filtration analysis (Figure 4-4-9) and fluorescence resonance energy transfer (FRET) detection (Figure 4-4-10). As can be seen in Figure 4-4-9, Rab7d-GG refolded in the presence of REP displayed two fractions, one eluted at 670 kDa and the other at 220 kDa, which correspond to oligomer and dimer of the complex, respectively. Figure 4-4-9 **B** blue line shows that dimer is the major component, while the fluorescence of dansyl was enhanced in the oligomeric protein so that a larger peak appeared at 670 kDa in the fluorescence GF-profile (Figure 4-4-9 **A**, blue line). The black profile in Figure 4-4-9 shows that Rab7d-GG:BSA is a heterogeneous mixture, addition of REP into it resulted in the formation of Rab7d-GG:REP complex characterized by appearance of a peak at 220 kDa (red line). The functionality of Rab7d-GG was also ascertained by FRET analysis. As shown in Figure 4-4-10 **A** and **B**, addition of REP or GDI to Rab7d-GG:BSA led to

reduction of FRET from tryptophan to dansyl. Assuming BSA bound Rab7d-GG has higher FRET efficiency than REP bound state, which could be a result of more tryptophans in BSA, shorter distance between tryptophan and dansyl in BSA bound state, or more oligomization of Rab7d-GG:BSA, decrease in FRET indicates transformation of Rab7d-GG:BSA to Rab7d-GG:REP. As a control, dansyl labeled unprenylated Rab7, Rab7Δ2C(dansyl)SCC (see Chapter 4.1.2), exhibited increase of FRET upon addition of REP, but no FRET on addition of GDI (Figure 4-4-10 **E**, **F**), consistent with the fact that REP can bind to unprenylated Rab but GDI cannot. In a positive control, a homogeneous complex of dansylated monoprenylated Rab7 (Rab7-A202C-E203K(dans)SC(GG)SC (Durek et al., 2004a), Rab7d-G) with βGGT that was shown to be functional by the same assays as those used for Rab7-G:βGGT (data not shown) displayed analogous decrease of FRET upon addition of REP or GDI (Figure 4-4-10 **C**, **D**). This suggests that translocation of Rab7d-G from βGGT to REP/GDI is characterized by decrease in FRET between trypophan and dansyl. These observations demonstrate that Rab7d-GG in the presence of BSA or βGGT, albeit heterogeneous, is functional and capable to a complex with REP and GDI.

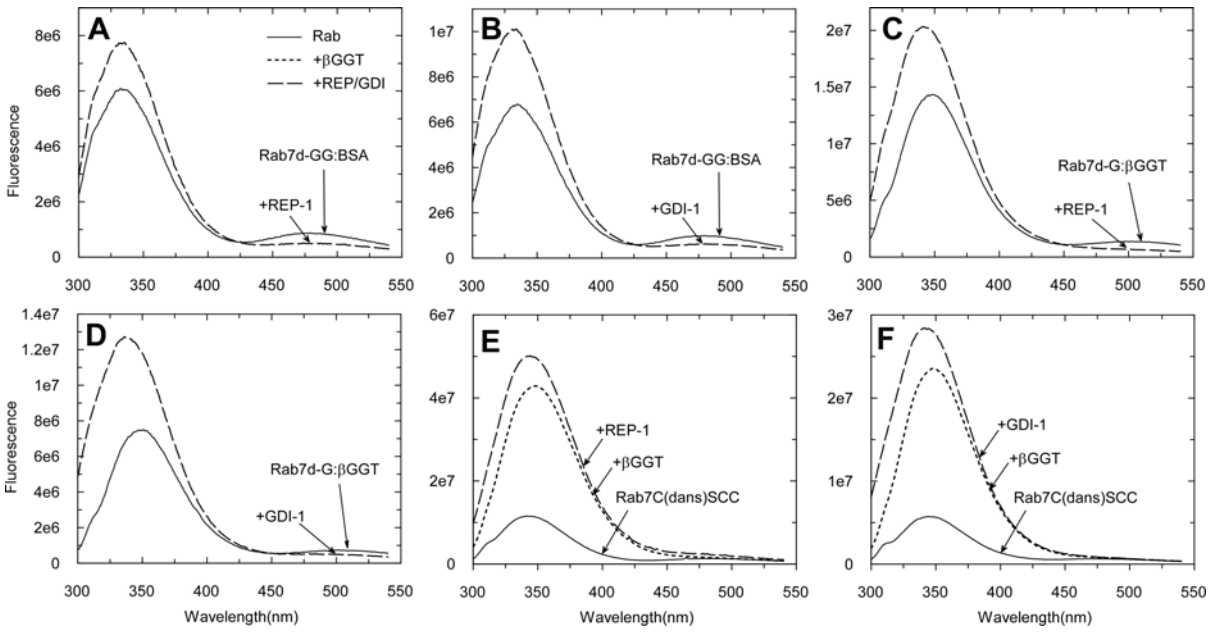

Figure 4-4-10. Emission spectra of Rab7d-GG:BSA (**A**-**B**), Rab7d-G:βGGT (**C**-**D**), Rab7Δ2C(dans)SCC (**E**-**F**) in the absence (solid line) the presence of REP/GDI (dashed line). Excitation was at 280nm to record the FRET from tryptophan to dansyl. 25 nM Rab7d-GG with 250 nM BSA, 100 nM Rab7d-G:βGGT, 150 nM Rab7Δ2C(dansyl) in E and 75 nM in F. 80 nM REP in A, 109 nM GDI in B, 120 nM REP in C, 218 nM GDI in D, 520 nM βGGT and 300 nM REP in E, 250 nM βGGT and 218 nM REP in F,

4.4.4 Quantitative analysis of the interaction of mono- and digeranylgeranylated Rab7 with REP and GDI

The availability of solubilized Rab7-G allowed us to devise an approach for monitoring its interaction with REP and GDI. Since Rab7-G by itself cannot be used as a reporter of the interaction, we decided to use the fluorescent Rab7-NF as a reporter. To this end 10nM Rab7-NF was mixed with 10nM Rab7-G:βGGT complex and the resulting solution was titrated with increasing concentrations of REP. As shown in Figure 4-4-11 **A**, there was an initial "lag" in the fluorescence increase, indicating that Rab7-G bound more strongly to the REP than Rab7-NF, initially resulting in the formation of a fluorescently silent complex. However, at higher REP concentrations, complex formation with Rab7-NF then occurs, leading to an increase in fluorescence intensity. Since the K_d value for the Rab7-NF:REP interaction had been determined independently, the data could be fitted numerically using a competitive binding model leading to a K_d value of 58 pM for the Rab7-G:REP. The same approach was applied to the analysis of the interaction of GDI with Rab7-G and determined a K_d value of 1.2 nM for this interaction (Figure 4-4-11 **B**).

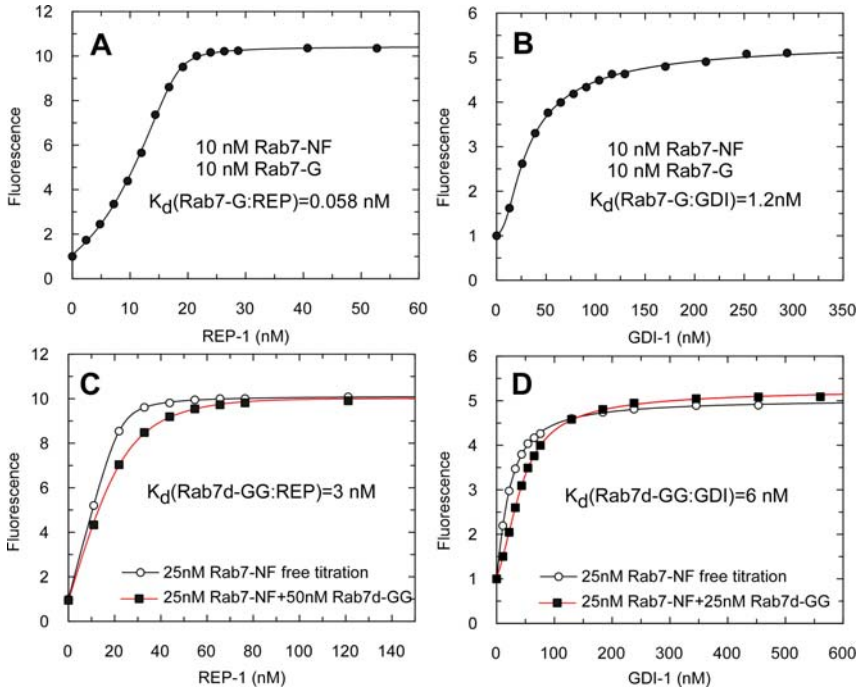

Figure 4-4-11. Analysis of interaction of mono- and digeranylgeranylated Rab7 with REP and GDI using Rab7-NF as a reporter. (**A** and **B**) Titration of REP (**A**) or GDI (**B**) to a mixture of 10 nM Rab7-G:βGGT and 10 nM Rab7-NF. (**C**) Titration of REP to 25 nM Rab7-NF (open cycle) and a mixture of 25nM Rab7-NF and 50 nM Rab7d-GG with 500 nM BSA (filled square). (**D**) Titration of GDI to 25 nM Rab7-NF (open cycle) and a mixture of 25nM Rab7-NF and 25 nM Rab7d-GG with 250 nM BSA (filled square) ($\lambda_{ex/em}$:479/525nm). The data were fitted to a competitive binding model to give K_d values of

Rab7-G and Rab7d-GG for REP and GDI, where K_d values of 0.22nM and 21nM of Rab7-NF for REP and GDI respectively were fixed.

A potential pitfall of this experiment relates to the influence of βGGT. This uncertainty comes from the unavailability of the affinity between Rab7-G and βGGT. Although this could in principle be included during fitting procedure, introduction of more parameters complicates the fitting and reduces the accuracy of simulation. However, the presence of low concentration of βGGT has negligible influence on Rab7-G:REP/GDI interaction. As shown in Figure 4-4-12, a series of titrations in the presence of different concentrations (<20 nM) of Rab7-G:βGGT complex resulted in identical K_d values for Rab7-G and REP/GDI interaction. Remarkably, Rab7-NF binds βGGT with relatively low affinity (K_d=114±0.1nM), and assuming a not dramatically higher affinity of Rab7-G, the presence of βGGT with a concentration far below K_d would not give rise to significant association with Rab7-NF and Rab7-G, so that the influence of these interactions on the calculation of K_d values for Rab7-G:REP/GDI can be ignored. Hence, the approximation is sound and sufficient for the mathematical simulation.

This argument, however, provokes another question: since Rab7-G is mostly dissociated from βGGT under such a low concentration, how could the prenylated Rab still be in the solution but not precipitate? We proposed that the dynamic equilibrium of interaction between Rab7-G and βGGT would transiently stabilize Rab7-G. This effect as well as the low concentration of protein may lead to a slow aggregation of Rab7-G so that it is available for titration that was typically completed within several minutes. Because the concentration of Rab7-G applied in titration is much higher than K_d values, its effective concentration could be accurately determined from the titration, which is quite close to the nominal concentration. This implies that most of Rab7-G is soluble and functional during the course of experiment.

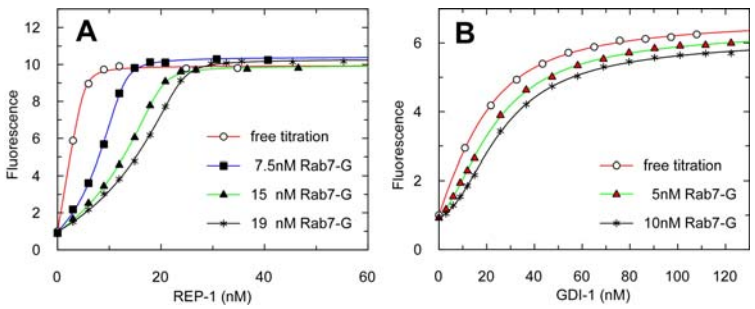

Concentration of Rab7-G:βGGT (nM)	K_d(Rab7-G:REP) (nM)	K_d(Rab7-G:GDI) (nM)
5		1.1
7.5	0.058	
10		0.88
15	0.081	
19	0.079	

Figure 4-4-12. (**A**) Titration of REP to 5 nM Rab7-NF in the presence of the indicated concentrations of Rab7-G:βGGT. (**B**) Titration of GDI to 19 nM Rab7-NF in the presence of indicated concentrations of

Rab7-G:βGGT. The data were processed as in Figure 4-4-11. The resulting K_d values were summarized in the table.

Natively monoprenylated Rab proteins comprise only a small subgroup of mammalian Rab GTPases and are absent in yeast. We therefore wished to explore the possible differences in the interaction of REP and GDI with the doubly and singly prenylated forms of Rab7. To measure the affinities for these interactions we used the above described competitive titration with Rab7-NF as a fluorescent reporter. A mixture of equimolar amount of Rab7-NF and Rab7d-GG was titrated with REP and GDI using only the NBD fluorescence as a signal (Figure 4-4-11 **C**,**D**). Remarkably, in this case the initial lag in fluorescence increase was not observed, suggesting that diprenylated Rab7 binds to its regulators more weakly than its monoprenylated form.

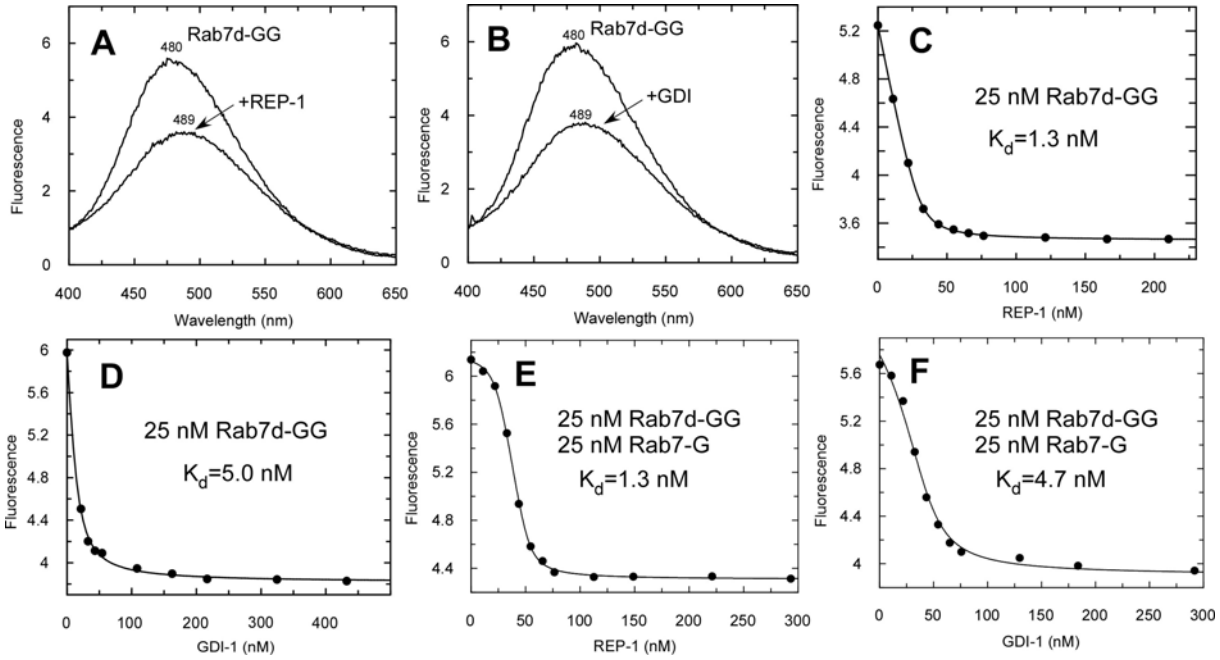

Figure 4-4-13. Interaction analysis of Rab7d-GG with REP and GDI. (**A** and **B**) The emission spectra of Rab7d-GG:BSA in the absence and the presence of REP(**A**) or GDI (**B**), λ_{ex}=340nm. (**C** and **D**) Titration of REP (**C**) or GDI (**D**) to 25 nM Rab7d-GG with 250 nM BSA ($\lambda_{ex/em}$: 340/479nm). K_d values were obtained by fitting the data to a quadratic equation. (**E** and **F**) Titration of REP (**E**) or GDI (**F**) to a mixture of 25nM Rab7d-GG with 250 nM BSA and 25nM Rab7-G:βGGT. ($\lambda_{ex/em}$: 340/479nm). K_d values were obtained by fitting the data by numerical simulation where the K_d values of 0.06nM and 1.5nM of Rab7-G for REP and GDI respectively were fixed.

To confirm these data using an independent approach we took advantage of the dansyl group at position 203 of Rab7 that provides a sensitive fluorescence change upon interaction of Rab7d-GG with REP or GDI (Figure 4-4-13 **A**, **B**) and was used as a reporter in the titrations. Competitive titration of an equimolar mixture of Rab7d-GG and Rab7-G with REP using the fluorescence of dansyl group, which displayed a lag in the fluorescence change (decrease in this case) arising from preferential binding to the non-fluorescent monoprenylated form (Figure 4-4-13 **E**, **F**). Numerical

fit of the data from the competitive titrations of the Rab7-NF/Rab7d-GG and the Rab7d-GG/Rab7-G mixture with REP and GDI gave K_d values consistent with those obtained from direct titrations [K_d(Rab7d-GG:REP)=1.3 nM, K_d(Rab7d-GG:GDI)=5.0 nM] (see Figure 4-4-13 **C**, **D**). The dissociation constants indicate that mono-prenylated Rab GTPase has a 20-fold higher affinity for REP than the doubly prenylated form, while in case of GDI the affinity difference is only 3-fold.

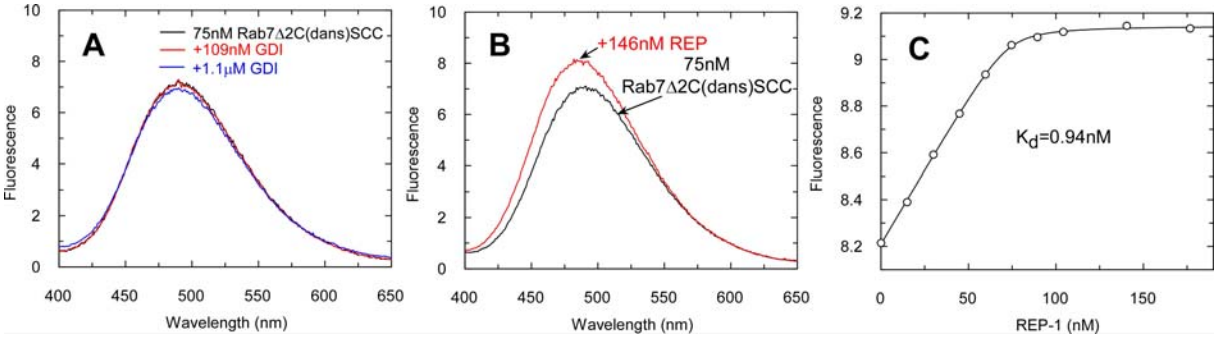

Figure 4-4-14. (**A** and **B**) The emission spectra of Rab7Δ2C(dans)SCC in the absence and in the presence of GDI (**A**) and REP (**B**), λ_{ex}=340nm. (**C**) Titration of REP to 75nM Rab7Δ2C(dans)SCC. (ex/em:340/486nm). The K_d value was obtained by fitting the data to a quadratic equation.

The REP/GDI-induced decrease in dansyl fluorescence is specific for prenylated Rab7. As shown in Figure 4-4-14 **A**, no fluorescence change was observed when GDI was added to unprenylated and dansylated Rab, Rab7Δ2C(dansyl)SCC, in agreement with previous observations and ITC result (Table 4-4-3). Addition of REP to Rab7Δ2C(dansyl)SCC resulted in ca. 10% fluorescence increase. These observations indicate that the observed quenching of dansyl fluorescence in the case of Rab7d-GG:REP/GDI interactions was indeed due to the presence of the isoprenoid moieties (Figure 4-4-14 **B**,**C**). The K_d value of Rab7Δ2C(dansyl)SCC:REP interaction was determined to be 1.1±0.3nM, in agreement with the previous report (Alexandrov et al., 1998).

It should be noted that the titration system for Rab7d-GG contains an excess of solubilizer, delipidated BSA (250 nM). However, the presence low micromolar BSA did not have obvious influence on the interactions of Rab7d-GG with REP and GDI (Figure 4-4-15). This could be interpreted to be a result of low affinity of Rab7d-GG for BSA, associated with that digeranylgeranylated Rab has to be solubilized with high concentration of delipidated BSA (section 4.4.3). Still, low concentration of delipidated BSA present in titration are sufficient to stabilize Rab7d-GG within the time frame of a titration (<10 min). Since the concentration of Rab7d-GG applied in REP titration is much higher than K_d value, its effective concentration could be

extracted reliably. The effective concentrations of Rab7d-GG obtained from titrations in the presence of different concentrations of BSA was close to the nominal one, indicating that Rab7d-GG is soluble and functional during the titration.

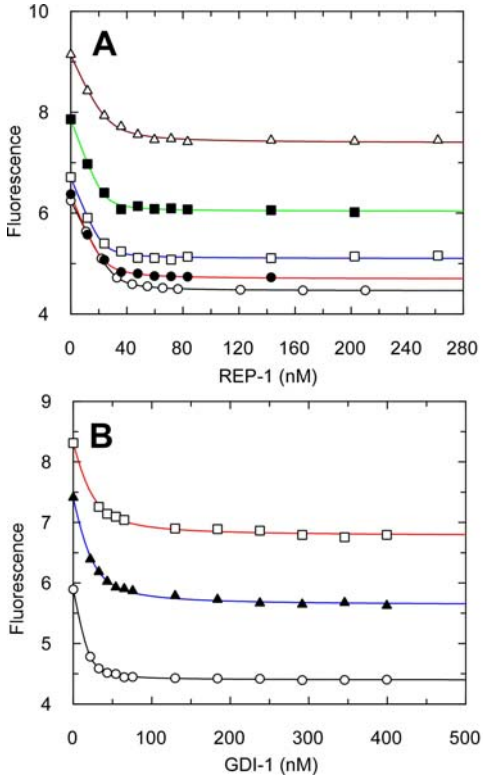

Table A.

Symbol	Concentration of BSA (μM)	K_d^{app} (nM)	Effective [Rab7d-GG] (nM)
	0.25	1.2	30
	1	1.7	22
	2	1.1	23
	5	1.0	24
	10	2.6	26

Table B.

Symbol	Concentration of BSA (μM)	K_d^{app} (nM)	Effective [Rab7d-GG] (nM)
	0.25	2.2	21
	5	7.3	24
	10	8.5	24

Figure 4-4-15. Titration of REP (**A**) and GDI (**B**) to nominal concentration of 30 nM of Rab7d-GG in the presence of indicated concentrations of delipidated BSA. Tables show the values of apparent K_d and effective concentration of Rab7d-GG obtained from titrations.

Table 4-4-2. Summery of dissociation constants and rate constants for interaction between prenylated Rab and REP/GDI.

Complex	K_d (nM)	k_{off} (s^{-1})
Rab7wt:REP-1	1[a]	0.012[a]
Rab7wt:GDI	> 5 ×10[4 b]	
Rab7Δ3CSC(NBD-farnesyl):REP-1	0.22±0.06	6.1±0.02 ×10^{-4}
Rab7Δ3CSC(NBD-farnesyl):GDI-1	14±5.5	0.031±0.001
Rab7Δ3CSC(NBD-farnesyl): β-GGT	114±0.1	0.13±0.01
Rab7Δ2SSCC(GG):REP-1	0.061±0.03	
Rab7Δ2SSCC(GG):GDI-1	1.5±0.3	
Rab7Δ6CK(Dans)SC(GG)SC-OMe:REP-1	0.41±0.06	
Rab7Δ6CK(Dans)SC(GG)SC-OMe:GDI-1	4.0±1.4	
Rab7Δ6CK(Dans)SC(GG)SC-OMe:β-GGT		0.1±0.01
Rab7Δ6CK(NBD)SCSC(GG)-OMe:REP-1	0.19±0.05	
Rab7Δ6CK(NBD)SCSC(GG)-OMe:GDI-1	2.5±0.4	
Rab7Δ6CK(NBD)SCSC(GG)-OMe: β-GGT		0.25±0.05
Rab7Δ6CK(Dans)SC(GG)SC(GG)-OMe:REP-1	1.3±0.2	0.002
Rab7Δ6CK(Dans)SC(GG)SC(GG)-OMe:GDI-1	5.2±2.2	0.0013±0.0005

[a](Alexandrov et al., 1998). [b] measurement by isothermal titration calorimetery (data not shown)

4.4.5 A model for Rab recycling

Table 4-4-3. K_d values of complexes of unprenylated wild type Rab7 and differently prenylated Rab7 with REP and GDI.

	K_d for REP (nM)	K_d for GDI (nM)
Rab7wt	1[a]	> $5x10^4$ [b]
Rab7-NBD-farnesyl	0.22±0.06	14±5.5
mono-geranylgeranylated Rab7	0.061±0.03	1.5±0.3
di-geranylgeranylated Rab7	1.3±0.2	5.2±2.2

[a](Alexandrov et al., 1998). [b] measured by isothermal titration calorimetery (data not shown)

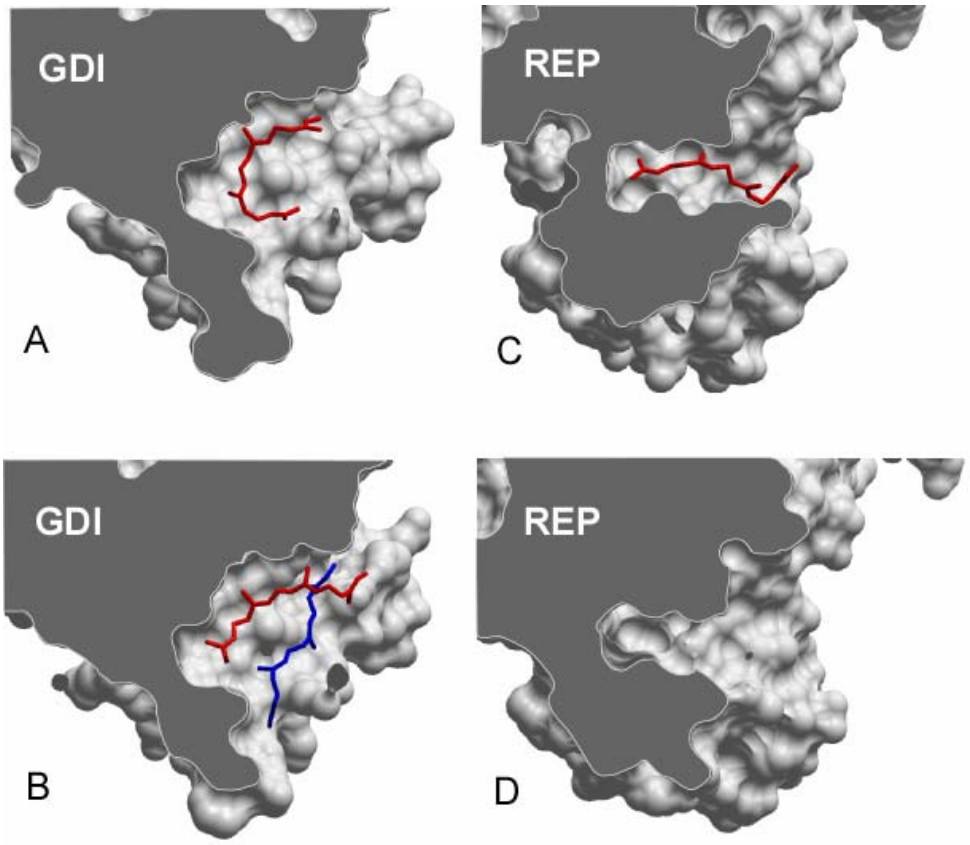

Figure 4-4-16. Comparison of lipid binding sites of GDI and REP molecules in complex with prenylated Rab GTPases. (**A**) monoprenylated Ypt1:GDI complex (1UKV), (**B**) di-prenylated Ypt1:GDI complex (2BCG), (**C**) monoprenylated Rab7:REP complex (1VG0) (**D**) unprenylated Rab7Δ22:REP complex (1VG9). The complexes were optimally superimposed and the domains II were sliced to expose the lipid binding site. All molecular manipulations including generation of images were performed with ICM browser Pro (Molsoft LLC).

The quantitative analysis results are summarized in Table 4-4-3, analysis of the interactions of prenylated Rab7 with REP and GDI revealed that they display comparable affinities to the di-prenylated form of this GTPase. In constrast, its monoprenylated form bound 3 times more tightly than the di-prenylated form to GDI

and nearly 20 times more tightly to REP. The latter observation finds support in earlier findings that unlike the diprenylated protein, the mono-prenylated Rab1 is not easily dissociated from REP by detergent and phospholipid, an observation that was interpreted as reflecting a higher affinity of the monoprenylated Rab form for REP compared to di-prenylated (Shen and Seabra, 1996). A small difference in the affinities of mono- and di-prenylated Rab7 for GDI can be rationalized on the basis of the recently solved structures of Ypt1:GDI complexes (Pylypenko et al., 2006; Rak et al., 2003). In the structure of the mono-prenylated Ypt1:GDI complex the conjugated lipid is inserted into the lipid binding pocket in a bent conformation with both ends being solvent exposed, partially occupying the binding sites of both lipids (Figure 4-4-16 **A**). In the doubly prenylated Ypt1:GDI complex, one isoprenoid is buried at the bottom of the hydrophobic binding site while the second stacks on top of it, forming relatively few contacts with GDI (Figure 4-4-16 **B**). Because of this, the overall contact area of the protein:lipid interface is increased only modestly upon conjugation of the second isoprenoid. The situation with the Rab:REP interaction appears to be more complex. Monoprenylation increases the affinity of the Rab:REP complex to an affinity of 60pM which is then reduced to ca. 1 nM after the attachment of the second lipid. This implies that the prenyl groups bound only very weakly to REP in the di-prenylated complex.

At the mechanistic level these observations can be rationalized in the following way: The binding site of REP is narrower than that of GDI and the lipid is inserted in an extended conformation (Figure 4-4-16 **C**). The structure of the doubly prenylated REP:Rab complex is not available, but should its lipid binding site be already fully dilated in the complex with the monoprenyated GTPase, then the second lipid could bind outside of it. This may also lead to partial displacement of the isoprenoid moiety from the lipid binding site, leading to the observed affinity decease. The “purpose” of this mechanism may be the retention of the monoprenylated reaction intermediate in the complex to assure its complete processing. However, this model raises the question about the way natively monoprenylated RabGTPases are processed, since they may form a complex too tight to be dissociated for membrane insertion. Indirect support of this idea comes form the observation that mono-cysteine Rab5a and Rab27a mutants are retained on the ER membrane and are not delivered to their native locations (Gomes et al., 2003). The answer probably lies in a large variation of affinities for the interaction of the Rab protein core with REP, with Rab7 being one

of the tightest binders (Rak et al., 2004). With many Rab:REP interactions displaying K_d values of several hundred nM, the overall affinity of monoprenylated complexes can be expected to remain in the nanomolar range.

Finally, and probably most importantly, our study provides evidence for a proposed model of RabGTPase membrane delivery and extraction (Figure 4-4-17). It was shown that REP appears to be much less efficient than GDI in Rab extraction. This difference in efficiency is in keeping with their biological roles, since REP is probably only involved in delivery of Rabs to membranes, whereas GDI, in addition to having this property, must also be able to extract them. These different properties can be explained by considering the affinities of REP/GDI for unmodified and prenylated forms of Rab, respectively. As shown in Table 4-4-2, whereas REP binds with the same high affinity to both unprenylated and di-prenylated Rab, enabling it to present the unprenylated form to RabGGTase, GDI binds to prenylated Rab with at least 1000-fold higher affinity than to unprenylated Rab. The large increase in affinity of GDI to Rab on docking of the C-terminus and the conjugated isopreniod groups is the driving force for the extraction process. Expressed in another manner, GDI is efficient in extraction of Rabs from membrane since there is a large difference in binding energy between the situations in which only the GTPase domain interacts with GDI and the situation in which the C-terminus and conjugated isopreniod moiety are also docked. Therefore, the difference in binding energies provides the thermodynamic driving force for the extraction from the membrane. In contrast, most of the binding energy in the case of REP comes from the interaction with the GTPase domain, with only very little or no driving force for the extraction provided by the interaction of the isoprenoid conjugated C-terminus. As a consequence, REP has very low potential to extract Rab from membranes, but can readily release the prenyl groups for insertion into the membrane. Therefore, the thermodynamic driving force in the process from B to C shown in Figure 4-4-17 determines the functional segregation of REP and GDI in extraction of Rab from membranes. A remaining problem concerns the dissociation of REP from a Rab molecule which has inserted its lipid into a membrane. Based on what is known about the kinetics of dissociation of REP from unprenylated Rab, this should occur at a rate of ca. 0.01 s-1, corresponding to a half-life in the range of 1 minute (Alexandrov et al., 1998). It is possible that this is rapid enough for the physiological role of REP, especially when it is considered that after GTP/GDP exchange, a process which happens on the

membrane, the affinity of REP for Rab is reduced by at least a factor of 10 through acceleration of the dissociation rate (Alexandrov et al., 1998). However, it is also possible that additional proteinaceous factors are involved, as already implied for GDI in several studies (Sivars et al., 2003; Dirac-Svejstrup AB et al., 1997).

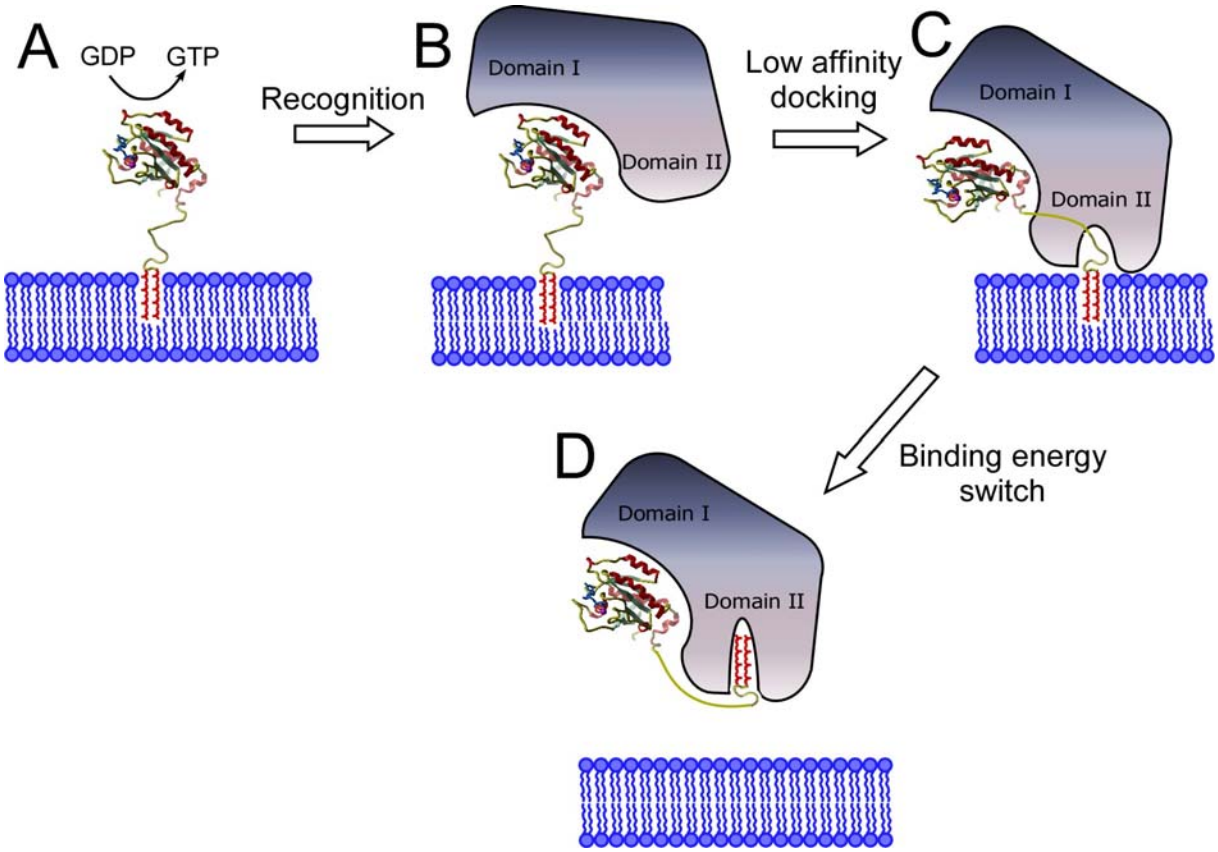

Figure 4-4-17. Model for the extraction of Rab from membranes by GDI or REP. (**A**) Membrane associated Rab proteins undergo hydrolysis of GTP to GDP after a round of vesicular transport. (**B**) Initial recognition of the GDP-bound Rab. (**C**) Formation of the membrane bound Rab:REP/GDI complex. (**D**) Translocation of the conjugated isoprenoid moieties to the GDI/REP and release form the membrane.

5. Materials and Methods

5.1 Materials

5.1.1 Chemicals

Chemicals	Supplier
Acetic acid,	Merck (Darmstadt, DE)
Acetonitrile	JT Baker (Deventer, NL)
Acetone	JT Baker (Deventer, NL)
Acrylamid/Bisacrylamide (37.5:1, 30 % w/v)	Applichem (Darmstadt, DE)
Ammonium carbonate	Riedel-de Haën (Seelze,DE)
Ammonium sulfate	Applichem (Darmstadt, DE)
Ammonium persulfate (APS)	Merck (Darmstadt, DE)
Ampicillin (Amp)	Serva (Heidelberg, DE)
Bradford reagent	Bio-Rad (München, DE)
Bromphenol blue	Serva (Heidelberg, DE)
Bovine serum albumine (BSA)	Sigma
Cetyltrimethylammoniumbromide (CTAB)	Roth (Karlsruhe, DE)
Chloroform	JT Baker (Deventer, NL)
3-[(3-Cholamidopropyl)dimethylammonio]-1-propanesulfonate (CHAPS)	Roth (Karlsruhe, DE)
Chloramphenicol (Cam)	Merck (Darmstadt, DE)
Coomassie Brilliant Blue G250+R250	Serva (Heidelberg, DE)
N-dodecyl-*N*,*N*-(dimethylammonio)butyrate (DDMAB)	Calbiochem
Deoxycholic acid sodium salt (DCS)	Serva (Heidelberg, DE)
Dichloromethane	JT Baker (Deventer, NL)
Dimethylsulfoxide(DMSO)	Fluka
Disodium hydrogenphosphate	JT Baker (Deventer, NL)
Dithioerythitol (DTE)	Gerbu (Gaiberg, DE)
Dithiothreitol (DTT)	Gerbu (Gaiberg, DE)
Ethylenediaminetetraacetic adic (EDTA)	Gerbu (Gaiberg, DE)
Ethanethiol	Fluka
Ethanol	JT Baker (Deventer, NL)

Ethidium bromide	Sigma
Farnesyl pyrophosphate (FPP)	Sigma
Farnesyl triphosphate (FTP)	Sigma
GdmHCl	Applichem (Darmstadt, DE)
Gernylgernyl monophosphate (GGMP)	Sigma
Gernylgernyl pyrophosphate (GGPP)	Sigma
Gernylgernyl trihosphate (GGTP)	Sigma
Glycerol	Gerbu Gaiberg, DE
Glycine	Roth (Karlsruhe, DE)
Guanosine diphophate (GDP)	Pharma Waldhof (Düsseldorf, DE)
4-(2-Hydroxyethyl)piperazine-1-ethanesulfonic acid (HEPES)	Gerbu (Gaiberg, DE)
Hydrochloric acid	JT Baker (Deventer, NL)
Imidazol	Gerbu (Gaiberg, DE)
Isopropyl-β-D-thiogalactopyranoside (IPTG)	Gerbu (Gaiberg, DE)
Kanamycin	Boehringer (Mannheim,DE)
Magnesium chloride	JT Baker (Deventer, NL)
Methanol	Applichem (Darmstadt, DE)
β-Mercaptoethanol	Serva (Heidelberg, DE)
Organic dyes	Molecular Probes (Eugene, OR, USA), ATTO-TEC GmbH (Siegen, DE), Dyomics GmbH (Jena, DE)
Phenylmethylsulfonylfluoride (PMSF)	Sigma
Potassium dihydrogenphosphate	JT Baker (Deventer, NL)
Potassium hydroxide	JT Baker (Deventer, NL)
2-Propanol	JT Baker (Deventer, NL)
Sinapinic acid	Sigma
Sodium chloride	Fluka
Sodium dihydrogenphosphate,	JT Baker (Deventer, NL)
Sodium dodecylsulphate (SDS)	Gerbu (Gaiberg, DE)
Sodium hydroxide	JT Baker (Deventer, NL)
Sodium lauryl sarcosine (SLS)	Sigma
Sodium 2-mercaptoehanesulfonate (MESNA)	Sigma
N,*N*,*N'*,*N'*-tetramethylethylendiamin (TEMED)	Roth (Karlsruhe, DE)
D(+)-trehalose	Roth (Karlsruhe, DE)

Trichloroacetic acid (TCA)	Fluka
Trifluoroacetic acid (TFA)	Fluka
Trihydroxymethylaminomethane (TRIS)	Roth (Karlsruhe, DE)
Triton X-100	Serva (Heidelberg, DE)
Urea	JT Baker (Deventer, NL)

5.1.2 Other chemicals from collaborators

The novel dyes I-SO-s-IA and I-BA-s-IA (Figure 4-1-8) were gifts from Prof. Dr. Klaus Hahn (The Scripps Research Institute, San Diego, USA). The fluorescent peptides shown in Figure 4-1-11, chapter 4.1.2.3 were obtained from Thermo Hybaid GmbH, Novabiochem and EMD Biosciences. The NBD-farnesylated peptide, C(S*t*Bu)SC(NBD-farensyl) (Scheme 4-7) was synthesized by Dr. Kui-Thong Tan in Prof. Waldmann´s group at the Max-Planck-Institute of Molecular Physiology, Dortmund and the Dortmund University. These peptides were stored as powder at -20°C under an atmosphere of argon, and were dissolved in DMSO to prepare solutions of 40mM before use. They were ligated to truncated Rab7 proteins by means of EPL.

NBD-FPP (Figure 4-1-17) was synthesized by Dr. Reinhard Reents and Dr. Kui-Thong Tan in Prof. Waldmann´s group. It was stored as power or 40 mM stock solution in 20 mM $(NH_4)_2CO_3$ at -20°C.

Table 5-1. Peptides used in this study.

Entry	Compounds	Mw (g/mol)	Supplier
1	CK(NBD)C	515.6	Thermo
2	CCK(NBD)	515.6	Thermo
3	CCK(dans)	585.8	Novabiochem
4	C(S*t*Bu)C(S*t*Bu)-dans	676.0	EMD
5	CK(ATTO425)C	735.9	Novabiochem
6	CCK(ATTO425)	735.9	Novabiochem
7	C(S*t*Bu)SC(NBD-farensyl)	782.0	Dr. Kui-Thong Tan
8	NBD-FPP	560.4	Dr. Reinhard Reents and Dr. Kui-Thong Tan

The peptide compounds for the screening of RabGGTase inhibitors (Figure 4-2-4 in chapter 4.2.3) were synthesized with purity >95% by Dr. Kui-Thong Tan and Dr.

Ester Guiu-Rozas in Prof. Waldmann´s group. Synthetic procedures and analytical data can be found in Kui-Thong Tan's PhD thesis (Dortmund University).

5.1.3 Other materials

Materials	Supplier
Amicon Ultra-4,15 (10K, 30K) Concentrator	Milipore (Ireland)
BioSep-SEC-2000 gel filtration	Phenomenex (Aschaffenburg, DE)
Chitin beads	New England Biolabs (Beverly, USA)
Dialysis membrane tubing (MWCO: 12-14 kDa, 5-8 kDa)	Spectrum Lab Inc. (Racho Dominguez, CA, USA)
DyeEx 2.0 Spin Kit	Qiagen GmbH (Hilden, DE)
Electroporation cuvettes	Bio-Rad (München,DE)
Eppendorf tube (0.5 mL, 1.5 mL, 2.0 mL)	Eppendorf (Hamburg,DE)
Falcon Tube (50 mL, 15 mL)	Falcon GmbH (Gräfeling-Locham, DE)
Glutathione Sepharose	GE Healthcare (Uppsala, SE)
HiTrap Ni-NTA column	Pharmacia Biotech (Uppsala, SE)
Jupiter 5μm C4 300A reverse phase column	Phenomenex (Aschaffenburg, DE)
Low molecular weight marker	Amersham Biosciences (Uppsala, SE)
NAP-5 desalting column	Amersham Biosciences (Uppsala, SE)
Nitrocellulose paper	Schleicher&Schuell (Dassel, DE)
PD-10 desalting column	Amersham Biosciences (Uppsala, SE)
PRCNTOSIL 120-5-C18-AQ 5 μm reverse phase column	Bischoff-Chrom (Leor, DE)
Quartz cuvette (1cm)	Hellma Optik GmbH (Jena, DE)
Superdex 75/200 Gel filtration	Pharmacia Biotech (Uppsala, SE)
Whatman FP 30/0.2, 0.4 μm cellulose filter	Schleicher&Schuell (Dassel, DE)
ZapCap filter	Nalgene (Rochaster, NY, USA)

5.1.4 Instruments

Instruments	Supplier
Äkta prime system with REC112 recorder	Pharmacia Biotech (Uppsala, SE)
Biorad PE 9700 thermocycler	Applied Biosystems (Weiterstadt, DE)
Centrifuge Allegra X-22R	Beckman Coulter (Palo Alto, USA)
Centrifuge Avanti J20-XP	Beckman Coulter (Palo Alto, USA)
Centrifuge Optima L-70K Ultracentrifuge	Beckman Coulter (Palo Alto, USA)
Centrifuge Eppendorf 5415C/D benchtop	Eppendorf (Hamburg, DE)
Electroporation device *E. coli* Pulser	Bio-Rad (München,DE)
Deionized water apparatus	Millipore (Eschborn, DE)
FLA-5000 (Fluorescence image reader)	Fujifilm (Japan)
Fluoroskan Ascent Fl type 374	Thermo BioAnalysis (Santa Fe, New Mexico, USA)
Gel-electrophoresis system	Bio-Rad (München, DE)
High pressure liquid chromatography (HPLC)	Waters (Eschborn, DE)
HPLC-ESI-MS	Agilent, Finnigan
Isothermal titration calorimeter	MicroCal (Northampton, USA)
MALDI-TOF-MS	Applied Biosystem (Darmstadt, DE)
Microfluidizer	Microfluidics (Newton, MA, USA)
PH-meter 761	Calimatic Knick (Berlin, DE)
SDS-PAGE Mini-Protean II system	Bio-Rad (München, DE)
Shaker	Infors (Bottmingen, CH)
Spex Fluoromax-3 Spectrofluorometer	Jobin Yvon Horiba Group (NJ, USA)
Stopped-flow spectrometer SX20	Applied Photophysics (Leatherhead, UK)
Thermomixer 5436 (1.5 mL)	Eppendorf (Hamburg, DE)
Ultrasonic cell disruptor (SONIFIER)	Branson (Danbury, CT, USA)
UV/Visible Spectrometer DU 640	Beckman Coulter (Palo Alto, USA)

Representations of crystal structures were created with the program Molsoft-ICM (Molsoft LLC, La Jolla, USA). Simulation of ternary Rab:REP:RabGGTase complex was carried out by Prof. Dr. Ruben Abagyan, The Scripps Research Institute (La Jolla, USA) using the ICM 3.4-8cj software package (Molsoft).

5.1.5 Buffers and growth media

LB medium

5 g/L	yeast extract
10 g/L	Tryptone
10 g/L	NaCl

LB agar plates

15 g/L	Bacto agar
50 mg/L	Ampicillin

Antibiotics

125 mg/L	Ampicillin
34 mg/L	Chloramphenicol
50 mg/L	Kanamycin

SDS-PAGE running buffer (10x)

0.25 M	Tris-HCl
2 M	Glycine
1% (w/v)	SDS

SDS-PAGE stacking gel buffer (4X)

0.5 M	Tris-HCl, pH 6.8
0.4 % (w/v)	SDS

SDS-PAGE resolving gel buffer(4X)

1.5 M	Tris-HCl, pH 8.8
0.4 % (w/v)	SDS

SDS-PAGE loading buffer (2x)

62.3 mM	Tris-HCl, pH 6.8
2 % (w/v)	SDS
10 % (v/v)	glycerol
5 % (v/v)	β-Mercaptoethanol
0.001 % (w/v)	bromophenol blue

Coomassie staining solution

10 % (v/v)	acetic acid
40 % (v/v)	ethanol
0.1 % (w/v)	Coomassie Brilliant Blue R250

Destaining solution

10 % (v/v)	acetic acid

TAE buffer (1x)

40 mM	Tris acetate, pH 8.5
2 mM	EDTA
20 mM	Glacial acetic acid

PBS (10x)

80 g/L	NaCl
2 g/L	KCl
14.4 g/L	$Na_2HPO_4 \cdot 2\ H_2O$
2.4 g/L	KH_2PO_4

DNA loading buffer (5x)

30 %(w/v)	Sucrose
20 % (v/v)	glycerol
0.2 % (w/v)	orange G

Bug Buffer

50 mM	NaH_2PO_4, pH 8.0
0.3 M	NaCl

Buffer A

50 mM	NaH_2PO_4, pH 8.0
0.3 M	NaCl
2 mM	β-mercaptoethanol

Buffer B

50 mM	NaH_2PO_4, pH 8.0
0.3 M	NaCl
2 mM	β-mercaptoethanol
0.5 M	Imidazole

Breaking Buffer

25 mM	NaH_2PO_4, pH 7.5
0.5 M	NaCl
2 mM	$MgCl_2$
10 μM	GDP

5.2 Molecular cloning methods

5.2.1 Plasmids and bacterial strains

Plasmids

Plasmid Name	Insert	Resistance/ Selection marker	Application and References
pTWIN2_Rab7Δ3	canine Rab7Δ3	Amp	Expression of Rab-intein-CBD fusion proteins and production of C-terminal α-thioesters. (Durek et al., 2004a; Alexandrov et al., 2002; Iakovenko et al., 2000)
pTYB1_Rab7Δ6	canine Rab7Δ6	Amp	
pTWIN1_Rab7Δ2SS	canine Rab7Δ2	Amp	
pTWIN1_Rab7Δ2SC	canine Rab7Δ2	Amp	
pTWIN1_Rab7Δ2CS	canine Rab7Δ2	Amp	
pGATEVmod_RabGGTase α	rat RabGGTase α	Amp	Coexpression of the RabGGTase subunits with a 6XHis-GST tag on the N-terminus of the α-subunit. The tag can be cleaved off by TEV protease. (Kalinin et al., 2001)
pET30_RabGGTase β	rat RabGGTase β	Kan	
pET19mod_yGDI	yeast GDI	Amp	Expression of the corresponding protein N-terminally containing a 6XHis tag, which can be cleaved off by TEV protease.
* pFastBac_GDI-1	bovine GDI-1	Amp	
* pVL_REP-1	rat REP-1	Amp	Expression of REP-1 or MRS6p with a 6XHis tag.(Armstrong et al., 1995a)
pET30a_MRS6	yeast MRS6p	Kan	
pIF-Rab7SSSC	Rab7C205S	Amp	Expression of Rab7 single cysteine mutants with a 6XHis-IF tag at the N-terminus, which can be cleaved off by TEV protease.
pIF-Rab7SCSS	Rab7C207S	Amp	
pMAL_Rab7	canine Rab7wt	Amp	Expression of Rab7wt and truncation mutants with 6XHis-MBP tag on the N-terminus, which can be cleaved off by TEV protease.
pMAL_Rab7delata14	Rab7Δ14	Amp	
pMAL_Rab7_ASA	Rab7_ASA	Amp	
pMAL_Rab7_TEV_ASA	Rab7_TEV_ASA	Amp	
pMAL_Rab7_WFY	Rab7_WFY	Amp	
pMAL_Rab7AAAAACSC	Rab7-5A	Amp	
pMAL_Rab7Δ204	Rab7Δ204	Amp	
pMAL_Rab7Δ203-204	Rab7Δ203-204	Amp	

pMAL_Rab7Δ202-204	Rab7Δ202-204	Amp	
pMAL_Rab7Δ201-204	Rab7Δ202-204	Amp	
pMAL_Rab7Δ199-204	Rab7Δ202-204	Amp	
pMAL_Rab7Δ198-204	Rab7Δ202-204	Amp	
pMAL_Rab7Δ197-204	Rab7Δ202-204	Amp	
pET19modRab7_L192S	Rab7 L192S	Amp	Expression of the corresponding protein N-terminally containing with a 6XHis tag, which can be removed by TEV protease.
pET19modRab7_I190H	Rab7 L192S	Amp	
pET19modRab7_I190H L192S	Rab7 I190H L192S	Amp	

Empty pTWIN and pTYB vectors were obtained from New England Biolabs (Beverly, MA, USA). Typically expression was performed using one of the *E. coli* strains listed below. * Expression in SF9 or SF21 cells upon infection with recombinant baculovirus. Amp = ampicillin, CBD = chitin-binding domain, Kan = kanamycin.

Bacterial strains	***Genotypes***
XL1 Blue (Stratagene)	*recA1, endA1*, *gyrA96*, thi-1, *hsdR17*, *supE44*, *relA1*, *lac* [F´, *proAB*, *lacI*^{q}ZΔM15, *Tn10* (Tet^r)]
BL21(DE3) (Novagen)	F$^-$, *ompT*, lon, *hsd*S (r_B^-, m_B^-), *dcm*, *gal*, λ(DE3)
BL21(DE3) Codon Plus RIL (Stratagene)	F$^-$, *ompT*, lon, *hsd*S (r_B^-, m_B^-), *dcm*, *gal*, λ(DE3), *endA,* Hte [*argU ileY leuW* Cam^R]
BL21(DE3) Codon Plus RP (Stratagene)	F$^-$, *ompT*, lon, *hsd*S (r_B^-, m_B^-), *dcm*, *gal*, λ(DE3), *endA,* Hte *[argU proL* Cam^R]
BL21(DE3) Rosetta (Novagen)	F$^-$, *ompT*, lon, *hsd*S (r_B^-, m_B^-), *dcm*, *gal*, λ(DE3), pRARE2 (Cam^R)

5.2.2 Preparation of competent cells

1 L of LB medium was inoculated with 1 mL of an overnight-grown culture of the desired *E.coli* strain. Cells possessing antibiotic resistance genes were grown in the presence of the corresponding antibiotics. The culture was incubated at 37° C on a shaker, until the OD_{600} reached 0.5 (ca. 3 - 4 h). The culture was cooled on ice for 20 min, transferred to sterile centrifugation vessels and centrifuged for 10 min at 4°C at 2000 g. The supernatant was discarded.

Electro-competent cells

The bacterial cell pellet was gently resuspended in 5 mL of ice-cold sterile GYT (0.125 % (w/v) yeast extract, 0.25 % (w/v) tryptone, 10 % (v/v) glycerol) and recentrifuged as described above. Cell pellet were resuspended in 1 mL GYT, dispensed in 50 µl aliquots, shock frozen in liquid nitrogen and stored at -80° C.

Chemical-competent cells

The pellet was gently resuspended in 20 mL of ice-cold sterile 100 mM $CaCl_2$ solution and incubated on ice for 30 min. The cells were centrifuged at 2000 g for 5 min at 4° C and were resuspended in 1 - 5 mL of TFBII buffer (10 mM MOPS, pH 7.0, 75 mM $CaCl_2$, 10 mM NaCl, 15 % glycerol). Aliquots of 50 - 100 µl were shock frozen in liquid nitrogen and stored frozen at -80° C.

5.2.3 Preparative PCR

The appropriate 5'- and 3'-primers were designed. The PCR reaction mixture was prepared in steps shown in Table 5-2 in a PCR tube. The mixture was incubated in Biorad PE 9700 thermocycler (Applied Biosystems) using PCR program as described in table 5-3.

Table 5-2. Preparation of PCR reaction mixture.

Step	Material	Volume (µL)
1	Sterile water	37
2	Buffer (Expend High Fidelity 10X)	5
3	DMSO	3
4	Template DNA (10-100 ng)	1
5	Primers (final conc. 1 µM)	1.5
6	dNTPs (10 mM, final conc. 200 µM)	1
7	Enzyme: 2-3 units of Expand High Fidelity Polymerase mix (Roche Diagnostics, Mannheim, DE)	1
	Total	50

Table 5-3. PCR program

Temp (°C)	Time	Step function
94	2-3 min	**Hold**
94	[cycle]40 s	**Denaturation**: the first cycling event causes melting of DNA template and primers.
50-62	[cycle] 30 s	**Annealing**: the temperature is dependent on melting temp (Tm) of primer, typically 3-5°C below Tm.
72	[cycle] 1 min/kb	**Extension**: the time is dependent on the length of amplifying fragment.
72	7-10 min	**Final elongation**: after the last PCR cycle to ensure that any remaining single-stranded DNA is fully extended.
4	indefinite	**Final Hold**: short-term storage of the reaction.

[cycle] PCR for 20-30 cycles.

5.2.4 Purification of PCR products by agarose gel electrophoresis

Depending on the size of the DNA fragment, the agarose concentration was between 0.8 and 2 % (w/v).

1| Dissolve the required amount of agarose by heating in TAE buffer.

2| Add ethidium bromide to a final concentration of 0.5 μg/mL

3| Pour the solution into the gel casting equipment and allowed to polymerize.

4| Mix the samples with 5X DNA loading buffer and load into the wells. A 1 kb DNA ladder (GibcoBRL) was used as a molecular weight standard.

5| Run the gels horizontally at 10 V/cm immersed in TAE-buffer until fragment separation was complete.

6| Excise the bands of interest and extract the DNA from the gel using a gel extraction kit from Qiagen according to the instructions of the manufacturer.

5.2.5 Subcloning

Restriction enzyme digestion

Both vector and purified PCR product were digested by the appropriate restriction enzymes. Digestions of DNA fragments were performed as recommended by the manufacturer at 37°C for 2 h. An example is shown in Table 5-4. The reaction was stopped by addition of DNA loading buffer. Fragments produced by restriction enzyme digestion were purified using agarose gel electrophoresis.

Table 5-4. Restriction enzyme digestions.

Step	Material	Volume (μL)	Volume (μL)
1	Sterile water	29	27
2	Buffer (NEB4 10X)	5	10
3	Vector (0.2 μg/μL) or PCR product (1 μg/μL)	Vector 10	PCR product 53
4	Enzyme: NdeI (20 U/μL)*	3	5
5	Enzyme: SapI (20 U/μL)	3	5
	Total	50	100

*1 unit of enzyme can digest 1 μg DNA.

Ligation

For ligation 1-10 *f*mol of linear plasmid DNA was mixed with a 10 fold molar excess of insert fragment. Ligation was performed in ligation buffer in a volume of 20 µl, using 5 units of T4 DNA ligase (Roche Diagnostics, Mannheim, Germany) for 1 h at 20°C. Subsequent deactivation was performed at 65°C for 10 min. An example is shown in Table 5-5.

Table 5-5. Preparation of ligation reaction mixture.

Step	Material	Volume (μL)
1	Vector (0.06 μg/μL)	3
2	Insert (0.3 μg/μL)	12
3	Ligation buffer (5X)	4
4	T4 DNA ligase (5 U/μL)	1
	Total	20

5.2.6 Chemical transformation

1| Add the ligation mixture containing approximately 1 ng of the desired plasmid DNA to 50 μL chemical competent cells. The mixture was incubated on ice for 30 min without shaking.

2| Heat the cells at 42° C for 1 min and immediately cooled on ice for 2 min.

3| Add 1 mL of LB medium was added to the cells.

4| Incubate at 37°C for 1 h on a shaker.

5| Spread 100 μL cells on agar plates supplemented with the corresponding antibiotics.

6| Invert plates and incubate overnight (12-16 h) at 37°C.

5.2.7 Colony PCR screen

1| Pick a single bacterial colony growing on LB agar plate with the corresponding antibiotics using a sterile inoculating loop.

2| Inoculate the colony into 2 mL of LB medium with the corresponding antibiotics.

3| After overnight growth, withdraw 10 μL culture and mix it with 10 μL 0.05% Triton-X 100 in a PCR test tube using sterile tips.

4| Heat the mixture at 95°C for 10 min.

5| Centrifuge the mixture at 4°C (16,000 g, 2min).

6| Perform PCR using 3 μL of the supernatant. The preparation of the PCR reaction mixture is depicted in Table 5-6.

Table 5-6. Preparation of colony PCR reaction mixture.

Step	Material	Volume (μL)
1	Sterile water	15.7
2	Buffer (Bio Therm 10X)	2.5
3	DMSO	1.5
4	Template DNA (mixture of cell lysate)	3
5	Primers (final conc. 1 μM)	1
6	dNTPs (10 mM, final conc. 200 μM)	0.5
7	Enzyme: 1 unit Bio Therm DNA polymerase	0.3
	Total	25

7| Analyze the PCR products by agarose gel electrophoresis. The one showing a band of PCR product at the expected molecular weight suggests a successful subcloning.

5.2.8 Preparation of plasmid DNA

Plasmid DNA was prepared using the plasmid mini-prep kit (Qiagen) as follows:

1| Pick a single bacterial colony to seed 2 mL of LB medium containing the appropriate antibiotics.

2| Grow the culture overnight (10 - 12 h) at 37°C.

3| Harvest cells by centrifugation (16,000 g, 1 min). Discard the supernatant.

4| Resuspend the cell pellet in 250 μL Buffer I with RNase A by vortex.

5| Add 250 μL Buffer II and mix extensively until the solution becomes clear.

6| Add 350 μL Buffer III into clear lysate to precipitate chromosomal DNA, lipids, and proteins.

7| Remove the precipitates by centrifugation (16,000 g, 15 min).

8| Load the supernatant on a silica spin column. Centrifuge the column for 0.5 min at 10,000 rpm.

9| Wash the column with 500 μL HB buffer, 700 μL wash buffer (with ethanol) for 2 times by centrifugation (10,000 rpm, 0.5 min).

10| Centrifuge the column for 1.5 min at 10,000 rpm to get rid of ethanol.

11| Elute the plasmid DNA with 30-50 μL EB buffer by centrifugation (10,000 rpm, 1 min).

5.2.9 DNA sequencing

For DNA sequencing, the cloned plasmid was subjected to PCR using the BigDyeDesoxy terminator cycle sequencing kit. The sequencing reactions were prepared as described in Table 5-7. And PCR program was set as shown in Table 5-8.

Table 5-7. Preparation of sequencing reaction mixture.

Step	Material	Volume (μL)
1	Sterile water	3
2	Plasmid (0.1 – 0.5 μg)	2
3	Primers (3 pmol)	1
4	BigDye mix	4
	Total	10

Table 5-8. PCR program

Temp (°C)	Time	Step
98	2 min	**Hold**
94	^{cycle}20 s	**Denaturation**
50	^{cycle} 30 s	**Annealing**

60	[cycle]4 min	**Extension**
4	indefinite	**Final Hold**

[cycle] PCR for 25 cycles.

Ethanol precipitation

1| Dilute the PCR product with 10 μL H_2O.

2| Add sodium acetate (pH 5.5) to a final concentration 250 - 300 mM to the sample.

3| Precipitate DNA by adding ethanol (96 %) to a final concentration of ca. 70 %

4| Incubate the sample for 15 min at room temperature.

5| Centrifuge the sample at 16,000 g for 10 min at 4°C. Remove the supernatant.

6| Wash the precipitate once with 50 μL 70 % ethanol. Centrifuge the sample at 16,000 g for 10 min at 4°C.

7| Dry the sample under vacuum.

The sample was analyzed by the in house sequencing facility.

5.2.10 Transformation by electroporation

1| Add ca. 1 ng of plasmid DNA in a volume of 0.5 μL to 50 μL electro-competent cell suspension in a chilled electroporation cuvette (0.2 μm path length).

2| Tap the cuvette to exclude air bubbles.

3| Apply a high voltage pulse using a *E.coli* Pulser from Biorad (conditions: 25 μF, 200 Ω, 2.5 kV).

4| Immediately add 1 mL of LB medium to the cuvette after pulsing.

5| Grow the culture at 37°C for 1 h on a shaker.

6| Spread 100 μL cell suspensions on agar plates containing the appropriate antibiotics.

7| Invert plates and incubate overnight (12-16 h) at 37°C.

5.3 Protein expression and purification methods

5.3.1. Expression and purification of RabGGTase, REP-1, RabGDI, Rab7wt and Rab7 mutants

Expression of Rab7 in E. coli

1| Transform BL21(DE3) cells with plasmid pMAL_Rab7 and select on a LB agar plate containing 50 mg/L ampicillin (Amp).

2| Pick a single colony from the agar plate using a sterile inoculating loop and inoculate it into 100 mL of LB-medium containing 125 mg/L ampicillin.

3| Incubate at 37°C at 160 rpm on a rotatory shaker overnight.

4| Inoculate this pre-culture into 5 L of LB-medium containing 125 mg/L Amp.

5| Grow cells in five 5 L flasks at 37°C on a shaker (160 rpm) until the absorbance at 600 nm (OD_{600}) reached 0.5-0.7 (ca. 4-6 h).

6| Put the flasks in the cold room to reduce the temperature of the culture to 20°C.

7| For induction of the protein expression, add IPTG to the culture to a final concentration of 0.1 mM.

8| Incubate at 20°C on a shaker (160 rpm) overnight (5-12 h).

9| Before harvesting cells, take a sample of 30 μL from the cell suspension, mix it with 30 μL 2×SDS sample buffer, boile at 95°C for 10 min and run a denaturing SDS-PAGE (see section 5.4.1) to estimate the protein expression level.

10| Harvest cells by centrifugation in the centrifuge Avanti J20-XP (Beckman Coulter) at 6000 rpm, 4°C for 20 min.

11| Discard the supernatant carefully and wash the cells with PBS by centrifugation in the centrifuge Allegra X-22R (Beckman Coulter) at 4000 rpm, 4°C for 15 min.

■ **PAUSE POINT** The cells can be frozen in liquid nitrogen and stored in -80°C.

Lysis of E. coli cells

12| Resuspend the cell pellet in 50 mL ice-cold Bug Buffer (50 mM NaH_2PO_4, pH 8.0, 0.3 M NaCl) freshly supplemented with 1 mM PMSF and 2 mM (140 μL/L) β-mercaptoenthanol. ▲CRITICAL The PMSF and β-mercaptoenthanol should be added freshly.

13| Pass the cell suspensions through the chilled pressure chamber of Microfluidizer twice at 40,000 psi.

14| Centrifuge the cell lysate in the ultracentrifuge Optima L-70K (Beckman Coulter) at 35,000 rpm, 4°C for 30 min.

15| Filter the supernatant through a 0.2 μm ZapCap filter (Nalgene).

Purification of Rab7

16| Load the filtrate with a flow rate of 2 mL/min on a 5 mL Hi-Trap Ni-NTA column that has been equilibrated with the Buffer A (50 mM NaH_2PO_4, pH 8.0, 0.3 M NaCl, 2 mM β-mercaptoethanol).

17| Wash the column with Buffer A with a flow rate of 3 mL/min until the absorbance reached the baseline.

18| Wash the column with 2% Buffer B (50 mM NaH_2PO_4, pH 8.0, 0.3 M NaCl, 2 mM β-mercaptoethanol, 0.5 M imidazole) with a flow rate of 3 mL/min until the absorbance reached the baseline.

19| Elute the column with a gradient of 2-100% Buffer B with a flow rate of 3 mL/min for 250 mL. Collect 5 mL/fraction.

20| Run SDS-PAGE and identify the fractions of interest.

21| Wash the column with 2 mM NaN_3.

22| Collect the fractions of interest and dialyze the sample against buffer for TEV-protease (25 mM Tris-HCl, pH 8.0, 100 mM NaCl, 4 mM sodium citrate, 2 mM β-mercaptoethanol).

23| Add TEV protease at 1:20 molar ratio to the protein in the dialysis membrane tubing.

24| After dialysis overnight, spin down the precipitates at 8000 rpm for 10 min.

25| Discard the pellet and collect the supernatant.

26| Add $MgCl_2$ and imidazole to the supernatant to a final concentration of 5 mM and 10 mM, respectively.

27| Load the cleavage mixture with a flow rate of 2 mL/min on a 5 mL Hi-Trap Ni-NTA column to remove the cleaved-off 6XHis-MBP tag and uncleaved 6XHis-MBP-Rab7.

28| Collect the flow-through and reload on the column.

29| Wash the column with 2% Buffer B with a flow rate of 3 mL/min until the absorbance reached the baseline and collect the flow-through.

30| Elute the column with 5% Buffer B and a gradient of 5-100% Buffer B with a flow rate of 3 mL/min for 150 mL. Collect 5 mL/fraction.

31| Concentrate the flow-through to 3-4 mL using a Centricon concentrator.

32| Centrifuge the sample in a benchtop centrifuge Eppendorf 5415C/D at 16,000 rpm, 4°C for 20 min.

33| Load the supernatant with a flow rate of 2 mL/min on the gel-filtration column Superdex-75 26/60 that has been equilibrated with the gel filtration buffer (25 mM HEPES, pH 7.2, 50 mM NaCl, 5 mM DTE, 2 mM $MgCl_2$, 20 μM GDP). Collect 5 mL/fraction. ▲CRITICAL Prepare fresh solution, filter the buffer through a 0.2 μm membrane filter (Whatman) and degas on a vacuum-membrane pump (ILM/VAC GmbH) by stirring for 0.5 h at room temperature (20°C).

34| Run SDS-PAGE and collect those fractions containing pure Rab7.

35| Concentrate the sample to 10 mg/mL, separate them in aliquots and froze them flashily in liquid nitrogen. Store the protein in -80°C.

The other proteins were purified in a similar protocol as Rab7. Mammalian RabGGTase was expressed in *E. coli* BL21(DE3) codon plus RIL cells, with a hexahistidine-GST tagged α-subunit and an untagged β-subunit (Kalinin et al., 2001). REP-1 and α-RabGDI were expressed in SF21 and SF9 insect cells, respectively, infected with recombinant baculovirus (Armstrong et al., 1995a) or from recombinant yeast *S. cerevisiae* (Sidorovitch et al., 2002). Rab7 wild-type and mutant proteins were expressed and purified in a similar manner.

5.3.2 Expression and purification of Rab-thioester proteins

The expression of the Rab-Intein-CBD fusion proteins was performed in a similar way as described in 5.3.1 (steps 1 to step 11).

Lysis of E. coli cells

1| Resuspend the cell pellet in 25 mL ice-cold Breaking Buffer (25 mM NaH_2PO_4, pH 7.5, 0.5 M NaCl, 1 mM $MgCl_2$) freshly supplemented with 1 mM PMSF, 10 μM GDP. ▲CRITICAL The PMSF and GDP should be added freshly. Don't add any reducing substances.

2| Pass the cell suspensions through the chilled pressure chamber of Microfluidizer twice at 40,000 psi.

3| Add new portion of PMSF to 0.5 mM and TritonX-100 to 1% (v/v). ▲CRITICAL The TritonX-100 should be added after breaking the cells.

4| Centrifuge the cell lysate in the ultracentrifuge Optima L-70K (Beckman Coulter) at 35,000 rpm, 4°C for 30 min.

Purification of Rab7 α-thioester

5| Transfer the supernatant to Falcon tubes.

6| Add an appropriate amount of chitin beads that have been washed with Breaking Buffer containing 1 % TritonX-100. ▲CRITICAL 1 mL beads can bind ca. 2-5 mg protein.

7| Incubate for 1 h on a rotating wheel at 4°C.

8| Centrifuge the suspension at 2500 g, 4°C for 5 min to remove the supernatant.

9| Wash the beads 5 times with 3X bed volume of Breaking Buffer containing 1 % TritonX-100

10| Wash the beads 5 times with 3X bed volume of Breaking Buffer.

11| Add sodium 2-mercaptoehanesulfonate (MESNA) powder to the beads suspension to a concentration of 0.5 M and incubate overnight on a rotating wheel at 20°C.

12| Collect the supernatant by centrifugation (2500 g, 4°C for 5 min) and concentrate it to 3-4 mL using a Centricon concentrator.

13| Run gel filtration on the Superdex-75 column using buffer (25mM NaH_2PO_4, pH 7.2, 30 mM NaCl, 1 mM $MgCl_2$, 20 μM GDP). ▲CRITICAL Prepare fresh solution, filter the buffer through a 0.2 μm membrane filter (Whatman) and degas on a vacuum-membrane pump (ILM/VAC GmbH) by stirring for 0.5 h at room temperature (20°C).

14| Run SDS-PAGE and collect those fractions containing pure Rab7 α-thioester.

15| Concentrate the sample to at least 10 mg/mL, separate them in aliquots and froze them flashily in liquid nitrogen. Store the protein in -80°C.

The proteins stored at -80°C for 2 years did not significantly reduce the ligation efficiency. Yields typically ranged from 5 - 10 mg of Rab thioester per liter of bacterial culture.

5.4 Analytical methods

5.4.1 Denaturing SDS-PAGE

Preparation of SDS-Polyacrylamide Gel Electrophoresis (PAGE) gels

1| Prepare the resolving gel by mixing the individual components as indicated in Table 5-9 following the adding sequence. ▲CRITICAL Finally add APS and TEMED to start polymerization.

2| Pour the solution into a Biorad Multi-casting apparatus (9 gels). Add 50% isopropanol on the top of the resolving gel. Incubate at room temperature until the resolving gel was polymerized (ca. 30 min).

3| Remove the isopropanol and add the stacking gel solution (prepared as shown in Table 5-9) atop the resolving gel. Insert combs immediately.

4| Incubate at room temperature until the stacking gel was polymerized (ca. 20 min). ■ **PAUSE POINT** The gels can be stored in 4°C in a wet paper packet.

Table 5-9: Receipts for making SDS-PAGE gels.

Adding sequence	**1**	**2**	**3**	**4**	**5**	**6**
Type of gel (%)	**Acrylamide/ bisacrylamide (29:1, 30 %)**	**Mili-Q H_2O**	**Resolving gel buffer (4X)**	**Stacking gel buffer (4X)**	**10 % APS**	**TEMED**
Resolving gel (60 mL)						
10 %	20 mL	25 mL	15 mL	–	300 µl	30 µl
15 %	30 mL	15 mL	15 mL	–	300 µl	30 µl
Stacking gel (30 mL)						
5 %	5 mL	17.5 mL	–	7.5 mL	240 µl	30 µl

TEMED: *N*,*N*,*N´*,*N´*-tetramethylethylendiamine, APS: ammoniumpersulfate.

Gel electrophoresis

5| Prepare protein samples by adding an equal amount of SDS-PAGE sample buffer (2x) and heat them for 5 min at 95°C.

6| Run gels electrophoresis at 50 A until the bromphenol blue front entered the buffer solution.

7| Visualize fluorescent proteins by exposing the unstained SDS-PAGE gel to UV light or fluorescent image reader.

8| Stain the proteins by heating the gels in the Coomassie staining solution (section 5.1.5) in a microwave. Incubate on a shaker at room temperature for 10 min.

9| Destain the gels by heating the gels in the destaining solution (section 5.1.5) in a microwave. Incubate on a shaker at room temperature.

15 % SDS-PAGE gels were used for the analysis of REP (73 kDa), RabGGTase α (63 kDa) and β subunit (37 kDa) and Rab proteins (24 kDa).

5.4.2 MALDI-TOF-mass spectrometry

Matrix Assisted Laser Desorbtion Ionization - Time Of Flight (MALDI-TOF) spectra were recorded on a Voyager-DE Pro Biospectrometry workstation from Applied Biosystems (Weiterstadt, Germany). Protein samples were desalted using small GF spin columns (DyeEx 2.0 Spin Kit, Qiagen, Hilden, Germany) and mixed with an equal volume of matrice (saturated sinapinic acid solution in 0.3 % TFA/acetonitrile (2:1 v/v)). The mixture was quickly spotted on a MALDI sample plate, air-dried. Spectra were measured with the following instrument settings: acceleration voltage = 25 kV, grid voltage = 93 %, extraction delay time = 750 ns and guide wire = 0.3 %. The laser intensity was manually adjusted during the measurements in order to obtain optimal signal to noise ratios. Calibrations were carried out using a protein mixture of defined molecular mass (Sigma). Spectra recording and data evaluation was performed using the supplied Voyager software package. The accuracy of the method for proteins within the molecular weight range of 20-30 kDa is ca. $\pm$ 20 Da.

5.4.3 LC-ESI-mass spectrometry

Liquid Chromatography-Electrospray Ionization-Mass Spectrometry (LC-ESI-MS) analysis was performed on an Agilent 1100 series chromatography system (Hewlett Packard) equipped with an LCQ ESI mass spectrometer (Finnigan, San Jose, USA) using Jupiter C4 columns (5 µm, 15 x 0.46 cm, 300 Å pore-size) from Phenomenex (Aschaffenburg, Germany) for proteins and 125/21 NUCLEODUR 5 µm C18 columns for peptides. For LC separation a gradient of buffer B (0.1 % formic acid in acetonitrile) in buffer A (0.1 % formic acid in water) with a constant flow-rate of 1 mL/min was applied, with a gradient program as shown in Table 5-10 and 5-11. Under these conditions, Rab proteins typically were eluted at 12-13 min. Mass spectra data evaluation and deconvolution was performed using the Xcalibur

software package. The accuracy of the method for proteins within the molecular weight range of 20 kDa is ca. ± 1-2 Da.

Table 5-10: Gradient program for LC-ESI-MS measurements of protein using a C4 column.

Time (min)	buffer A (0.1% FA, H_2O) %	buffer B (0.1% FA, ACN) %
5	20	80
15	70	30
17	90	10
19	90	10
20	20	80
22	20	80

Table 5-11: Gradient program for LC-ESI-MS measurements of peptide using a C18 column.

Time (min)	buffer A (0.1% FA, H_2O) %	buffer B (0.1% FA, ACN) %
1	90	10
17	60	40
22	20	80
25	20	80
26	90	10
30	90	10

5.4.4 Analytical reversed-phase (RP)- and gel filtration (GF)-HPLC

Analytical reversed-phase (RP) and gel filtration (GF) chromatography were performed on a Waters 600 chromatography instrument equipped with a Waters 2487 absorbance detector and a Waters 2475 fluorescence detector (Waters, Milford, MA, USA). Jupiter C4 column (5 µm, 15 x 0.46 cm, 300 Å pore-size) from Phenomenex (Aschaffenburg, Germany) was used for RP-HPLC, while Biosep-SEC-2000 column (60 x 0.78 cm, separation range 1-300 kDa, Phenomenex), Superdex 75 HR 10/30 column (separation range 3-70 kDa) or Superdex 200 HR 10/30 column (separation range 10-600 kDa) from Pharmacia Biotech (Uppsala, SE) was used for GF-HPLC. GF chromatography were carried out using a running buffer (50 mM HEPES, pH 7.2, 50 mM NaCl, 2 mM $MgCl_2$, 5 mM DTE, 10 µM GDP) at a flow rate of 0.5 mL/min.

For RP-HPLC the gradient of buffer B (0.1 % TFA in acetonitrile) in buffer A (0.1 % TFA in water) at a flow rate of 1 mL/min was applied using a gradient program described in Table 5-12. Under these conditions, unprenylated Rab proteins typically

were eluted at ca. 17 min. Data analysis was carried out using the software package provided by Waters.

Table 5-12: Gradient program for HPLC measurements of protein using a C4 column.

Time (min)	buffer A (0.1% TFA, H_2O) %	buffer B (0.1% TFA, ACN) %
2	95	5
17	30	70
22	30	70
24	0	100
26	0	100
28	95	5
30	95	5

5.4.5 Ion exchange chromatography

Poros HQ (PerSeptive Biosystem) and HiTrap Q Sepharose (Amersham Biosciences) anion-exchange columns were used for ion exchange chromatography. The columns were washed with buffer A (10 mM NaH_2PO_4, pH 7.5, **2 M NaCl**, 1 mM $MgCl_2$) and subsequently equilibrated with buffer B (10 mM NaH_2PO_4, pH 7.5, **10 mM NaCl**, 1 mM $MgCl_2$, 5 mM MESNA). The proteins were loaded onto the column and eluted with a linear gradient from 10 mM (buffer B) to 500 mM NaCl (buffer C: 10 mM NaH_2PO_4, pH 7.5, **500 mM NaCl**, 1 mM $MgCl_2$, 5 mM MESNA).

5.5 Biochemical methods

5.5.1 Conjugation of organic dyes to Rab7 α-thioester

50-100 μM protein in buffer (25 mM NaH_2PO_4, pH 7.2, 30 mM NaCl, 1 mM $MgCl_2$, 20 μM GDP) was added with 2-10 eq. (versus cysteine) thio-reactive organic dyes from a stock solution in DMSO. The final concentration of DMSO as a cosolvent is typical 5% (v/v). The reaction mixture was incubated at room temperature (20°C) for 0.5-1 h under an atmosphere of argon. The reaction was quenched by adding MESNA to a final concentration of 10 mM. After reaction, dyes were removed by a NAP-5 desalting column (Amersham) equilibrated with buffer (25 mM NaH_2PO_4, pH 7.2, 30 mM NaCl, 1 mM $MgCl_2$, 20 μM GDP, 10 mM MESNA). The protein conjugates were further purified by ion exchange chromatography on a 1 mL Poros HQ anion-exchange column. The fractions of interest were collected and carried out buffer exchange using a NAP-5 desalting column equilibrated with ligation buffer (25 mM NaH_2PO_4, pH 7.5, 30 mM NaCl, 1 mM $MgCl_2$, 100 μM GDP, 10 mM MESNA). The flow-through was concentrated to 5-10 mg/mL with VIVASPIN 500 (MWCO: 10kDa) (Vivascience AG, Hannover, Germany).

5.5.2 Ligation of unprenylated peptide to Rab α-thioester

5-10 mg/mL Rab α-thioester in ligation buffer (25 mM NaH_2PO_4, pH 7.5, 30 mM NaCl, 1 mM $MgCl_2$, 100 μM GDP, 10 mM MESNA) was supplemented with 100 mM MESNA (final concentration). The reaction was initiated by adding fluorescently labeled or unlabeled peptide in a final concentration of 2-4 mM (20 eq.) from a stock solution in DMSO. The final concentration of DMSO as a cosolvent is typical 5% (v/v). The reaction mixture was incubated at room temperature (20°C) overnight (10-12h). After reaction, unreacted peptides were removed by a NAP-5 desalting column or dialysis against buffer (25 mM NaH_2PO_4, pH 7.2, 30 mM NaCl, 1 mM $MgCl_2$, 20 μM GDP, 2 mM DTE).

5.5.3 Ligation of prenylated peptide to Rab α-thioester

Ligation of the mono- and di-geranylgeranylated peptide to Rab7Δ6 and Rab7Δ2SS α-thioester to prepare Rab7-C205S-CC(GG) and Rab7-A202C-

E203K(dans)SC(GG)SC(GG) was previously performed by Dr. Thomas Durek in MPI-Dortmund (Durek et al., 2004a; Rak et al., 2003).

To prepare Rab7CSC(NBD-farnesyl) (Rab7-NF), Rab7Δ3-MESNA thioester protein (>10 mg/mL) in ligation buffer was supplemented with 40 mM CTAB and 100 mM MESNA. Ligation was initiated by adding >2mM peptide C(S*t*Bu)SC(NBD-farnesyl) from a ca. 40 mM stock solution in DMSO. The reaction mixture was incubated overnight at 40°C with vigorous agitation. The reaction mixture was centrifuged, and the supernatant was removed. The pellet was washed 4 times with methanol, 4 times with of dichloromethane, 4 times with methanol, and 4 times with Milli-Q water at room temperature in order to remove contaminating peptide and unligated protein. The precipitate was dissolved in denaturation buffer (100 mM Tris-HCl, pH 8.0, 6 M guanidinium-HCl, 100 mM DTE, 1% CHAPS, 1 mM EDTA) to a final protein concentration of 0.5-1.0 mg/mL and incubated overnight at 4°C with slight agitation. The solution was cleared by centrifugation. The solution can be stored at this point at -80°C.

5.5.4 Refolding of the prenylated Rab

Mono-, di-geranylgeranylated or NBD-farnesylated Rab7 in denaturation buffer was renatured by diluting it at least 30-fold dropwise into refolding buffer (50 mM HEPES, pH 7.5, 2.5 mM DTE, 2 mM MgCl2, 100 μM GDP, 1% CHAPS, 400 mM arginine-HCl, 400 mM trehalose, 1 mM PMSF) in the presence or the absence of an equimolar amount of RabGGTase beta subunit (βGGT) with gentle stirring at room temperature. Alternatively 10 molar excess of delipidated BSA was used. The mixture was incubated for 30min at room temperature and 60 min on ice, and concentrated to 2-5 mg/mL using Amicon Ultra-5 concentrator (MWCO: 10 kDa) from Milipore. The concentrated mixture was dialyzed overnight against two 2 L changes of dialysis buffer (25 mM HEPES, pH 7.5, 50 mM $(NH_4)_2SO_4$, 50mM NaCl, 2 mM $MgCl_2$, 2.5 mM DTE, 10 μM GDP, 10% glycerol, 1 mM PMSF). The dialyzed material was centrifuged at 16,000 g for 10 min to remove aggregates and subsequently loaded on a Superdex-200 HR 10/30 gel filtration column (Pharmacia Biotech) equilibrated with gel filtration buffer (50 mM HEPES, pH 7.2, 50mM NaCl, 5 mM DTE, 2 mM MgCl2, 10 μM GDP). The fractions containing the Rab7:βGGT complex or Rab7(NBD-farnesyl) were collected, concentrated to 2mg/mL, flash-frozen in liquid nitrogen in multiple aliquots and stored at -80°C.

5.5.5 *In vitro* prenylation to prepare Rab7-NF:REP-1 complex

Single cysteine mutant Rab7C207S (0.4 mg, 16.7 nmol) was mixed with 1.22 mg REP-1 (16.7 nmol) and 2.6 mg GST-RabGGTase (20 nmol) in prenylation buffer (25 mM HEPES, pH 7.2, 50 mM NaCl, 3 mM $MgCl_2$, 5 mM DTE,10 μM GDP). 167 nmol (10 eq.) of NBD-farnesyl pyrophosphate (NBD-FPP) from a 10 mM stock solution in 25 mM $(NH_4)_2CO_3$ was added to initiate the reaction. The reaction mixture was incubated at 20°C for 1h followed by dilution to 4 mL with prenylation buffer containing 5% CHAPS. The solution was passed three times over a glutathione Sepharose column (Pharmacia, 0.5 mL bed volume) equilibrated with the same buffer. The flow-through was collected and dialyzed against gel filtration buffer (50 mM NaH_2PO_4, pH 7.2, 50 mM NaCl, 1 mM $MgCl_2$, 10 μM GDP, 2 mM β-mercaptoethanol). After dialysis, the sample was concentrated to 300 μL and loaded on a Superdex 200 HR 10/30 GF column (Pharmacia) equilibrated with gel filtration buffer. Fractions containing binary Rab7-NF:REP-1 complex were pooled, concentrated to approximately 20 mg/mL and stored at -80°C in multiple aliquots.

5.5.6 Screening of RabGGTase inhibitors by 96-well plate assay

1| Prepare fresh prenylation buffer (50 mM HEPES, pH7.2, 50 mM NaCl, 2 mM $MgCl_2$, 5 mM DTE, 20 μM GDP, 0.01% TritonX-100), filter the buffer through a 0.2 μm membrane filter (Whatman) and degas on a vacuum-membrane (ILM/VAC GmbH) pump by stirring for 0.5 h at room temperature.

2| Switch on the Fluoroskan Acsent Fl machine (Thermo BioAnalysis, Santa Fe, New Mexico, USA), set the system temperature to 37°C, and let it equilibrate while preparing test samples.

3| Dispense 50 μl 4 μM NBD-FPP (560.4 Da) and 40 nM RabGGTase (100 kDa) cocktail from a groove to each well of a 95-well plate using a 8-channel multipipette. The number of wells should correspond to the number of test samples, positive and negative controls in triplicate. In the case of the positive control no inhibitor is added to the solution.

4| If performing inhibitor screening, add the desired compounds at the selected concentrations to the plate. Typically 0.5 μl of 10 mM compound in DMSO is added to reach a final concentration of 50 μM in each reaction.

5| Mix the plate on an orbital shaker integrated in the Fluoroskan machine.

6| Incubate the plate with cover at 37°C for 5 min.

7| Incubate the 4 μM Rab7 (24 kDa) and 4 μM REP-1 (76 kDa) protein substrate cocktail and prenylation buffer at 37°C for 5 min.

8| Dispense 50 μl of the Rab7:REP-1 protein substrate cocktail from a groove to the wells for the corresponding samples and positive controls using a multipipette. For the negative controls, add 50 μl of prenylation buffer instead.

9| Immediately start measuring the fluorescence intensity of each well over a time period of 10-20 min (with approximately 30-50 individual measurements per well). Use an excitation cut-off filter of 485 nm and an emission cut-off filter of 538 nm.

10| After measurement, reactions were quenched by addition of 1 μl 10% trifluoroacetic acid (TFA) quenching buffer, final concentration of TFA is 0.1% (v/v).

11| Process the time-dependent fluorescence change of each well to obtain the average rate with the Acsent FI software provided by the manufacturer.

Before start a screening of compounds, a series of test experiments where the different combinations of the concentrations of Rab7:REP-1, NBD-FPP and RabGGTase should be performed to find out those conditions providing enough signal to noise ratio. Then the screening follows the step 1 to 11. The IC_{50} was calculated as described in section 4.2.1.

5.5.7 SDS-PAGE end-point assay to investigate selectivity of inhibitors

In the SDS-polyacrylamide gel electrophoresis end-point assay for inhibitors of FTase, GGTase-I and RabGGTase, recombinant protein substrate GST-KiRas , GST-RhoA and Rab7, and fluorescent lipid substrate NBD-GPP and NBD-FPP were used, respectively. In the prenylation buffer (50 mM HEPES, pH 7.2, 50 mM NaCl, 2 mM $MgCl_2$, 2 mM DTE, 0.01% Triton X-100), a 10 μl mixture of FTase with NBD-GPP, GGTase-I with NBD-FPP, RabGGTase with NBD-FPP in the presence and the absence of various concentrations of inhibitor were incubated for 5 minutes at 37°C, the same volume of protein substrate GST-KiRas , GST-RhoA and Rab7 with REP-1 were added to initiate the reaction. For the FTase assay, 3 μM GST-KiRas, 2 μM

NBD-FPP, and 20 nM FTase, for the GGTase-I assay, 6 μM GST-RhoA, 6 μM NBD-FPP, and 1 μM GGTase-I; for the RabGGTase assay 3 μM Rab, 3 μM REP, 2 μM NBD-FPP, and 40 nM RabGGTase, respectively, were used. In the negative controls, the enzymes were omitted. Reactions were run for the same period of time (10 min) and quenched by adding cold 2X SDS sample buffer. The reaction mixtures were resolved by 15% SDS-PAGE and the gel was scanned using a Fluorescent Image Reader FLA-5000 (Fujifilm) (excitation laser at 473 nm and emission cutoff filter at 510 nm). The fluorescent bands corresponding to the formation of the prenylated product were quantified using the AIDA densitometry software. The data were processed in the same way as in the plate assay.

5.6 Biophysical methods

Fluorescence measurements were performed on a Spex Fluoromax-3 spectrofluorometer (Jobin Yvon, Edison, NJ, USA). Measurements were carried out in 1 mL quartz cuvettes (Hellma) with continuous stirring and thermostated at 25° C unless otherwise indicated. Transient kinetics was recorded on a stopped-flow spectrometer SX20 (Applied Photophysics, Leatherhead, UK). Isothermal titration calorimetry (ITC) measurements were carried out on a VP-isothermal titration calorimeter (MicroCal, Northampton, USA). All buffers used in these experiments were filtered through a 0.2 μm membrane filter (Whatman) and degassed on a vacuum-membrane (ILM/VAC GmbH) pump by stirring for 0.5 h at room temperature.

5.6.1 Continuous fluorometric assay for Rab prenylation

To perform the assay using fluorescent Rab7 proteins, 100-200 nM of fluorescently labeled Rab7 was mixed with an equal amount of REP-1 and RabGGTase in a quartz cuvette, containing 1 mL of prenylation buffer (50 mM HEPES, pH 7.2, 50 mM NaCl, 5 mM DTE, 2 mM $MgCl_2$, 10 μM GDP). After a 5 min-incubation at 25°C, the reaction was initiated by adding geranylgeranyl pyrophosphate (GGPP) to a final concentration of ca. 10 μM. Excitation and emission monochromators settings were dependent on the feature of dyes. The fluorescence (count/sec) was related to the amount of prenylated product formation (μM) using the following equation:

$$P(\mu M) = [F(count/\sec)] \cdot \left[\frac{1}{m} \left(\frac{\mu M}{count/\sec} \right) \right] \cdot \left(\frac{e}{e-1} \right)$$

where P is the amount of product, F is the fluorescent intensity, e is the fluorescence enhancement factor, i.e. the ratio of the fluorescence of the prenylated product to the fluorescence of the starting material, m is the conversion factor, i.e. the slope of the line generated in a plot of concentration of prenylated protein substrate versus fluorescence intensity. e and m should be measured at the same conditions.

To perform the assay using NBD-FPP, 1 μM of REP-1 and RabGGTase in a quartz cuvette were mixed with 4 μM NBD-FPP in the same buffer. Rab7 wild-type or mutants were added to a final concentration of 1 μM to start the reaction. Excitation and emission monochromators were set to 479 nm and 520 nm, respectively. The

traces were fitted to a single or double exponential equation using GraFit 5.0 (Erithacus software, Surrey, UK):

$$F = F_0 + A\, e^{-k\, t}$$

$$F = F_0 + A_1 e^{-k_1 t} + A_2 e^{-k_2 t}$$

where F is the observed fluorescence intensity, F_0 is the fluorescence intensity at $t = \infty$, A, A_1 and A_2 are the amplitudes, t is the time, k, k_1 and k_2 are the rate constants.

5.6.2 Fluorescence titrations – determination of K_d

Fluorescence titrations were performed in titration buffer (50 mM HEPES, pH 7.2, 50 mM NaCl and 5 mM DTE). Fluorescently labelled reactant A was added to a quartz cuvette containing 1 mL buffer with continuous stirring. Small aliquots of titrant E were then added to the cuvette, until the fluorescence signal change reached situation. The change in fluorescence was corrected for light scattering as well as dilution and plotted as a function of the reactant concentration. The data was fitted to the following equation using GraFit 5.0 (Erithacus software, Surrey, UK):

$$F = F_{\min} + \left(K_d + A_0 + E_0 - \sqrt{\left(K_d + A_0 + E_0\right)^2 - 4A_0E_0} \right) \frac{F_{\max} - F_{\min}}{2A_0}$$

where F is the observed fluorescence intensity after each step of titrant E addition, E_0 is the total (cumulative) concentration of titrant E, A_0 is the concentration of fluorescent reactant A, F_{min} is the initial fluorescence intensity at $E_0 = 0$, F_{max} is the final fluorescence intensity at $E_0 = \infty$, and K_d is the equilibrium constant, which is to be determined (see Appendix 6.1 for a derivation of this equation).

Competitive titration was performed by titrating of competitor B to a preformed A:E complex. Co-titration was carried out by titrating of reactant E to a mixture of A and competitor B. Data analysis was performed with the program SCIENTIST (MicroMath Scientific Software, Saint Louis, Missouri USA). A description of equations is in Appendix 6.2.

5.6.3 Transient kinetics

Stopped-flow measurements

Fluorescent reactant A in buffer (50 mM HEPES, pH 7.2, 50 mM NaCl, 5 mM DTE) was rapidly mixed in the stopped-flow apparatus with an equal volume of reactant B in the same buffer. Excitation was at 479 nm for NBD, while fluorescene was recorded through a 530 nm cut-off filter. Mixing and measuring chamber were thermostated at 25° C using a water bath. Typically, traces of 3 independent experiments were averaged using the software package provided by Applied Photophysics.

Determination of k_{off}

Fluorescent A complexed with E was displaced from E by addition of excess amount of competitor B. The dissociation was monitored either in Fluoromax-3 for slow dissociation process or stopped-flow machine for fast dissociation process. The measurements were performed at 25°C in buffer (50 mM HEPES, pH 7.2, 50 mM NaCl and 5 mM DTE). The obtained dissociation traces could be fitted to a single exponential equation:

$$F = F_0 + Ae^{-k_{off}t}$$

where F is the observed fluorescence, F_0 is the offset, A is the signal amplitude, t is the time, and k_{off} is the dissociation rate constant. Data analysis was carried out using GraFit 5.0 (Erithacus software).

5.6.4 Isothermal titration calorimetry (ITC)

ITC measurements were carried out in the ITC buffer (50 mM HEPES, pH7.2, 50 mM NaCl, 0.2 mM β-mercaptoethanol) at 25°C.

1| Dialyze both protein reactants against the same ITC buffer. In the case of titration with a compound, the protein was dialyzed against ITC buffer, while the ligand was dissolved in the same buffer.

2| Centrifuge the protein and the ligand solution to remove any unsoluble material. Degas the samples in a ThermoVac degassing apparatus (MicroCal) thermostated at 25°C to remove residual air bubbles.

3| Slowly withdraw 2 ml of 50 μM protein into the filling syringe with a long needle.

4| Remove all air from the filling syringe by tapping the syringe. ▲CRITICAL Do not allow air bubbles to be introduced into the cell.

5| Inject the solution with an abrupt spurt of ca. 0.25 mL into the cell until you see it spill out the top of the cell stem. ▲CRITICAL This bursting of solution will help

remove bubbles that may rest on the edges of the coin shaped area where the junction of the stem is.

6| Drain off the solution overflow. ▲CRITICAL Place the syringe on the ledge at the top of the metal cell stem and remove the excess solution.

7| Fill the reference cell with water as above.

8| Attach the tube of the plastic filling syringe to the filling port of the injection syringe. Click on the **Open Fill Port** button in the ITC Controls window.

9| Slowly withdraw the plunger of the plastic filling syringe to draw up the 0.5 mM ligand from a 500 μL reservoir until you see the solution exit through the top filling port. Then click on the **Close Fill Port** button. ▲CRITICAL Keep submersing the pipette tip in eppendorf tube containing ligand solution.

10| Click on the **Purge->ReFill** button to apply two purge/refill procedures in order to dislodge any air bubbles from inside walls of the injection syringe. ▲CRITICAL The long needle and stir paddle on the pipette injection syringe must not be bent even slightly.

11| Carefully insert the pipette into the sample cell access tube. Watch the end paddle of the long needle to insure it is inserted directly into the access hole, hold the pipette vertical and slowly lower the pipette. When the pipette is completely inserted, push down slightly to compensate for the resistance of the rubber o-ring to seat the pipette.

12| Set the run parameters. Total number of injections: 26, Injection volume: 8 μL, Duration: 16 sec (injection time, this value yields an injection rate of 0.5 μL/sec), Spacing: 240 sec (the interval between injections), Cell temperature: 25°C, Reference Power: 18 μCal/sec (large exothermic reactions require 30 μCal/sec, large endothermic reactions require 2 μCal/sec), Stirring Speed: 310 rpm.

13| Start to run an ITC experiment. ▲CRITICAL Make a small first injection (2 μL) to avoid a smaller heat effect that may be resulted from leakage or bending the syringe needle. Then delete the first data point before doing curve-fitting.

14| Perform control experiments to determine the heat of dilution of the ligand by titrating the ligand into the buffer in the same way as the experiment with protein present. ▲CRITICAL These heats of dilution should be subtracted from the corresponding injection into the protein solution.

15| Perform least-squares fit to a single-site binding model using the program Origin that includes routines designed to analyze ITC data (MicroCal).

6. Appendices

6.1 Equilibrium titration

In a reversible second-order reaction:

$$A + E \underset{k_{off}}{\overset{k_{on}}{\rightleftharpoons}} AE$$

the dissociation constant is defined as:

$$K_d = \frac{A \cdot E}{AE} = \frac{k_{off}}{k_{on}}$$

where A, E and AE are the equilibrium concentrations of labeled ligand A, titrant E and complex AE, respectively. K_d is the dissociation constant.

The mass conservation relations $A = A_0 - AE \qquad E = E_0 - AE$

result in $$K_d = \frac{(A_0 - AE)\cdot(E_0 - AE)}{AE}$$

where A_0 and E_0 are the total concentrations (free and bound) of labeled ligand A and titrant E, respectively.

This can be rearranged to $(AE)^2 - AE(K_d + A_0 + E_0) + A_0E_0 = 0$

The solutions of this quadratic equation are :

$$AE = \frac{1}{2}\left[(K_d + A_0 + E_0) \pm \sqrt{(K_d + A_0 + E_0)^2 - 4A_0E_0}\right]$$

The relation $AE \leq E_0$ gives

$$AE = \frac{1}{2}\left[(K_d + A_0 + E_0) - \sqrt{(K_d + A_0 + E_0)^2 - 4A_0E_0}\right] \qquad \text{(eq. 1)}$$

The fractional completion of the binding reaction (r) can be observed using spectroscopic techniques and corresponds to :

$$r = \frac{AE}{A_0} = \frac{F - F_{\min}}{F_{\max} - F_{\min}}$$

where F is the experimentally observed signal, such as fluorescence intensity, anisotropy or absorbance, F_{min} is the initial signal at $E_0 = 0$, F_{max} is the final signal at $E_0 = \infty$. This equation is only valid if the quantity of F is a linear function of the

fractional completion of the reaction and does not depend on other reactions. This equation can be rearranged to:

$$F = F_{\min} + AE\frac{F_{\max} - F_{\min}}{A_0} \qquad \text{(eq. 2)}$$

Replacing AE in eq. 2 with eq. 1 results in:

$$F = F_{\min} + \left(K_d + A_0 + E_0 - \sqrt{(K_d + A_0 + E_0)^2 - 4A_0E_0} \right)\frac{F_{\max} - F_{\min}}{2A_0}$$

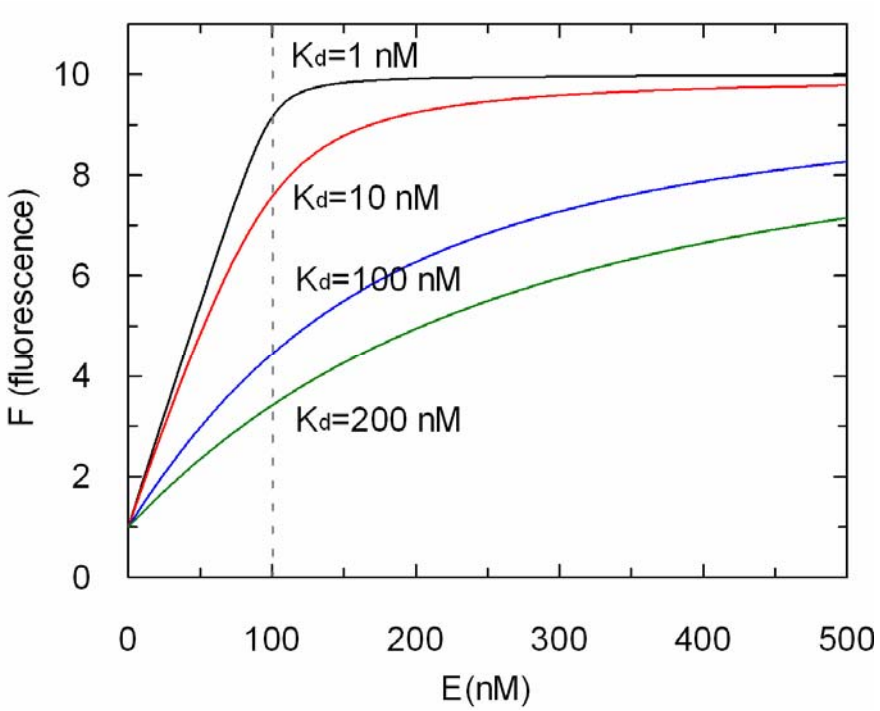

Figure 6-1. Simulation of titration curves. In all cases 100 nM labeled ligand A (A0=100 nM) is titrated with increasing concentrations of binder E. F_{max} and F_{min} are set to 10 and 1, respectively. K_d=1 nM (black), K_d=10nM (red), K_d=100nM (blue), K_d=200 nM (green).

6.2 Competitive titration

A and B competitively bind to E:

$$A + E \underset{k_{-1}}{\overset{k_{+1}}{\rightleftharpoons}} AE \quad K_{dA} \quad \text{Labeled}$$

$$B + E \underset{k_{-2}}{\overset{k_{+2}}{\rightleftharpoons}} BE \quad K_{dB} \quad \text{Unlabeled}$$

the dissociation constant is defined as:

$$K_{dA} = \frac{A \cdot E}{AE} \qquad K_{dB} = \frac{B \cdot E}{BE}$$

where A, B, E, AE and BE are the equilibrium concentrations of labeled ligand A, unlabeled competitor B, binder E, complex AE and complex BE, respectively. K_{dA} is the dissociation constant of AE, K_{dB} is the dissociation constant of BE.

There are mass conservation relations:

$$A = A_0 - AE$$
$$B = B_0 - BE$$
$$E = E_0 - AE - BE$$

where A_0, B_0 and E_0 are the total concentrations (free and bound) of labeled ligand A, competitor B and binder E, respectively.

The signal observed has the relation:

$$F = Y_a \cdot A + Y_{ae} \cdot AE$$

where F is the experimentally observed signal, Y_a and Y_{ae} are the quantum yields or extinction coefficients of ligand A and complex AE, respectively. These two values can be estimated by the initial signal at $E_0 = 0$, $F_{min} = Y_a * A_0$, and the final signal at $E_0 = \infty$, $F_{max} = Y_{ae} * A_0$.

The K_{dA} of the reporter is first determined by titrating binder E to a fixed concentration of ligand A as described in 6.1. Competition titrations can be done in two ways: (a) competitive titration: a complex of E and A at concentrations above its determined K_{dA} is pre-formed followed by titrating with competitor B (Figure 6-3); (b) co-titration: A is premixed with B, and E is titrated into the mixture (Figure 6-2). This value K_{dA} is fixed during the simulation of competitive titration data, allowing calculation of K_{dB} using the equations described above.

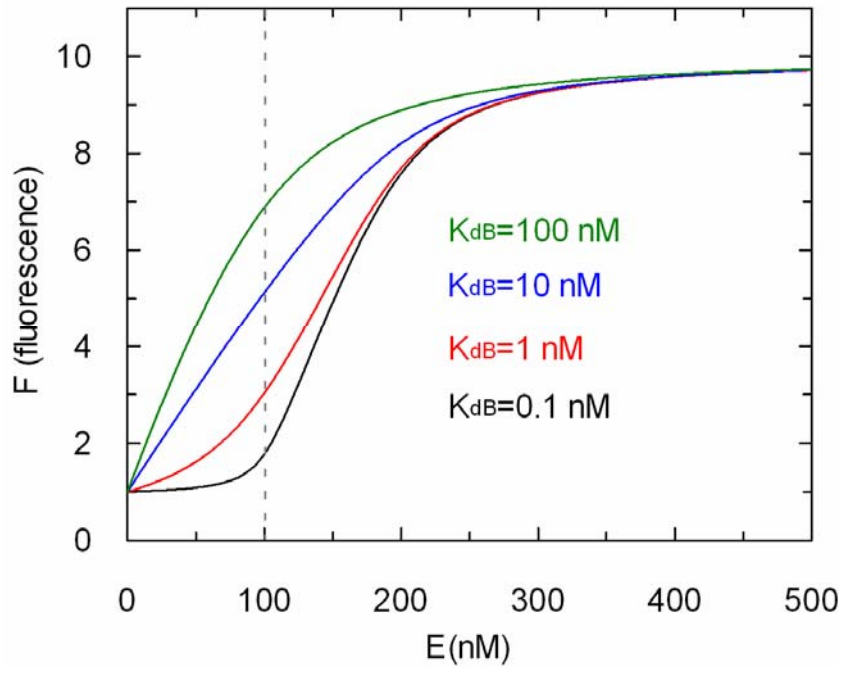

Figure 6-2. Simulation of co-titration curves. In all cases 100 nM labeled ligand A mixed with 100 nM competitor B is titrated with increasing concentrations of binder E. Y_a and Y_{ae} are set to 0.01 and 0.1, respectively. K_{dB}=0.1 nM (black), K_{dB}=1 nM (red), K_{dB}=10 nM (blue), K_{dB}=100 nM (green).

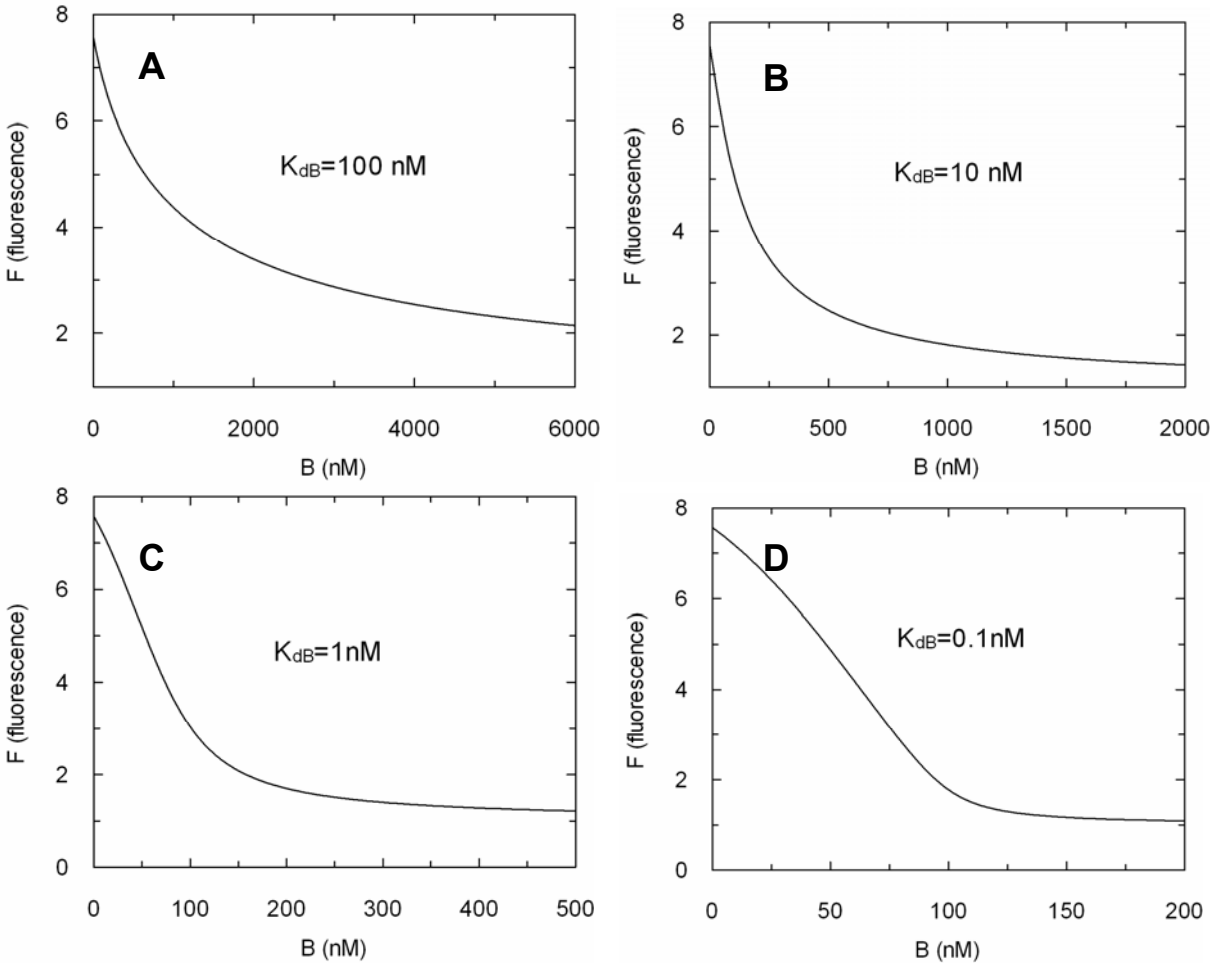

Figure 6-3. Simulation of competitive titration curves. In all cases 100 nM labeled ligand A pre-mixed with 100 nM binder E is titrated with increasing concentrations of competitor B. Y_a and Y_{ae} are set to 0.01 and 0.1, respectively. K_{dB}=100 nM (**A**), K_{dB}=10 nM (**B**), K_{dB}=1 nM (**C**), K_{dB}=0.1 nM (**D**).

6.3 Dissociation kinetics

The two competitive reaction models shown in 6.2 can be transformed as:

$$AE \underset{k_{+1}}{\overset{k_{-1}}{\rightleftharpoons}} A + E + B \underset{k_{-2}}{\overset{k_{+2}}{\rightleftharpoons}} BE$$

where k_{+1} and k_{-1} are association and dissociation rate constant of a labeled ligand A from its complex AE, respectively, and k_{+2} and k_{-2} are association and dissociation rate constant of a unlabeled ligand B (competitor) from its complex BE, respectively.

The decay of AE can be described by

$$\frac{dAE}{dt} = k_{+1} \cdot A \cdot E - k_{-1} \cdot AE \,. \qquad \text{(eq. 3)}$$

In the present case it is assumed that both the labeled and the unlabeled ligand interact with the protein in a similar manner. If a large excess of unlabeled ligand B is applied (B>>A, E), the association rate of the competitor B with the free protein E is significantly faster than the association of the labeled ligand A (i.e. k_2*B >> k_1*A*E), which would drive the reaction towards the formation of BE complex and make the dissociation of AE pseudo-irreversible. Under such conditions the concentration of free (unbound) protein E is very low (E → 0) and thereby k_1*A*E is negligible. This will give

$$\frac{dAE}{dt} = -k_{-1} \cdot AE \qquad \text{(eq. 4)}$$

integration gives a single exponential equation:

$$AE = AE_0 e^{-k_{-1}t}$$

where AE_0 is the concentration of the complex AE when B_0 = 0.

6.4 Consecutive reaction kinetics

A simple model of a first order consecutive reaction is:

$$S \xrightarrow{k_1} I \xrightarrow{k_2} P$$

The substrate (S) decays with a transient increase and then decay of the intermediate (I) and the emergence of the product (P).

$$\frac{dS}{dt} = -k_1 \cdot S \qquad \text{(eq. 5)}$$

$$\frac{dI}{dt} = k_1 \cdot S - k_2 \cdot I \qquad \text{(eq. 6)}$$

$$\frac{dS}{dt} = k_2 \cdot I \qquad \text{(eq. 7)}$$

Integrations give equations:

$$S = S_0 e^{-k_1 t}$$

$$I = \frac{k_1 S_0}{(k_1 - k_2)}\left[e^{-k_2 t} - e^{-k_1 t}\right]$$

$$P = S_0\left[1 - \frac{1}{k_1 - k_2}\left(k_1 e^{-k_2 t} - k_2 e^{-k_1 t}\right)\right]$$

where S_0 is the concentration of substrate at the beginning of the reaction. A simulation of the reaction is shown in Figure 6-4.

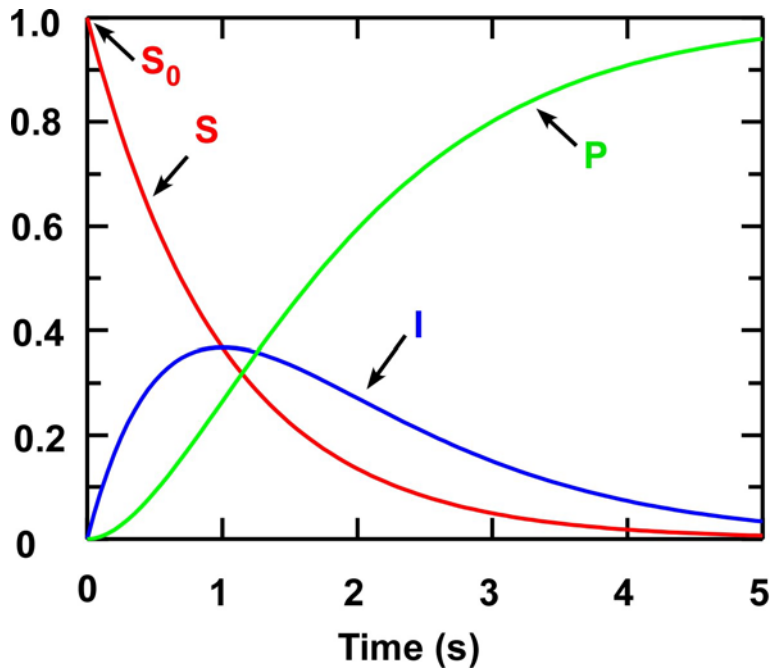

Figure 6-4. Simulation of the process of a first order consecutive reaction. S: concentration of substrate (red), I: concentration of intermediate (blue), P: concentration of product (green).

The prenylation reaction described in Scheme 4-3 (section 4.1.3.2) is shown in a simple way (Scheme 6-1) and give a set of differential equations (eq. 8-17).

Scheme 6-1.

$$A + E \underset{k_{-1}}{\overset{k_1}{\rightleftharpoons}} AE$$

$$AE + N \underset{k_{-2}}{\overset{k_2}{\rightleftharpoons}} AEN$$

$$AEN \xrightarrow{k_3} BE$$

$$BE \underset{k_4}{\overset{k_{-4}}{\rightleftharpoons}} B + E$$

$$BE + N \underset{k_{-5}}{\overset{k_5}{\rightleftharpoons}} BEN$$

$$BEN \xrightarrow{k_6} CE$$

$$CE \underset{k_7}{\overset{k_{-7}}{\rightleftharpoons}} C+E$$

where A is Rab7:REP, E is RabGGTase, N is NBD-FPP, B is Rab7_NF:REP, C is Rab7_NFNF:REP.

$$\frac{dA}{dt} = k_{-1} \cdot AE - k_1 \cdot A \cdot E \quad \text{(eq. 8)}$$

$$\frac{dE}{dt} = k_{-1} \cdot AE - k_1 \cdot A \cdot E + k_{-4} \cdot BE - k_4 \cdot B \cdot E + k_{-7} \cdot CE - k_7 \cdot C \cdot E \quad \text{(eq. 9)}$$

$$\frac{dAE}{dt} = k_1 \cdot A \cdot E - k_{-1} \cdot AE + k_{-2} \cdot AEN - k_2 \cdot AE \cdot N \quad \text{(eq. 10)}$$

$$\frac{dN}{dt} = k_{-2} \cdot AEN - k_2 \cdot AE \cdot N + k_{-5} \cdot BEN - k_5 \cdot BE \cdot N \quad \text{(eq. 11)}$$

$$\frac{dAEN}{dt} = k_2 \cdot AE \cdot N - k_{-2} \cdot AEN - k_3 \cdot AEN \quad \text{(eq. 12)}$$

$$\frac{dBE}{dt} = k_3 \cdot AEN - k_{-4} \cdot BE + k_4 \cdot B \cdot E - k_5 \cdot BE \cdot N + k_{-5} \cdot BEN \quad \text{(eq. 13)}$$

$$\frac{dB}{dt} = k_{-4} \cdot BE - k_4 \cdot B \cdot E \quad \text{(eq. 14)}$$

$$\frac{dBEN}{dt} = k_5 \cdot BE \cdot N - k_{-5} \cdot BEN - k_6 \cdot BEN \quad \text{(eq. 15)}$$

$$\frac{dCE}{dt} = k_6 \cdot BEN - k_{-7} \cdot CE - k_7 \cdot C \cdot E \quad \text{(eq. 16)}$$

$$\frac{dC}{dt} = k_{-7} \cdot CE - k_7 \cdot C \cdot E \quad \text{(eq. 17)}$$

6.5 Isothermal titration calorimetry (ITC)

ITC (Lewis and Murphy, 2005) is a quantitative approach for measuring protein-protein/ligand interactions. It does not rely on the presence of chromophores or fluorophores, nor does it require an enzymatic assay. ITC detects a heat effect upon binding. An ITC experiment can be used to determine the binding the binding constant (K_a), the enthalpy of binding (ΔH), and the stoichiometry (n) or number of binding sites. The entropy change (ΔS) of binding is calculated from ΔH and K_a:

$$\Delta G = -RT \ln K_a = \Delta H - T\Delta S$$

where ΔG is Gibbs free energy, R is gas constant, T is absolute temperature.

At the beginning of an experiment, the cell of calorimeter is filled with macromolecule solution (working volume V_0) and the injection of ligand solution drives an equivalent volume (V_{inj}) of solution out of the cell. The concentration of macromolecule decreases at injection number *i* as:

$$M_{tot,i} = nM_{tot,0}\left(1-\frac{V_{inj}}{V_0}\right)^i \quad \text{(eq. 18)}$$

where $M_{tot,i}$ is the total concentration of protein in the cell after injection step i, $M_{tot,0}$ is the total concentration of protein in the cell before injection, which is known quantity. V_0 is the volume of the cell, V_{inj} is the injection volume, and n is the number of binding sites.

The total concentration of the titrant ligand increases with each injection step as:

$$L_{tot,i} = L_{tot,0}\left(\frac{V_{inj}}{V_0}\right)^i \quad \text{(eq. 19)}$$

where $L_{tot,i}$ is the total concentration of ligand in the cell after injection step I and $L_{tot,0}$ is the total concentration of ligand in the injection syringe.

The total concentration of macromolecule and ligand is equal to the sum of the bound and the free (unbound) forms at injection number i, and is given as:

$$M_{tot,i} = M_i + ML_i = M_i(1+K_aL_i) \quad \text{(eq. 20)}$$

$$L_{tot,i} = L_i + ML_i = L_i(1+K_aM_i) \quad \text{(eq. 21)}$$

where M_i, L_i and ML_i are the concentrations of free macromolecule, free ligand and ML complex at injection number i, K_a is the binding constant.

Eq. 20 can be rearranged to give the concentration of free M as:

$$M_i = \frac{M_{tot,i}}{1+K_aL_i} \quad \text{(eq. 22)}$$

Eq. 22 can be substituted into eq. 21 and rearranged to give the following quadratic expression:

$$K_aL_i^2 + \left[1+K_a\left(M_{tot,i}-L_{tot,i}\right)\right]L_i - L_{tot,i} = 0 \quad \text{(eq. 23)}$$

The meaningful solution of this quadratic equation gives the concentration of free ligand after any injection step:

$$L_i = \frac{-\left[1+K_a\left(M_{tot,i}-L_{tot,i}\right)\right]+\sqrt{\left[1+K_a\left(M_{tot,i}-L_{tot,i}\right)\right]^2+4K_aL_{tot,i}}}{2K_a} \quad \text{(eq. 24)}$$

The heat that is absorbed or produced for each injection in an ITC experiment is the difference in heat content before and after the injection. The heat for injection number i is defined as:

$$Q_i = \left\langle \Delta H \right\rangle_i M_{tot,i}V_0 - \left\langle \Delta H \right\rangle_{i-1} M_{tot,i-1}\left(V_0 - V_{inj}\right) \quad \text{(eq. 25)}$$

where $\langle \Delta H \rangle$ is the cumulative enthalpy change per mole of macromolecule.

In case of one to one binding, the cumulative enthalpy change is given as:

$$\left\langle \Delta H \right\rangle_i = \Delta H \frac{ML_i}{M_{tot,i}} = \Delta H \frac{ML_i}{M + ML_i} = \Delta H \frac{K_a L_i}{1 + K_a L_i} \qquad \text{(eq. 26)}$$

where ΔH is the enthalpy change for binding one mole of ligand to one mole of macromolecule, $M_{tot,i}$ and ML_i are the concentrations of total and bound macromolecule at injection number i.

Replacing $\langle \Delta H \rangle$ in eq. 26 with eq. 25 results in:

$$Q_i = \frac{\Delta H K_a L_i M_{tot,i} V_0}{1 + K_a L_i} - \frac{\Delta H K_a L_{i-1} M_{tot,i-1} \left(V_0 - V_{inj}\right)}{1 + K_a L_{i-1}} \qquad \text{(eq. 27)}$$

where the $M_{tot,i}$ and $L_{tot,i}$ can be calculated from eq. 18 and 19, respectively, while L_i can be substituted using eq. 24. Therefore, eq. 27 is a quadratic equation of K_a. Fitting the ITC data to this equation allows for direct determination of ΔH, K_a and n.

7. References

Adamson,P., Marshall,C.J., Hall,A., and Tilbrook,P.A. (1992). Post-translational modifications of p21rho proteins. J. Biol. Chem. *267*, 20033-20038.

Aivazian,D., Serrano,R.L., and Pfeffer,S. (2006). TIP47 is a key effector for Rab9 localization. J. Cell Biol. *173*, 917-926.

Alexandrov,K., Heinemann,I., Durek,T., Sidorovitch,V., Goody,R.S., and Waldmann,H. (2002). Intein-mediated synthesis of geranylgeranylated Rab7 protein in vitro. J Am Chem Soc 2002. May. 22. ;124. (20.):5648. -9. *124*, 5648-5649.

Alexandrov,K., Horiuchi,H., Steele-Mortimer,O., Seabra,M.C., and Zerial,M. (1994). Rab escort protein-1 is a multifunctional protein that accompanies newly prenylated rab proteins to their target membranes. EMBO J. *13*, 5262-5273.

Alexandrov,K., Scheidig,A.J., and Goody,R.S. (2001). Fluorescence methods for monitoring interactions of Rab proteins with nucleotides, Rab escort protein, and geranylgeranyltransferase. Methods Enzymol. *329*, 14-31.

Alexandrov,K., Simon,I., Iakovenko,A., Holz,B., Goody,R.S., and Scheidig,A.J. (1998). Moderate discrimination of REP-1 between Rab7 x GDP and Rab7 x GTP arises from a difference of an order of magnitude in dissociation rates. FEBS Lett. *425*, 460-464.

Alexandrov,K., Simon,I., Yurchenko,V., Iakovenko,A., Rostkova,E., Scheidig,A.J., and Goody,R.S. (1999). Characterization of the ternary complex between Rab7, REP-1 and Rab geranylgeranyl transferase. Eur. J. Biochem. *265*, 160-170.

Ali,B.R., Wasmeier,C., Lamoreux,L., Strom,M., and Seabra,M.C. (2004). Multiple regions contribute to membrane targeting of Rab GTPases. J. Cell Sci. *117*, 6401-6412.

Allan,B.B., Moyer,B.D., and Balch,W.E. (2000). Rab1 recruitment of p115 into a cis-SNARE complex: Programming budding COPII vesicles for fusion. Science *289*, 444-448.

Alory,C. and Balch,W.E. (2000). Molecular basis for Rab prenylation. J Cell Biol *150*, 89-103.

Alory,C. and Balch,W.E. (2001). Organization of the rab-gdi/chm superfamily: the functional basis for choroideremia disease. Traffic. *2*, 532-543.

Alory,C. and Balch,W.E. (2003). Molecular evolution of the Rab-escort-protein/guanine-nucleotide-dissociation-inhibitor superfamily. Mol. Biol. Cell 2003. Sep. ;14(9.):3857. -67. Epub. 2003. May. 29. *14*, 3857-3867.

Anant,J.S., Desnoyers,L., Machius,M., Demeler,B., Hansen,J.C., Westover,K.D., Deisenhofer,J., and Seabra,M.C. (1998). Mechanism of Rab geranylgeranylation: formation of the catalytic ternary complex. Biochemistry *37*, 12559-12568.

Andres,D.A., Seabra,M.C., Brown,M.S., Armstrong,S.A., Smeland,T.E., Cremers,F.P., and Goldstein,J.L. (1993). cDNA cloning of component A of Rab geranylgeranyl transferase and demonstration of its role as a Rab escort protein. Cell *73*, 1091-1099.

Araki,S., Kikuchi,A., Hata,Y., Isomura,M., and Takai,Y. (1990). Regulation of reversible binding of smg p25A, a ras p21-like GTP- binding protein, to synaptic plasma membranes and vesicles by its specific regulatory protein, GDP dissociation inhibitor. Journal of Biological Chemistry *265*, 13007-13015.

Armstrong,S.A., Brown,M.S., Goldstein,J.L., and Seabra,M.C. (1995a). Preparation of recombinant Rab geranylgeranyltransferase and Rab escort proteins. Methods Enzymol. *257*, 30-41.

Armstrong,S.A., Hannah,V.C., Goldstein,J.L., and Brown,M.S. (1995b). CAAX geranylgeranyl transferase transfers farnesyl as efficiently as geranylgeranyl to RhoB. J. Biol. Chem. *270*, 7864-7868.

Ayers,B., Blaschke,U.K., Camarero,J.A., Cotton,G.J., Holford,M., and Muir,T.W. (1999). Introduction of unnatural amino acids into proteins using expressed protein ligation. Biopolymers *51*, 343-354.

Bang,D., Pentelute,B.L., and Kent,S.B. (2006). Kinetically controlled ligation for the convergent chemical synthesis of proteins. Angew. Chem. Int. Ed Engl. *45*, 3985-3988.

Barawkar,D.A. and Ganesh,K.N. (1995). Fluorescent D(Cgcgaattcgcg) - Characterization of Major Groove Polarity and Study of Minor-Groove Interactions Through A Major Groove Semantophore Conjugate. Nucleic Acids Research *23*, 159-164.

Barbacid,M. (1987). ras genes. [Review]. Annual Review of Biochemistry *56*, 779-827.

Basso,A.D., Kirschmeier,P., and Bishop,W.R. (2006). Lipid posttranslational modifications. Farnesyl transferase inhibitors. J. Lipid Res. *47*, 15-31.

Beard,M., Satoh,A., Shorter,J., and Warren,G. (2005). A cryptic Rab1-binding site in the p115 tethering protein. J. Biol. Chem. *280*, 25840-25848.

Bentley,M., Liang,Y.J., Mullen,K., Xu,D.L., Sztul,E., and Hay,J.C. (2006). SNARE status regulates tether recruitment and function in homotypic COPII vesicle fusion. Journal of Biological Chemistry *281*, 38825-38833.

Beranger,F., Paterson,H., Powers,S., de,G.J., and Hancock,J.F. (1994). The effector domain of Rab6, plus a highly hydrophobic C terminus, is required for Golgi apparatus localization. Mol. Cell Biol. *14*, 744-758.

Bergo,M.O., Leung,G.K., Ambroziak,P., Otto,J.C., Casey,P.J., Gomes,A.Q., Seabra,M.C., and Young,S.G. (2001). Isoprenylcysteine carboxyl methyltransferase deficiency in mice. J. Biol. Chem. *276*, 5841-5845.

Bergo,M.O., Lieu,H.D., Gavino,B.J., Ambroziak,P., Otto,J.C., Casey,P.J., Walker,Q.M., and Young,S.G. (2004). On the physiological importance of endoproteolysis of CAAX proteins: heart-specific RCE1 knockout mice develop a lethal cardiomyopathy. J. Biol. Chem. *279*, 4729-4736.

Bielli,A., Haney,C.J., Gabreski,G., Watkins,S.C., Bannykh,S.I., and Aridor,M. (2005). Regulation of Sar1 NH2 terminus by GTP binding and hydrolysis promotes membrane deformation to control COPII vesicle fission. J. Cell Biol. *171*, 919-924.

Bivona,T.G., Quatela,S.E., Bodemann,B.O., Ahearn,I.M., Soskis,M.J., Mor,A., Miura,J., Wiener,H.H., Wright,L., Saba,S.G., Yim,D., Fein,A., Perez de Castro,I., Li,C., Thompson,C.B., Cox,A.D., and Philips,M.R. (2006). PKC regulates a farnesyl-electrostatic switch on K-Ras that promotes its association with Bcl-XL on mitochondria and induces apoptosis. Molecular Cell *21*, 481-493.

Bos,J.L. (1988). The ras gene family and human carcinogenesis. Mutat. Res. *195*, 255-271.

Bos,J.L., Rehmann,H., and Wittinghofer,A. (2007). GEFs and GAPs: critical elements in the control of small G proteins. Cell *129*, 865-877.

Bourne,H.R., Sanders,D.A., and McCormick,F. (1991). The Gtpase Superfamily - Conserved Structure and Molecular Mechanism. Nature *349*, 117-127.

Boyartchuk,V.L., Ashby,M.N., and Rine,J. (1997). Modulation of Ras and a-factor function by carboxyl-terminal proteolysis. Science *275*, 1796-1800.

Brenner,C., Jan,G., Chevalier,Y., and Wroblewski,H. (1995). Evaluation of the efficacy of zwitterionic dodecyl carboxybetaine surfactants for the extraction and the separation of mycoplasma membrane protein antigens. Anal. Biochem. *224*, 515-523.

Brennwald,P. and Novick,P. (1993). Interactions of three domains distinguishing the Ras-related GTP-binding proteins Ypt1 and Sec4. Nature *362*, 560-563.

Brown,M.S., Faust,J.R., Goldstein,J.L., Kaneko,I., and Endo,A. (1978). Induction of 3-hydroxy-3-methylglutaryl coenzyme A reductase activity in human fibroblasts incubated with compactin (ML-236B), a competitive inhibitor of the reductase. J. Biol. Chem. *253*, 1121-1128.

Brune,M., Hunter,J.L., Corrie,J.E.T., and Webb,M.R. (1994). Direct, Real-Time Measurement of Rapid Inorganic-Phosphate Release Using A Novel Fluorescent-Probe and Its Application to Actomyosin Subfragment-1 Atpase. Biochemistry *33*, 8262-8271.

Buskirk,A.R., Ong,Y.C., Gartner,Z.J., and Liu,D.R. (2004). Directed evolution of ligand dependence: small-molecule-activated protein splicing. Proc. Natl. Acad. Sci. U. S A *101*, 10505-10510.

Cai,H., Yu,S., Menon,S., Cai,Y., Lazarova,D., Fu,C., Reinisch,K., Hay,J.C., and Ferro-Novick,S. (2007). TRAPPI tethers COPII vesicles by binding the coat subunit Sec23. Nature *445*, 941-944.

Calero,M., Chen,C.Z., Zhu,W.Y., Winand,N., Havas,K.A., Gilbert,P.M., Burd,C.G., and Collins,R.N. (2003). Dual prenylation is required for Rab protein localization and function. Molecular Biology of the Cell *14*, 1852-1867.

Cantalupo,G., Alifano,P., Roberti,V., Bruni,C.B., and Bucci,C. (2001). Rab-interacting lysosomal protein (RILP): the Rab7 effector required for transport to lysosomes. EMBO J. *20*, 683-693.

Carroll,K.S., Hanna,J., Simon,I., Krise,J., Barbero,P., and Pfeffer,S.R. (2001). Role of Rab9 GTPase in facilitating receptor recruitment by TIP47. Science *292*, 1373-1376.

Casey,P.J. and Seabra,M.C. (1996). Protein prenyltransferases. [Review]. Journal of Biological Chemistry *271*, 5289-5292.

Casey,P.J., Thissen,J.A., and Moomaw,J.F. (1991). Enzymatic modification of proteins with a geranylgeranyl isoprenoid. Proc. Natl. Acad. Sci. U. S. A *88*, 8631-8635.

Castro,A.F., Rebhun,J.F., Clark,G.J., and Quilliam,L.A. (2003). Rheb binds tuberous sclerosis complex 2 (TSC2) and promotes S6 kinase activation in a rapamycin- and farnesylation-dependent manner. J. Biol. Chem. *278*, 32493-32496.

Cavasotto,C.N. and Abagyan,R.A. (2004). Protein flexibility in ligand docking and virtual screening to protein kinases. J. Mol. Biol. *337*, 209-225.

Cavasotto,C.N., Ortiz,M.A., Abagyan,R.A., and Piedrafita,F.J. (2006). In silico identification of novel EGFR inhibitors with antiproliferative activity against cancer cells. Bioorg. Med. Chem. Lett. *16*, 1969-1974.

Cerione,R.A. (1994). Fluorescence assays for G-protein interactions. Methods Enzymol. *237*, 409-423.

Chavrier,P., Gorvel,J.P., Stelzer,E., Simons,K., Gruenberg,J., and Zerial,M. (1991). Hypervariable C-terminal domain of rab proteins acts as a targeting signal. Nature *353*, 769-772.

Chehade,K.A., Kiegiel,K., Isaacs,R.J., Pickett,J.S., Bowers,K.E., Fierke,C.A., Andres,D.A., and Spielmann,H.P. (2002). Photoaffinity analogues of farnesyl pyrophosphate transferable by protein farnesyl transferase. J. Am. Chem. Soc. *124*, 8206-8219.

Chelsky,D., Ruskin,B., and Koshland,D.E., Jr. (1985). Methyl-esterified proteins in a mammalian cell line. Biochemistry *24*, 6651-6658.

Chen,C.Y. and Balch,W.E. (2006). The Hsp90 chaperone complex regulates GDI-dependent Rab recycling. Mol. Biol. Cell *17*, 3494-3507.

Chen,W.J., Moomaw,J.F., Overton,L., Kost,T.A., and Casey,P.J. (1993). High level expression of mammalian protein farnesyltransferase in a baculovirus system. The purified protein contains zinc. J. Biol. Chem. *268*, 9675-9680.

Chen,Z., Sun,J., Pradines,A., Favre,G., Adnane,J., and Sebti,S.M. (2000). Both farnesylated and geranylgeranylated RhoB inhibit malignant transformation and suppress human tumor growth in nude mice. J. Biol. Chem. *275*, 17974-17978.

Cherfils,J. and Chardin,P. (1999). GEFs: structural basis for their activation of small GTP-binding proteins. Trends in Biochemical Sciences *24*, 306-311.

Chevalier,Y., Storet,Y., Pourchet,S., and Leperchec,P. (1991). Tensioactive Properties of Zwitterionic Carboxybetaine Amphiphiles. Langmuir *7*, 848-853.

Chong,S., Mersha,F.B., Comb,D.G., Scott,M.E., Landry,D., Vence,L.M., Perler,F.B., Benner,J., Kucera,R.B., Hirvonen,C.A., Pelletier,J.J., Paulus,H., and Xu,M.Q. (1997). Single-column purification of free recombinant proteins using a self- cleavable affinity tag derived from a protein splicing element. Gene *192*, 271-281.

Chong,S.R., Williams,K.S., Wotkowicz,C., and Xu,M.Q. (1998). Modulation of protein splicing of the Saccharomyces cerevisiae vacuolar membrane ATPase intein. Journal of Biological Chemistry *273*, 10567-10577.

Clark,E.A., Golub,T.R., Lander,E.S., and Hynes,R.O. (2000). Genomic analysis of metastasis reveals an essential role for RhoC. Nature *406*, 532-535.

Clark,E.D., Schwarz,E., and Rudolph,R. (1999). Inhibition of aggregation side reactions during in vitro protein folding. Amyloid, Prions, and Other Protein Aggregates *309*, 217-236.

Clarke,S. (1992). Protein isoprenylation and methylation at carboxyl-terminal cysteine residues. Annu. Rev. Biochem. *61*, 355-386.

Clarke,S., Vogel,J.P., Deschenes,R.J., and Stock,J. (1988). Posttranslational modification of the Ha-ras oncogene protein: evidence for a third class of protein carboxyl methyltransferases. Proc. Natl. Acad. Sci. U. S. A *85*, 4643-4647.

Clausen,V.A., Edelstein,R.L., and Distefano,M.D. (2001). Stereochemical analysis of the reaction catalyzed by human protein geranylgeranyl transferase. Biochemistry *40*, 3920-3930.

Cohen,B.E., Pralle,A., Yao,X.J., Swaminath,G., Gandhi,C.S., Jan,Y.N., Kobilka,B.K., Isacoff,E.Y., and Jan,L.Y. (2005). A fluorescent probe designed for studying protein conformational change. Proceedings of the National Academy of Sciences of the United States of America *102*, 965-970.

Constantinescu,A.T., Rak,A., Alexandrov,K., Esters,H., Goody,R.S., and Scheidig,A.J. (2002). Rab-subfamily-specific regions of Ypt7p are structurally different from other RabGTPases. Structure (Camb.) *10*, 569-579.

Cotton,G.J., Ayers,B., Xu,R., and Muir,T.W. (1999). Insertion of a synthetic peptide into a recombinant protein framework: A protein biosensor. Journal of the American Chemical Society *121*, 1100-1101.

Cotton,G.J. and Muir,T.W. (2000). Generation of a dual-labeled fluorescence biosensor for Crk-II phosphorylation using solid-phase expressed protein ligation. Chem. Biol. *7*, 253-261.

Cox,A.D., Garcia,A.M., Westwick,J.K., Kowalczyk,J.J., Lewis,M.D., Brenner,D.A., and Der,C.J. (1994). The CAAX peptidomimetic compound B581 specifically blocks farnesylated, but not geranylgeranylated or myristylated, oncogenic ras signaling and transformation. J. Biol. Chem. *269*, 19203-19206.

Coxon,F.P., Helfrich,M.H., Larijani,B., Muzylak,M., Dunford,J.E., Marshall,D., McKinnon,A.D., Nesbitt,S.A., Horton,M.A., Seabra,M.C., Ebetino,F.H., and Rogers,M.J. (2001). Identification of a novel

phosphonocarboxylate inhibitor of Rab geranylgeranyl transferase that specifically prevents Rab prenylation in osteoclasts and macrophages. J. Biol. Chem.

Coxon,F.P., Helfrich,M.H., Van't,H.R., Sebti,S., Ralston,S.H., Hamilton,A., and Rogers,M.J. (2000). Protein geranylgeranylation is required for osteoclast formation, function, and survival: inhibition by bisphosphonates and GGTI-298. J. Bone Miner. Res. *15*, 1467-1476.

Cremers,F.P., Armstrong,S.A., Seabra,M.C., Brown,M.S., and Goldstein,J.L. (1994). REP-2, a Rab escort protein encoded by the choroideremia-like gene. Journal of Biological Chemistry *269*, 2111-2117.

Cser,A., Nagy,K., and Biczok,L. (2002). Fluorescence lifetime of Nile Red as a probe for the hydrogen bonding strength with its microenvironment. Chemical Physics Letters *360*, 473-478.

Dan,H.C., Jiang,K., Coppola,D., Hamilton,A., Nicosia,S.V., Sebti,S.M., and Cheng,J.Q. (2004). Phosphatidylinositol-3-OH kinase/AKT and survivin pathways as critical targets for geranylgeranyltransferase I inhibitor-induced apoptosis. Oncogene *23*, 706-715.

Daugherty,D.L. and Gellman,S.H. (1999). A fluorescence assay for leucine zipper dimerization: Avoiding unintended consequences of fluorophore attachment. Journal of the American Chemical Society *121*, 4325-4333.

Dawson,P.E., Churchill,M.J., Ghadiri,M.R., and Kent,S.B.H. (1997a). Modulation of reactivity in native chemical ligation through the use of thiol additives. Journal of the American Chemical Society *119*, 4325-4329.

Dawson,P.E., Churchill,M.J., Ghadiri,M.R., and Kent,S.B.H. (1997b). Modulation of reactivity in native chemical ligation through the use of thiol additives. Journal of the American Chemical Society *119*, 4325-4329.

Dawson,P.E. and Kent,S.B. (2000). Synthesis of native proteins by chemical ligation. Annu. Rev. Biochem. *69*, 923-960.

Dawson,P.E., Muir,T.W., Clark-Lewis,I., and Kent,S.B. (1994). Synthesis of proteins by native chemical ligation. Science *266*, 776-779.

de Hoop,M.J., Huber,L.A., Stenmark,H., Williamson,E., Zerial,M., Parton,R.G., and Dotti,C.G. (1994). The involvement of the small GTP-binding protein Rab5a in neuronal endocytosis. Neuron *13*, 11-22.

De Lorimier,R.M., Smith,J.J., Dwyer,M.A., Looger,L.L., Sali,K.M., Paavola,C.D., Rizk,S.S., Sadigov,S., Conrad,D.W., Loew,L., and Hellinga,H.W. (2002). Construction of a fluorescent biosensor family. Protein Science *11*, 2655-2675.

Delprato,A. and Lambright,D.G. (2007). Structural basis for Rab GTPase activation by VPS9 domain exchange factors. Nat. Struct. Mol. Biol. *14*, 406-412.

Delprato,A., Merithew,E., and Lambright,D.G. (2004). Structure, exchange determinants, and family-wide rab specificity of the tandem helical bundle and Vps9 domains of Rabex-5. Cell *118*, 607-617.

Desnos,C., Huet,S., and Darchen,F. (2007). 'Should I stay or should I go?': myosin V function in organelle trafficking. Biol. Cell *99*, 411-423.

Detter,J.C., Zhang,Q., Mules,E.H., Novak,E.K., Mishra,V.S., Li,W., McMurtrie,E.B., Tchernev,V.T., Wallace,M.R., Seabra,M.C., Swank,R.T., and Kingsmore,S.F. (2000). Rab geranylgeranyl transferase alpha mutation in the gunmetal mouse reduces Rab prenylation and platelet synthesis. Proc. Natl. Acad. Sci. U. S A *97*, 4144-4149.

Diaz,E. and Pfeffer,S.R. (1998). TIP47: a cargo selection device for mannose 6-phosphate receptor trafficking. Cell *93*, 433-443.

Dirac-Svejstrup AB, Sumizawa T, and Pfeffer SR. Identification of a GDI displacement factor that releases endosomal Rab GTPases from Rab-GDI. EMBO J 16, 465-472. 1997. Ref Type: Abstract

Dirac-Svejstrup,A.B., Soldati,T., Shapiro,A.D., and Pfeffer,S.R. (1994). Rab-GDI presents functional Rab9 to the intracellular transport machinery and contributes selectivity to Rab9 membrane recruitment. Journal of Biological Chemistry *269*, 15427-15430.

Diwu,Z., Lu,Y.X., Zhang,C.L., Klaubert,D.H., and Haugland,R.P. (1997). Fluorescent molecular probes .2. The synthesis, spectral properties and use of fluorescent solvatochromic Dapoxyl(TM) dyes. Photochemistry and Photobiology *66*, 424-431.

Dolence,J.M. and Poulter,C.D. (1995). A mechanism for posttranslational modifications of proteins by yeast protein farnesyltransferase. Proceedings of the National Academy of Sciences of the United States of America *92*, 5008-5011.

Dong,G., Medkova,M., Novick,P., and Reinisch,K.M. (2007). A catalytic coiled coil: structural insights into the activation of the Rab GTPase Sec4p by Sec2p. Mol. Cell *25*, 455-462.

Du,W., Lebowitz,P.F., and Prendergast,G.C. (1999). Cell growth inhibition by farnesyltransferase inhibitors is mediated by gain of geranylgeranylated RhoB. Mol. Cell Biol. *19*, 1831-1840.

Du,W. and Prendergast,G.C. (1999). Geranylgeranylated RhoB mediates suppression of human tumor cell growth by farnesyltransferase inhibitors. Cancer Res. *59*, 5492-5496.

Dubendorff,J.W. and Studier,F.W. (1991). Controlling basal expression in an inducible T7 expression system by blocking the target T7 promoter with lac repressor. J. Mol. Biol. *219*, 45-59.

Dumas,J.J., Zhu,Z., Connolly,J.L., and Lambright,D.G. (1999). Structural basis of activation and GTP hydrolysis in Rab proteins. Structure. Fold. Des *7*, 413-423.

Duncan,J.A. and Gilman,A.G. (1998). A cytoplasmic acyl-protein thioesterase that removes palmitate from G protein alpha subunits and p21(RAS). J. Biol. Chem. *273*, 15830-15837.

Durek,T., Alexandrov,K., Goody,R.S., Hildebrand,A., Heinemann,I., and Waldmann,H. (2004a). Synthesis of fluorescently labeled mono- and diprenylated Rab7 GTPase. J. Am. Chem. Soc. *126*, 16368-16378.

Durek,T., Goody,R.S., and Alexandrov,K. (2004b). In vitro semisynthesis and applications of C-terminally modified rab proteins. Methods Mol. Biol. *283*, 233-244.

Durek,T., Torbeev,V.Y., and Kent,S.B. (2007). Convergent chemical synthesis and high-resolution x-ray structure of human lysozyme. Proc. Natl. Acad. Sci. U. S A *104*, 4846-4851.

Dursina,B., Reents,R., Delon,C., Wu,Y., Kulharia,M., Thutewohl,M., Veligodsky,A., Kalinin,A., Evstifeev,V., Ciobanu,D., Szedlacsek,S.E., Waldmann,H., Goody,R.S., and Alexandrov,K. (2006). Identification and specificity profiling of protein prenyltransferase inhibitors using new fluorescent phosphoisoprenoids. J. Am. Chem. Soc. *128*, 2822-2835.

Dursina,B., Thoma,N.H., Sidorovitch,V., Niculae,A., Iakovenko,A., Rak,A., Albert,S., Ceacareanu,A.C., Kolling,R., Herrmann,C., Goody,R.S., and Alexandrov,K. (2002). Interaction of yeast rab geranylgeranyl transferase with its protein and lipid substrates. Biochemistry *41*, 6805-6816.

Dursina,B.E., Reents,R., Niculae,A., Veligodsky,A., Breitling,R., Pyatkov,K., Waldmann,H., Goody,R.S., and Alexandrov,K. (2005). A genetically encodable microtag for chemo-enzymatic derivatization and purification of recombinant proteins. Protein Expr. Purif. 2005. Jan. ;39. (1):71. -81. *39*, 71-81.

Dwars,T., Paetzold,E., and Oehme,G. (2005). Reactions in micellar systems. Angewandte Chemie-International Edition *44*, 7174-7199.

Eastman,R.T., Buckner,F.S., Yokoyama,K., Gelb,M.H., and Van Voorhis,W.C. (2006). Thematic review series: lipid posttranslational modifications. Fighting parasitic disease by blocking protein farnesylation. J. Lipid Res. *47*, 233-240.

Eathiraj,S., Mishra,A., Prekeris,R., and Lambright,D.G. (2006). Structural basis for Rab11-mediated recruitment of FIP3 to recycling endosomes. J. Mol. Biol. *364*, 121-135.

Echard,A., Jollivet,F., Martinez,O., Lacapere,J.J., Rousselet,A., Janoueix-Lerosey,I., and Goud,B. (1998). Interaction of a Golgi-associated kinesin-like protein with Rab6. Science *279*, 580-585.

Edeling,M.A., Smith,C., and Owen,D. (2006). Life of a clathrin coat: insights from clathrin and AP structures. Nat. Rev. Mol. Cell Biol. *7*, 32-44.

Edelstein,R.L., Weller,V.A., Distefano,M.D., and Tung,J.S. (1998). Stereochemical analysis of the reaction catalyzed by yeast protein farnesyltransferase. Journal of Organic Chemistry *63*, 5298-5299.

El,O.F., Cohen,L.H., van der Marel,G.A., and Overhand,M. (2006). Inhibitors of protein: geranylgeranyl transferases. Curr. Med. Chem. *13*, 2385-2427.

Endo,A. (1992). The discovery and development of HMG-CoA reductase inhibitors. J. Lipid Res. *33*, 1569-1582.

Engel,P.C. (1996). Patterns of Enzyme Inhibition. In Enzymology LABFAX, (San Diego, CA and Oxford, UK: Academic Press and BIOS Scientific Publishers), pp. 115-170.

Etienne-Manneville,S. and Hall,A. (2002). Rho GTPases in cell biology. Nature *420*, 629-635.

Evans,T.C., Benner,J., and Xu,M.Q. (1998). Semisynthesis of cytotoxic proteins using a modified protein splicing element. Protein Science *7*, 2256-2264.

Fairbanks,K.P., Witte,L.D., and Goodman,D.S. (1984). Relationship between mevalonate and mitogenesis in human fibroblasts stimulated with platelet-derived growth factor. J. Biol. Chem. *259*, 1546-1551.

Falsetti,S.C., Wang,D.A., Peng,H., Carrico,D., Cox,A.D., Der,C.J., Hamilton,A.D., and Sebti,S.M. (2007). Geranylgeranyltransferase I inhibitors target RalB to inhibit anchorage-dependent growth and induce apoptosis and RalA to inhibit anchorage-independent growth. Mol. Cell Biol. *27*, 8003-8014.

Farnsworth,C.C., Gelb,M.H., and Glomset,J.A. (1990). Identification of geranylgeranyl-modified proteins in HeLa cells. Science *247*, 320-322.

Farnsworth,C.C., Wolda,S.L., Gelb,M.H., and Glomset,J.A. (1989). Human lamin B contains a farnesylated cysteine residue. J Biol. Chem *264*, 20422-20429.

Fasshauer,D., Sutton,R.B., Brunger,A.T., and Jahn,R. (1998). Conserved structural features of the synaptic fusion complex: SNARE proteins reclassified as Q- and R-SNAREs. Proc. Natl. Acad. Sci. U. S A *95*, 15781-15786.

Fath,S., Mancias,J.D., Bi,X.P., and Goldberg,J. (2007). Structure and organization of coat proteins in the COPII cage. Cell *129*, 1325-1336.

Feng,B.Y., Shelat,A., Doman,T.N., Guy,R.K., and Shoichet,B.K. (2005). High-throughput assays for promiscuous inhibitors. Nature Chemical Biology *1*, 146-148.

Fielding,A.B., Schonteich,E., Matheson,J., Wilson,G., Yu,X., Hickson,G.R., Srivastava,S., Baldwin,S.A., Prekeris,R., and Gould,G.W. (2005). Rab11-FIP3 and FIP4 interact with Arf6 and the exocyst to control membrane traffic in cytokinesis. EMBO J. *24*, 3389-3399.

Finder,J.D., Litz,J.L., Blaskovich,M.A., McGuire,T.F., Qian,Y., Hamilton,A.D., Davies,P., and Sebti,S.M. (1997). Inhibition of protein geranylgeranylation causes a superinduction of nitric-oxide synthase-2 by interleukin-1beta in vascular smooth muscle cells. J. Biol. Chem. *272*, 13484-13488.

Fotin,A., Cheng,Y.F., Grigorieff,N., Walz,T., Harrison,S.C., and Kirchhausen,T. (2004a). Structure of an auxilin-bound clathrin coat and its implications for the mechanism of uncoating. Nature *432*, 649-653.

Fotin,A., Cheng,Y.F., Sliz,P., Grigorieff,N., Harrison,S.C., Kirchhausen,T., and Walz,T. (2004b). Molecular model for a complete clathrin lattice from electron cryomicroscopy. Nature *432*, 573-579.

Fukuda,M. and Kuroda,T.S. (2002). Slac2-c (synaptotagmin-like protein homologue lacking C2 domains-c), a novel linker protein that interacts with Rab27, myosin Va/VIIa, and actin. J. Biol. Chem. *277*, 43096-43103.

Fukuda,M., Kuroda,T.S., and Mikoshiba,K. (2002). Slac2-a/melanophilin, the missing link between Rab27 and myosin Va: implications of a tripartite protein complex for melanosome transport. J. Biol. Chem. *277*, 12432-12436.

Fukui,K., Sasaki,T., Imazumi,K., Matsuura,Y., Nakanishi,H., and Takai,Y. (1997). Isolation and characterization of a GTPase activating protein specific for the Rab3 subfamily of small G proteins. J. Biol. Chem. *272*, 4655-4658.

Furfine,E.S., Leban,J.J., Landavazo,A., Moomaw,J.F., and Casey,P.J. (1995). Protein farnesyltransferase: kinetics of farnesyl pyrophosphate binding and product release. Biochemistry *34*, 6857-6862.

Gangopadhyay,J.P., Jiang,S.Q., and Paulus,H. (2003). An in vitro screening system for protein splicing inhibitors based on green fluorescent protein as an indicator. Anal. Chem. *75*, 2456-2462.

Gelb,M.H. (1997). Protein prenylation, et cetera: signal transduction in two dimensions [comment]. Science *275*, 1750-1751.

Gelb,M.H. (2007). Drug discovery for malaria: a very challenging and timely endeavor. Curr. Opin. Chem. Biol. *11*, 440-445.

Gelb,M.H., Brunsveld,L., Hrycyna,C.A., Michaelis,S., Tamanoi,F., Van Voorhis,W.C., and Waldmann,H. (2006). Therapeutic intervention based on protein prenylation and associated modifications. Nat. Chem. Biol. *2*, 518-528.

Gelb,M.H., Reiss,Y., Ghomashchi,F., and Farnsworth,C.C. (1995). Exploring the Specificity of Prenyl Protein-Specific Methyltransferase with Synthetic Prenylated Rab Peptides. Bioorganic & Medicinal Chemistry Letters *5*, 881-886.

Georgiou,G. and Valax,P. (1996). Expression of correctly folded proteins in Escherichia coli. Current Opinion in Biotechnology *7*, 190-197.

Gether,U., Lin,S., and Kobilka,B.K. (1995). Fluorescent labeling of purified beta 2 adrenergic receptor. Evidence for ligand-specific conformational changes. J. Biol. Chem. *270*, 28268-28275.

Ghomashchi,F., Zhang,X., Liu,L., and Gelb,M.H. (1995). Binding of prenylated and polybasic peptides to membranes: affinities and intervesicle exchange. Biochemistry *34*, 11910-11918.

Gibbs,J.B. (1991). Ras C-terminal processing enzymes--new drug targets? Cell *65*, 1-4.

Gibbs,R.A., Zahn,T.J., and Sebolt-Leopold,J.S. (2001). Non-peptidic prenyltransferase inhibitors: diverse structural classes and surprising anti-cancer mechanisms. Curr. Med. Chem. *8*, 1437-1465.

Gilardi,G., Mei,G., Rosato,N., Agro,A.F., and Cass,A.E. (1997). Spectroscopic properties of an engineered maltose binding protein. Protein Eng *10*, 479-486.

Gilardi,G., Zhou,L.Q., Hibbert,L., and Cass,A.E.G. (1994). Engineering the Maltose-Binding Protein for Reagentless Fluorescence Sensing. Analytical Chemistry *66*, 3840-3847.

Giriat,I. and Muir,T.W. (2003). Protein semi-synthesis in living cells. J. Am. Chem. Soc. *125*, 7180-7181.

Gitler,C., Zarmi,B., and Kalef,E. (1995). Use of Cationic Detergents to Enhance Reactivity of Protein Sulfhydryls. Biothiols, Pt A *251*, 366-375.

Giuliano,K.A. and Taylor,D.L. (1998). Fluorescent-protein biosensors: new tools for drug discovery. Trends in Biotechnology *16*, 135-140.

Glomset,J.A. and Farnsworth,C.C. (1994). Role of protein modification reactions in programming interactions between ras-related GTPases and cell membranes. Annu. Rev. Cell Biol. *10*, 181-205.

Glomset,J.A., Gelb,M.H., and Farnsworth,C.C. (1990). Prenyl proteins in eukaryotic cells: a new type of membrane anchor. Trends Biochem. Sci. *15*, 139-142.

Goldstein,J.L. and Brown,M.S. (1990). Regulation of the mevalonate pathway. Nature *343*, 425-430.

Gomes,A.Q., Ali,B.R., Ramalho,J.S., Godfrey,R.F., Barral,D.C., Hume,A.N., and Seabra,M.C. (2003). Membrane targeting of rab GTPases is influenced by the prenylation motif. Mol. Biol. Cell *14*, 1882-1899.

Goodwin,J.S., Drake,K.R., Rogers,C., Wright,L., Lippincott-Schwartz,J., Philips,M.R., and Kenworthy,A.K. (2005). Depalmitoylated Ras traffics to and from the Golgi complex via a nonvesicular pathway. J. Cell Biol. *170*, 261-272.

Goody,R.S., Rak,A., and Alexandrov,K. (2005). The structural and mechanistic basis for recycling of Rab proteins between membrane compartments. Cell Mol. Life Sci. *62*, 1657-1670.

Grabowski,Z.R., Rotkiewicz,K., and Rettig,W. (2003). Structural changes accompanying intramolecular electron transfer: Focus on twisted intramolecular charge-transfer states and structures. Chemical Reviews *103*, 3899-4031.

Graham,S.M., Oldham,S.M., Martin,C.B., Drugan,J.K., Zohn,I.E., Campbell,S., and Der,C.J. (1999). TC21 and Ras share indistinguishable transforming and differentiating activities. Oncogene *18*, 2107-2116.

Graham,S.M., Vojtek,A.B., Huff,S.Y., Cox,A.D., Clark,G.J., Cooper,J.A., and Der,C.J. (1996). TC21 causes transformation by Raf-independent signaling pathways. Mol. Cell Biol. *16*, 6132-6140.

Grosshans,B.L., Ortiz,D., and Novick,P. (2006). Rabs and their effectors: achieving specificity in membrane traffic. Proc. Natl. Acad. Sci. U. S A *103*, 11821-11827.

Gurkan,C., Stagg,S.M., LaPointe,P., and Balch,W.E. (2006). The COPII cage: unifying principles of vesicle coat assembly. Nat. Rev. Mol. Cell Biol. *7*, 727-738.

Hackeng,T.M., Griffin,J.H., and Dawson,P.E. (1999). Protein synthesis by native chemical ligation: Expanded scope by using straightforward methodology. Proceedings of the National Academy of Sciences of the United States of America *96*, 10068-10073.

Hahn,K., Debiasio,R., and Taylor,D.L. (1992). Patterns of Elevated Free Calcium and Calmodulin Activation in Living Cells. Nature *359*, 736-738.

Hahn,K.M., Waggoner,A.S., and Taylor,D.L. (1990). A Calcium-Sensitive Fluorescent Analog of Calmodulin Based on A Novel Calmodulin-Binding Fluorophore. Journal of Biological Chemistry *265*, 20335-20345.

Hales,C.M., Vaerman,J.P., and Goldenring,J.R. (2002). Rab11 family interacting protein 2 associates with Myosin Vb and regulates plasma membrane recycling. J. Biol. Chem. *277*, 50415-50421.

Hamachi,I., Nagase,T., and Shinkai,S. (2000). A general semisynthetic method for fluorescent saccharide-biosensors based on a lectin. Journal of the American Chemical Society *122*, 12065-12066.

Hammarstrom,P., Owenius,R., Martensson,L.G., Carlsson,U., and Lindgren,M. (2001). High-resolution probing of local conformational changes in proteins by the use of multiple labeling: unfolding and self-assembly of human carbonic anhydrase II monitored by spin, fluorescent, and chemical reactivity probes. Biophys. J. *80*, 2867-2885.

Han,W.G., Liu,T.Q., Himo,F., Toutchkine,A., Bashford,D., Hahn,K.M., and Noodleman,L. (2003). A theoretical study of the UV/visible absorption and emission solvatochromic properties of solvent-sensitive dyes. Chemphyschem *4*, 1084-1094.

Hancock,J.F., Cadwallader,K., Paterson,H., and Marshall,C.J. (1991). A CAAX or a CAAL motif and a second signal are sufficient for plasma membrane targeting of ras proteins. EMBO J. *10*, 4033-4039.

Hancock,J.F., Magee,A.I., Childs,J.E., and Marshall,C.J. (1989). All ras proteins are polyisoprenylated but only some are palmitoylated. Cell *57*, 1167-1177.

Hanson,P.I., Roth,R., Morisaki,H., Jahn,R., and Heuser,J.E. (1997). Structure and conformational changes in NSF and its membrane receptor complexes visualized by quick-freeze/deep-etch electron microscopy. Cell *90*, 523-535.

Hartman,H.L., Hicks,K.A., and Fierke,C.A. (2005). Peptide specificity of protein prenyltransferases is determined mainly by reactivity rather than binding affinity. Biochemistry *44*, 15314-15324.

Hashimoto,M., Ikegami,T., Seino,S., Ohuchi,N., Fukada,H., Sugiyama,J., Shirakawa,M., and Watanabe,T. (2000). Expression and characterization of the chitin-binding domain of chitinase A1 from Bacillus circulans WL-12. Journal of Bacteriology *182*, 3045-3054.

Haugland,R.P. (2002). Thio-reactive probes. In Handbook of Fluorescent Probes and Research Products, 9th Edition, (Eugene, USA: Molecular Probes), pp. 79-98.

Head,J.E. and Johnston,S.R. (2003). Protein farnesyltransferase inhibitors. Expert. Opin. Emerg. Drugs *8*, 163-178.

Heo,W.D., Inoue,T., Park,W.S., Kim,M.L., Park,B.O., Wandless,T.J., and Meyer,T. (2006). PI(3,4,5)P3 and PI(4,5)P2 lipids target proteins with polybasic clusters to the plasma membrane. Science *314*, 1458-1461.

Hicks,K.A., Hartman,H.L., and Fierke,C.A. (2005). Upstream polybasic region in peptides enhances dual specificity for prenylation by both farnesyltransferase and geranylgeranyltransferase type I. Biochemistry *44*, 15325-15333.

Hightower,K.E., Casey,P.J., and Fierke,C.A. (2001). Farnesylation of nonpeptidic thiol compounds by protein farnesyltransferase. Biochemistry *40*, 1002-1010.

Hightower,K.E. and Fierke,C.A. (1999). Zinc-catalyzed sulfur alkyation:insights from protein farnesyltransferase. Curr. Opin. Chem Biol *3*, 176-181.

Hightower,K.E., Huang,C.C., Casey,P.J., and Fierke,C.A. (1998). H-Ras peptide and protein substrates bind protein farnesyltransferase as an ionized thiolate. Biochemistry *37*, 15555-15562.

Hinshaw,J.E. (2000). Dynamin and its role in membrane fission. Annual Review of Cell and Developmental Biology *16*, 483-+.

Hirel,P.H., Schmitter,J.M., Dessen,P., Fayat,G., and Blanquet,S. (1989). Extent of N-Terminal Methionine Excision from Escherichia-Coli Proteins Is Governed by the Side-Chain Length of the Penultimate Amino-Acid. Proceedings of the National Academy of Sciences of the United States of America *86*, 8247-8251.

Hoffman,G.R., Nassar,N., and Cerione,R.A. (2000). Structure of the Rho family GTP-binding protein Cdc42 in complex with the multifunctional regulator RhoGDI. Cell *100*, 345-356.

Hong,W. (2005). SNAREs and traffic. Biochim. Biophys. Acta *1744*, 120-144.

Huang,C., Hightower,K.E., and Fierke,C.A. (2000). Mechanistic studies of rat protein farnesyltransferase indicate an associative transition state. Biochemistry *39*, 2593-2602.

Huang,C.C., Casey,P.J., and Fierke,C.A. (1997). Evidence for a catalytic role of zinc in protein farnesyltransferase. Spectroscopy of Co2+-farnesyltransferase indicates metal coordination of the substrate thiolate. J. Biol. Chem. *272*, 20-23.

Huber,S.K. and Scheidig,A.J. (2005). High resolution crystal structures of human Rab4a in its active and inactive conformations. FEBS Lett. *579*, 2821-2829.

Hudson,E.N. and Weber,G. (1973). Synthesis and Characterization of 2 Fluorescent Sulfhydryl Reagents. Biochemistry *12*, 4154-4161.

Iakovenko,A., Rostkova,E., Merzlyak,E., Hillebrand,A.M., Thoma,N.H., Goody,R.S., and Alexandrov,K. (2000). Semi-synthetic Rab proteins as tools for studying intermolecular interactions. FEBS Lett. *468*, 155-158.

Ikegami,T., Okada,T., Hashimoto,M., Seino,S., Watanabe,T., and Shirakawa,M. (2000). Solution structure of the chitin-binding domain of Bacillus circulans WL-12 chitinase A1. J. Biol. Chem. *275*, 13654-13661.

Isaksson,M., Kalinin,S., Lobov,S., Ny,T., and Johansson,L.B.A. (2003). An environmental-sensitive BODIPY (R)-derivative with bioapplication: Spectral and photophysical properties. Journal of Fluorescence *13*, 379-384.

Itzen,A., Pylypenko,O., Goody,R.S., Alexandrov,K., and Rak,A. (2006). Nucleotide exchange via local protein unfolding--structure of Rab8 in complex with MSS4. EMBO J. *25*, 1445-1455.

Jahn,R. and Scheller,R.H. (2006). SNAREs--engines for membrane fusion. Nat. Rev. Mol. Cell Biol. *7*, 631-643.

Jalaie,M. and Shanmugasundaram,V. (2006). Virtual screening: are we there yet? Mini. Rev. Med. Chem. *6*, 1159-1167.

James,G., Goldstein,J.L., and Brown,M.S. (1996). Resistance of K-RasBV12 proteins to farnesyltransferase inhibitors in Rat1 cells. Proc. Natl. Acad. Sci. U. S A *93*, 4454-4458.

James,G.L., Goldstein,J.L., and Brown,M.S. (1995). Polylysine and CVIM sequences of K-RasB dictate specificity of prenylation and confer resistance to benzodiazepine peptidomimetic in vitro. J. Biol. Chem. *270*, 6221-6226.

James,G.L., Goldstein,J.L., Brown,M.S., Rawson,T.E., Somers,T.C., McDowell,R.S., Crowley,C.W., Lucas,B.K., Levinson,A.D., and Marsters,J.C., Jr. (1993). Benzodiazepine peptidomimetics: potent inhibitors of Ras farnesylation in animal cells. Science *260*, 1937-1942.

Jedd,G., Mulholland,J., and Segev,N. (1997). Two new Ypt GTPases are required for exit from the yeast trans-Golgi compartment. J. Cell Biol. *137*, 563-580.

Jiang,K., Coppola,D., Crespo,N.C., Nicosia,S.V., Hamilton,A.D., Sebti,S.M., and Cheng,J.Q. (2000). The phosphoinositide 3-OH kinase/AKT2 pathway as a critical target for farnesyltransferase inhibitor-induced apoptosis. Mol. Cell Biol. *20*, 139-148.

Johansson,M., Rocha,N., Zwart,W., Jordens,I., Janssen,L., Kuijl,C., Olkkonen,V.M., and Neefjes,J. (2007). Activation of endosomal dynein motors by stepwise assembly of Rab7-RILP-p150Glued, ORP1L, and the receptor betalll spectrin. J. Cell Biol. *176*, 459-471.

Johnson,E.C.B. and Kent,S.B.H. (2006). Insights into the mechanism and catalysis of the native chemical ligation reaction. Journal of the American Chemical Society *128*, 6640-6646.

Jones,S., Newman,C., Liu,F., and Segev,N. (2000). The TRAPP complex is a nucleotide exchanger for Ypt1 and Ypt31/32. Mol. Biol. Cell *11*, 4403-4411.

Jordens,I., Fernandez-Borja,M., Marsman,M., Dusseljee,S., Janssen,L., Calafat,J., Janssen,H., Wubbolts,R., and Neefjes,J. (2001). The Rab7 effector protein RILP controls lysosomal transport by inducing the recruitment of dynein-dynactin motors. Curr. Biol. *11*, 1680-1685.

Jordens,I., Marsman,M., Kuijl,C., and Neefjes,J. (2005). Rab proteins, connecting transport and vesicle fusion. Traffic *6*, 1070-1077.

Kalinin,A., Thoma,N.H., Iakovenko,A., Heinemann,I., Rostkova,E., Constantinescu,A.T., and Alexandrov,K. (2001). Expression of Mammalian Geranylgeranyltransferase Type-II in Escherichia coli and Its Application for in Vitro Prenylation of Rab Proteins. Protein Expr. Purif. *22*, 84-91.

Kamasani,U., Duhadaway,J.B., Alberts,A.S., and Prendergast,G.C. (2007). mDia Function is Critical for the Cell Suicide Program Triggered by Farnesyl Transferase Inhibition. Cancer Biol. Ther. *6*.

Kamasani,U., Huang,M., Duhadaway,J.B., Prochownik,E.V., Donover,P.S., and Prendergast,G.C. (2004). Cyclin B1 is a critical target of RhoB in the cell suicide program triggered by farnesyl transferase inhibition. Cancer Res. *64*, 8389-8396.

Kane,P.M., Yamashiro,C.T., Wolczyk,D.F., Neff,N., Goebl,M., and Stevens,T.H. (1990). Protein splicing converts the yeast TFP1 gene product to the 69-kD subunit of the vacuolar H(+)-adenosine triphosphatase. Science *250*, 651-657.

Kanno,A., Ozawa,T., and Umezawa,Y. (2006a). Genetically encoded optical probe for detecting release of proteins from mitochondria toward cytosol in living cells and mammals. Anal. Chem. *78*, 8076-8081.

Kanno,A., Ozawa,T., and Umezawa,Y. (2006b). Intein-mediated reporter gene assay for detecting protein-protein interactions in living mammalian cells. Anal. Chem. *78*, 556-560.

Kim,S.B., Ozawa,T., and Umezawa,Y. (2005). Genetically encoded stress indicator for noninvasively imaging endogenous corticosterone in living mice. Anal. Chem. *77*, 6588-6593.

Kim,S.B., Ozawa,T., Watanabe,S., and Umezawa,Y. (2004). High-throughput sensing and noninvasive imaging of protein nuclear transport by using reconstitution of split Renilla luciferase. Proc. Natl. Acad. Sci. U. S A *101*, 11542-11547.

Klabunde,T., Sharma,S., Telenti,A., Jacobs,W.R., Jr., and Sacchettini,J.C. (1998). Crystal structure of GyrA intein from Mycobacterium xenopi reveals structural basis of protein splicing. Nat. Struct. Biol. *5*, 31-36.

Kohl,N.E., Mosser,S.D., deSolms,S.J., Giuliani,E.A., Pompliano, DL, Graham,S.L., Smith,R.L., Scolnick,E.M., Oliff,A., and Gibbs,J.B. (1993). Selective inhibition of ras-dependent transformation by a farnesyltransferase inhibitor [see comments]. Science *260*, 1934-1937.

Kohl,N.E., Omer,C.A., Conner,M.W., Anthony,N.J., Davide,J.P., deSolms,S.J., Giuliani,E.A., Gomez,R.P., Graham,S.L., Hamilton,K., and . (1995). Inhibition of farnesyltransferase induces regression of mammary and salivary carcinomas in ras transgenic mice. Nat. Med. *1*, 792-797.

Konstantinopoulos,P.A., Karamouzis,M.V., and Papavassiliou,A.G. (2007). Post-translational modifications and regulation of the RAS superfamily of GTPases as anticancer targets. Nat. Rev. Drug Discov. *6*, 541-555.

Korlach,J., Baird,D.W., Heikal,A.A., Gee,K.R., Hoffman,G.R., and Webb,W.W. (2004). Spontaneous nucleotide exchange in low molecular weight GTPases by fluorescently labeled gamma-phosphate-

linked GTP analogs (vol 101, pg 2800, 2004). Proceedings of the National Academy of Sciences of the United States of America *101*, 5180.

Kusama,T., Mukai,M., Tatsuta,M., Nakamura,H., and Inoue,M. (2006). Inhibition of transendothelial migration and invasion of human breast cancer cells by preventing geranylgeranylation of Rho. Int. J. Oncol. *29*, 217-223.

Kwon,Y., Coleman,M.A., and Camarero,J.A. (2006). Selective immobilization of proteins onto solid supports through split-intein-mediated protein trans-splicing. Angew. Chem. Int. Ed Engl. *45*, 1726-1729.

Lackner,M.R., Kindt,R.M., Carroll,P.M., Brown,K., Cancilla,M.R., Chen,C., de Silva,H., Franke,Y., Guan,B., Heuer,T., Hung,T., Keegan,K., Lee,J.M., Manne,V., O'Brien,C., Parry,D., Perez-Villar,J.J., Reddy,R.K., Xiao,H., Zhan,H., Cockett,M., Plowman,G., Fitzgerald,K., Costa,M., and Ross-Macdonald,P. (2005). Chemical genetics identifies Rab geranylgeranyl transferase as an apoptotic target of farnesyl transferase inhibitors. Cancer Cell 2005. Apr;7. (4):325. -36. *7*, 325-336.

Lakowicz,J.R. (1999). Solvent Effects on Emission Spectra. In Principles of Fluorescence Spectroscopy, 2nd Ed., (New York: Kluwer Academic Publishiers/Plenum Publishing Group), pp. 185-210.

Lane,K.T. and Beese,L.S. (2006). Structural biology of protein farnesyltransferase and geranylgeranyltransferase type I. Journal of Lipid Research *47*, 681-699.

Larijani,B., Hume,A.N., Tarafder,A.K., and Seabra,M.C. (2003). Multiple factors contribute to inefficient prenylation of Rab27a in Rab prenylation diseases. J. Biol. Chem. *278*, 46798-46804.

Law,B.K., Norgaard,P., and Moses,H.L. (2000). Farnesyltransferase inhibitor induces rapid growth arrest and blocks p70s6k activation by multiple stimuli. J. Biol. Chem. *275*, 10796-10801.

Lebowitz,P.F., Casey,P.J., Prendergast,G.C., and Thissen,J.A. (1997). Farnesyltransferase inhibitors alter the prenylation and growth-stimulating function of RhoB. J. Biol. Chem. *272*, 15591-15594.

Lebowitz,P.F., Davide,J.P., and Prendergast,G.C. (1995). Evidence that farnesyltransferase inhibitors suppress Ras transformation by interfering with Rho activity. Mol. Cell Biol. *15*, 6613-6622.

Lee,M.C., Orci,L., Hamamoto,S., Futai,E., Ravazzola,M., and Schekman,R. (2005). Sar1p N-terminal helix initiates membrane curvature and completes the fission of a COPII vesicle. Cell *122*, 605-617.

Lenevich,S., Xu,J., Hosokawa,A., Cramer,C.J., and Distefano,M.D. (2007). Transition state analysis of model and enzymatic prenylation reactions. J. Am. Chem. Soc. *129*, 5796-5797.

Leung,K.F., Baron,R., Ali,B.R., Magee,A.I., and Seabra,M.C. (2007). Rab GTPases containing a CAAX motif are processed post-geranylgeranylation by proteolysis and methylation. J. Biol. Chem. *282*, 1487-1497.

Lewis,E.A. and Murphy,K.P. (2005). Isothermal titration calorimetry. Methods Mol. Biol. *305*, 1-16.

Li,G. and Stahl,P.D. (1993a). Post-translational processing and membrane association of the two early endosome-associated rab GTP-binding proteins (rab4 and rab5). Arch. Biochem. Biophys. *304*, 471-478.

Li,G. and Stahl,P.D. (1993b). Post-translational processing and membrane association of the two early endosome-associated rab GTP-binding proteins (rab4 and rab5). Arch. Biochem. Biophys. *304*, 471-478.

Liang,P.H., Ko,T.P., and Wang,A.H. (2002). Structure, mechanism and function of prenyltransferases. Eur. J Biochem. *269*, 3339-3354.

Liang,Y., Morozova,N., Tokarev,A.A., Mulholland,J.W., and Segev,N. (2007). The role of Trs65 in the Ypt/Rab guanine nucleotide exchange factor function of the TRAPP II complex. Mol. Biol. Cell *18*, 2533-2541.

Lim,K.H., Baines,A.T., Fiordalisi,J.J., Shipitsin,M., Feig,L.A., Cox,A.D., Der,C.J., and Counter,C.M. (2005). Activation of RalA is critical for Ras-induced tumorigenesis of human cells. Cancer Cell *7*, 533-545.

Lin,R.C. and Scheller,R.H. (1997). Structural organization of the synaptic exocytosis core complex. Neuron *19*, 1087-1094.

Lipinski,C.A., Lombardo,F., Dominy,B.W., and Feeney,P.J. (2001). Experimental and computational approaches to estimate solubility and permeability in drug discovery and development settings. Advanced Drug Delivery Reviews *46*, 3-26.

Lippincott-Schwartz,J. and Liu,W. (2006). Insights into COPI coat assembly and function in living cells. Trends Cell Biol. *16*, e1-e4.

Liu,A., Du,W., Liu,J.P., Jessell,T.M., and Prendergast,G.C. (2000). RhoB alteration is necessary for apoptotic and antineoplastic responses to farnesyltransferase inhibitors. Mol. Cell Biol. *20*, 6105-6113.

Liu,A. and Prendergast,G.C. (2000). Geranylgeranylated RhoB is sufficient to mediate tissue-specific suppression of Akt kinase activity by farnesyltransferase inhibitors. FEBS Lett. *481*, 205-208.

Liu,A.X., Rane,N., Liu,J.P., and Prendergast,G.C. (2001). RhoB is dispensable for mouse development, but it modifies susceptibility to tumor formation as well as cell adhesion and growth factor signaling in transformed cells. Mol. Cell Biol. *21*, 6906-6912.

Liu,T.Q., Han,W.G., Himo,F., Ullmann,G.M., Bashford,D., Toutchkine,A., Hahn,K.M., and Noodleman,L. (2004). Density functional vertical self-consistent reaction field theory for solvatochromism - Studies of solvent-sensitive dyes. Journal of Physical Chemistry A *108*, 3545-3555.

Lobell,R.B., Omer,C.A., Abrams,M.T., Bhimnathwala,H.G., Brucker,M.J., Buser,C.A., Davide,J.P., deSolms,S.J., Dinsmore,C.J., Ellis-Hutchings,M.S., Kral,A.M., Liu,D., Lumma,W.C., Machotka,S.V., Rands,E., Williams,T.M., Graham,S.L., Hartman,G.D., Oliff,A.I., Heimbrook,D.C., and Kohl,N.E. (2001). Evaluation of farnesyl:protein transferase and geranylgeranyl:protein transferase inhibitor combinations in preclinical models. Cancer Res. *61*, 8758-8768.

Long,S.B., Casey,P.J., and Beese,L.S. (1998). Cocrystal structure of protein farnesyltransferase complexed with a farnesyl diphosphate substrate. Biochemistry *37*, 9612-9618.

Long,S.B., Casey,P.J., and Beese,L.S. (2002). Reaction path of protein farnesyltransferase at atomic resolution. Nature *419*, 645-650.

Luan,P., Balch,W.E., Emr,S.D., and Burd,C.G. (1999). Molecular dissection of guanine nucleotide dissociation inhibitor function in vivo. Rab-independent binding to membranes and role of Rab recycling factors. J. Biol. Chem. *274*, 14806-14817.

Lupashin,V. and Sztul,E. (2005). Golgi tethering factors. Biochim. Biophys. Acta *1744*, 325-339.

Lutz,H.P. and Luisi,P.L. (1983). Correction for Inner Filter Effects in Fluorescence Spectroscopy. Helvetica Chimica Acta *66*, 1929-1935.

Machner,M.P. and Isberg,R.R. (2007). A bifunctional bacterial protein links GDI displacement to Rab1 activation. Science *318*, 974-977.

Maltese,W.A. and Sheridan,K.M. (1987). Isoprenylated proteins in cultured cells: subcellular distribution and changes related to altered morphology and growth arrest induced by mevalonate deprivation. J. Cell Physiol *133*, 471-481.

Mangues,R., Corral,T., Kohl,N.E., Symmans,W.F., Lu,S., Malumbres,M., Gibbs,J.B., Oliff,A., and Pellicer,A. (1998). Antitumor effect of a farnesyl protein transferase inhibitor in mammary and lymphoid tumors overexpressing N-ras in transgenic mice. Cancer Res. *58*, 1253-1259.

Marrari,Y., Crouthamel,M., Irannejad,R., and Wedegaertner,P.B. (2007). Assembly and trafficking of heterotrimeric G proteins. Biochemistry *46*, 7665-7677.

Marvin,J.S. and Hellinga,H.W. (1998). Engineering biosensors by introducing fluorescent allosteric signal transducers: Construction of a novel glucose sensor. Journal of the American Chemical Society *120*, 7-11.

Maurer-Stroh,S., Washietl,S., and Eisenhaber,F. (2003). Protein prenyltransferases. Genome Biol. 2003. ;4(4):212. Epub. 2003. Apr 1. *4*, 212.

Mayer,A., Wickner,W., and Haas,A. (1996). Sec18p (NSF)-driven release of Sec17p (alpha-SNAP) can precede docking and fusion of yeast vacuoles. Cell *85*, 83-94.

Mazieres,J., Tillement,V., Allal,C., Clanet,C., Bobin,L., Chen,Z., Sebti,S.M., Favre,G., and Pradines,A. (2005). Geranylgeranylated, but not farnesylated, RhoB suppresses Ras transformation of NIH-3T3 cells. Exp. Cell Res. *304*, 354-364.

McBride,H.M., Rybin,V., Murphy,C., Giner,A., Teasdale,R., and Zerial,M. (1999). Oligomeric complexes link Rab5 effectors with NSF and drive membrane fusion via interactions between EEA1 and syntaxin 13. Cell *98*, 377-386.

McGovern,S.L., Caselli,E., Grigorieff,N., and Shoichet,B.K. (2002). A common mechanism underlying promiscuous inhibitors from virtual and high-throughput screening. Journal of Medicinal Chemistry *45*, 1712-1722.

McGovern,S.L., Helfand,B.T., Feng,B., and Shoichet,B.K. (2003). A specific mechanism of nonspecific inhibition. Journal of Medicinal Chemistry *46*, 4265-4272.

McLauchlan,H., Newell,J., Morrice,N., Osborne,A., West,M., and Smythe,E. (1998). A novel role for Rab5-GDI in ligand sequestration into clathrin-coated pits. Curr. Biol. *8*, 34-45.

McNew,J.A., Weber,T., Engelman,D.M., Sollner,T.H., and Rothman,J.E. (1999). The length of the flexible SNAREpin juxtamembrane region is a critical determinant of SNARE-dependent fusion. Mol. Cell *4*, 415-421.

McNew,J.A., Weber,T., Parlati,F., Johnston,R.J., Melia,T.J., Sollner,T.H., and Rothman,J.E. (2000). Close is not enough: SNARE-dependent membrane fusion requires an active mechanism that transduces force to membrane anchors. J. Cell Biol. *150*, 105-117.

McNiven,M.A. and Thompson,H.M. (2006). Vesicle formation at the plasma membrane and trans-Golgi network: the same but different. Science *313*, 1591-1594.

Memon,A.R. (2004). The role of ADP-ribosylation factor and SARI in vesicular trafficking in plants. Biochimica et Biophysica Acta-Biomembranes *1664*, 9-30.

Menasche,G., Ho,C.H., Sanal,O., Feldmann,J., Tezcan,I., Ersoy,F., Houdusse,A., Fischer,A., and de Saint,B.G. (2003). Griscelli syndrome restricted to hypopigmentation results from a melanophilin defect (GS3) or a MYO5A F-exon deletion (GS1). J. Clin. Invest *112*, 450-456.

Menasche,G., Pastural,E., Feldmann,J., Certain,S., Ersoy,F., Dupuis,S., Wulffraat,N., Bianchi,D., Fischer,A., Le,D.F., and de Saint,B.G. (2000). Mutations in RAB27A cause Griscelli syndrome associated with haemophagocytic syndrome. Nat. Genet. *25*, 173-176.

Merithew,E., Hatherly,S., Dumas,J.J., Lawe,D.C., Heller-Harrison,R., and Lambright,D.G. (2001). Structural plasticity of an invariant hydrophobic triad in the switch regions of Rab GTPases is a determinant of effector recognition. J Biol. Chem. *276*, 13982-13988.

Meutermans,W.D.F., Golding,S.W., Bourne,G.T., Miranda,L.P., Dooley,M.J., Alewood,P.F., and Smythe,M.L. (1999). Synthesis of difficult cyclic peptides by inclusion of a novel photolabile auxiliary in a ring contraction strategy. Journal of the American Chemical Society *121*, 9790-9796.

Michaelson,D., Silletti,J., Murphy,G., D'Eustachio,P., Rush,M., and Philips,M.R. (2001). Differential localization of Rho GTPases in live cells: regulation by hypervariable regions and RhoGDI binding. J. Cell Biol. *152*, 111-126.

Milburn,M.V., Tong,L., Devos,A.M., Brunger,A., Yamaizumi,Z., Nishimura,S., and Kim,S.H. (1990). Molecular Switch for Signal Transduction - Structural Differences Between Active and Inactive Forms of Protooncogenic Ras Proteins. Science *247*, 939-945.

Mills,K.V., Lew,B.M., Jiang,S., and Paulus,H. (1998). Protein splicing in trans by purified N- and C-terminal fragments of the Mycobacterium tuberculosis RecA intein. Proc. Natl. Acad. Sci. U. S A *95*, 3543-3548.

Mitchell,D.A., Vasudevan,A., Linder,M.E., and Deschenes,R.J. (2006). Protein palmitoylation by a family of DHHC protein S-acyltransferases. J. Lipid Res. *47*, 1118-1127.

Montal,M. and Gitler,C. (1973). Surface Potential and Energy-Coupling in Bioenergy-Conserving Membrane Systems. Journal of Bioenergetics *4*, 363-382.

Moomaw,J.F. and Casey,P.J. (1992). Mammalian protein geranylgeranyltransferase. Subunit composition and metal requirements. J. Biol. Chem. *267*, 17438-17443.

Moore,I., Schell,J., and Palme,K. (1995). Subclass-specific sequence motifs identified in Rab GTPases. Trends Biochem. Sci. *20*, 10-12.

Mootz,H.D., Blum,E.S., and Muir,T.W. (2004). Activation of an autoregulated protein kinase by conditional protein splicing. Angew. Chem. Int. Ed Engl. *43*, 5189-5192.

Mootz,H.D., Blum,E.S., Tyszkiewicz,A.B., and Muir,T.W. (2003). Conditional protein splicing: a new tool to control protein structure and function in vitro and in vivo. J. Am. Chem. Soc. *125*, 10561-10569.

Mootz,H.D. and Muir,T.W. (2002). Protein splicing triggered by a small molecule. J. Am. Chem. Soc. *124*, 9044-9045.

Morgan,M.A., Sebil,T., Aydilek,E., Peest,D., Ganser,A., and Reuter,C.W. (2005). Combining prenylation inhibitors causes synergistic cytotoxicity, apoptosis and disruption of RAS-to-MAP kinase signalling in multiple myeloma cells. Br. J. Haematol. *130*, 912-925.

Morgan,M.A., Wegner,J., Aydilek,E., Ganser,A., and Reuter,C.W. (2003). Synergistic cytotoxic effects in myeloid leukemia cells upon cotreatment with farnesyltransferase and geranylgeranyl transferase-I inhibitors. Leukemia *17*, 1508-1520.

Morii,T., Sugimoto,K., Makino,K., Otsuka,M., Imoto,K., and Mori,Y. (2002). A new fluorescent biosensor for inositol trisphosphate. Journal of the American Chemical Society *124*, 1138-1139.

Moyer,B.D., Allan,B.B., and Balch,W.E. (2001). Rab1 interaction with a GM130 effector complex regulates COPII vesicle cis-Golgi tethering. Traffic *2*, 268-276.

Mu,Y.Q., Omer,C.A., and Gibbs,R.A. (1996). On the stereochemical course of human protein-farnesyl transferase. Journal of the American Chemical Society *118*, 1817-1823.

Muir,T.W. (2003). Semisynthesis of proteins by expressed protein ligation. Annu. Rev. Biochem. *72*, 249-289.

Muir,T.W., Sondhi,D., and Cole,P.A. (1998). Expressed protein ligation: a general method for protein engineering. Proc. Natl. Acad. Sci. U. S A *95*, 6705-6710.

Musha,T., Kawata,M., and Takai,Y. (1992). The geranylgeranyl moiety but not the methyl moiety of the smg-25A/rab3A protein is essential for the interactions with membrane and its inhibitory GDP/GTP exchange protein. J. Biol. Chem. *267*, 9821-9825.

Nagashima,K., Torii,S., Yi,Z., Igarashi,M., Okamoto,K., Takeuchi,T., and Izumi,T. (2002). Melanophilin directly links Rab27a and myosin Va through its distinct coiled-coil regions. FEBS Lett. *517*, 233-238.

Nalbant,P., Hodgson,L., Kraynov,V., Toutchkine,A., and Hahn,K.M. (2004). Activation of endogenous Cdc42 visualized in living cells. Science *305*, 1615-1619.

Nguyen,U.T.T., Cramer,J., Gomis,J., Reents,R., Gutierrez-Rodriguez,M., Goody,R.S., Alexandrov,K., and Waldmann,H. (2007). Exploiting the substrate tolerance of farnesyltransferase for site-selective protein derivatization. Chembiochem *8*, 408-423.

Nichols,B.J., Ungermann,C., Pelham,H.R., Wickner,W.T., and Haas,A. (1997). Homotypic vacuolar fusion mediated by t- and v-SNAREs [see comments]. Nature *387*, 199-202.

Nomanbhoy,T. and Cerione,R.A. (1999). Fluorescence assays of Cdc42 interactions with target/effector proteins. Biochemistry *38*, 15878-15884.

Offer,J., Boddy,C.N.C., and Dawson,P.E. (2002). Extending synthetic access to proteins with a removable acyl transfer auxiliary. Journal of the American Chemical Society *124*, 4642-4646.

Omer,C.A., Chen,Z., Diehl,R.E., Conner,M.W., Chen,H.Y., Trumbauer,M.E., Gopal-Truter,S., Seeburger,G., Bhimnathwala,H., Abrams,M.T., Davide,J.P., Ellis,M.S., Gibbs,J.B., Greenberg,I., Koblan,K.S., Kral,A.M., Liu,D., Lobell,R.B., Miller,P.J., Mosser,S.D., O'Neill,T.J., Rands,E., Schaber,M.D., Senderak,E.T., Oliff,A., and Kohl,N.E. (2000). Mouse mammary tumor virus-Ki-rasB transgenic mice develop mammary carcinomas that can be growth-inhibited by a farnesyl:protein transferase inhibitor. Cancer Res. *60*, 2680-2688.

Onganer,Y., Yin,M., Bessire,D.R., and Quitevis,E.L. (1993). Dynamic Solvation Effects on the Cis-Trans Isomerization Reaction - Photoisomerization of Merocyanine-540 in Polar-Solvents. Journal of Physical Chemistry *97*, 2344-2354.

Ortiz,D., Medkova,M., Walch-Solimena,C., and Novick,P. (2002). Ypt32 recruits the Sec4p guanine nucleotide exchange factor, Sec2p, to secretory vesicles; evidence for a Rab cascade in yeast. J. Cell Biol. *157*, 1005-1015.

Ossig,R., Laufer,W., Schmitt,H.D., and Gallwitz,D. (1995). Functionality and Specific Membrane Localization of Transport Gtpases Carrying C-Terminal Membrane Anchors of Synaptobrevin-Like Proteins. EMBO J. *14*, 3645-3653.

Ossig,R., Schmitt,H.D., de,G.B., Riedel,D., Keranen,S., Ronne,H., Grubmuller,H., and Jahn,R. (2000). Exocytosis requires asymmetry in the central layer of the SNARE complex. EMBO J. *19*, 6000-6010.

Ostermeier,C. and Brunger,A.T. (1999). Structural basis of Rab effector specificity: crystal structure of the small G protein Rab3A complexed with the effector domain of rabphilin- 3A. Cell *96*, 363-374.

Otomo,T., Ito,N., Kyogoku,Y., and Yamazaki,T. (1999). NMR observation of selected segments in a larger protein: central-segment isotope labeling through intein-mediated ligation. Biochemistry *38*, 16040-16044.

Overmeyer,J.H., Wilson,A.L., and Maltese,W.A. (2001). Membrane targeting of a Rab GTPase that fails to associate with Rab escort protein (REP) or guanine nucleotide dissociation inhibitor (GDI). Journal of Biological Chemistry *276*, 20379-20386.

Ozawa,T., Kaihara,A., Sato,M., Tachihara,K., and Umezawa,Y. (2001). Split luciferase as an optical probe for detecting protein-protein interactions in mammalian cells based on protein splicing. Anal. Chem. *73*, 2516-2521.

Ozawa,T., Nogami,S., Sato,M., Ohya,Y., and Umezawa,Y. (2000). A fluorescent indicator for detecting protein-protein interactions in vivo based on protein splicing. Anal. Chem. *72*, 5151-5157.

Pagano,A., Crottet,P., Prescianotto-Baschong,C., and Spiess,M. (2004). In vitro formation of recycling vesicles from endosomes requires adaptor protein-1/clathrin and is regulated by rab4 and the connector rabaptin-5. Mol. Biol. Cell *15*, 4990-5000.

Pais,J.E., Bowers,K.E., and Fierke,C.A. (2006). Measurement of the alpha-secondary kinetic isotope effect for the reaction catalyzed by mammalian protein farnesyltransferase. Journal of the American Chemical Society *128*, 15086-15087.

Pais,J.E. and Fierke,C.A. (2007). Measurement of kinetic isotope effects to probe the reaction mechanism catalyzed by mammalian protein farnesyltransferase. Faseb Journal *21*, A275.

Pan,X., Eathiraj,S., Munson,M., and Lambright,D.G. (2006). TBC-domain GAPs for Rab GTPases accelerate GTP hydrolysis by a dual-finger mechanism. Nature *442*, 303-306.

Pasqualato,S., Senic-Matuglia,F., Renault,L., Goud,B., Salamero,J., and Cherfils,J. (2004). The structural GDP/GTP cycle of Rab11 reveals a novel interface involved in the dynamics of recycling endosomes. J. Biol. Chem. *279*, 11480-11488.

Paulmurugan,R., Umezawa,Y., and Gambhir,S.S. (2002). Noninvasive imaging of protein-protein interactions in living subjects by using reporter protein complementation and reconstitution strategies. Proc. Natl. Acad. Sci. U. S A *99*, 15608-15613.

Peranen,J., Auvinen,P., Virta,H., Wepf,R., and Simons,K. (1996). Rab8 promotes polarized membrane transport through reorganization of actin and microtubules in fibroblasts. J. Cell Biol. *135*, 153-167.

Pereira-Leal,J.B. and Seabra,M.C. (2000). The mammalian Rab family of small GTPases: definition of family and subfamily sequence motifs suggests a mechanism for functional specificity in the Ras superfamily. J Mol. Biol *301*, 1077-1087.

Pereira-Leal,J.B. and Seabra,M.C. (2001). Evolution of the Rab family of small GTP-binding proteins. J Mol. Biol. *313*, 889-901.

Peterson,Y.K., Kelly,P., Weinbaum,C.A., and Casey,P.J. (2006). A novel protein geranylgeranyltransferase-I inhibitor with high potency, selectivity, and cellular activity. J. Biol. Chem. *281*, 12445-12450.

Pfeffer,S. and Aivazian,D. (2004). Targeting Rab GTPases to distinct membrane compartments. Nat. Rev. Mol. Cell Biol. 2004. Nov. ;5(11):886. -96. *5*, 886-896.

Pfeffer,S.R. (2005). Structural clues to Rab GTPase functional diversity. J. Biol. Chem. 2005. Apr 22. ;280. (16.):15485. -8. Epub. 2005. Mar. 3. *280*, 15485-15488.

Pfeffer,S.R. (2007). Unsolved mysteries in membrane traffic. Annu. Rev. Biochem. *76*, 629-645.

Pham,W., Pantazopoulos,P., and Moore,A. (2006). Imaging farnesyl protein transferase using a topologically activated probe. Journal of the American Chemical Society *128*, 11736-11737.

Pickett,W.C., Zhang,F.L., Silverstrim,C., Schow,S.R., Wick,M.M., and Kerwar,S.S. (1995). A fluorescence assay for geranylgeranyl transferase type I. Anal. Biochem. *225*, 60-63.

Pompliano,D.L., Gomez,R.P., and Anthony,N.J. (1992a). Intramolecular fluorescence enhancement - a continuous assay of ras farnesyl - protein transferase. Journal of the American Chemical Society *114*, 7945-7946.

Pompliano,D.L., Rands,E., Schaber,M.D., Mosser,S.D., Anthony, NJ, and Gibbs,J.B. (1992b). Steady-state kinetic mechanism of Ras farnesyl:protein transferase. Biochemistry *31*, 3800-3807.

Pompliano,D.L., Schaber,M.D., Mosser,S.D., Omer,C.A., Shafer,J.A., and Gibbs,J.B. (1993). Isoprenoid diphosphate utilization by recombinant human farnesyl: protein transferase: interactive binding between substrates and a preferred kinetic pathway. Biochemistry *32*, 8341-8347.

Post,P.L., Trybus,K.M., and Taylor,D.L. (1994). A Genetically-Engineered, Protein-Based Optical Biosensor of Myosin-Ii Regulatory Light-Chain Phosphorylation. Journal of Biological Chemistry *269*, 12880-12887.

Praefcke,G.J.K. and McMahon,H.T. (2004). The dynamin superfamily: Universal membrane tubulation and fission molecules? Nature Reviews Molecular Cell Biology *5*, 133-147.

Prendergast,F.G., Meyer,M., Carlson,G.L., Iida,S., and Potter,J.D. (1983). Synthesis, Spectral Properties, and Use of 6-Acryloyl-2-Dimethylaminonaphthalene (Acrylodan) - A Thiol-Selective, Polarity-Sensitive Fluorescent-Probe. Journal of Biological Chemistry *258*, 7541-7544.

Prendergast,G.C. (2001). Actin' up: RhoB in cancer and apoptosis. Nat. Rev. Cancer *1*, 162-168.

Prendergast,G.C., Davide,J.P., deSolms,S.J., Giuliani,E.A., Graham,S.L., Gibbs,J.B., Oliff,A., and Kohl,N.E. (1994). Farnesyltransferase inhibition causes morphological reversion of ras-transformed cells by a complex mechanism that involves regulation of the actin cytoskeleton. Mol. Cell Biol. *14*, 4193-4202.

Presley,J.F., Ward,T.H., Pfeifer,A.C., Siggia,E.D., Phair,R.D., and Lippincott-Schwartz,J. (2002). Dissection of COPI and Arf1 dynamics in vivo and role in Golgi membrane transport. Nature *417*, 187-193.

Pruyne,D., Legesse-Miller,A., Gao,L., Dong,Y., and Bretscher,A. (2004). Mechanisms of polarized growth and organelle segregation in yeast. Annu. Rev. Cell Dev. Biol. *20*, 559-591.

Pylypenko,O., Rak,A., Durek,T., Kushnir,S., Dursina,B.E., Thomae,N.H., Constantinescu,A.T., Brunsveld,L., Watzke,A., Waldmann,H., Goody,R.S., and Alexandrov,K. (2006). Structure of doubly prenylated Ypt1:GDI complex and the mechanism of GDI-mediated Rab recycling. EMBO J. *25*, 13-23.

Pylypenko,O., Rak,A., Reents,R., Niculae,A., Sidorovitch,V., Cioaca,M.D., Bessolitsyna,E., Thoma,N.H., Waldmann,H., Schlichting,I., Goody,R.S., and Alexandrov,K. (2003). Structure of rab escort protein-1 in complex with rab geranylgeranyltransferase. Mol. Cell *11*, 483-494.

Qiu,X., Valentijn,J.A., and Jamieson,J.D. (2001). Carboxyl-methylation of Rab3D in the rat pancreatic acinar tumor cell line AR42J. Biochem. Biophys. Res. Commun. *285*, 708-714.

Quimby,B.B. and Dasso,M. (2003). The small GTPase Ran: interpreting the signs. Curr. Opin. Cell Biol. *15*, 338-344.

Rak,A., Niculae,A., Kalinin,A., Thoma,N.H., Sidorovitch,V., Goody,R.S., and Alexandrov,K. (2002). In vitro assembly, purification, and crystallization of the rab geranylgeranyl transferase:substrate complex. Protein Expr. Purif. *25*, 23-30.

Rak,A., Pylypenko,O., Durek,T., Watzke,A., Kushnir,S., Brunsveld,L., Waldmann,H., Goody,R.S., and Alexandrov,K. (2003). Structure of Rab GDP-dissociation inhibitor in complex with prenylated YPT1 GTPase. Science *302*, 646-650.

Rak,A., Pylypenko,O., Niculae,A., Pyatkov,K., Goody,R.S., and Alexandrov,K. (2004). Structure of the Rab7:REP-1 complex: insights into the mechanism of Rab prenylation and choroideremia disease. Cell *117*, 749-760.

Reid,T.S., Terry,K.L., Casey,P.J., and Beese,L.S. (2004). Crystallographic analysis of CaaX prenyltransferases complexed with substrates defines rules of protein substrate selectivity. J. Mol. Biol. *343*, 417-433.

Reiss,Y., Brown,M.S., and Goldstein,J.L. (1992). Divalent cation and prenyl pyrophosphate specificities of the protein farnesyltransferase from rat brain, a zinc metalloenzyme. J. Biol. Chem. *267*, 6403-6408.

Reiss,Y., Goldstein,J.L., Seabra,M.C., Casey,P.J., and Brown,M.S. (1990). Inhibition of purified p21ras farnesyl:protein transferase by Cys-AAX tetrapeptides. Cell *62*, 81-88.

Reiss,Y., Seabra,M.C., Armstrong,S.A., Slaughter,C.A., Goldstein,J.L., Brown, and MS. (1991). Nonidentical subunits of p21H-ras farnesyltransferase. Peptide binding and farnesyl pyrophosphate carrier functions. Journal of Biological Chemistry *266*, 10672-10677.

Ren,B.Y., Gao,F., Tong,Z., and Yan,Y. (1999). Solvent polarity scale on the fluorescence spectra of a dansyl monomer copolymerizable in aqueous media. Chemical Physics Letters *307*, 55-61.

Resh,M.D. (2006). Trafficking and signaling by fatty-acylated and prenylated proteins. Nat. Chem. Biol. *2*, 584-590.

Rink,J., Ghigo,E., Kalaidzidis,Y., and Zerial,M. (2005). Rab conversion as a mechanism of progression from early to late endosomes. Cell *122*, 735-749.

Rishton,G.M. (1997). Reactive compounds and in vitro false positives in HTS. Drug Discovery Today *2*, 382-384.

Rocks,O., Peyker,A., and Bastiaens,P.I. (2006). Spatio-temporal segregation of Ras signals: one ship, three anchors, many harbors. Curr. Opin. Cell Biol. *18*, 351-357.

Rocks,O., Peyker,A., Kahms,M., Verveer,P.J., Koerner,C., Lumbierres,M., Kuhlmann,J., Waldmann,H., Wittinghofer,A., and Bastiaens,P.I. (2005). An acylation cycle regulates localization and activity of palmitoylated Ras isoforms. Science *307*, 1746-1752.

Roelofs,A.J., Hulley,P.A., Meijer,A., Ebetino,F.H., Russell,R.G., and Shipman,C.M. (2006). Selective inhibition of Rab prenylation by a phosphonocarboxylate analogue of risedronate induces apoptosis, but not S-phase arrest, in human myeloma cells. Int. J. Cancer *119*, 1254-1261.

Romanelli,A., Shekhtman,A., Cowburn,D., and Muir,T.W. (2004). Semisynthesis of a segmental isotopically labeled protein splicing precursor: NMR evidence for an unusual peptide bond at the N-extein-intein junction. Proc. Natl. Acad. Sci. U. S A *101*, 6397-6402.

Roskoski,R., Jr. and Ritchie,P. (1998). Role of the carboxyterminal residue in peptide binding to protein farnesyltransferase and protein geranylgeranyltransferase. Arch. Biochem. Biophys. *356*, 167-176.

Rowell,C.A., Kowalczyk,J.J., Lewis,M.D., and Garcia,A.M. (1997). Direct demonstration of geranylgeranylation and farnesylation of Ki-Ras in vivo. J. Biol. Chem. *272*, 14093-14097.

Rybin V, Ullrich O, Rubino M, Alexandrov K, Simon I, Seabra C M, Goody R, and Zerial M (1996). GTPase activity of Rab5 acts as a timer for endocytic membrane fusion. Nature *383*, 266-269.

Saderholm,M.J., Hightower,K.E., and Fierke,C.A. (2000). Role of metals in the reaction catalyzed by protein farnesyltransferase. Biochemistry *39*, 12398-12405.

Sakagami,Y., Isogai,A., Suzuki,A., Tamura,S., Tsuchiya,E., and Fukui,S. (1978). Isolation of A Novel Sex-Hormone, Tremerogen A-10, Controlling Conjugation Tube Formation in Tremella-Mesenterica Fries. Agricultural and Biological Chemistry *42*, 1093-1094.

Sakisaka,T., Meerlo,T., Matteson,J., Plutner,H., and Balch,W.E. (2002). Rab-alphaGDI activity is regulated by a Hsp90 chaperone complex. EMBO J *21*, 6125-6135.

Sanford JC, Yu J, Pan JY, and Wessling-Resnick M. GDP dissociation inhibitor serves as a cytosolic acceptor for newly synthesized and prenylated Rab5. J Biol Chem 270[45], 26904-26909. 1995. Ref Type: Abstract

Sanford,J.C., Pan,Y., and Wessling-Resnick,M. (1993). Prenylation of Rab5 is dependent on guanine nucleotide binding. J. Biol. Chem. *268*, 23773-23776.

Sasaki,T., Kikuchi,A., Araki,S., Hata,Y., Isomura,M., Kuroda,S., and Takai,Y. (1990). Purification and characterization from bovine brain cytosol of a protein that inhibits the dissociation of GDP from and the subsequent binding of GTP to smg p25A, a ras p21-like GTP-binding protein. Journal of Biological Chemistry *265*, 2333-2337.

Sato,K. and Nakano,A. (2007). Mechanisms of COPII vesicle formation and protein sorting. FEBS Lett. *581*, 2076-2082.

Schalk,I., Zeng,K., Wu,S.K., Stura,E.A., Matteson,J., Huang,M., Tandon,A., Wilson,I.A., and Balch,W.E. (1996). Structure and mutational analysis of Rab GDP-dissociation inhibitor. Nature *381*, 42-48.

Scheffzek,K., Ahmadian,M.R., Kabsch,W., Wiesmuller,L., Lautwein,A., Schmitz,F., and Wittinghofer,A. (1997). The Ras-RasGAP complex: structural basis for GTPase activation and its loss in oncogenic Ras mutants [see comments]. Science *277*, 333-338.

Scheffzek,K., Ahmadian,M.R., and Wittinghofer,A. (1998). GTPase-activating proteins: helping hands to complement an active site. Trends Biochem. Sci. *23*, 257-262.

Schein,C.H. and Noteborn,M.H.M. (1988). Formation of Soluble Recombinant Proteins in Escherichia-Coli Is Favored by Lower Growth Temperature. Bio-Technology *6*, 291-294.

Schlichting,I., Almo,S.C., Rapp,G., Wilson,K., Petratos,K., Lentfer,A., Wittinghofer,A., Kabsch,W., Pai,E.F., Petsko,G.A., and . (1990). Time-resolved X-ray crystallographic study of the conformational change in Ha-Ras p21 protein on GTP hydrolysis. Nature *345*, 309-315.

Schmidt,R.A., Schneider,C.J., and Glomset,J.A. (1984). Evidence for post-translational incorporation of a product of mevalonic acid into Swiss 3T3 cell proteins. J. Biol. Chem. *259*, 10175-10180.

Schnolzer,M. and Kent,S.B. (1992). Constructing proteins by dovetailing unprotected synthetic peptides: backbone-engineered HIV protease. Science *256*, 221-225.

Scott,C.P., bel-Santos,E., Wall,M., Wahnon,D.C., and Benkovic,S.J. (1999). Production of cyclic peptides and proteins in vivo. Proc. Natl. Acad. Sci. U. S A *96*, 13638-13643.

Seabra,M.C. (1996a). New insights into the pathogenesis of choroideremia: a tale of two REPs. Ophthalmic Genet. *17*, 43-46.

Seabra,M.C. (1996b). Nucleotide dependence of Rab geranylgeranylation. Rab escort protein interacts preferentially with GDP-bound Rab. Journal of Biological Chemistry *271*, 14398-14404.

Seabra,M.C., Brown,M.S., and Goldstein,J.L. (1993). Retinal degeneration in choroideremia: deficiency of rab geranylgeranyl transferase. Science *259*, 377-381.

Seabra,M.C., Brown,M.S., Slaughter,C.A., Sudhof,T.C., and Goldstein,J.L. (1992a). Purification of component A of Rab geranylgeranyl transferase: possible identity with the choroideremia gene product. Cell *70*, 1049-1057.

Seabra,M.C. and Coudrier,E. (2004). Rab GTPases and myosin motors in organelle motility. Traffic *5*, 393-399.

Seabra,M.C., Goldstein,J.L., Sudhof,T.C., and Brown,M.S. (1992b). Rab geranylgeranyl transferase. A multisubunit enzyme that prenylates GTP-binding proteins terminating in Cys-X-Cys or Cys- Cys. Journal of Biological Chemistry *267*, 14497-14503.

Seabra,M.C., Ho,Y.K., and Anant,J.S. (1995). Deficient geranylgeranylation of Ram/Rab27 in choroideremia. Journal of Biological Chemistry *270*, 24420-24427.

Seabra,M.C., Mules,E.H., and Hume,A.N. (2002). Rab GTPases, intracellular traffic and disease. Trends Mol. Med. *8*, 23-30.

Seabra,M.C., Reiss,Y., Casey,P.J., Brown,M.S., and Goldstein,J.L. (1991). Protein farnesyltransferase and geranylgeranyltransferase share a common alpha subunit. Cell *65*, 429-434.

Sebti,S.M. (2005). Protein farnesylation: implications for normal physiology, malignant transformation, and cancer therapy. Cancer Cell *7*, 297-300.

Severinov,K. and Muir,T.W. (1998). Expressed protein ligation, a novel method for studying protein-protein interactions in transcription. J. Biol. Chem. *273*, 16205-16209.

Shahinian,S. and Silvius,J.R. (1995). Doubly-lipid-modified protein sequence motifs exhibit long-lived anchorage to lipid bilayer membranes. Biochemistry *34*, 3813-3822.

Shao,Y. and Paulus,H. (1997). Protein splicing: estimation of the rate of O-N and S-N acyl rearrangements, the last step of the splicing process. J Pept. Res. *50*, 193-198.

Shao,Y., Xu,M.Q., and Paulus,H. (1996). Protein splicing: evidence for an N-O acyl rearrangement as the initial step in the splicing process. Biochemistry *35*, 3810-3815.

Shapiro,A.D. and Pfeffer,S.R. (1995). Quantitative analysis of the interactions between prenyl Rab9, GDP dissociation inhibitor-alpha, and guanine nucleotides. Journal of Biological Chemistry *270*, 11085-11090.

Shen,F. and Seabra,M.C. (1996). Mechanism of digeranylgeranylation of Rab proteins. Formation of a complex between monogeranylgeranyl-Rab and Rab escort protein. Journal of Biological Chemistry *271*, 3692-3698.

Shiba,T., Koga,H., Shin,H.W., Kawasaki,M., Kato,R., Nakayama,K., and Wakatsuki,S. (2006). Structural basis for Rab11-dependent membrane recruitment of a family of Rab11-interacting protein 3 (FIP3)/Arfophilin-1. Proc. Natl. Acad. Sci. U. S A *103*, 15416-15421.

Shults,M.D. and Imperiali,B. (2003). Versatile fluorescence probes of protein kinase activity. J. Am. Chem. Soc. *125*, 14248-14249.

Sidorovitch,V., Niculae,A., Kan,N., Ceacareanu,A., and Alexandrov,K. (2002). Expression of mammalian Rab Escort Protein-1 and -2 in yeast Saccharomyces cerevisiae. Protein Expr. Purif. *26*, 50.

Silvius,J.R. and l'Heureux,F. (1994). Fluorimetric evaluation of the affinities of isoprenylated peptides for lipid bilayers. Biochemistry *33*, 3014-3022.

Sivars,U., Aivazian,D., and Pfeffer,S.R. (2003). Yip3 catalyses the dissociation of endosomal Rab-GDI complexes. Nature 2003. Oct. 23;425. (6960.):856. -9. *425*, 856-859.

Sklan,E.H., Serrano,R.L., Einav,S., Pfeffer,S.R., Lambright,D.G., and Glenn,J.S. (2007). TBC1D20 is a RAB1 GAP that mediates HCV replication. J. Biol. Chem.

Skretas,G. and Wood,D.W. (2005). Regulation of protein activity with small-molecule-controlled inteins. Protein Sci. *14*, 523-532.

Sloan,D.J. and Hellinga,H.W. (1998). Structure-based engineering of environmentally sensitive fluorophores for monitoring protein-protein interactions. Protein Engineering *11*, 819-823.

Smeland,T.E., Seabra,M.C., Goldstein,J.L., and Brown,M.S. (1994). Geranylgeranylated Rab proteins terminating in Cys-Ala-Cys, but not Cys-Cys, are carboxyl-methylated by bovine brain membranes in vitro. Proceedings of the National Academy of Sciences of the United States of America *91*, 10712-10716.

Soldati,T., Shapiro,A.D., Svejstrup,A.B., and Pfeffer,S.R. (1994). Membrane targeting of the small GTPase Rab9 is accompanied by nucleotide exchange [see comments]. Nature *369*, 76-78.

Sollner,T., Bennett,M.K., Whiteheart,S.W., Scheller,R.H., and Rothman,J.E. (1993). A protein assembly-disassembly pathway in vitro that may correspond to sequential steps of synaptic vesicle docking, activation, and fusion. Cell *75*, 409-418.

Soper,S.A. and Mattingly,Q.L. (1994). Steady-State and Picosecond Laser Fluorescence Studies of Nonradiative Pathways in Tricarbocyanine Dyes - Implications to the Design of Near-Ir Fluorochromes with High Fluorescence Efficiencies. Journal of the American Chemical Society *116*, 3744-3752.

Southworth,M.W., Adam,E., Panne,D., Byer,R., Kautz,R., and Perler,F.B. (1998). Control of protein splicing by intein fragment reassembly. EMBO J. *17*, 918-926.

Souza-Schorey,C. and Chavrier,P. (2006). ARF proteins: roles in membrane traffic and beyond. Nat. Rev. Mol. Cell Biol. *7*, 347-358.

Sprang,S.R. (1997). G protein mechanisms: insights from structural analysis. Annu. Rev. Biochem. *66*, 639-678.

Stagg,S.M., Gurkan,C., Fowler,D.M., LaPointe,P., Foss,T.R., Potter,C.S., Carragher,B., and Balch,W.E. (2006). Structure of the Sec13/31 COPII coat cage. Nature *439*, 234-238.

Starai,V.J., Jun,Y., and Wickner,W. (2007). Excess vacuolar SNAREs drive lysis and Rab bypass fusion. Proc. Natl. Acad. Sci. U. S A *104*, 13551-13558.

Stenmark,H. and Olkkonen,V.M. (2001). The Rab GTPase family. Genome Biol *2*, REVIEWS3007.

Stenmark,H., Parton,R.G., Steele-Mortimer,O., Lutcke,A., Gruenberg,J., and Zerial,M. (1994a). Inhibition of rab5 GTPase activity stimulates membrane fusion in endocytosis. EMBO J. *13*, 1287-1296.

Stenmark,H., Valencia,A., Martinez,O., Ullrich,O., Goud,B., and Zerial,M. (1994b). Distinct structural elements of rab5 define its functional specificity. EMBO J. *13*, 575-583.

Strickland,C.L., Windsor,W.T., Syto,R., Wang,L., Bond,R., Wu,Z., Schwartz,J., Le,H.V., Beese,L.S., and Weber,P.C. (1998). Crystal structure of farnesyl protein transferase complexed with a CaaX peptide and farnesyl diphosphate analogue. Biochemistry *37*, 16601-16611.

Strom,M., Hume,A.N., Tarafder,A.K., Barkagianni,E., and Seabra,M.C. (2002). A family of Rab27-binding proteins. Melanophilin links Rab27a and myosin Va function in melanosome transport. J. Biol. Chem. *277*, 25423-25430.

Stroupe,C. and Brunger,A.T. (2000). Crystal structures of a Rab protein in its inactive and active conformations. J. Mol. Biol. *304*, 585-598.

Sun,J., Ohkanda,J., Coppola,D., Yin,H., Kothare,M., Busciglio,B., Hamilton,A.D., and Sebti,S.M. (2003). Geranylgeranyltransferase I inhibitor GGTI-2154 induces breast carcinoma apoptosis and tumor regression in H-Ras transgenic mice. Cancer Res. *63*, 8922-8929.

Sutton,R.B., Fasshauer,D., Jahn,R., and Brunger,A.T. (1998). Crystal structure of a SNARE complex involved in synaptic exocytosis at 2.4 A resolution. Nature *395*, 347-353.

Suvorova,E.S., Duden,R., and Lupashin,V.V. (2002). The Sec34/Sec35p complex, a Ypt1p effector required for retrograde intra-Golgi trafficking, interacts with Golgi SNAREs and COPI vesicle coat proteins. J. Cell Biol. *157*, 631-643.

Swanson,K.M. and Hohl,R.J. (2006). Anti-cancer therapy: targeting the mevalonate pathway. Curr. Cancer Drug Targets. *6*, 15-37.

Swarthout,J.T., Lobo,S., Farh,L., Croke,M.R., Greentree,W.K., Deschenes,R.J., and Linder,M.E. (2005). DHHC9 and GCP16 constitute a human protein fatty acyltransferase with specificity for H- and N-Ras. J. Biol. Chem. *280*, 31141-31148.

Sztul,E. and Lupashin,V. (2006). Role of tethering factors in secretory membrane traffic. Am. J. Physiol Cell Physiol *290*, C11-C26.

Takai,Y., Sasaki,T., and Matozaki,T. (2001). Small GTP-binding proteins. Physiol Rev. *81*, 153-208.

Tanford,C. and Reynolds,J.A. (1976). Characterization of Membrane Proteins in Detergent Solutions. Biochimica et Biophysica Acta *457*, 133-170.

Tascioglu,S. (1996). Micellar solutions as reaction media. Tetrahedron *52*, 11113-11152.

Taylor,J.S., Reid,T.S., Terry,K.L., Casey,P.J., and Beese,L.S. (2003). Structure of mammalian protein geranylgeranyltransferase type-I. EMBO J. *22*, 5963-5974.

Thomä,N. and Goody,R.S. (2003). What to do if there is no signal: using competition experiments to determine binding parameters. In Kinetic Analysis of Macromolecules, K.A.Johnson, ed. (Oxford: Oxford University Press), pp. 153-170.

Thoma,N.H., Iakovenko,A., Goody,R.S., and Alexandrov,K. (2001a). Phosphoisoprenoids modulate association of Rab geranylgeranyltransferase with REP-1. J. Biol. Chem.

Thoma,N.H., Iakovenko,A., Kalinin,A., Waldmann,H., Goody,R.S., and Alexandrov,K. (2001b). Allosteric regulation of substrate binding and product release in geranylgeranyltransferase type II. Biochemistry *40*, 268-274.

Thoma,N.H., Iakovenko,A., Owen,D., Scheidig,A.S., Waldmann,H., Goody,R.S., and Alexandrov,K. (2000). Phosphoisoprenoid Binding Specificity of Geranylgeranyltransferase Type II. Biochemistry *39*, 12043-12052.

Thoma,N.H., Niculae,A., Goody,R.S., and Alexandrov,K. (2001c). Double prenylation by RabGGTase can proceed without dissociation of the mono-prenylated intermediate. J. Biol. Chem. *276*, 48631-48636.

Thutewohl,M., Kissau,L., Popkirova,B., Karaguni,I.M., Nowak,T., Bate,M., Kuhlmann,J., Muller,O., and Waldmann,H. (2002). Solid-phase synthesis and biological evaluation of a pepticinnamin E library. Angewandte Chemie-International Edition *41*, 3616-3620.

Tolbert,T.J. and Wong,C.H. (2000). Intein-mediated synthesis of proteins containing carbohydrates and other molecular probes. Journal of the American Chemical Society *122*, 5421-5428.

Toutchkine,A., Kraynov,V., and Hahn,K. (2003). Solvent-sensitive dyes to report protein conformational changes in living cells. Journal of the American Chemical Society *125*, 4132-4145.

Trueblood,C.E., Boyartchuk,V.L., Picologlou,E.A., Rozema,D., Poulter,C.D., and Rine,J. (2000). The CaaX proteases, Afc1p and Rce1p, have overlapping but distinct substrate specificities. Mol. Cell Biol. *20*, 4381-4392.

Trueblood,C.E., Ohya,Y., and Rine,J. (1993). Genetic evidence for in vivo cross-specificity of the CaaX-box protein prenyltransferases farnesyltransferase and geranylgeranyltransferase-I in Saccharomyces cerevisiae. Mol. Cell Biol. *13*, 4260-4275.

Tschantz,W.R., Furfine,E.S., and Casey,P.J. (1997). Substrate binding is required for release of product from mammalian protein farnesyltransferase. J. Biol. Chem. *272*, 9989-9993.

Tsuchiya,E., Fukui,S., Kamiya,Y., Sakagami,Y., and Fujino,M. (1978). Requirements of chemical structure of hormonal activity of lipopeptidyl factors inducing sexual differentiation in vegetative cells of heterobasidiomycetous yeasts. Biochem. Biophys. Res. Commun. *85*, 459-463.

Ullrich,O., Horiuchi,H., Bucci,C., and Zerial,M. (1994). Membrane association of Rab5 mediated by GDP-dissociation inhibitor and accompanied by GDP/GTP exchange [see comments]. Nature *368*, 157-160.

Ungar,D., Oka,T., Krieger,M., and Hughson,F.M. (2006). Retrograde transport on the COG railway. Trends Cell Biol. *16*, 113-120.

Ungar,D., Oka,T., Vasile,E., Krieger,M., and Hughson,F.M. (2005). Subunit architecture of the conserved oligomeric Golgi complex. J. Biol. Chem. *280*, 32729-32735.

Valencia,A., Chardin,P., Wittinghofer,A., and Sander,C. (1991). The Ras Protein Family - Evolutionary Tree and Role of Conserved Amino-Acids. Biochemistry *30*, 4637-4648.

Valentijn,J.A. and Jamieson,J.D. (1998). Carboxyl methylation of rab3D is developmentally regulated in the rat pancreas: correlation with exocrine function. Eur. J. Cell Biol. *76*, 204-211.

Van Voorhis,W.C., Schlekewy,L., and Trong,H.L. (1991). Molecular mimicry by Trypanosoma cruzi: the F1-160 epitope that mimics mammalian nerve can be mapped to a 12-amino acid peptide. Proc. Natl. Acad. Sci. U. S. A *88*, 5993-5997.

Vetter,I.R. and Wittinghofer,A. (2001). The guanine nucleotide-binding switch in three dimensions. Science *294*, 1299-1304.

Vojtek,A.B. and Der,C.J. (1998). Increasing complexity of the Ras signaling pathway. J. Biol. Chem. *273*, 19925-19928.

Wada,A., Mie,M., Aizawa,M., Lahoud,P., Cass,A.E.G., and Kobatake,E. (2003). Design and construction of glutamine binding proteins with a self-adhering capability to unmodified hydrophobic surfaces as reagentless fluorescence sensing devices. Journal of the American Chemical Society *125*, 16228-16234.

Wada,M., Nakanishi,H., Satoh,A., Hirano,H., Obaishi,H., Matsuura,Y., and Takai,Y. (1997). Isolation and characterization of a GDP/GTP exchange protein specific for the Rab3 subfamily small G proteins. J. Biol. Chem. *272*, 3875-3878.

Wagner,W., Bielli,P., Wacha,S., and Ragnini-Wilson,A. (2002). Mlc1p promotes septum closure during cytokinesis via the IQ motifs of the vesicle motor Myo2p. EMBO J. *21*, 6397-6408.

Waldmann,H. and Thutewohl,M. (2001). Ras-farnesyltransferase-inhibitors as promising anti-tumor drugs. Bioorganic Chemistry of Biological Signal Transduction *211*, 117-130.

Walkup,G.K. and Imperiali,B. (1996). Design and evaluation of a peptidyl fluorescent chemosensor for divalent zinc. Journal of the American Chemical Society *118*, 3053-3054.

Walters,C.E., Pryce,G., Hankey,D.J., Sebti,S.M., Hamilton,A.D., Baker,D., Greenwood,J., and Adamson,P. (2002). Inhibition of Rho GTPases with protein prenyltransferase inhibitors prevents leukocyte recruitment to the central nervous system and attenuates clinical signs of disease in an animal model of multiple sclerosis. J. Immunol. *168*, 4087-4094.

Wang,D.A. and Sebti,S.M. (2005). Palmitoylated cysteine 192 is required for RhoB tumor-suppressive and apoptotic activities. J. Biol. Chem. *280*, 19243-19249.

Wang,Q.Z. and Lawrence,D.S. (2005). Phosphorylation-driven protein-protein interactions: A protein kinase sensing system. Journal of the American Chemical Society *127*, 7684-7685.

Weber,T., Zemelman,B.V., McNew,J.A., Westermann,B., Gmachl,M., Parlati,F., Sollner,T.H., and Rothman,J.E. (1998). SNAREpins: minimal machinery for membrane fusion. Cell *92*, 759-772.

Weller,V.A. and Distefano,M.D. (1998). Measurement of the alpha-secondary kinetic isotope effect for a prenyltransferase by MALDI mass spectrometry. Journal of the American Chemical Society *120*, 7975-7976.

Welling-Wester,S., Feijlbrief,M., Koedijk,D.G., and Welling,G.W. (1998). Detergent extraction of herpes simplex virus type 1 glycoprotein D by zwitterionic and non-ionic detergents and purification by ion-exchange high-performance liquid chromatography. J. Chromatogr. A *816*, 29-37.

Wennerberg,K., Rossman,K.L., and Der,C.J. (2005). The Ras superfamily at a glance. J. Cell Sci. *118*, 843-846.

Whyte,D.B., Kirschmeier,P., Hockenberry,T.N., Nunez-Oliva,I., James,L., Catino,J.J., Bishop,W.R., and Pai,J.K. (1997). K- and N-Ras are geranylgeranylated in cells treated with farnesyl protein transferase inhibitors. J. Biol. Chem. *272*, 14459-14464.

Willets,K.A., Ostroverkhova,O., He,M., Twieg,R.J., and Moerner,W.E. (2003). Novel fluorophores for single-molecule imaging. Journal of the American Chemical Society *125*, 1174-1175.

Williams,N.K., Prosselkov,P., Liepinsh,E., Line,I., Sharipo,A., Littler,D.R., Curmi,P.M., Otting,G., and Dixon,N.E. (2002). In vivo protein cyclization promoted by a circularly permuted Synechocystis sp. PCC6803 DnaB mini-intein. J. Biol. Chem. *277*, 7790-7798.

Wilson,A.L., Erdman,R.A., Castellano,F., and Maltese,W.A. (1998). Prenylation of Rab8 GTPase by type I and type II geranylgeranyl transferases. Bochem. J *333*, 497-504.

Wilson,G.M., Fielding,A.B., Simon,G.C., Yu,X., Andrews,P.D., Hames,R.S., Frey,A.M., Peden,A.A., Gould,G.W., and Prekeris,R. (2005). The FIP3-Rab11 protein complex regulates recycling endosome targeting to the cleavage furrow during late cytokinesis. Mol. Biol. Cell *16*, 849-860.

Woo,J.T., Kasai,S., Stern,P.H., and Nagai,K. (2000). Compactin suppresses bone resorption by inhibiting the fusion of prefusion osteoclasts and disrupting the actin ring in osteoclasts. J. Bone Miner. Res. *15*, 650-662.

Woo,J.T., Nakagawa,H., Krecic,A.M., Nagai,K., Hamilton,A.D., Sebti,S.M., and Stern,P.H. (2005). Inhibitory effects of mevastatin and a geranylgeranyl transferase I inhibitor (GGTI-2166) on mononuclear osteoclast formation induced by receptor activator of NF kappa B ligand (RANKL) or tumor necrosis factor-alpha (TNF-alpha). Biochem. Pharmacol. *69*, 87-95.

Wright,L.P. and Philips,M.R. (2006). Thematic review series: lipid posttranslational modifications. CAAX modification and membrane targeting of Ras. J. Lipid Res. *47*, 883-891.

Wu,C.W., Yarbrough,L.R., and Wu,F.Y.H. (1976). N-(1-Pyrene)Maleimide - Fluorescent Cross-Linking Reagent. Biochemistry *15*, 2863-2868.

Wu,H., Hu,Z., and Liu,X.Q. (1998a). Protein trans-splicing by a split intein encoded in a split DnaE gene of Synechocystis sp. PCC6803. Proc. Natl. Acad. Sci. U. S A *95*, 9226-9231.

Wu,M., Wang,T., Loh,E., Hong,W., and Song,H. (2005). Structural basis for recruitment of RILP by small GTPase Rab7. EMBO J. *24*, 1491-1501.

Wu,X., Bowers,B., Rao,K., Wei,Q., and Hammer,J.A., III (1998b). Visualization of melanosome dynamics within wild-type and dilute melanocytes suggests a paradigm for myosin V function In vivo. J. Cell Biol. *143*, 1899-1918.

Wu,X., Wang,F., Rao,K., Sellers,J.R., and Hammer,J.A., III (2002a). Rab27a is an essential component of melanosome receptor for myosin Va. Mol. Biol. Cell *13*, 1735-1749.

Wu,X.S., Rao,K., Zhang,H., Wang,F., Sellers,J.R., Matesic,L.E., Copeland,N.G., Jenkins,N.A., and Hammer,J.A., III (2002b). Identification of an organelle receptor for myosin-Va. Nat. Cell Biol. *4*, 271-278.

Wu,Y.W., Waldmann,H., Reents,R., Ebetino,F.H., Goody,R.S., and Alexandrov,K. (2006). A protein fluorescence amplifier: continuous fluorometric assay for rab geranylgeranyltransferase. Chembiochem. *7*, 1859-1861.

Wurmser,A.E., Sato,T.K., and Emr,S.D. (2000). New component of the vacuolar class C-Vps complex couples nucleotide exchange on the Ypt7 GTPase to SNARE-dependent docking and fusion. J. Cell Biol. *151*, 551-562.

Xu,M.Q., Comb,D.G., Paulus,H., Noren,C.J., Shao,Y., and Perler,F.B. (1994). Protein splicing: an analysis of the branched intermediate and its resolution by succinimide formation. EMBO J. *13*, 5517-5522.

Xu,M.Q. and Evans,T.C., Jr. (2001). Intein-mediated ligation and cyclization of expressed proteins. Methods 2001. Jul. ;24. (3):257. -77. *24*, 257-277.

Xu,M.Q. and Evans,T.C., Jr. (2005). Recent advances in protein splicing: manipulating proteins in vitro and in vivo. Curr. Opin. Biotechnol. *16*, 440-446.

Xu,M.Q., Paulus,H., and Chong,S. (2000). Fusions to self-splicing inteins for protein purification. Methods Enzymol. *326*, 376-418.

Xu,M.Q. and Perler,F.B. (1996). The mechanism of protein splicing and its modulation by mutation. EMBO J. *15*, 5146-5153.

Xu,M.Q., Southworth,M.W., Mersha,F.B., Hornstra,L.J., and Perler,F.B. (1993). In vitro protein splicing of purified precursor and the identification of a branched intermediate. Cell *75*, 1371-1377.

Xu,R., Ayers,B., Cowburn,D., and Muir,T.W. (1999a). Chemical ligation of folded recombinant proteins: Segmental isotopic labeling of domains for NMR studies. Proceedings of the National Academy of Sciences of the United States of America *96*, 388-393.

Xu,R., Ayers,B., Cowburn,D., and Muir,T.W. (1999b). Chemical ligation of folded recombinant proteins: segmental isotopic labeling of domains for NMR studies. Proc. Natl. Acad. Sci. U. S A *96*, 388-393.

Ye,J., Wang,C., Sumpter,R., Jr., Brown,M.S., Goldstein,J.L., and Gale,M., Jr. (2003). Disruption of hepatitis C virus RNA replication through inhibition of host protein geranylgeranylation. Proc. Natl. Acad. Sci. U. S A *100*, 15865-15870.

Yeh,R.H., Yan,X.W., Cammer,M., Bresnick,A.R., and Lawrence,D.S. (2002). Real time visualization of protein kinase activity in living cells. Journal of Biological Chemistry *277*, 11527-11532.

Yokoyama,K., Goodwin,G.W., Ghomashchi,F., Glomset,J.A., and Gelb,M.H. (1991). A protein geranylgeranyltransferase from bovine brain: implications for protein prenylation specificity. Proc. Natl. Acad. Sci. U. S. A *88*, 5302-5306.

Yokoyama,K., McGeady,P., and Gelb,M.H. (1995). Mammalian protein geranylgeranyltransferase-I: substrate specificity, kinetic mechanism, metal requirements, and affinity labeling [published erratum appears in Biochemistry 1995 Oct 31; 34(43):14270]. Biochemistry *34*, 1344-1354.

Yokoyama,K., Zimmerman,K., Scholten,J., and Gelb,M.H. (1997). Differential prenyl pyrophosphate binding to mammalian protein geranylgeranyltransferase-I and protein farnesyltransferase and its consequence on the specificity of protein prenylation. J. Biol. Chem. *272*, 3944-3952.

Zeidler,M.P., Tan,C., Bellaiche,Y., Cherry,S., Hader,S., Gayko,U., and Perrimon,N. (2004). Temperature-sensitive control of protein activity by conditionally splicing inteins. Nat. Biotechnol. *22*, 871-876.

Zerial,M. and McBride,H. (2001). Rab proteins as membrane organizers. Nat. Rev. Mol. Cell Biol. *2*, 107-117.

Zhang,F.L. and Casey,P.J. (1996). Protein prenylation: molecular mechanisms and functional consequences. Annu. Rev. Biochem. *65*, 241-269.

Zhang,F.L., Kirschmeier,P., Carr,D., James,L., Bond,R.W., Wang,L., Patton,R., Windsor,W.T., Syto,R., Zhang,R., and Bishop,W.R. (1997). Characterization of Ha-ras, N-ras, Ki-Ras4A, and Ki-Ras4B as in

vitro substrates for farnesyl protein transferase and geranylgeranyl protein transferase type I. J Biol. Chem *272*, 10232-10239.

Zhang,F.L., Moomaw,J.F., and Casey,P.J. (1994). Properties and kinetic mechanism of recombinant mammalian protein geranylgeranyltransferase type I. J. Biol. Chem. *269*, 23465-23470.

Zhu,G., Zhai,P., Liu,J., Terzyan,S., Li,G., and Zhang,X.C. (2004). Structural basis of Rab5-Rabaptin5 interaction in endocytosis. Nat. Struct. Mol. Biol. *11*, 975-983.

Acknowledgements

This is not the end of the story, instead a new beginning for my future. No matter how successful I was and will be, people are always the most important factor in the past and coming events. Thus I would like to appreciate those people who have helped me during my Ph.D. study. The most prominent people among these are my supervisors Prof. Dr. Roger Goody and Dr. Kirill Alexandrov. Both of them have been so kind to spend their time in instructing me knowledge and share creative ideas with me. They have provided me a lot of freedom to do my research and many training opportunities in communication, organization and leadership. Moreover, I am grateful for their continuous encouragement and their concerns for me.

I would like to thank my third supervisor and reviewer of my thesis, Prof. Dr. Herbert Waldmann for his supervision of part of my Ph.D. work, particularly in the RabGGTase inhibitor project. My Ph.D. work was performed in close collaboration with the people in Prof. Dr. Waldmann' group and the colleagues in our group. The RabGGTase inhibitor project was carried out by a team including chemists, biochemists, crystallographers and cell biologists. The fluorescent phosphoisoprenoids and prenylated peptides were synthesized by Dr. Reinhard Reents and Dr. Kui-Thong Tan. The peptide compounds for RabGGTase inhibitor study were synthesized by Dr. Kui-Thong Tan and Dr. Ester Guiu-Rozas. The crystal structures of RabGGTase complexed with inhibitors were solved by Zhong Guo and Dr. Wulf Blankenfeldt, the cellular activity of the inhibitors was evaluated by Dr. Christine Delon. Here, I would like to express my thanks to all these people.

I would like to thank Prof. Dr. Ruben Abagyan who did the simulation of Rab:REP:RabGGTase ternary complex together with me. And the virtual ligand screening was also performed in his lab.

I am grateful to Dr. Thomas Durek who has assisted me a lot in both work and life at the beginning of my Ph.D. study.

I am also thankful to all colleagues in the Alexandrov's group, particularly the skilful technicians who have provided a very good platform for my study, including cloning and protein purification.

Many thanks go to Dr. Aymelt Itzen and Ms. Thi Thanh Uyen Nguyen for their kind help in my Ph.D. thesis.

I would also like to appreciate Dr. Alex Rak and Dr. Lena Pylypenko for their kind guidance to me in crystallizing and solving the structure of beta subunit of RabGGTase.

Thanks are also assigned to the members in Alexandrov's group, Rak's group and Blankenfeldt's group in the MPI Dortmund who have contributed to a friendly and helpful working atmosphere.

Another kind person I would like to appreciate is Dr. Waltraud Hoffmann-Goody. It was she who asked me by chance about my future plan after my master. Without her introducing me to Roger, I would not have chance to do my Ph.D. in this lab. Moreover, she has been persistently helpful to me in the past few years.

Last but not least, I am greatly indebted to my family members who have always given me support and understanding in all circumstances of my life.

Publication

“Structure of Rab geranylgeranyl transferase:substrate/product complexes provide insights into evolution of protein prenylation”
Z. Guo*, **Y. W. Wu***, D. Das, J. Cramer, S, Yu, H. Waldmann, R.S. Goody, L. Brunsveld, W. Blankenfeldt, K. Alexandrov
EMBO J. 2008, in press (*equal contribution)

“Development of selective RabGGTase inhibitors and crystal structure of a RabGGTase-inhibitor complex”
Z. Guo*, **Y.W. Wu***, K.T Tan, R. Bon, E. Guiu-Rozas, C. Delon, U. T. Nguyen, S. Wetzel, S. Arndt, R. S. Goody, W. Blankenfeldt, K. Alexandrov, H. Waldmann
Angew. Chem. Int. Ed. Engl. 2008, 47(20): 3747-3750 (*equal contribution)

“Synthesis of a fluorescent analogue of geranylgeranyl pyrophosphate and its use in a high-throughput fluorometric assay for Rab geranylgeranyltransferase”
Y.W. Wu, K. Alexandrov, L. Brunsveld
Nature Protocols, 2007, 2, 2704-2711.

“Interaction analysis of prenylated Rab GTPase with Rab escort protein and GDP dissociation inhibitor explains the need for both regulators”
Y.W. Wu, K.T. Tan, H. Waldmann, R.S. Goody, K. Alexandrov
Proc. Natl. Acad. Sci. U. S. A. 2007, 104(30):12294-1299

“A synthetic supramolecular construct modulating protein assembly in cells”
L. Zhang, **Y. Wu**, L. Brunsveld
Angew. Chem. Int. Ed. Engl. 2007, 46(11):1798-1802

“A protein fluorescence amplifier: continuous fluorometric assay for Rab geranylgeranyl transferase”
Y.W. Wu, H. Waldmann, R. Reents, F.H. Ebetino, R.S. Goody, K. Alexandrov
Chembiochem. 2006, 7(12):1859-1861

“Identification and specificity profiling of protein prenyltransferase inhibitors using new fluorescent phosphoisoprenoids”
B. Dursina, R. Reents, C. Delon, **Y. Wu**, M. Kulharia, M. Thutewohl, A. Veligodsky, A. Kalinin, V. Evstifeev, D. Ciobanu, S. E. Szedlacsek, H. Waldmann, R. S. Goody, K. Alexandrov
J. Am. Chem. Soc. 2006, 128(9), 2822-2835